RELATION OF METAL SULFIDE MINERALIZATION TO ANHYDRITE CAP ROCK FORMATION AT HOCKLEY SALT DOME, HARRIS COUNTY, TEXAS

APPROVED:

Supervisc [redacted]

RELATION OF METAL SULFIDE MINERALIZATION TO ANHYDRITE CAP ROCK FORMATION AT HOCKLEY SALT DOME, HARRIS COUNTY, TEXAS

by

William Norris Agee, Jr., B.S.

THESIS

Presented to the Faculty of the Graduate School of

The University of Texas at Austin

in Partial Fulfillment

of the Requirements

for the Degree of

Master of Arts

THE UNIVERSITY OF TEXAS AT AUSTIN

May, 1990

ACKNOWLEDGMENTS

I wish to thank J. Richard Kyle for providing the direction and means of support necessary to complete this project. Harry H. Posey and Lynton S. Land critically read versions of this thesis and provided many valuable insights. I would like to thank Leon E. Long for reviewing the Pb isotope section of this thesis. It has been a pleasure to have studied under these faculty members. I am grateful to student editors Carl Fiduk and Larry Mack (Pb isotope section) for their editorial comments and Rachel Eustice for running PREQPITZ in my absence. Also, student assistants, David, Devin, and Scott, are to be commended for their efforts of data entry and core polishing.

Hockley Dome cap rock core was made available for study by Marathon Oil Company through Peter E. Price. Access to drill core from Hockley Dome was provided by Bill Warren (Warren Ranch) and the University of Texas Bureau of Economic Geology, Core Research Facility. Sulfur Isotope data reported in Kyle and Price (1986) were determined at McMaster University, Hamilton, Ontario. All subsequent sulfide analyses were performed at the United States Geological Survey National Headquarters, Reston, Virginia, utilizing the sulfur isotope facilities of W.C. Shanks III. Individual analyses were generated by Richard Kyle and T. W. Johnson. Common Pb data presented in Kyle and Price (1986) were determined at the Department of Physics, University of Alberta, Edmonton, Alberta. Additional Pb analyses were determined at laboratories of The University of California, Santa Barbara, California, and The University of Texas, Austin, Texas. Common Pb analyses of cap rock sulfides were provided by Nick Walker.

This research was supported by National Science Foundation grants EAR-8407736 and EAR-8709319 to Richard Kyle and by fellowships from the U.S. Department of the Interior's Mineral Institutes Program administered by the Bureau of Mines under allotment grant numbers G1154146 and G1164147 to the Texas Mining and Mineral Resources Research Institute. Research grants were also provided by Gulf Coast Association of Geological Societies and Gulf Coast Section Society of Economic Paleontologist and Mineralogist.

Finally, I would like to thank my parents, Lois and Norris Agee, for their support and encouragement throughout my academic endeavors. Leon Long also deserves credit and much appreciation for his persuasive introduction of geology to me. I am especially grateful to my wife, Leigh, for her help and understanding over the "long" four years I spent in graduate school. No doubt, I have benefitted from her laboratory assistance and many editorial comments. A very special acknowledgement goes to my son Chris, who has shown me that smiling can get you further than bawling, and that there is more to life than having a clean diaper (but not much).

ABSTRACT

RELATION OF METAL SULFIDE MINERALIZATION TO ANHYDRITE CAP ROCK FORMATION AT HOCKLEY SALT DOME, HARRIS COUNTY, TEXAS

by

William Norris Agee, Jr., B.S.

SUPERVISING PROFESSOR: James Richard Kyle

The Gulf Coast basin is a dynamic hydrologic environment for which mixing of multisource fluids is an attractive and plausible mechanism to explain metal and isotopic variations of sulfide concentrations in the cap rock of the Hockley salt dome. Textural evidence indicates that most metal concentrations are stratiform sulfides that were precipitated at the salt/cap rock contact as the anhydrite zone accumulated by sequential underplating. Because sulfides occur throughout the 935-ft cap rock and show vertical (paragenetic) trends with regard to metal ratios and sulfur isotope composition, the evolution of rock-fluid interactions in the cap rock environment can be evaluated. Reservoirs of reduced sulfur and metals evolved or mixed during the accumulation history of the anhydrite cap rock.

Extensive core drilling at Hockley Dome has defined an annular zone of metal sulfides in both the calcite and anhydrite cap rock zones. Marcasite is the dominant sulfide and is associated with lesser amounts of pyrite, sphalerite, galena, and rare acanthite. Significant concentrations of sulfides occur within a 150-ft zone in the central cap rock "stratigraphy". These zones may be related to decreased cap rock accumulation rates and increased supply of metalliferous fluids. The general metal trend in the Hockley cap rock is an overall increase of Zn relative to Pb downward in

the anhydrite cap rock. A high concentration of Ag appears in the lower part of the anhydrite cap rock. Metal assay data suggest that the sulfide-precipitating fluid became more Zn- and Ag-rich during cap rock accumulation.

$\delta^{34}S$ values of sulfide minerals within the Hockley cap rock range from +4 to -35 ‰ (CDT) (96 analyses). A single drill hole (HH2) profile of $\delta^{34}S$ pyrite values indicates that sulfide minerals become progressively heavier with depth to the approximate middle of the cap rock where the isotopic trend is reversed. The inflection point corresponds to a local highly mineralized biogenic calcite zone. The complementary metal and $\delta^{34}S$ data for HH2 indicate two isotopically distinct sulfur components. A mixing model involving relative contributions of isotopically heavy and light sulfur end-members is offered as an explanation for the observed isotopic trends. The isotopically light H_2S component is believed to be related to biogenic reduction of aqueous sulfate derived from anhydrite cap rock. The correlation between intensity of sulfide mineralization and sulfide $\delta^{34}S$ indicates a genetic relationship between the generation of heavy H_2S and the supply of metals by relatively hot, deep-sourced formation waters. A possible source of heavy H_2S is local thermochemical sulfate reduction of cap rock sulfate. Conversely, heavy H_2S could have been supplied along with metals in the formation waters. If these sulfides originated during anhydrite underplating, then metals from basinally derived fluids appear to have increased during the early stages of anhydrite cap rock formation. These events resulted in a greater contribution of heavy H_2S to the mixed sulfur reservoir, either through extrensic supply or by local thermochemical production. However, in younger cap rock, biogenic H_2S began to dominate the mixed sulfur reservoir resulting in a -15 ‰ shift and relatively lighter $\delta^{34}S$ values of pyrite to the present cap rock/salt contact.

It is proposed that fluid mixing and rock-water interactions produced the complex $\delta^{34}S$ isotopic and metal patterns within the anhydrite cap rock. The sulfide-depositing system at Hockley Dome resulted from interactions of cool acetate-type water with warmer metalliferous formation water that migrated up the salt dome flanks. Brines moved updip from the overpressured deep Gulf of Mexico basin via formational aquifers and major fault systems. The stratigraphic relationship of sulfide $\delta^{34}S$ values and metal concentrations suggests that basin-derived fluids were continuously leaked into the cap rock environment, but it appears that only prolonged episodes of fluid flow were maintained during the Eocene (Claiborne and Jackson time) and to a lesser extent the Oligocene (Vicksburg and Frio time). The metalliferous formation waters responsible for cap rock mineralization likely originate from deeply buried Mesozoic (carbonate) reservoirs.

TABLE OF CONTENTS

LIST OF TABLES

LIST OF FIGURES

Chapter 1

INTRODUCTION

Scientific and economic interests in salt domes have steadily increased as new mineral resources and uses have been recognized. Historically, the search for salt in shallow diapirs, limestone, gypsum, and sulfur in cap rocks, and structural traps of oil and gas was economically motivated. However, during the last few decades researchers have expanded their traditional interests (i.e., hydrocarbon accumulation) to include more diverse topics. The mechanisms responsible for Gulf Coast diapirism, cap rock formation and diagenesis, and fluid flow within the cap rock forming environment are presently being addressed (Seni and Jackson, 1984; Kyle and Agee, 1988; Posey and Kyle, 1988; Prikryl et al., 1988). Metallic minerals have long been known from cap rocks of many Gulf Coast salt domes (Hanna and Wolf, 1934), but these mineralized zones were regarded as little more than mineralogic curiosities (Smith, 1970). Recently, Zn-Pb-Ag sulfide concentrations within salt dome cap rocks have been evaluated in terms of their commercial potential, with principal interest centering on Hockley Dome (Price et al., 1983; Kyle and Price, 1985, 1986; Kyle and Agee, 1988; Agee, 1988; Fig. 1.1).

Gulf Coast salt dome cap rocks provide an interesting geologic framework for investigating metallic mineralization as an aspect of fluid-rock interactions in a young sedimentary basin. Cap rock metal concentrations have genetic affinities with classic ore deposits of the Mississippi Valley and sedimentary exhalative types (Kyle and Price, 1986). Modern analogs of the ore-forming fluids, for all three deposit types, appear to be metalliferous formation waters of the type that have been well documented in the Gulf Coast (Sharp et al., 1988; Carpenter et al., 1974; Land and Prezbindowski,

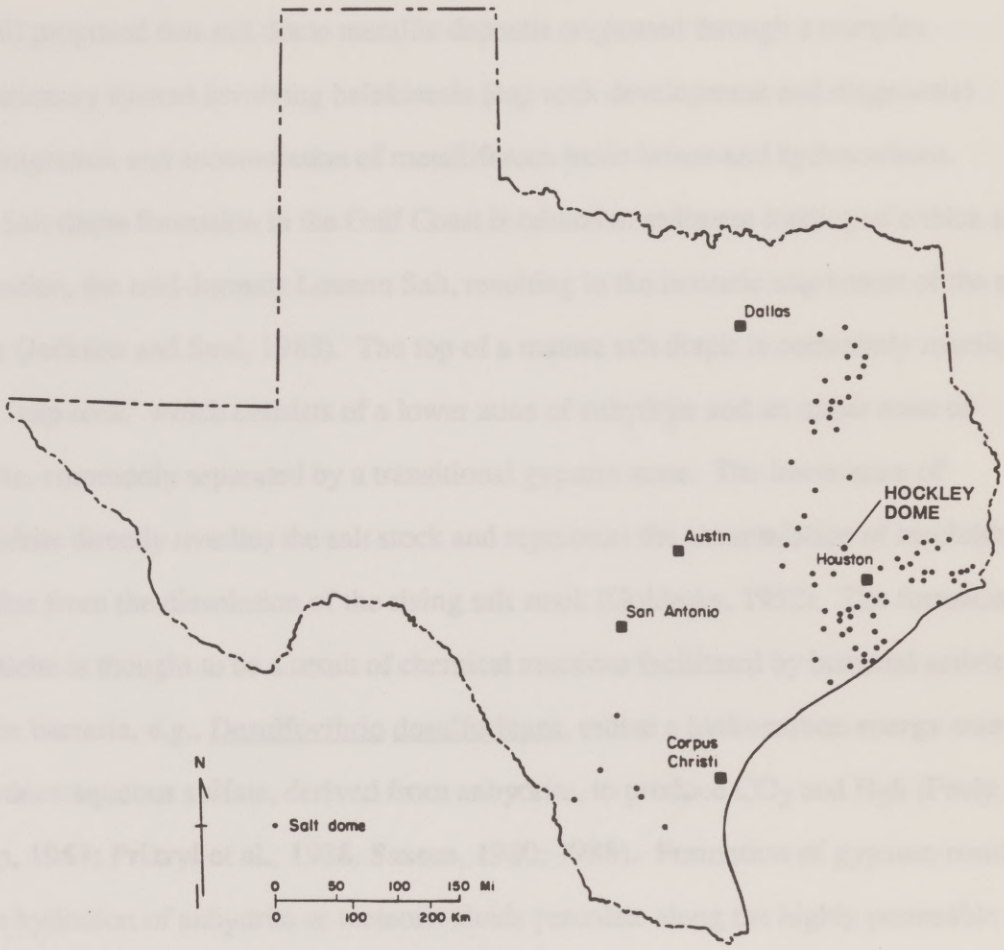

Fig. 1.1. Distribution of Texas salt domes, showing location map of Hockley Dome.

1981; Lydon, 1983; Sverjensky, 1984; Kharaka et al., 1980, 1987). These warm saline solutions migrate within aquifers to sites of ore deposition within the sedimentary basin (Land and Prezbindowski, 1981; Cathles and Smith, 1983). Kyle and Price (1986) proposed that salt dome metallic deposits originated through a complex evolutionary system involving halokinesis (cap rock development and diagenesis) and migration and accumulation of metalliferous basin brines and hydrocarbons.

Salt dome formation in the Gulf Coast is related to sediment loading of a thick salt formation, the mid-Jurassic Louann Salt, resulting in the isostatic movement of the salt mass (Jackson and Seni, 1983). The top of a mature salt diapir is commonly mantled by a "cap rock" which consists of a lower zone of anhydrite and an upper zone of calcite, commonly separated by a transitional gypsum zone. The lower zone of anhydrite directly overlies the salt stock and represents the accumulation of insoluble residue from the dissolution of the rising salt stock (Goldman, 1952). The formation of calcite is thought to be a result of chemical reactions facilitated by bacterial activity. These bacteria, e.g., Desulfovibrio desulfuricans, utilize a hydrocarbon energy source to reduce aqueous sulfate, derived from anhydrite, to produce CO_2 and H_2S (Feely and Kulp, 1957; Prikryl et al., 1988, Sassen, 1980, 1988). Formation of gypsum results from hydration of anhydrite as meteoric fluids percolate along the highly permeable anhydrite/calcite contact (Feely and Kulp, 1957).

Sulfide mineralization appears to be an integral aspect of cap rock formation (Kyle and Price, 1985). The textural relationship and genetic significance of euhedral anhydrite grains surrounded by sulfides was first documented by Ulrich et al. (1984) at the Winnfield Dome in northern Louisiana. Anhydrite grains that are completely surrounded by sulfides are euhedral and undeformed, similar to anhydrite disseminated throughout the salt mass. Anhydrite grains outside the mineralized zones are deformed

and tightly intergrown (Ulrich et al., 1984). These same textural relationships have also been identified at the Hockley Dome. Related sulfide concentrations have been observed at several other domes and represent mineralization during "underplating" of the anhydrite cap rock (Ulrich et al., 1984; Kyle et al., 1987). As mineralizing fluids entered the salt/anhydrite cap rock interface along the zone of salt dissolution, sulfide precipitation cemented some anhydrite grains prior to accretion and compaction. These sulfide-precipitating events are recorded as discrete zones of euhedral anhydrite grains surrounded or cemented by sulfides. Thus, the anhydrite cap rock and the stratiform sulfide zones formed in an orderly inverted sequence. Cap rock accretion results in the earliest formed sulfides at the top of the anhydrite rock column with sulfide layers becoming progressively younger toward the base. This systematic paragenesis provides the conceptual basis to evaluate the evolution of the sulfide mineralization system.

Hockley Dome was the site of mineral exploration programs that identified concentrations of marcasite, pyrite, sphalerite, galena, acanthite and barite within the calcite and anhydrite cap rock zones (Price et al. 1983; Kyle and Price, 1986). In the initial phase of the Hockley Dome project, beginning in 1977, ASARCO intersected low-grade Pb-Zn sulfides in three of five core holes drilled into the cap rock. Chevron acquired the mineral rights and drilled five additional core holes in 1978. Marathon Mineral Resources, Inc. became a joint venture partner with Chevron in 1980.

During the early 1980's Marathon Mineral Resources, Inc. was the principal operator and drilled an additional 55 core holes that penetrated the entire cap rock section (Appendix Ia and Ib). Preliminary ore reserve calculations (13 mt of 3.1 % Pb+Zn), based on drilling results to the end of 1982, were not encouraging enough

to justify further expenditures and in view of the prevailing low metal prices, the exploration program was discontinued. The extensive core library from Hockley metals exploration provided an excellent opportunity to study a sulfide-rich cap rock. These cores are presently stored at the Well Sample Library of the University of Texas Bureau of Economic Geology in Austin.

The intent of this thesis is to document the complex nature of sulfide and associated mineral concentrations at Hockley Dome and to relate mineralization to basin dewatering and timing of cap rock growth. Isotopic characteristics, i.e., $\delta^{34}S$ and common Pb, were used to evaluate possible sulfur and Pb sources. Hockley metal assay data was integrated with these isotopic studies, and evaluated with respect to documented Gulf Coast Mesozoic and Cenozoic metalliferous brines. These formation waters were evaluated as potential source fluids for cap rock mineralization. Therefore, attention was focused on the relationship of metal- and H_2S-bearing formation waters to sulfide mineralization. Ultimately, the ability to establish a temporal relationship between cap rock growth and stratiform sulfide mineralization may permit the timing of basin dewatering events to be defined.

Interpretations from electric-logs provided the stratigraphic data base for local structural cross-sections through the Hockley area. Cap rock stratigraphy was determined from synthesized core hole information and selected core hole logs. Polished thin sections of cap rock core were examined in transmitted, reflected, and ultraviolet light. Petrographic examination of sulfide concentrations in host rocks was used to determine paragenetic relationships among minerals. Base metal sulfides were evaluated by microprobe analysis, scanning electron microscopy, metal assay synthesis, and sulfur and Pb isotope measurements. Metal assay data, provided by the principal operator, were used to evaluate possible changes in fluid chemistry during

the history of basin dewatering. In contrast, microprobe studies were used to examine subtle compositional changes of trace metals within sulfides. These analyses identified trace Ag and Cd that occur in solid solution with sphalerite and galena. Such metals are considered anomalous in sedimentary terrains and may therefore represent a geochemical marker - a potential aid in identifying their origin. Isotope studies involved selected sulfides obtained from calcite, gypsum, and anhydrite cap rock zones, as well as from sediments overlying the cap rock. Samples from a pilot $\delta^{34}S$ and common Pb study (Kyle and Price, 1986) concentrated on textural and host rock types and were collected from core holes spaced around the dome. Subsequent work resulted in a vertical $\delta^{34}S$ (Kyle and Agee, 1988) and common Pb isotope profile from a single core hole (HH2). Examination of succeeding stratiform sulfide laminae proved to be a viable approach to evaluate the evolving mineralizing system.

Chapter 2

GEOLOGIC SETTING

Hockley Dome is located in western Harris Co. (Fig. 2.1), approximately 30 mi northwest of Houston, Texas (Fig. 1.1). The dome is emplaced within Cenozoic siliciclastic-dominated sediments of the Gulf Coastal Plain (Barnes, 1968) and resides in the Wilcox geothermal fairway (Morton et al., 1983; Fig. 2.2). There is no pronounced topographic expression of the salt stock even though the cap rock is covered by as little as 40 ft of Plio-Pleistocene sediments (Fig. 2.3). The average cap rock depth over the crest of the dome is approximately 100 ft, but steeply plunging margins are encountered at the -200-ft contour. Cap rock overlies the crest of the salt stock, at an average elevation of -850 ft, and drapes down the steeply dipping flanks of the salt. Hockley Dome is elongate in the northwest-southeast direction with dimensions of 14,000 ft by 10,000 ft at the -600-ft level. Hockley Dome occurs along the interior margin of a belt of oil-producing salt domes in the Houston diapir province (Deussen and Lane, 1926). A small oil field on the southwestern flank of Hockley Dome (Fig. 2.3) has yielded approximately 750,000 bbls of oil (Halbouty, 1979), a relatively minor amount for Gulf Coast salt domes.

Texas coastal salt domes are surrounded by thick sequences of Tertiary siliciclastic sediments (20,000 to 35,000 ft) and Cretaceous basinal deposits (approximately 10,000 ft) (Buffler and Sawyer, 1985). These thick sedimentary sequences overlie the Upper Jurassic siliciclastics and the Middle Jurassic Louann salt (Fig. 2.4). Hockley Dome resides within the northwestern part of the Houston Diapir Province (Fig. 2.2) and was mobilized by thick sedimentary basin infill. Movement of salt structures in combination with nearly continuous sedimentation has profoundly affected Gulf Coast

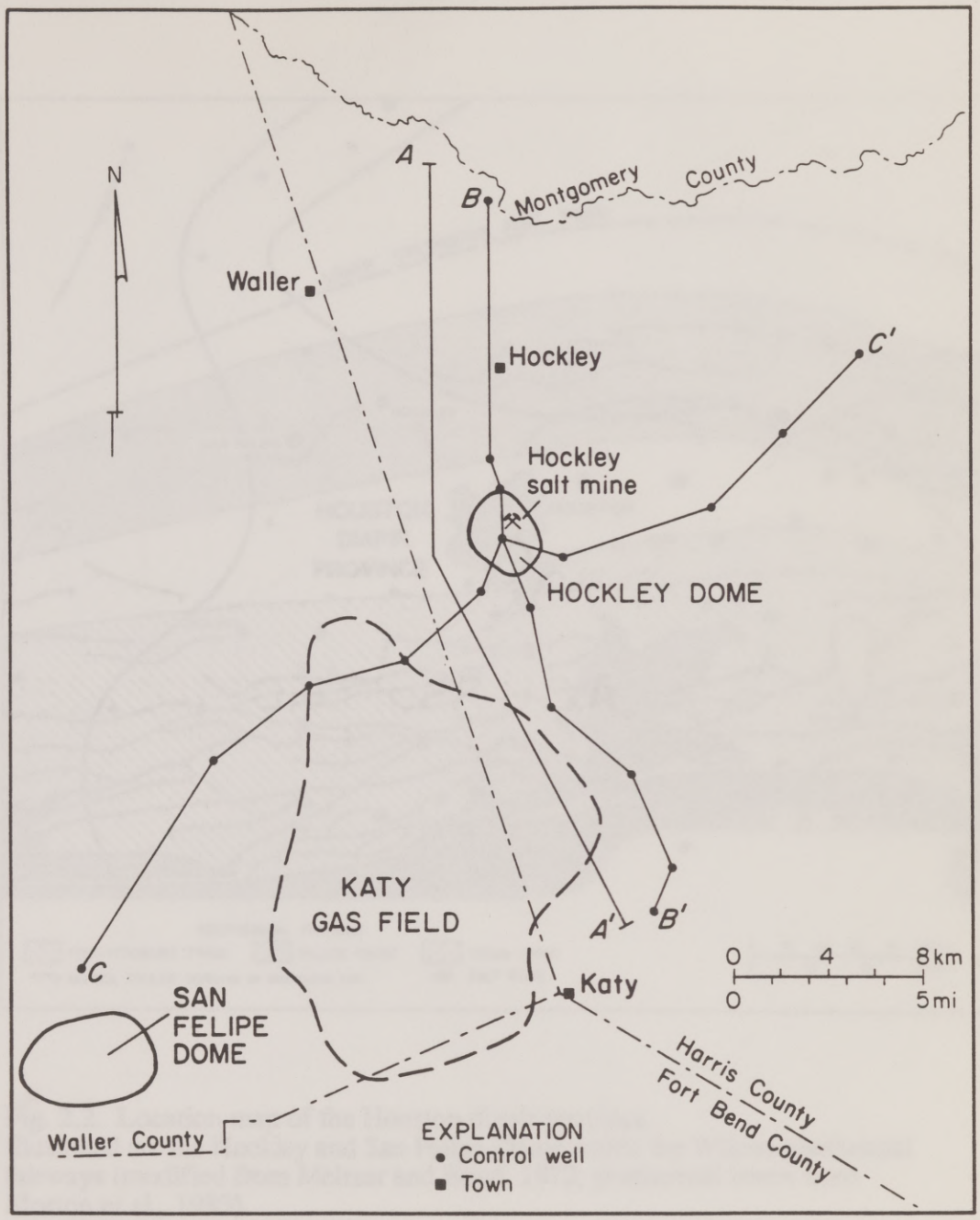

Fig. 2.1. Location map of Hockley study area showing geologic sections through the salt dome and associated withdrawal basin.
Also shown are neighboring San Felipe Dome and Katy Gas Field.

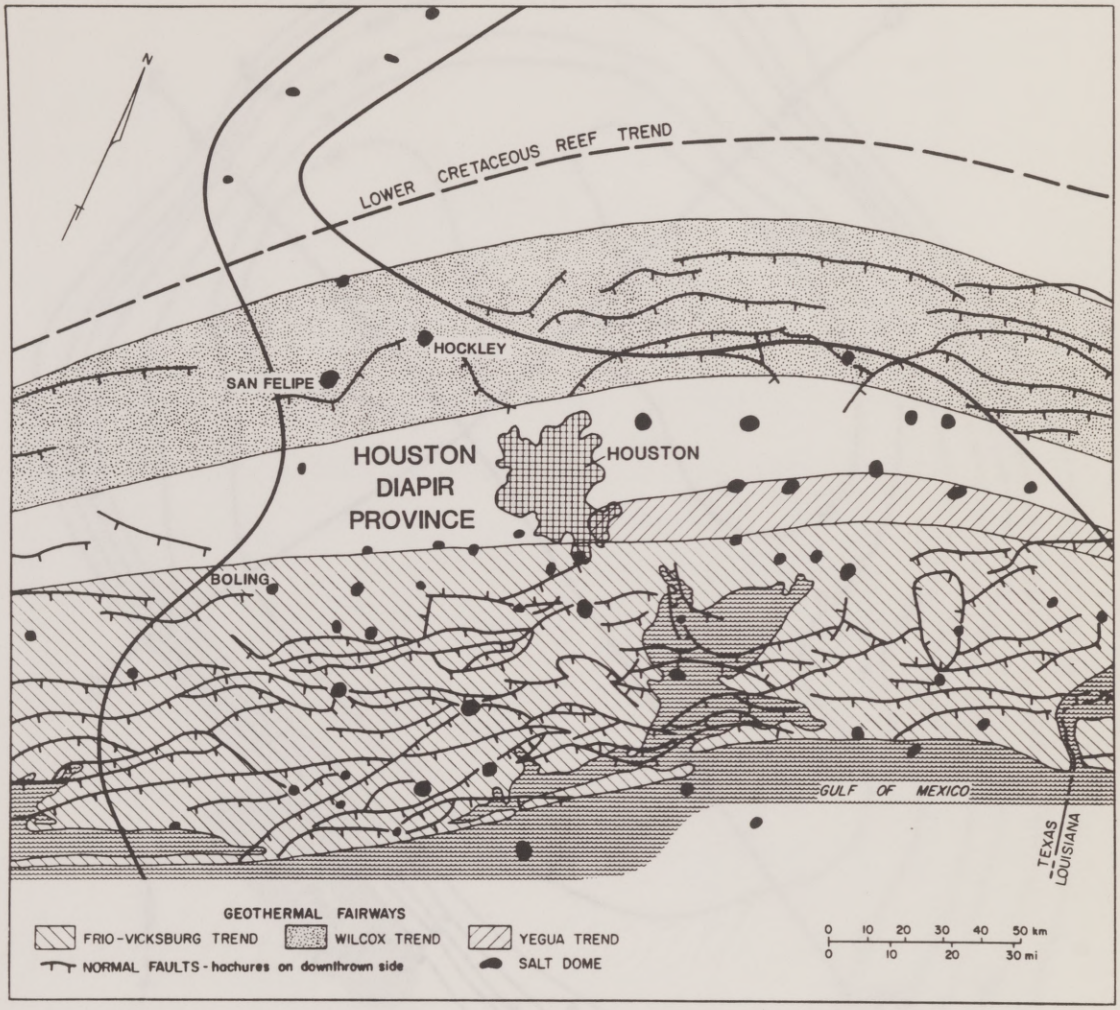

Fig. 2.2. Location map of the Houston diapir province.
Illustrated are the Hockley and San Felipe Dome within the Wilcox geothermal fairways (modified from Meltzer and Boyd, 1972; geothermal zones from Morton et al., 1983).

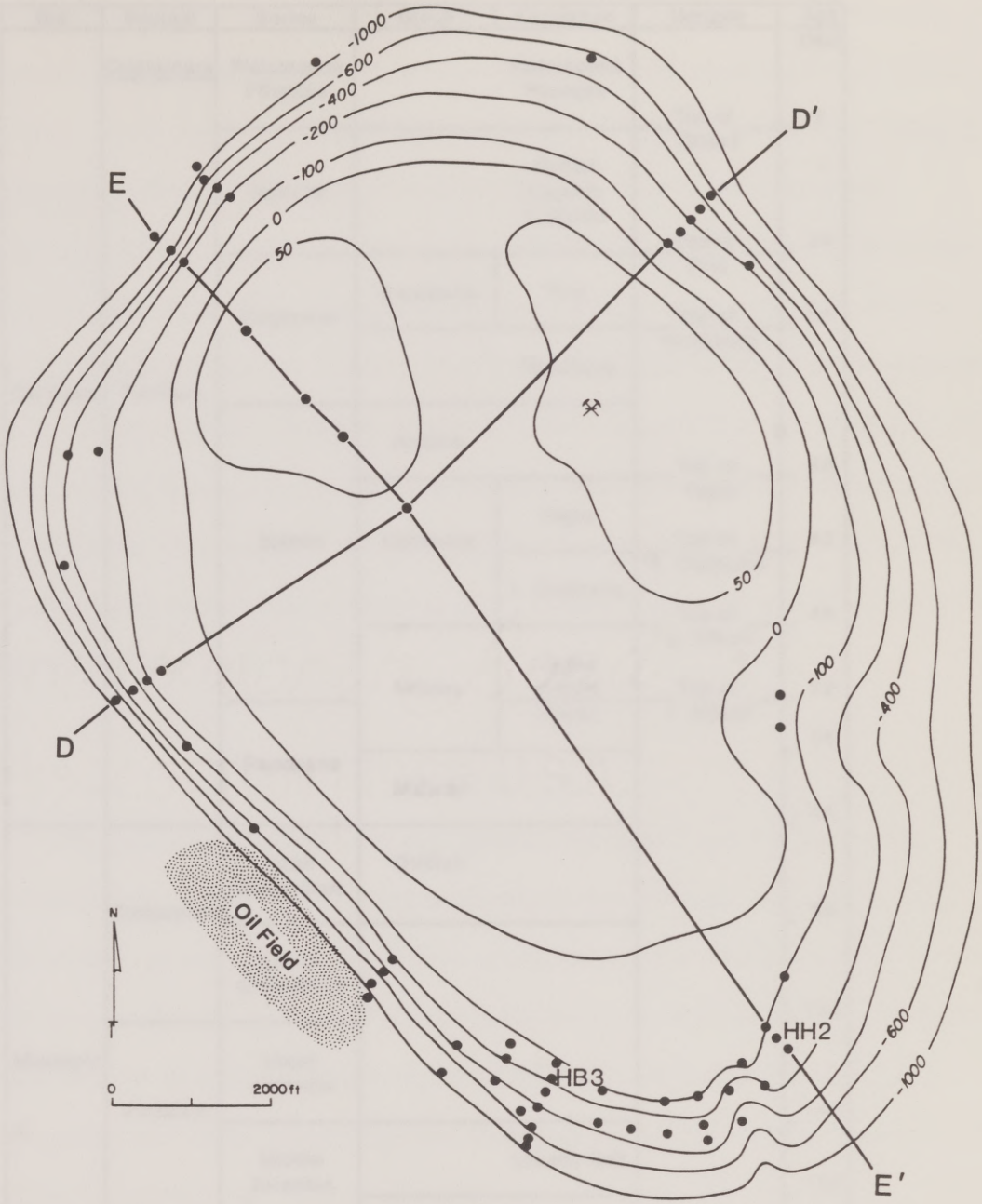

Fig. 2.3. Plan map of Hockley Dome showing elevation (relative to MSL) of top of cap rock in feet (modified from Price et al., 1983).
Locations of drill holes (filled circles) utilized in this study are illustrated (Appendix Ia and Ib). Also shown are type core holes HB3 and HH2, Oil field, United Salt Mine, and lines of section.

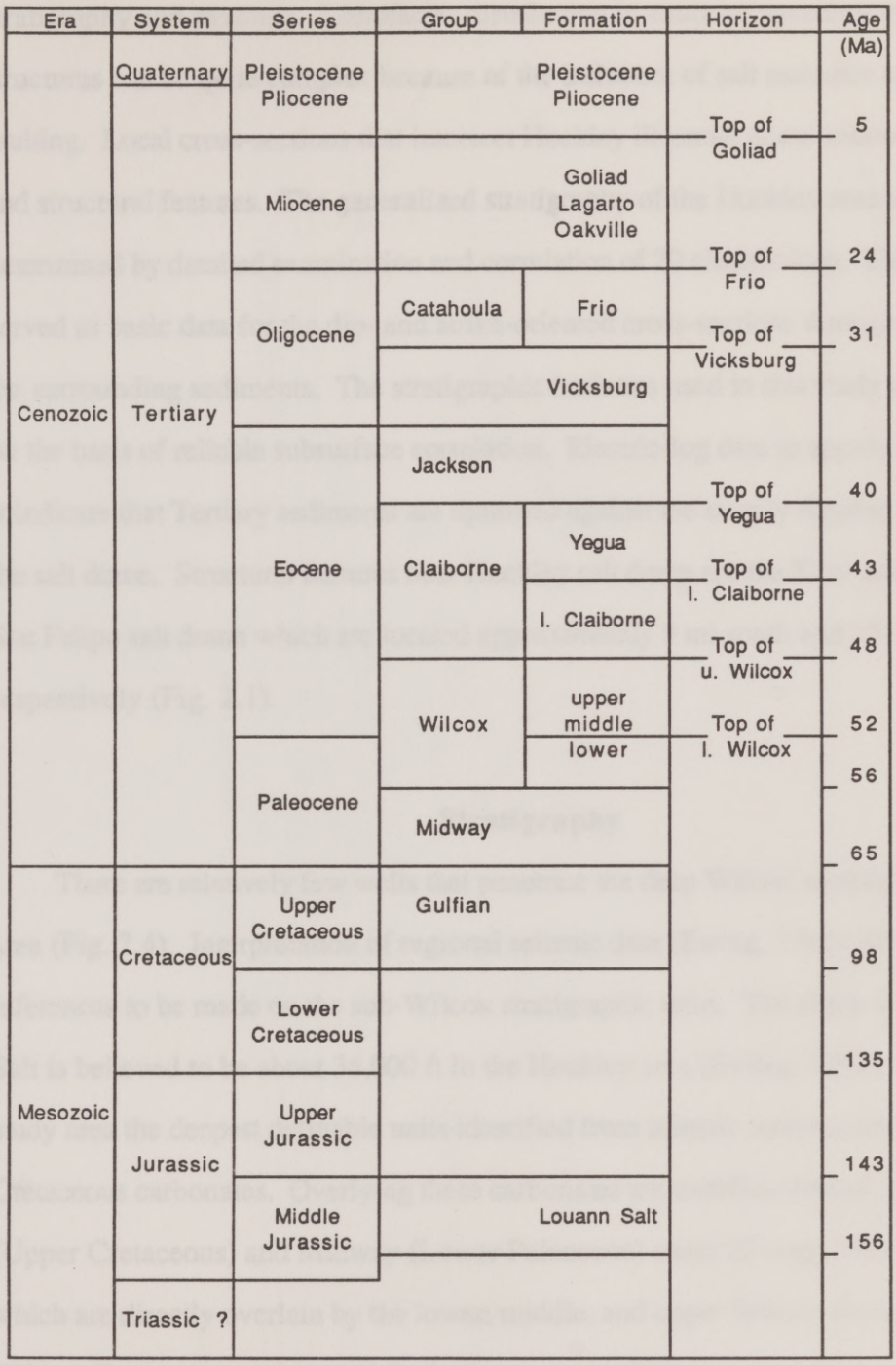

Fig. 2.4. Stratigraphic column of the Gulf Coast Basin.
Cross-section horizons were selected on the basis of reliable regional subsurface correlation. Chart and geochronology modified from Seni and Jackson (1984) and Jackson and Galloway (1984).

stratigraphy and structure. Lithofacies distribution in strata surrounding these salt structures can be quite complex because of the influence of salt tectonics and growth faulting. Local cross-sections that intersect Hockley illustrate dome-related stratigraphy and structural features. The generalized stratigraphy of the Hockley area was determined by detailed examination and correlation of 20 electric-logs. Electric-logs served as basic data for the dip- and strike-oriented cross-sections through Hockley and the surrounding sediments. The stratigraphic horizons used in this study were selected on the basis of reliable subsurface correlation. Electric-log data to approximately 7,000 ft indicate that Tertiary sediments are upturned against the steeply dipping margins of the salt dome. Structural features near Hockley salt dome are the Katy anticline and San Felipe salt dome which are located approximately 9 mi south and 15 mi southwest, respectively (Fig. 2.1).

Stratigraphy

There are relatively few wells that penetrate the deep Wilcox section in this area (Fig. 2.4). Interpretation of regional seismic data (Ewing, 1986) allows some inferences to be made on the sub-Wilcox stratigraphic units. The depth to the Louann Salt is believed to be about 36,000 ft in the Hockley area (Ewing, 1986). Within the study area the deepest definable units identified from seismic sections are Lower Cretaceous carbonates. Overlying these carbonates are undifferentiated marine Gulfian (Upper Cretaceous) and Midway (Lower Paleocene) strata (Ewing, 1986; Fig. 2.5), which are directly overlain by the lower, middle, and upper Wilcox Group. The lower Wilcox Group is a sandstone-rich clastic sequence (Fisher and McGowen, 1967) ranging in thickness from 3,600 ft to more than 6,000 ft within the Hockley area (Ewing, 1986). The upper Wilcox Group is also a sandstone-rich sequence, but is

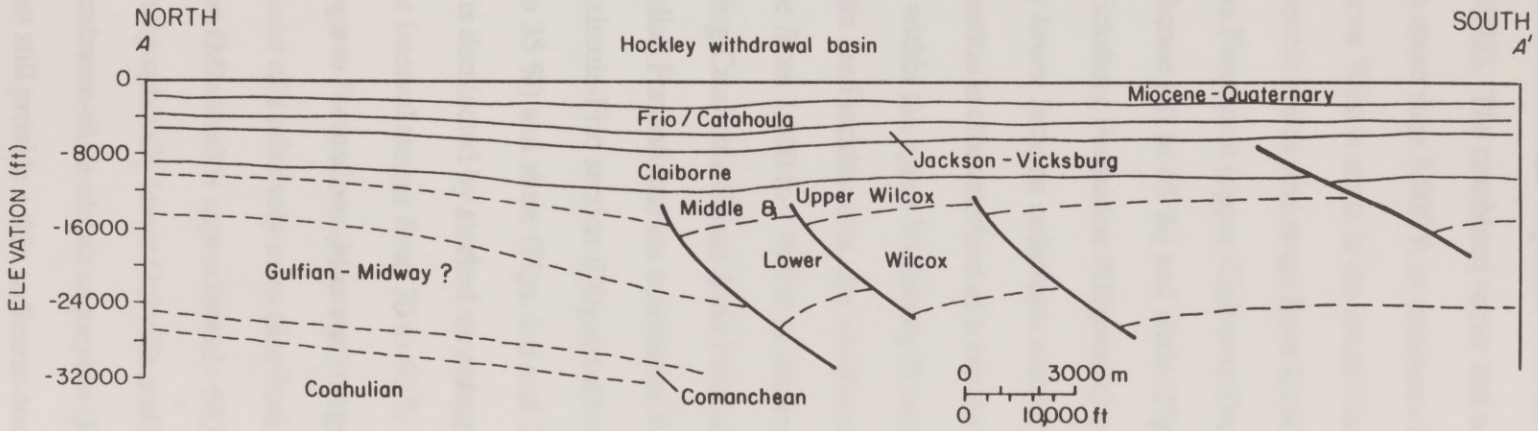

Fig. 2.5. Dip oriented structural cross-section (A-A') across Hockley withdrawal basin, Harris County, Texas.
Line of section shown in Figure 2.1. Note the thinning of Gulfian and Midway strata beneath the Hockley withdrawal basin. Modified from parallel line of section, San Felipe withdrawal basin (Ewing, 1986).

separated by a sandstone-shale sequence from the middle Wilcox Group (Bebout et al., 1982). The combined upper and middle Wilcox Group ranges from 1,700 ft to more than 3,000 ft in thickness (Ewing, 1986; Fig. 2.5).

Directly above Wilcox strata is the lower Claiborne Group which consists exclusively of neritic shales that range from 2,200 to 2,800 ft thick within the Hockley area. The Yegua Formation (upper Claiborne Group) is characterized as 1,700 to 1,900 ft of sandstone (45 to 65 %) and shale (Figs. 2.6 and 2.7). The Jackson Group (Eocene) and Vicksburg Formation (Oligocene) overlies the Claiborne Group. The stratigraphically lower Jackson sediments consist mostly of marine shales, whereas the Vicksburg Formation is characterized as a sandstone-shale sequence. Generally, these sandstone units within the upper Vicksburg Formation are better developed toward the dome. Within the Hockley area, the combined Jackson Group and Vicksburg Formation range from 1,300 to 1,900 ft in thickness (Figs. 2.6 and 2.7).

The overlying Catahoula Group (Frio Formation) and younger strata (Oakville, Lagarto, and Goliad Formations) are nonmarine fluvial streamplain sediments (Hamlin, 1986). The Catahoula-Frio section (Oligocene) consists of 1,700 to 2,800 ft of sandstone (20 to 35 %) and shale (Figs. 2.6 and 2.7). However, the lower half of the Frio Formation is dominated by stacked sandstone channels that thicken toward the dome; this lower interval ranges from 30 to 60 % sandstone. Local thicknesses in Oakville and Lagarto Formations (Miocene) range from 2,000 to 2,400 ft (Figs. 2.6 and 2.7) and consist of a relatively even distribution of sandstone and shale. The Goliad Formation (Miocene) is approximately 600 ft thick and is sedimentologically similar to the stratigraphically lower Oakville and Lagarto Formations. Plio-Pleistocene strata are also sandstone-shale clastic sequences (Barnes, 1968) that are partially penetrated by, but still provide a thin sediment cover over, Hockley Dome.

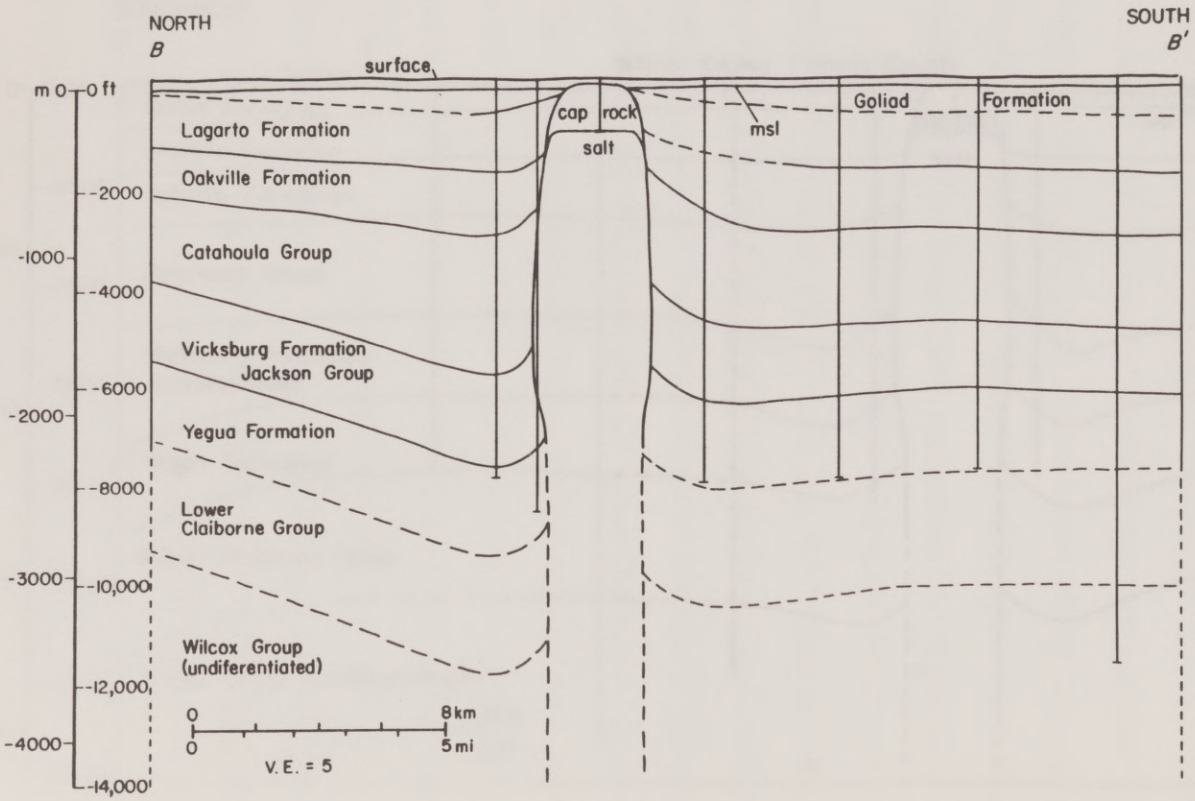

Fig. 2.6. Dip oriented structural cross-section (B-B') across Hockley Dome. Geopressure occurs at top of Wilcox. Line of section shown in Figure 2.1.

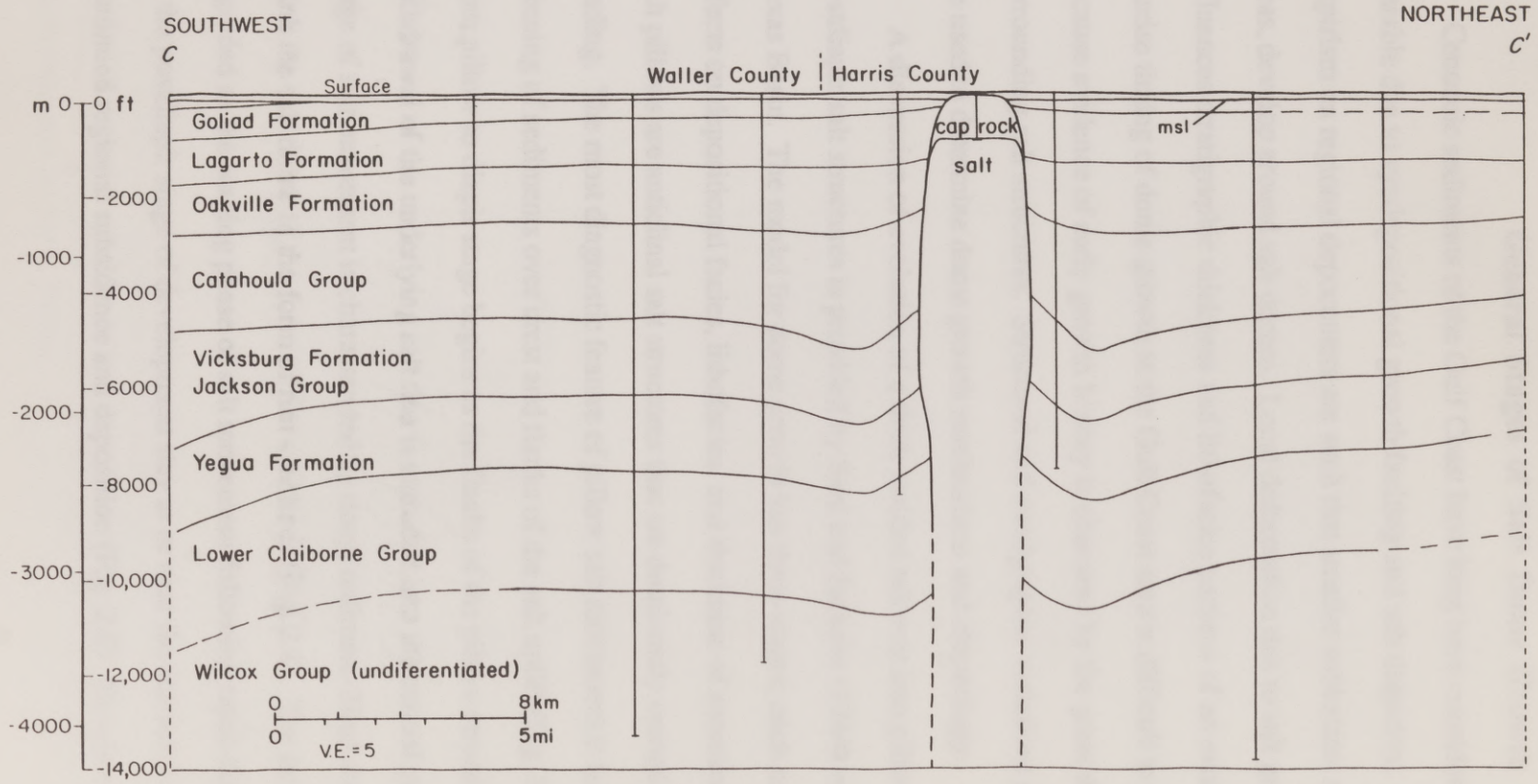

Fig. 2.7. Strike oriented structural cross-section (C-C') across Hockley Dome. Geopressure occurs at top of Wilcox. Line of section shown in Figure 2.1.

General Stages of Salt Dome Growth

Cenozoic sediments of the Gulf Coast have long been considered structurally unstable due to syndepositional growth faulting and salt diapirism. The effects of diapirism on regional depocenters are such that smaller subbasins, separated by uplifted areas, develop around salt domes. Local deformation due to salt growth consistently influences stratigraphic thickness and lithofacies patterns of an evolving subbasin. Precise timing of dome growth in the Gulf Coast area is difficult to determine because evidence of early growth history is obscured by the great thickness of strata surrounding salt structures. Structural and stratigraphic variations around the dome are used to determine dome growth mechanisms and chronology.

A discussion of evolution of a thick bedded salt unit into pillow, diapir, and postdiapir salt structures is provided by Seni and Jackson (1984) who studied the East Texas Basin. The model for dome growth has three-stages; each stage has distinctive effects on depositional facies, lithofacies, and thickness of surrounding sediments. Salt pillows are anticlinal salt structures that are dominantly caused by uneven sediment loading. The most diagnostic feature of pillow salt movement is syndepositional thinning of sediments over crest and flanks of the salt uplift (Fig. 2.8). A transition from pillow to diapir stage begins as the flanks of the pillow structures deflate due to withdrawal of the underlying salt that is extruded into the central growing diapir. This stage of salt movement is characterized by deep, sediment-filled sinks that surround or flank the salt dome in the form of rim synclines (Fig. 2.8). The postdiapir stage can be regarded as the waning phase of salt movement following rapid diapir growth. Domes in the postdiapir stage of development stay at or near the sediment surface regardless of continued regional subsidence and deposition (Fig. 2.8). However, some changes in

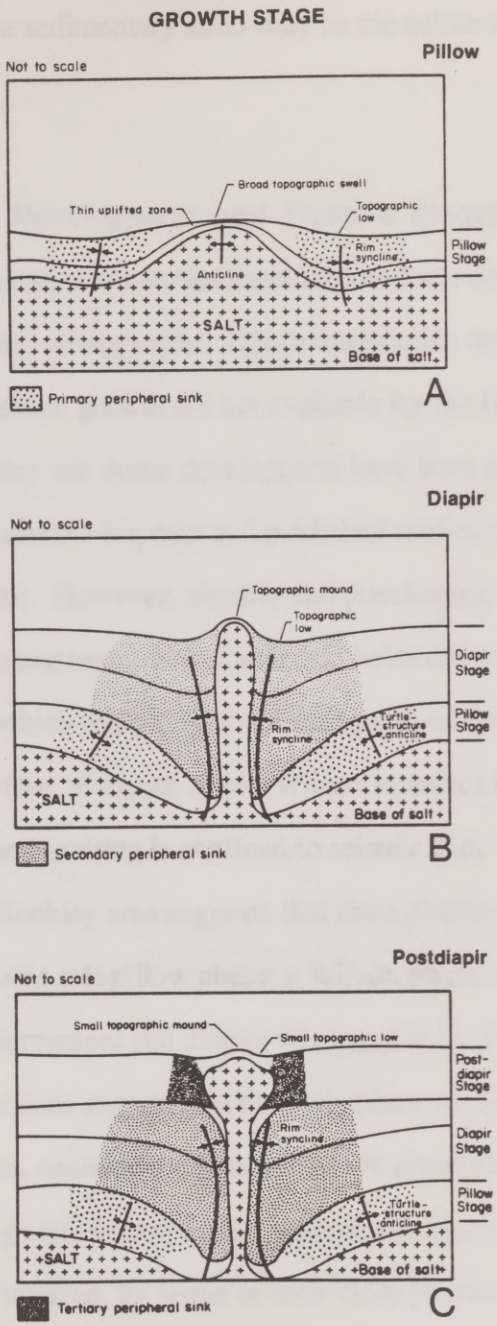

Fig. 2.8. Schematic evolution of salt dome growth.
Typical thickness variations in strata above and around the salt structures are shown for (A) pillow stage, (B) diapir stage, and (C) postdiapir stage (from Seni and Jackson, 1984).

thickness from these sedimentary sinks may be too subtle to be recognized (Seni and Jackson, 1984).

Structural Development and Growth Stages of Hockley Dome

Processes affecting sediment accumulation and salt dome evolution are complex, dynamic, and variable through time. Deep stratigraphic data necessary to interpret the multiple phases of dome growth are not available for the Houston diapir province. The stages of Hockley salt dome development have been examined using cross-sections derived from local electric-log data and published studies of the Katy area (Ewing, 1986; Hamlin, 1986). However, diapiric and postdiapiric stages of dome growth only could be evaluated because available drill holes did not penetrate the sub-Wilcox stratigraphic units which would allow the evaluation of the early pillow stage of halokinesis. Therefore, evidence of pre-Wilcox tectonics involving pillow stage salt structures and growth faulting is confined to seismic data. A seismic and electric-log study of the Katy/Hockley area suggests that three phases of structural development are indicated: a Mesozoic salt-pillow phase; a Wilcox phase of growth faulting; and a post-Wilcox phase of piercement salt diapirs (Ewing, 1986). However, examination of published cross-sections suggest that the main phase of salt diapirism was initiated in the lower Wilcox, contrary to the post-Wilcox phase proposed by Ewing (1986) (Fig. 2.5). Although this interpretation is based on seismic data related to the San Felipe Dome, it is inferred, by virtue of their close proximity, that Hockley experienced a similar depositional event initiating salt dome growth (Halbouty, 1979; Fig. 2.9). Diapiric histories of the two associated domes diverged quickly after Frio time, at which time San Felipe diapirism apparently ceased; i.e., it is deeply buried by Frio and younger sediments. This feature suggests that San Felipe Dome growth stalled because

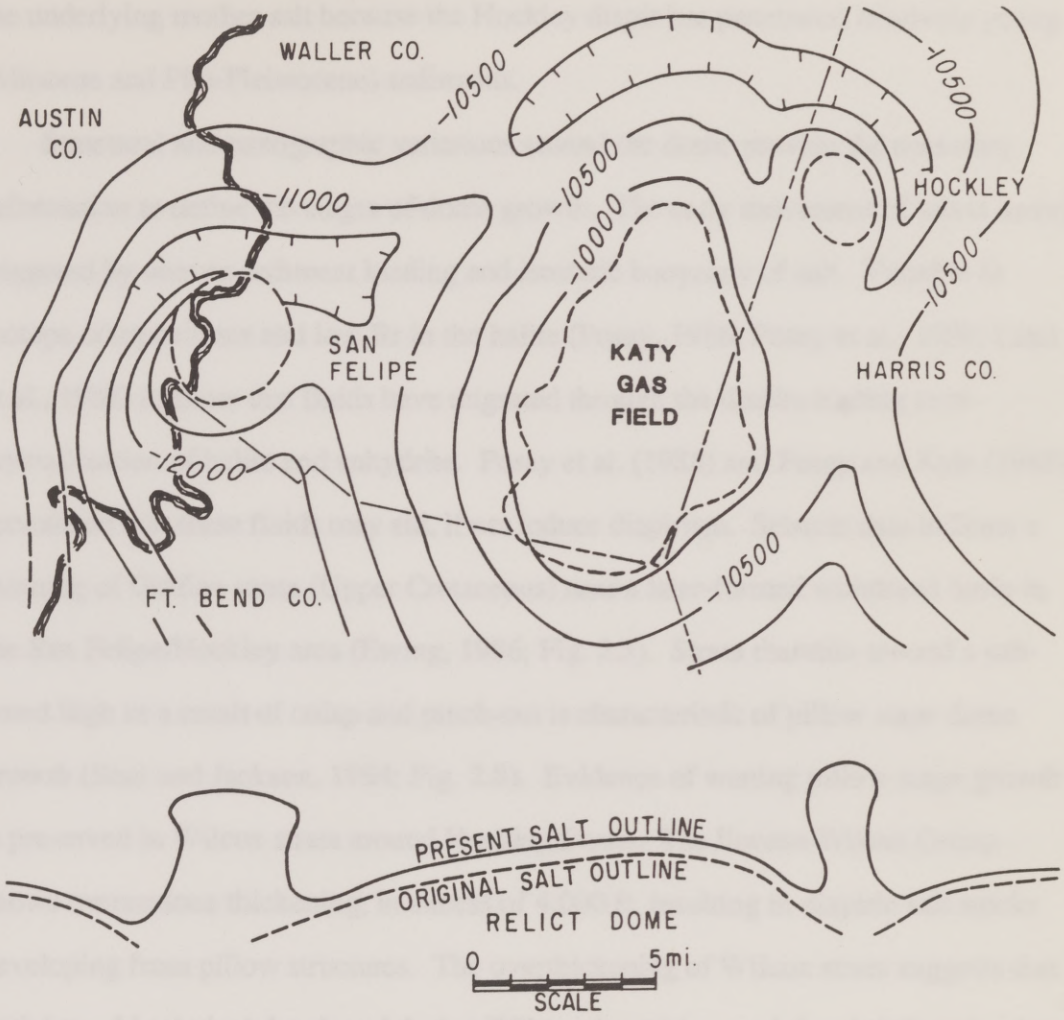

Fig. 2.9. Structure map on top of Wilcox and idealized section of the San Felipe-Katy-Hockley area (modified from Halbouty, 1979).

of an exhausted salt supply. Presumably, Hockley has maintained communication with the underlying mother salt because the Hockley diapir has penetrated relatively young (Miocene and Plio-Pleistocene) sediments.

Structural and stratigraphic variations around the dome provide the necessary information to define the stages of dome growth. The early movement of salt is mainly triggered by uneven sediment loading and isostatic buoyancy of salt. Variable Sr isotope compositions and low Br in the halite (Posey, 1986; Posey et al., 1988; Land et al., 1988) indicate that fluids have migrated through the diapirs leading to re-crystallization of halite and anhydrite. Posey et al. (1988) and Posey and Kyle (1988) speculated that these fluids may aid, if not induce diapirism. Seismic data indicate a thinning of Gulfian strata (Upper Cretaceous) near a later-formed withdrawl basin in the San Felipe/Hockley area (Ewing, 1986; Fig. 2.5). Strata that thin toward a salt-cored high as a result of onlap and pinch-out is characteristic of pillow stage dome growth (Seni and Jackson, 1984; Fig. 2.8). Evidence of waning pillow stage growth is preserved in Wilcox strata around Hockley Dome. The Eocene Wilcox Group shows tremendous thickening, in excess of 4,000 ft, resulting in diapiric salt stocks developing from pillow structures. The overthickening of Wilcox strata suggests that a withdrawal basin had developed during Wilcox deposition, and thus is inferred to have initiated diapirism in this area (Figs. 2.5 and 2.8). During this time withdrawal basin sediments substantially increased by roughly 40 % (Fig. 2.5). An extremely rapid growth rate is indicated by sediment overthickening during Wilcox deposition (duration 8 m.y.). For example, post-Wilcox strata are roughly the same thickness although they represent a vastly longer period of sedimentation (48 m.y.).

Wilcox phase growth faults trend southwest-northeast across San Felipe and Hockley salt dome areas (Ewing, 1986). Seismic information indicates that sediment expansion across these faults is considerable (i.e., up to 4,000 ft). The fault system appears to flatten with depth suggesting that a dècollement plane may extend above or into Lower Cretaceous carbonates (Fig. 2.5). Expansion across these large displacement growth faults was in response to deltaic systems burying salt pillows in a mass of unstable sediments (Ewing, 1986). During lower Wilcox deposition salt tectonism was extremely active; therefore, salt stocks at San Felipe and Hockley Domes were present during the main period of growth faulting. The stabilization of these growth faults did not occur until middle to upper Wilcox time. Downdip of the Hockley growth fault system, geopressured sandstone reservoirs are found within Wilcox Group sediments (Ewing, 1986).

After Wilcox time, detailed stratigraphic sections indicate that salt tectonism continued to be the dominant feature of the area (Figs. 2.6 and 2.7). During initial stages of diapirism Hockley salt stock pierced and deformed Wilcox strata and major fault planes (Ewing, 1986; Hamlin, 1986). Post-Wilcox sediments accumulated in deep, sediment-filled sinks that developed around the dome in the form of cresent-shaped rim synclines. Hockley Dome is surrounded by a prominent, post-Wilcox salt-withdrawal basin containing approximately 27 mi^3 of overthickened strata (Figs. 2.6 and 2.7). The accumulation of extra-thick sediments (in a salt-withdrawal basin) is in direct response to and theoretically equal to the volume of salt that migrated into the diapir. Given this one-to-one relationship, salt withdrawal was greatest from the updip side of Hockley. For example, Claiborne, Vicksburg, Jackson, and Catahoula strata thickened by approximately 23 % on the updip side of the subbasin as opposed to a 13 % gain on the downdip side (Fig. 2.6).

Activity during Claiborne time (including Yegua) was confined to continued uplift of the salt stock and sinking of the withdrawal basin. During this event sediment expansion, within the subbasin, is approximately 24 % and represents the transition from rapid to more moderate diapir growth rates. The rate of salt-withdrawal and associated subbasin subsidence appears to have been sustained or slightly decreased (roughly 16 % overthickening) during Vicksburg and Jackson time. However, withdrawal basin thickening increased by 64 % during Catahoula-Frio time (Fig. 2.6). Growth of the Hockley Dome during this time must have been exceptionally vigorous and rapid. Although diapiric dome growth decreased markedly during the Miocene and Plio-Pleistocene, it continued to pierce and deform these sediments. In summary, Hockley salt dome has experienced sporadic growth over a long history of halokinesis.

Cap Rock Forming Environment

Murray (1966) proposed a general cap rock forming model consisting of the following sequence of events (Fig. 2.10): (1) intrusion of a salt plug into a zone of active water circulation; (2) dissolution of the top of salt mass and accumulation of insoluble components; (3) compaction and intergrowth of the residual anhydrite to form cap rock; (4) repetition of steps 2 and 3 to develop the banding commonly observed in anhydrite cap rock; (5) bacterial alteration of aqueous sulfate (dissolved anhydrite/gypsum) to calcite; (6) influx of solutions that hydrate anhydrite to gypsum; and (7) influx of oxidizing solutions that oxidize H_2S to native sulfur and form secondary calcite. Relationships observed at numerous Gulf Coast domes support this generalized sequence (Kreitler and Dutton, 1983; Posey and Kyle, 1988).

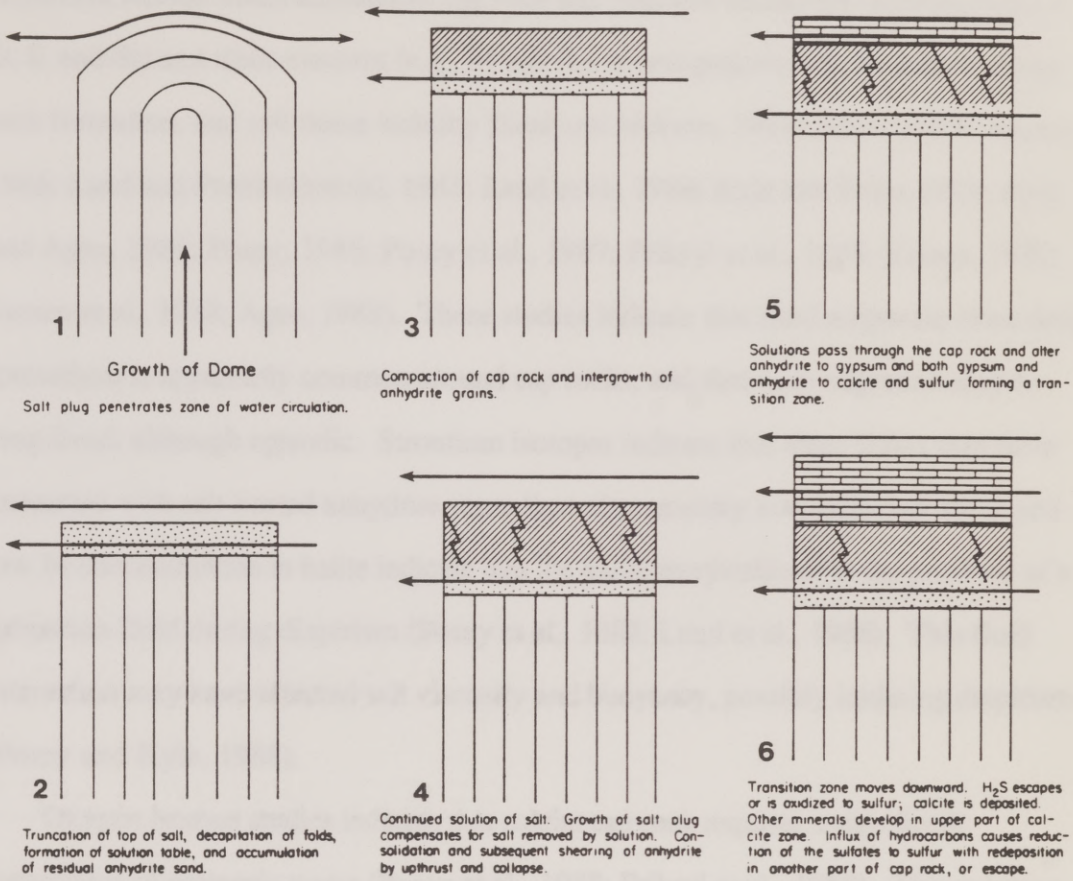

Fig. 2.10. Schematic illustration of stages of cap rock formation. Horizontal arrows show water flow (from Kreitler and Dutton, 1983; modified from Murray, 1966).

Renewed interest in the geochemistry of salt domes has caused reevaluation of traditional models explaining salt dome and cap rock formation. Much of the current research focuses on basin brine evolution, fluid evolution and transport related to salt diapirism, sulfide mineralization in cap rock and adjacent sediments, isotopic (e.g., C, O, S, and Sr) and trace-element (e.g., Sr and Br) investigations into the nature of cap rock formation, and salt dome stability (Seni and Jackson, 1984; Hanor and Workman, 1986; Land and Prezbindowski, 1981; Land et al., 1988; Kyle and Price, 1986; Kyle and Agee, 1988; Posey, 1986; Posey et al., 1987; Prikryl et al., 1988; Sassen, 1980; Sassen et al., 1988; Agee, 1988). These studies indicate that fluid migration from deep formations is apparently common around cap rocks, and that such migration may be long-lived, although episodic. Strontium isotopes indicate that these fluids may have interacted with salt-hosted anhydrite some time after primary evaporite deposition and low Br concentrations in halite indicate that the halite recrystallized in the presence of a formation fluid during diapirism (Posey et al., 1988; Land et al., 1988). This fluid interaction may have affected salt viscosity and buoyancy, possibly initiating diapirism (Posey and Kyle, 1988).

Oxygen isotope studies indicate that calcite cap rock requires a significant component of meteoric water (Posey et al., 1988; Prikryl et al., 1988). This assumes that calcite is a product of bacterial sulfate reduction and that such activity proceeds at low temperatures (< 70°C). Calcite cap rocks that have $\delta^{13}C$ ratios heavier than approximately < 30 ‰ (PDB) require liquid hydrocarbons to provide the carbon source; those with lighter values (i.e., -30 ‰) require a CH_4 source (Posey, 1986; Prikryl et al., 1988; Posey and Kyle, 1988). Sulfur isotopes of sulfates and sulfides in cap rocks suggest that marine sulfate of Jurassic age was the principal source of sulfur for all sulfur-bearing species (with the exception of barite) in cap rock. Metal sulfides

with $\delta^{34}S$ values lighter than -20 ‰ (CDT) require a biogenic H_2S source. However, those with heavier values, some of which reach +4 ‰, require thermochemically derived H_2S (Kyle and Agee, 1988). Results from these studies require previous theories for the formation of salt domes and cap rocks be modified to accommodate additional information.

Chapter 3

GEOLOGY OF HOCKLEY DOME

Extensive core drilling at Hockley Dome permits the study of cap rock features and associated sulfide concentrations. Hockley cap rock consists of a layered sequence of calcite, gypsum, and anhydrite as much as 925 ft thick (Fig. 3.1). The calcite portion is an irregular and discontinuous zone ranging in thickness from less than 10 to slightly over 300 ft. This zone is commonly fractured and brecciated with the open spaces containing calcite, barite, elemental sulfur and late-stage base metal sulfides. The anhydrite section may be as thick as 825 ft over the center of the dome and is typically characterized by sutured anhydrite crystals and thin (1 to 5 mm) sulfide laminae. An anhydrite zone is also present along the flanks of the dome extending to depths greater than 1,400 ft. A limited number of drill holes intersect a lower calcite zone that occurs within the anhydrite zone. This calcite zone is texturally similar to the upper calcite zone, but contains major base metal sulfide concentrations.

Salt Dome Lithology

Salt-Stock Lithology

The top of Hockley halite is overlain by anhydrite cap rock and is defined by coring a few feet below the salt/anhydrite interface. The salt/cap rock contact is semi-horizontal over the middle of the dome and is approximately 850 ft below sea level; the steeply plunging salt stock margins occur at about -900 ft (Fig. 3.2). Salt stock samples used in this study were collected from a salt mine located roughly 2,300 ft north and 1,500 ft east from the center of the dome (Fig. 2.3; Appendix Ia). United Salt Corporation actively mines rock salt from a 1,500 by 1,250 ft underground

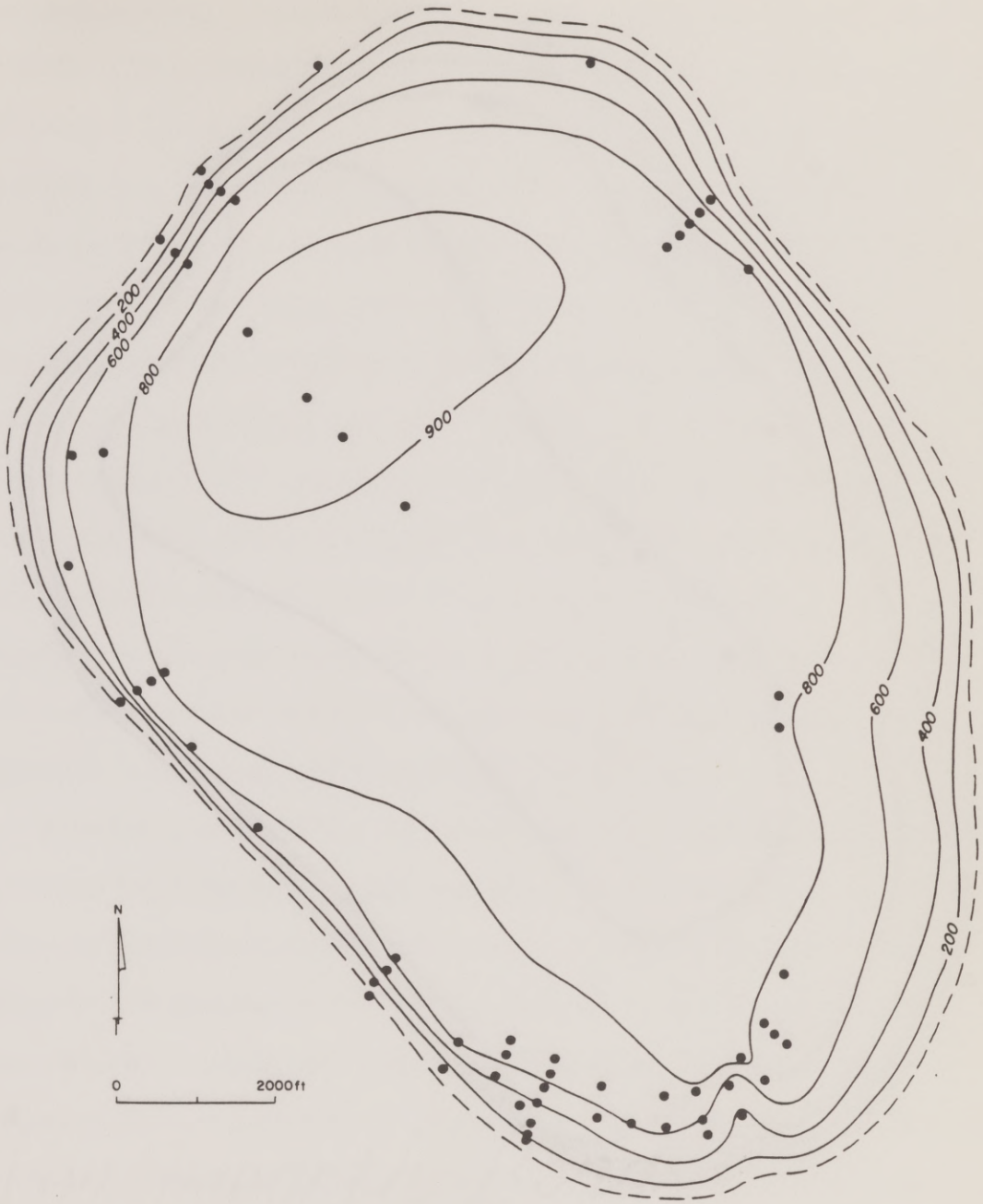

Fig. 3.1. Plan map of Hockley Dome showing isopach thickness of cap rock in feet. Dashed outermost line represents the inferred extent of cap rock.

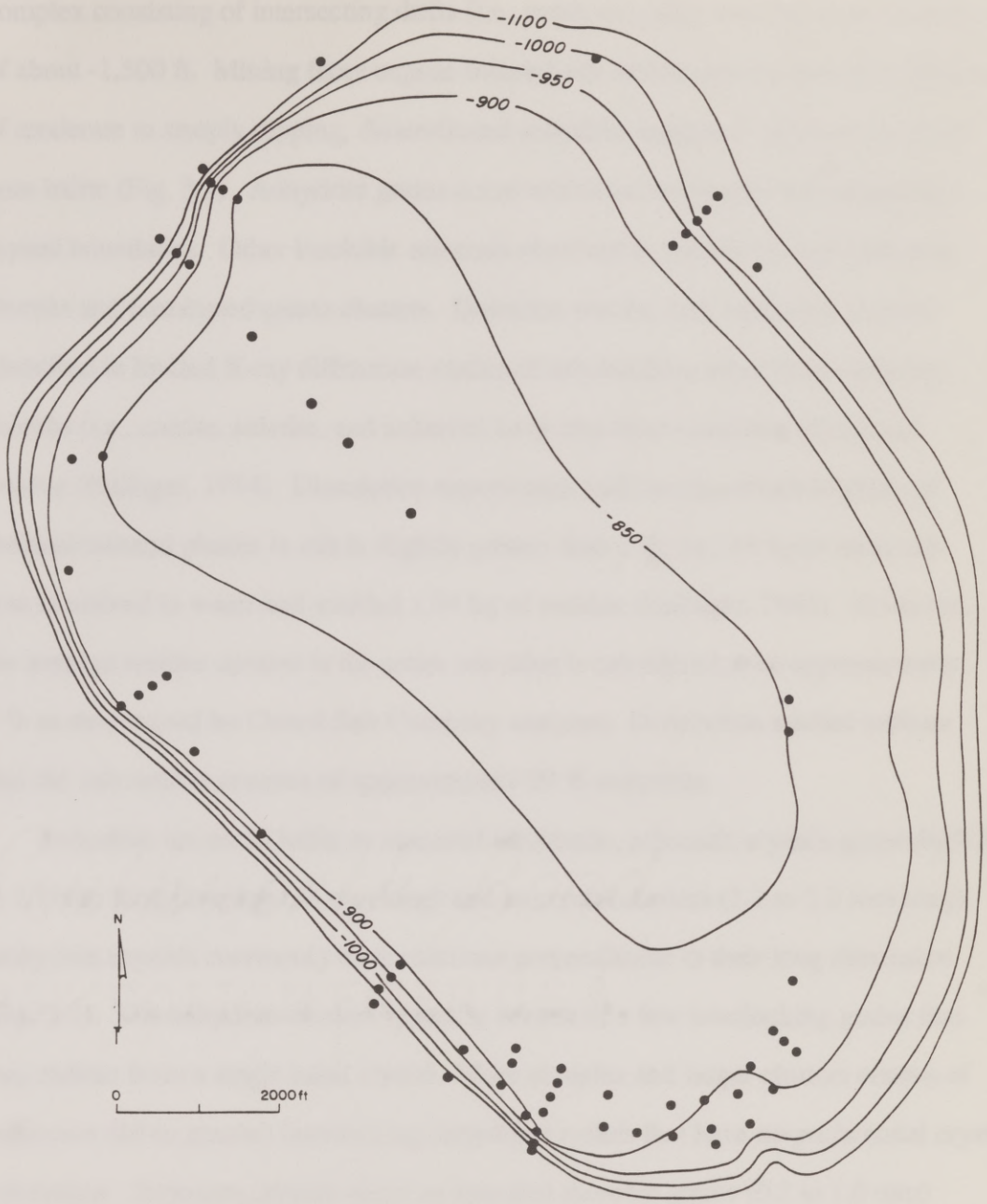

Fig. 3.2. Plan map of Hockley Dome showing elevation (relative to MSL) of top of salt in feet.

complex consisting of intersecting drifts (i.e., room and pillar mining) at an elevation of about -1,500 ft. Mining faces expose foliated salt which contains numerous layers of moderate to steeply dipping, disseminated anhydrite separated by zones of nearly pure halite (Fig. 3.3). Anhydrite grains occur within halite crystals and along halite crystal boundaries. Other insoluble minerals observed in the salt are rare carbonate rhombs and terminated quartz clusters. Dolomite was the only carbonate mineral identified in limited X-ray diffraction studies of salt residues; other trace carbonate rhombs (i.e., calcite, siderite, and ankerite) have also been identified from a salt residue (Hallager, 1984). Dissolution experiments indicate that concentrations of residual mineral phases in salt is slightly greater than 2 %; i.e., 45 kg of mine salt was dissolved in water and yielded 1.04 kg of residue (Hallager, 1984). However, the average residue content in the entire salt mine is considered to be approximately 5 % as determined by United Salt Company analyses. Dissolution studies indicate that the salt residue consists of approximately 99 % anhydrite.

Anhydrite occurs in halite as scattered idioblastic, prismatic crystals generally 0.3 to 1.3 mm long (average 0.8 mm long) and as crystal clusters (1.2 to 2.0 mm long). Anhydrite crystals commonly have striations perpendicular to their long dimension (Fig. 3.4). The anhydrite clusters typically consist of a few interlocking grains that may radiate from a single basal crystal. More complex and larger clusters consist of numerous (20 or greater) interlocking anhydrite crystals that have no preferential crystal orientation. Dolomite crystals occur as euhedral rhombic grains (0.2 to 1.0 mm) occasionally intergrown with anhydrite crystals and clusters (Fig. 3.5). Rare quantities of quartz also occur within the salt stock and are characterized as radiating clusters (0.5 to 0.7 mm) of terminated prisms (Fig. 3.6) intergrown with anhydrite crystals.

Fig. 3.3. Underground photograph of production face in the United Salt mine. Mining faces expose anhydrite foliations within salt stock. Mine location shown in Figure 2.3.

Fig. 3.4. SEM photomicrograph of a prismatic anhydrite crystal from Hockley salt stock.
Note the geometric, step-like ridges along crystal faces. SEM photo width is 0.7 mm.

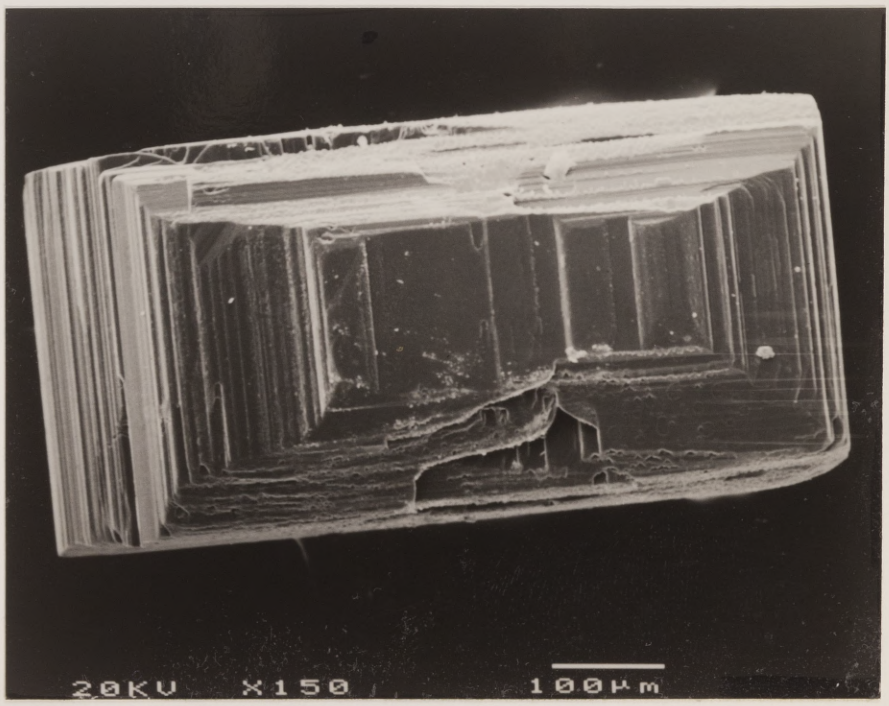
20KV X150
100µm

Fig. 3.5. SEM photomicrograph of a euhedral dolomite rhomb (do) intergrown with anhydrite (an) from Hockley salt stock.
SEM photo width is 0.7 mm.

Fig. 3.6. SEM photomicrograph of a radiating quartz cluster from Hockley salt stock.
SEM photo width is 0.7 mm.

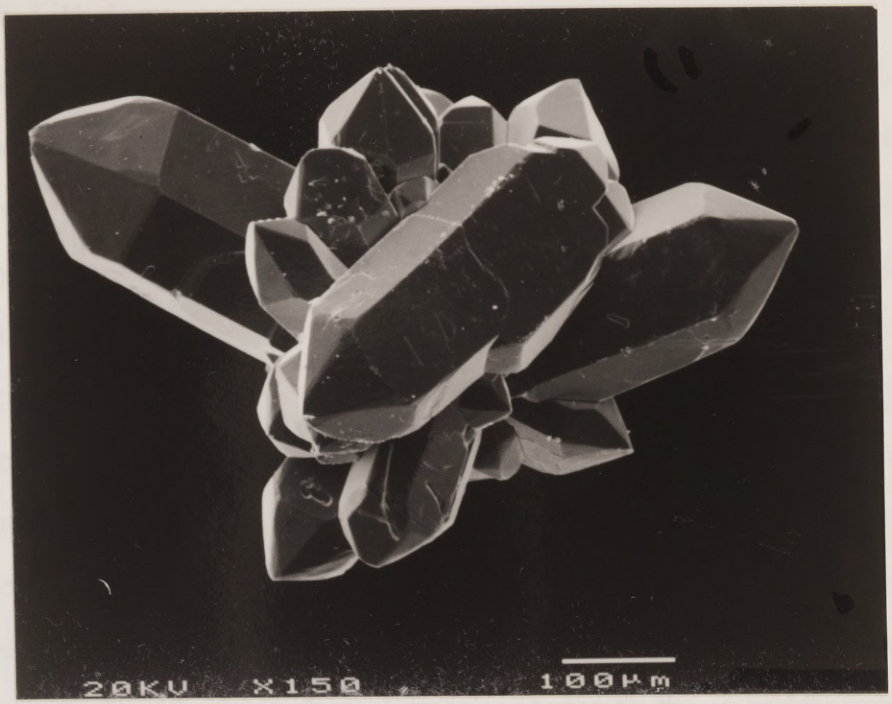
20KV X150
100µm

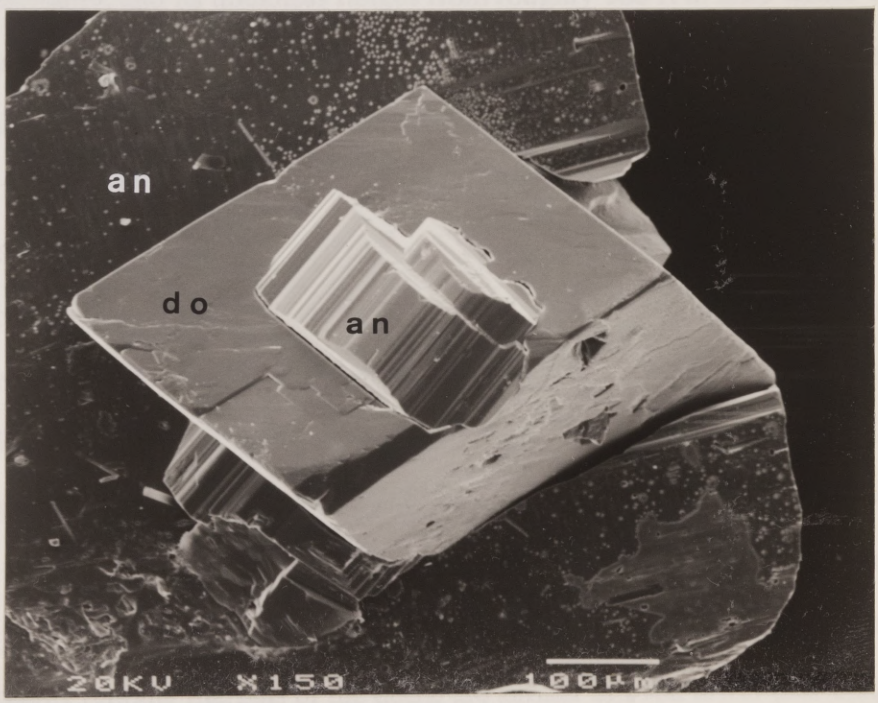
an
do
an
20KV X150

Cap Rock Lithology

Slightly over 36,000 ft of cap rock core was recovered from Hockley Dome. Cap rock is divided into three major lithic zones and is in sharp contact with overlying sediments and underlying salt (Figs. 3.7 and 3.8). The lower zone of the cap rock is primarily anhydrite with varying amounts of sulfide laminae and minor gypsum. Within this zone a lower (internal) calcite interval is locally present; however, it is volumetrically insignificant. The structural top of anhydrite ranges from 22 to -1,200 ft. The average elevation over the crest of the dome is approximately -80 ft; the steeply plunging margins are encountered at the -400-ft contour (Fig. 3.9). Excluding the thinning dome margins, isopach thickness of anhydrite ranges from about 850 to 600 ft with an average value of 750 ft (Fig. 3.10). Thicknesses may be as little as 3 ft where cap rock extends along the deep salt stock margins (Appendix Ib). A middle zone of gypsum cap rock forms between the anhydrite and calcite zones. The gypsum zone varies considerably, and its thickness ranges from roughly 100 ft to sites where very little gypsum marks the transition from calcite to anhydrite cap rock (Appendix Ib).

The calcite portion consists of an upper and lower (internal) zone which are commonly fractured and brecciated. The upper calcite zone has an irregular surface and is mapped as top of cap rock. Surface elevation over this portion of the dome ranges from 165 to 204 ft. In some instances top of calcite cap rock was estimated from logs for holes penetrated by rotary drilling. Elevation of the top of cap rock ranges from 97 to -1176 ft in the mineral exploration holes with an average elevation of about -50 ft over the crest of the dome (Fig. 2.3). Calcite thickness ranges from 3 to 323 ft with an average value of approximately 25 ft over a similar area. The greater thicknesses of calcite cap rock are restricted to margins of the dome (Fig. 3.11). Calcite thickness along the steeply dipping margins of the dome are similar or even lower than calcite

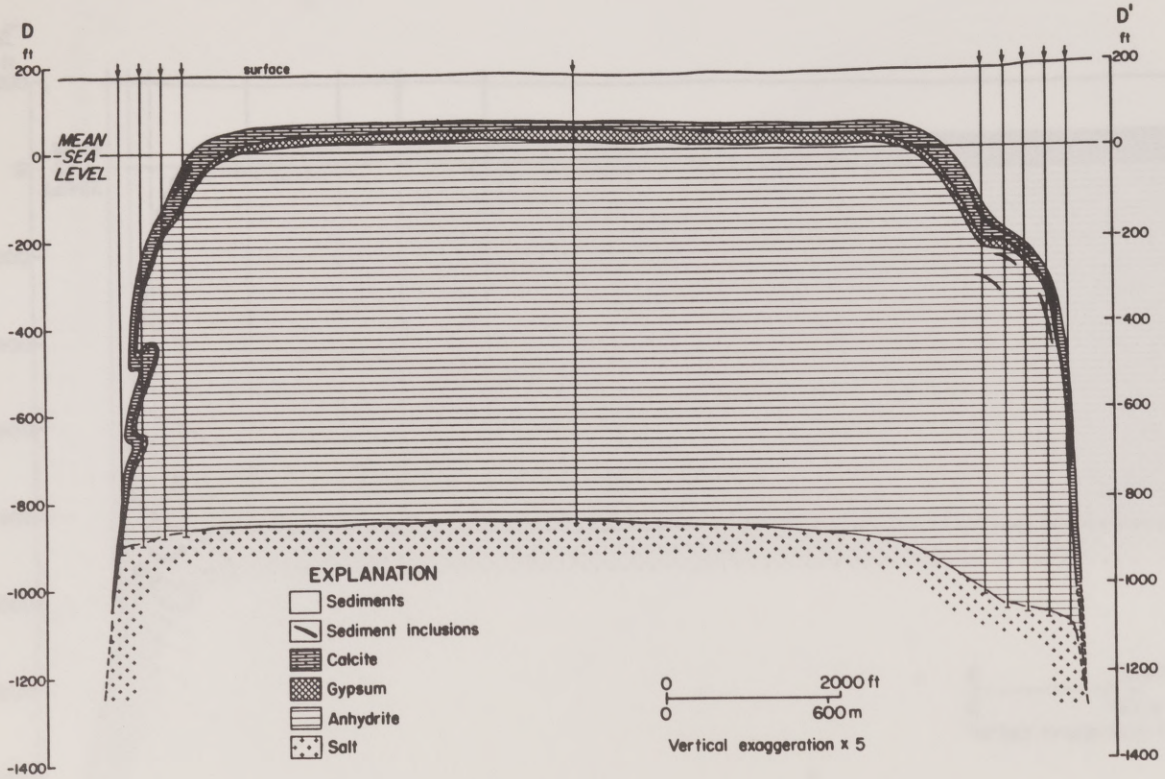

Fig. 3.7. Southwest-northeast cross-section of Hockley salt dome, D-D'.
Line of section shown in Figure 2.3.

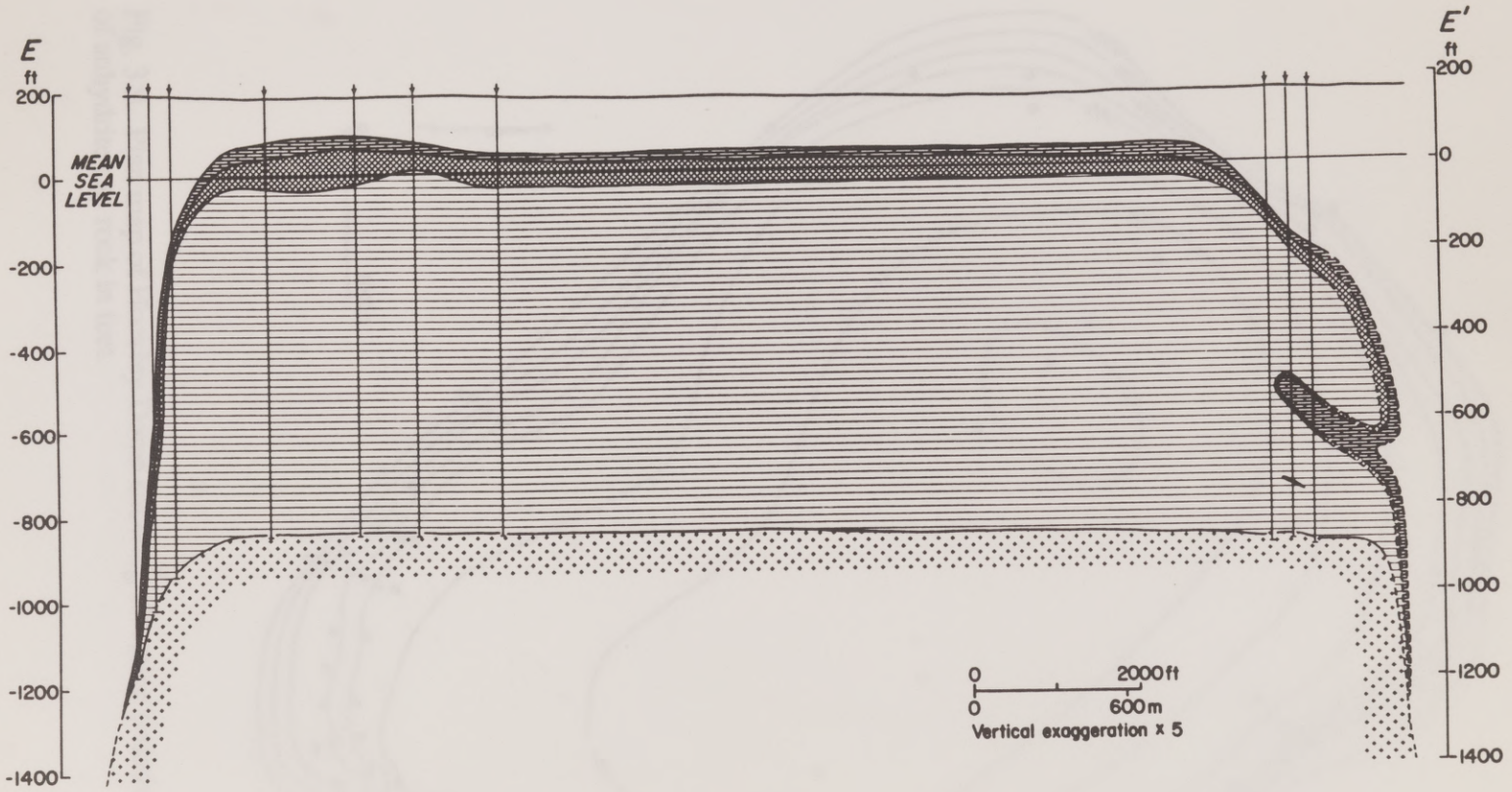

Fig. 3.8. Northwest-southeast cross-section of Hockley salt dome, E-E'.
Line of section shown in Figure 2.3. Note a lower calcite zone occurs entirely within the
southeast portion of the anhydrite cap rock. See Figure 3.7 for explanation of cap rock lithologies.

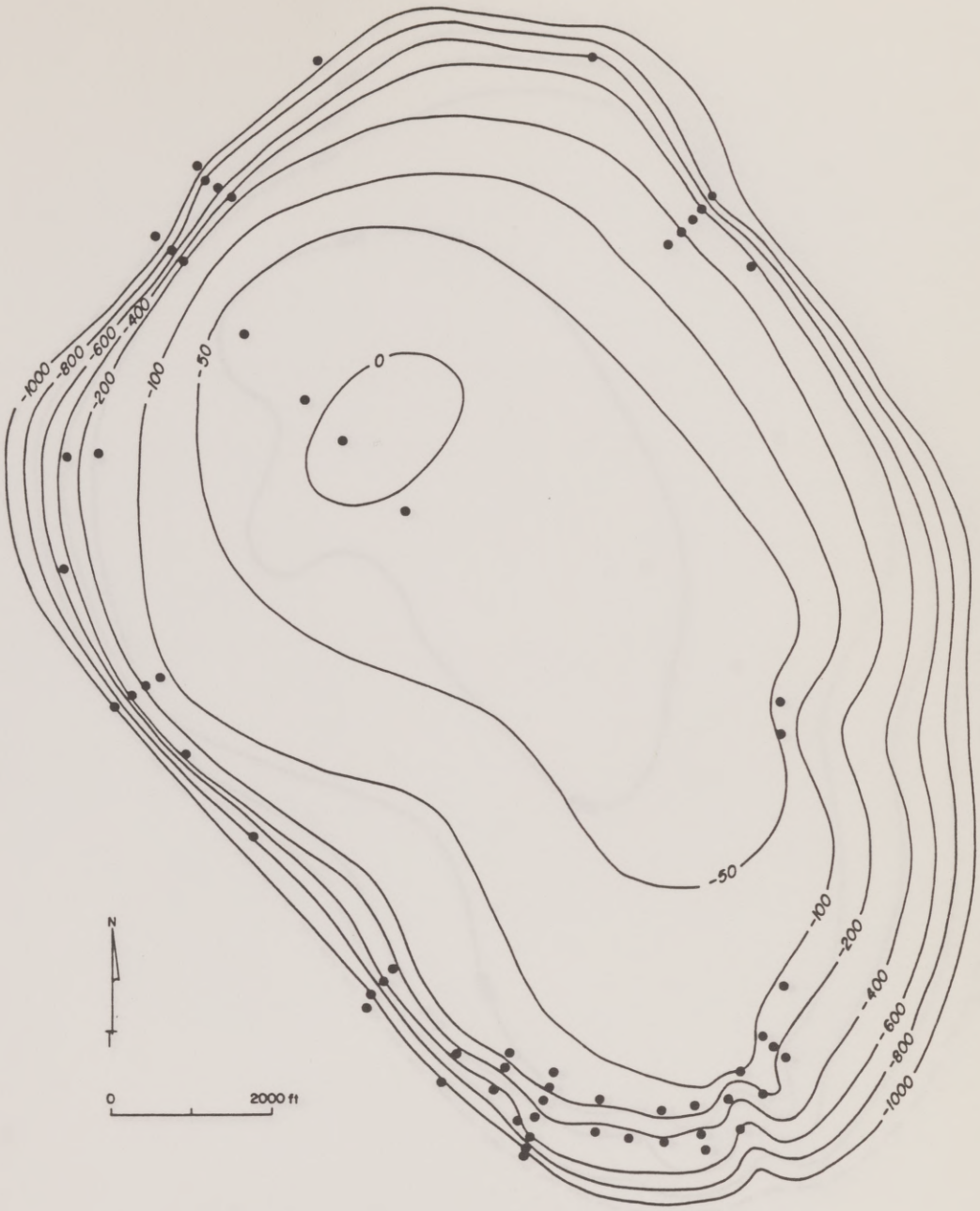

Fig. 3.9. Plan map of Hockley Dome showing elevation (relative to MSL) of top of anhydrite cap rock in feet.

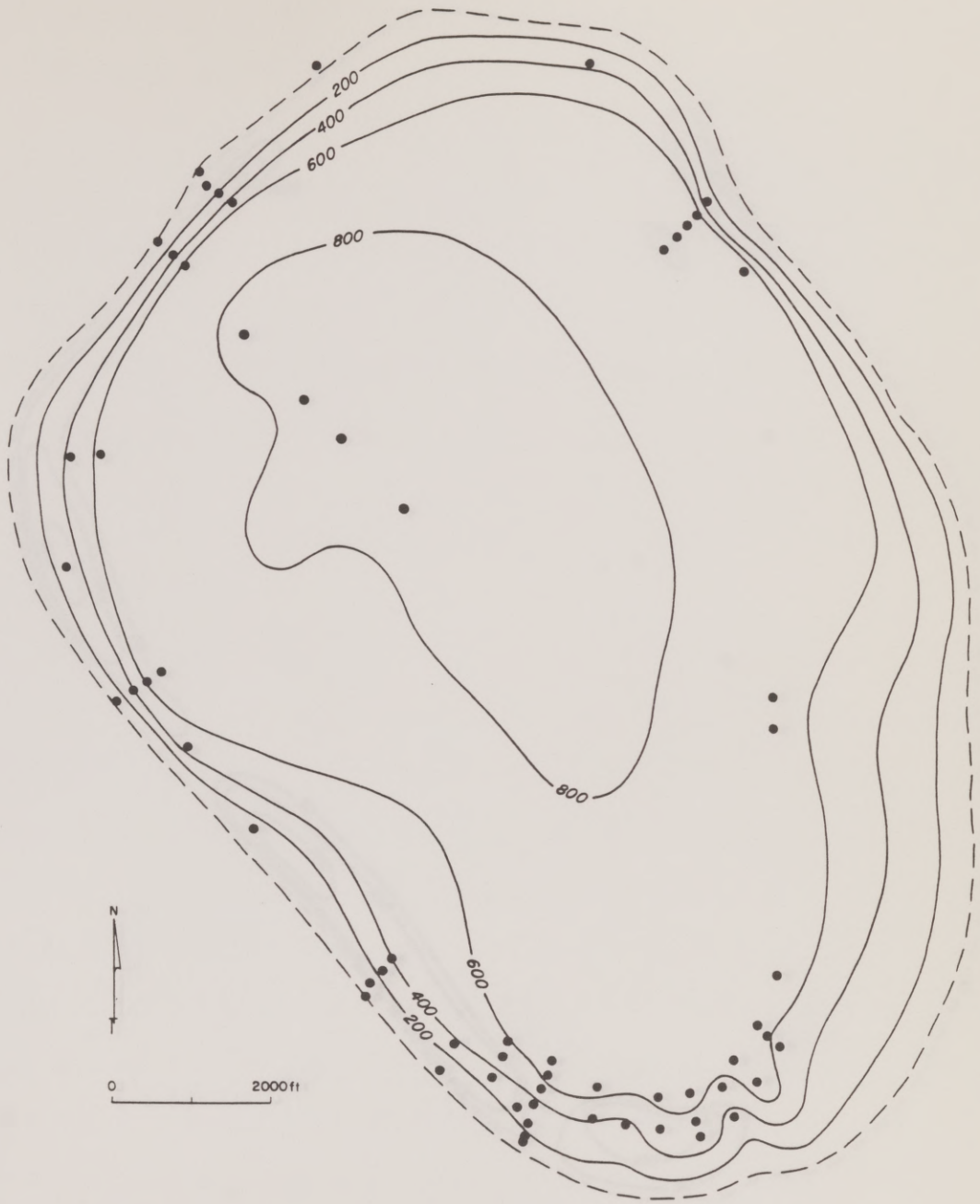

Fig. 3.10. Plan map of Hockley Dome showing isopach thickness of anhydrite in feet. Dashed outermost line represents the inferred extent of cap rock.

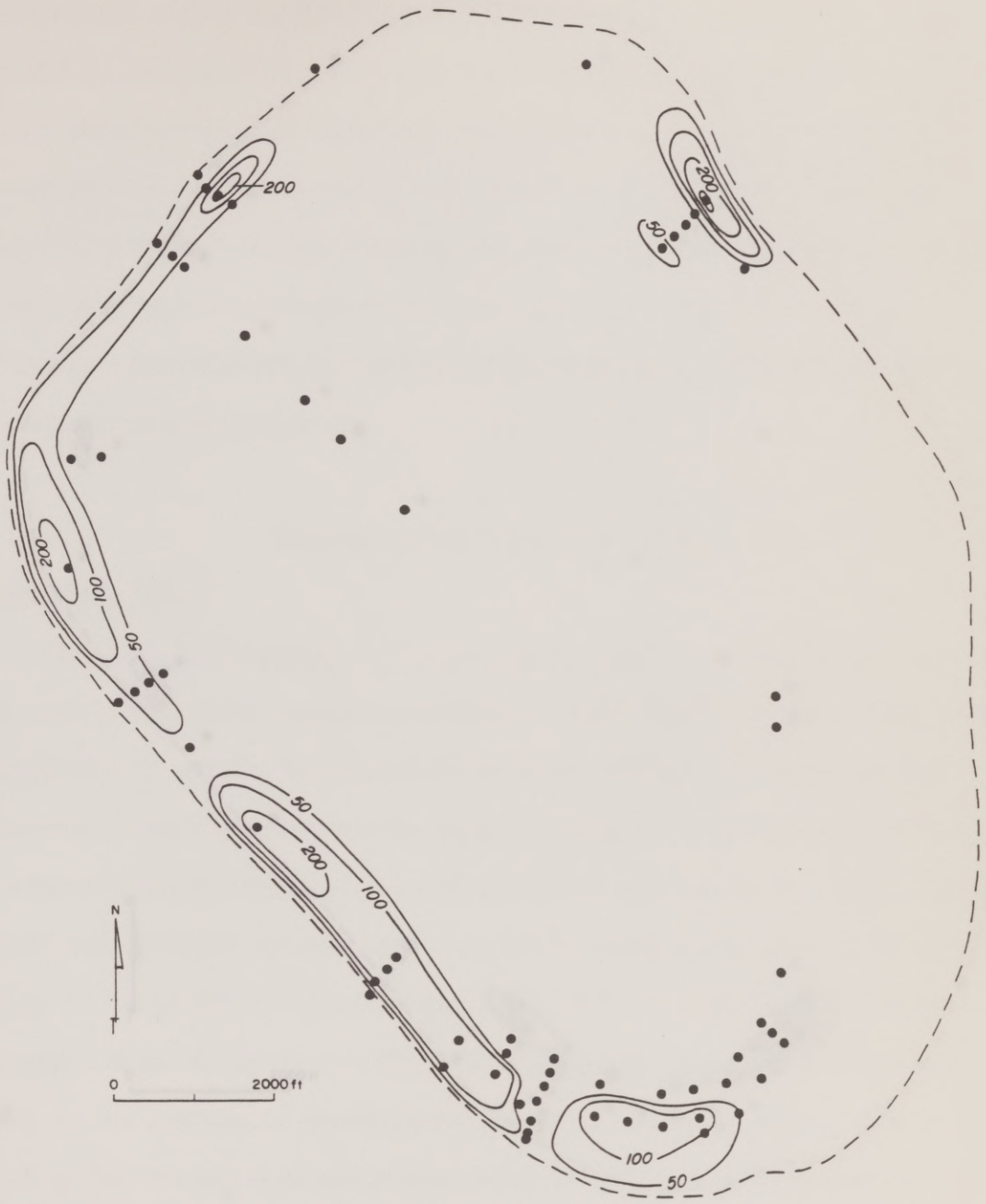

Fig. 3.11. Plan map of Hockley Dome showing isopach thickness of upper calcite in feet.
Note that greatest thicknesses are along the dome margins. Dashed outermost line represents the inferred extent of cap rock.

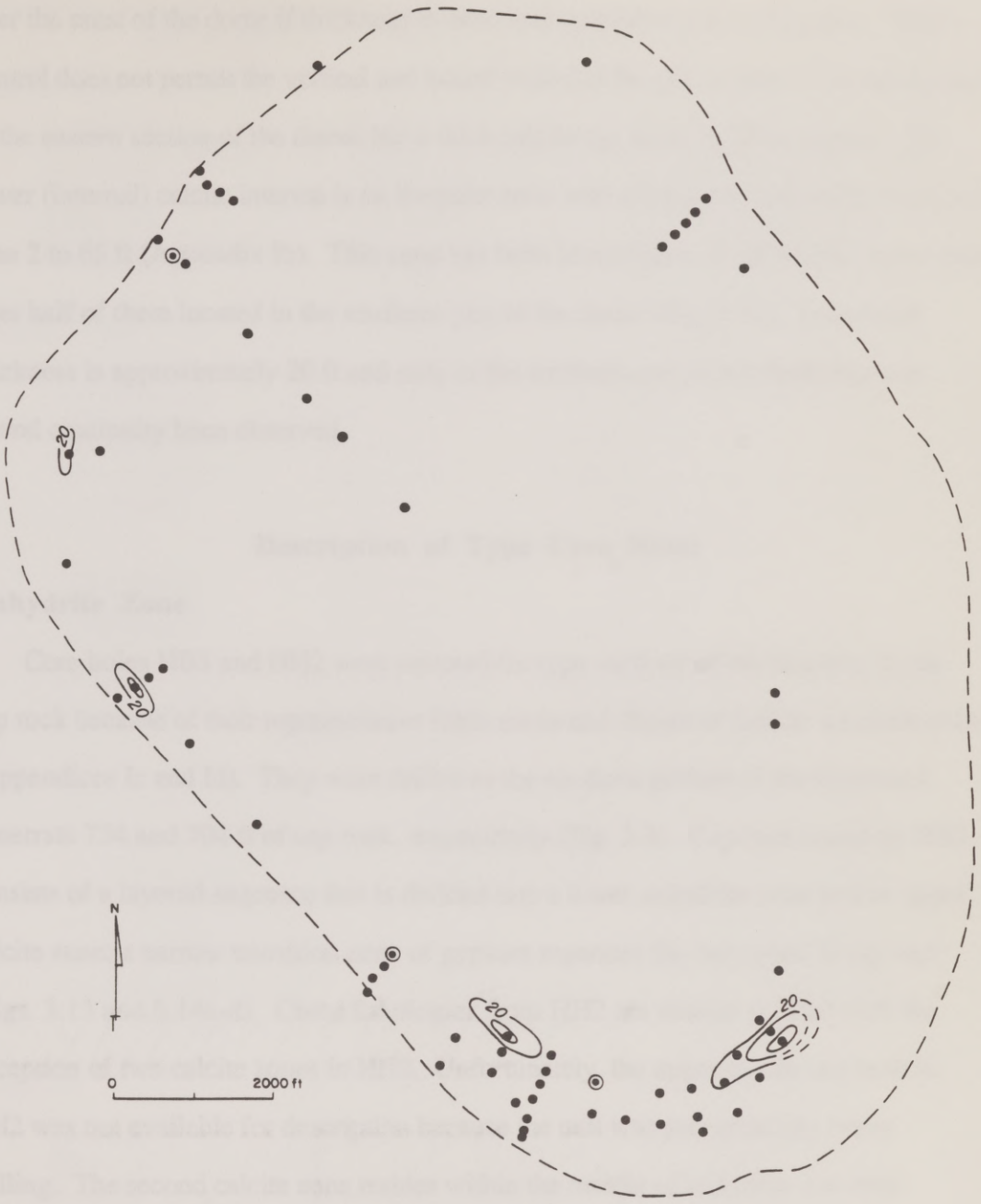

Fig. 3.12. Plan map of Hockley Dome showing isopach thickness of lower calcite in feet.
Most of these internal calcite zones are located in the southern portion of the dome. Drill holes denoted with small circles contain three ft of calcite or less. Dashed outermost line represents the inferred extent of cap rock.

over the crest of the dome if thickness is measured perpendicular to anhydrite. Well control does not permit the vertical and lateral extent of the calcite zone to be determined in the eastern section of the dome, but a thick calcite cap rock could be present. The lower (internal) calcite interval is an irregular zone with thicknesses that range from less than 2 to 65 ft (Appendix Ib). This zone has been identified in 10 of 65 core holes with over half of them located in the southern part of the dome (Fig. 3.12). Its average thickness is approximately 20 ft and only in the southern part of the dome has any lateral continuity been observed.

Description of Type Core Holes

Anhydrite Zone

Core holes HB3 and HH2 were selected for type sections of the Hockley Dome cap rock because of their representative lithic zones and degree of sulfide mineralization (Appendices Ic and Id). They were drilled in the southern portion of the dome and penetrate 734 and 704 ft of cap rock, respectively (Fig. 2.3). Cap rock cored by HB3 consists of a layered sequence that is divided into a lower anhydrite zone and an upper calcite zone; a narrow transition zone of gypsum separates the two types of cap rock (Figs. 3.13 and 3.14a-d). Cored lithologies from HH2 are similar to HB3 with the exception of two calcite zones in HH2. Unfortunately, the upper calcite cap rock in HH2 was not available for description because the unit was penetrated by rotary drilling. The second calcite zone resides within the middle of anhydrite cap rock (Figs. 3.15 and 3.16a-f). Internal calcite lenses appear to be concentrated in the southern part of the dome; drill hole density is also greatest in that area (Fig. 3.12).

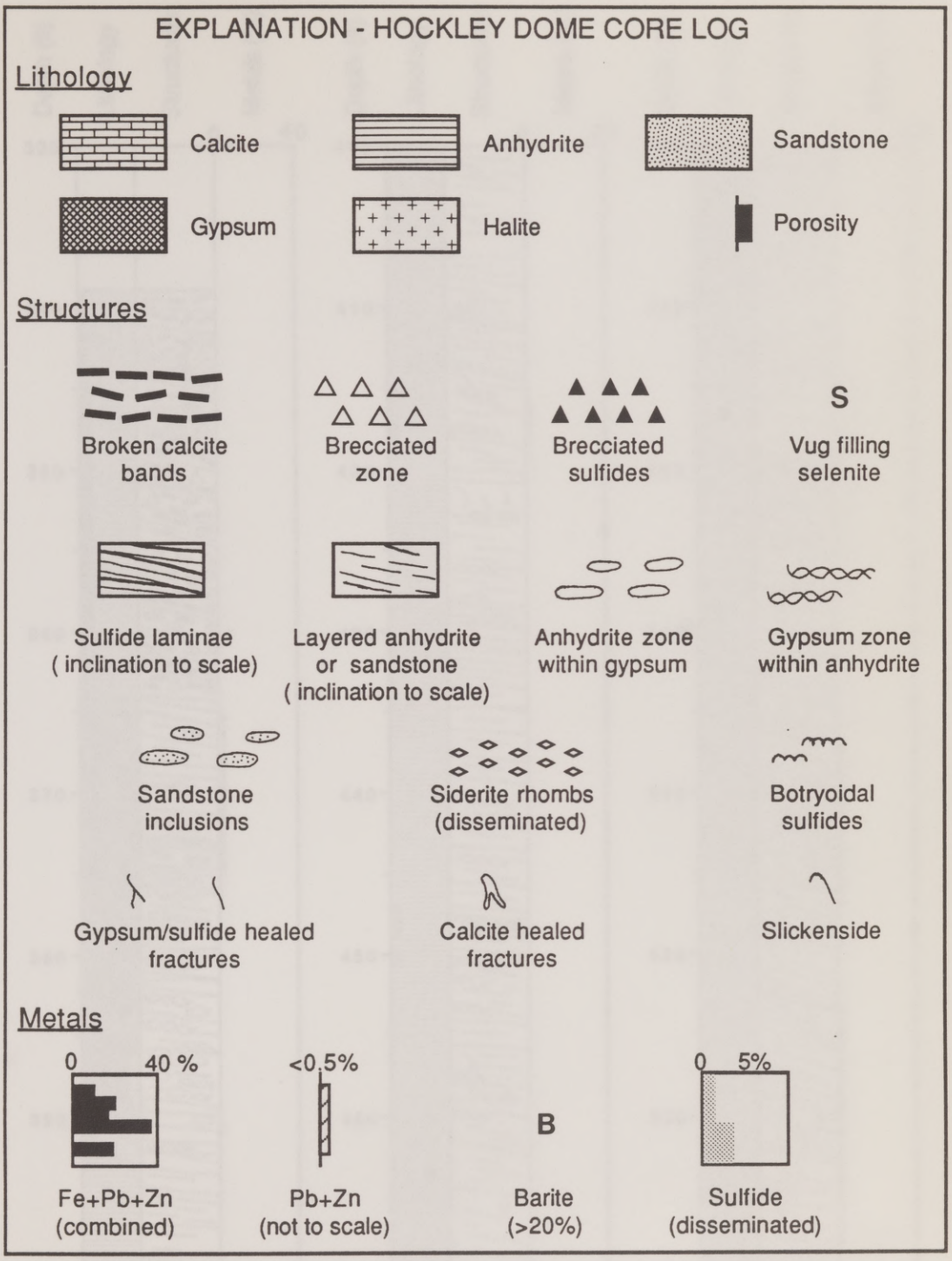

Fig. 3.13. Graphic cap rock description of type hole HB3.

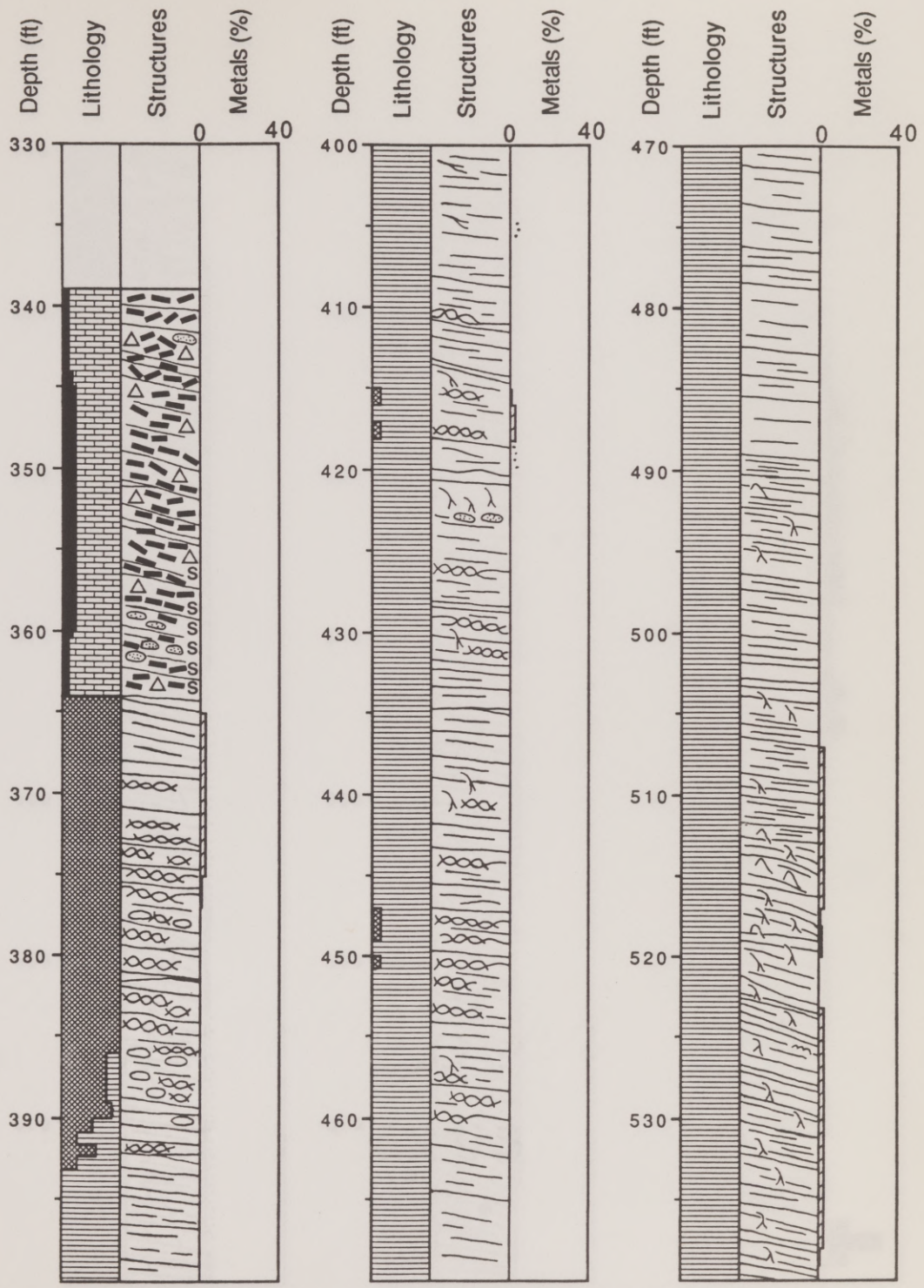

Fig. 3.13. Graphic cap rock description of type hole HB3 (cont.).

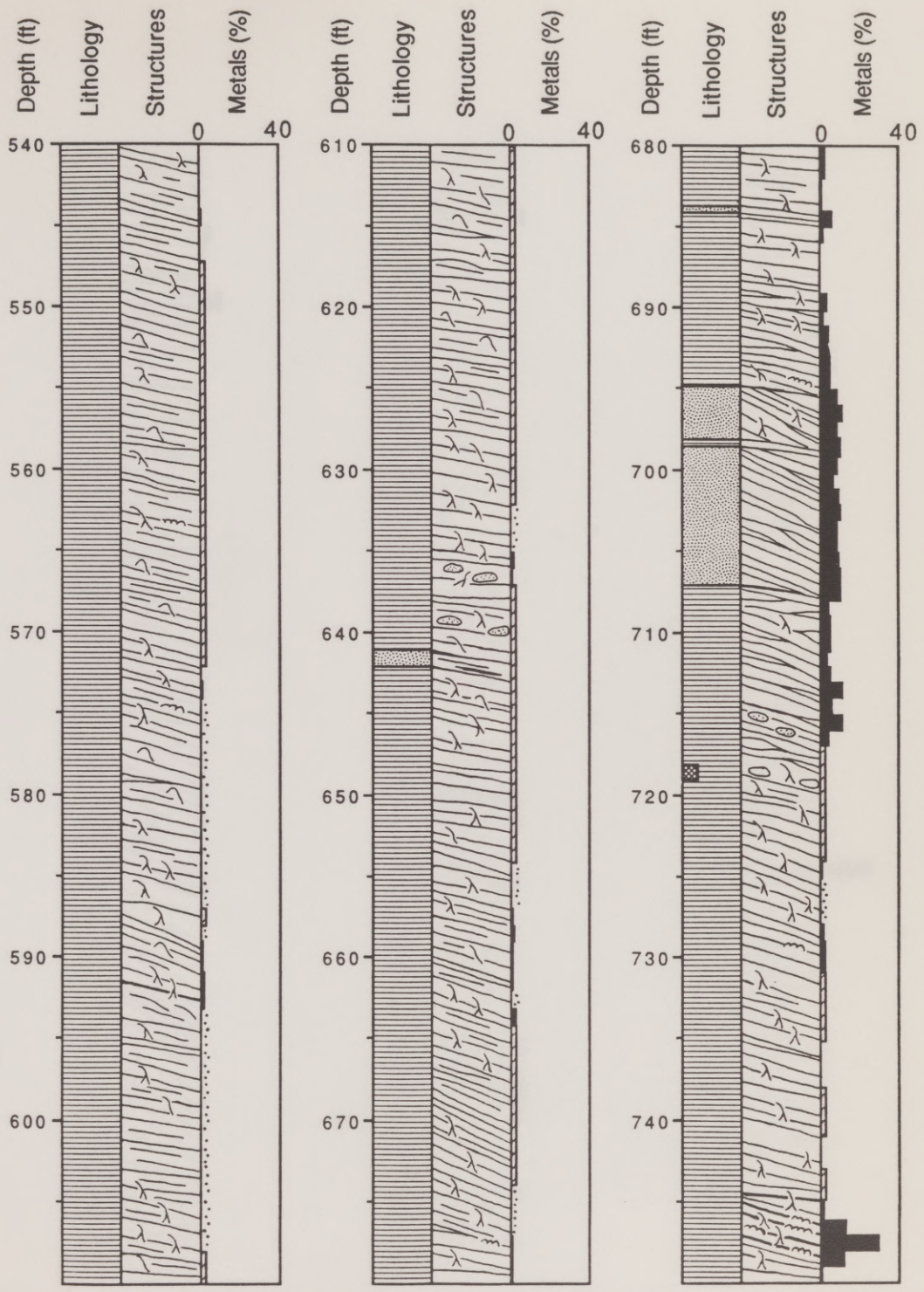

Fig. 3.13. Graphic cap rock description of type hole HB3 (cont.).

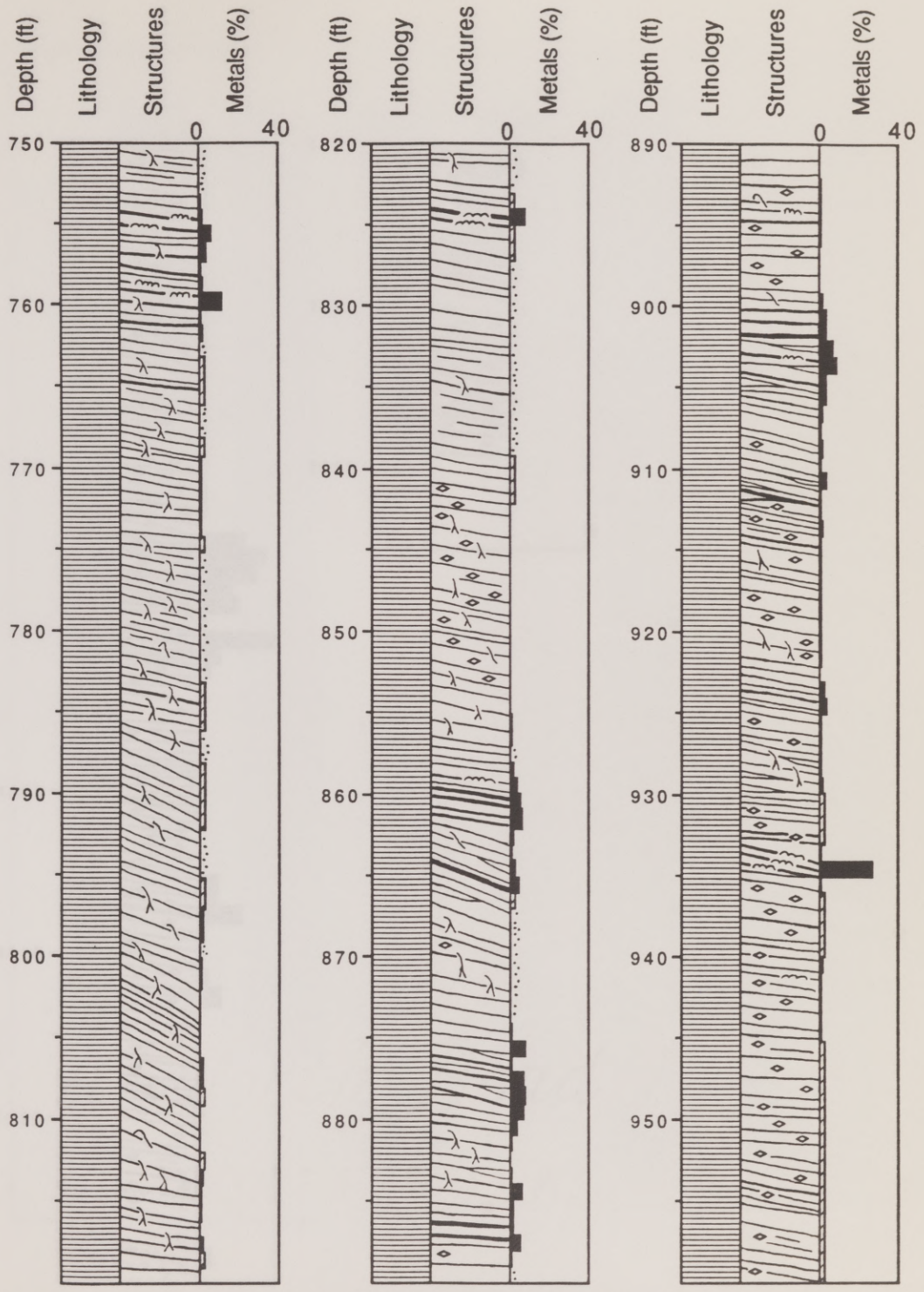

Fig. 3.13. Graphic cap rock description of type hole HB3 (cont.).

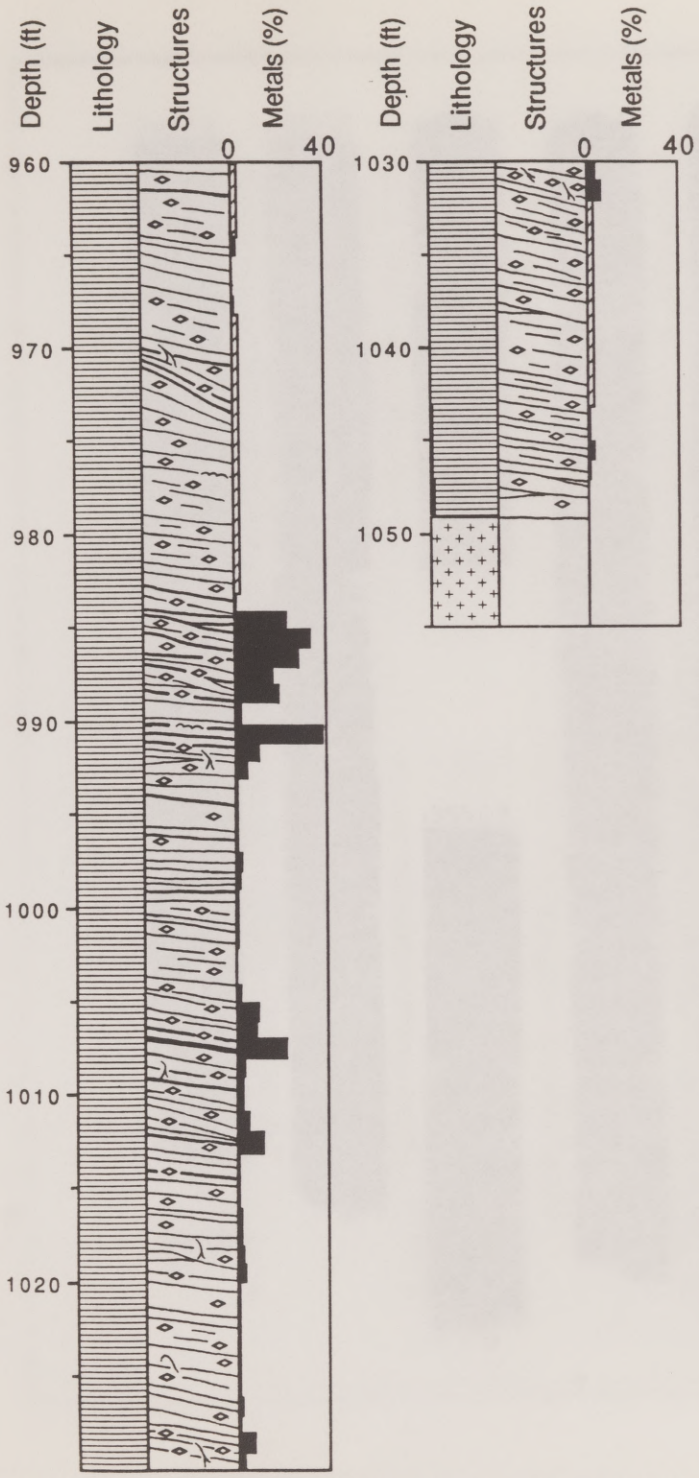

Fig. 3.13. Graphic cap rock description of type hole HB3 (cont.).

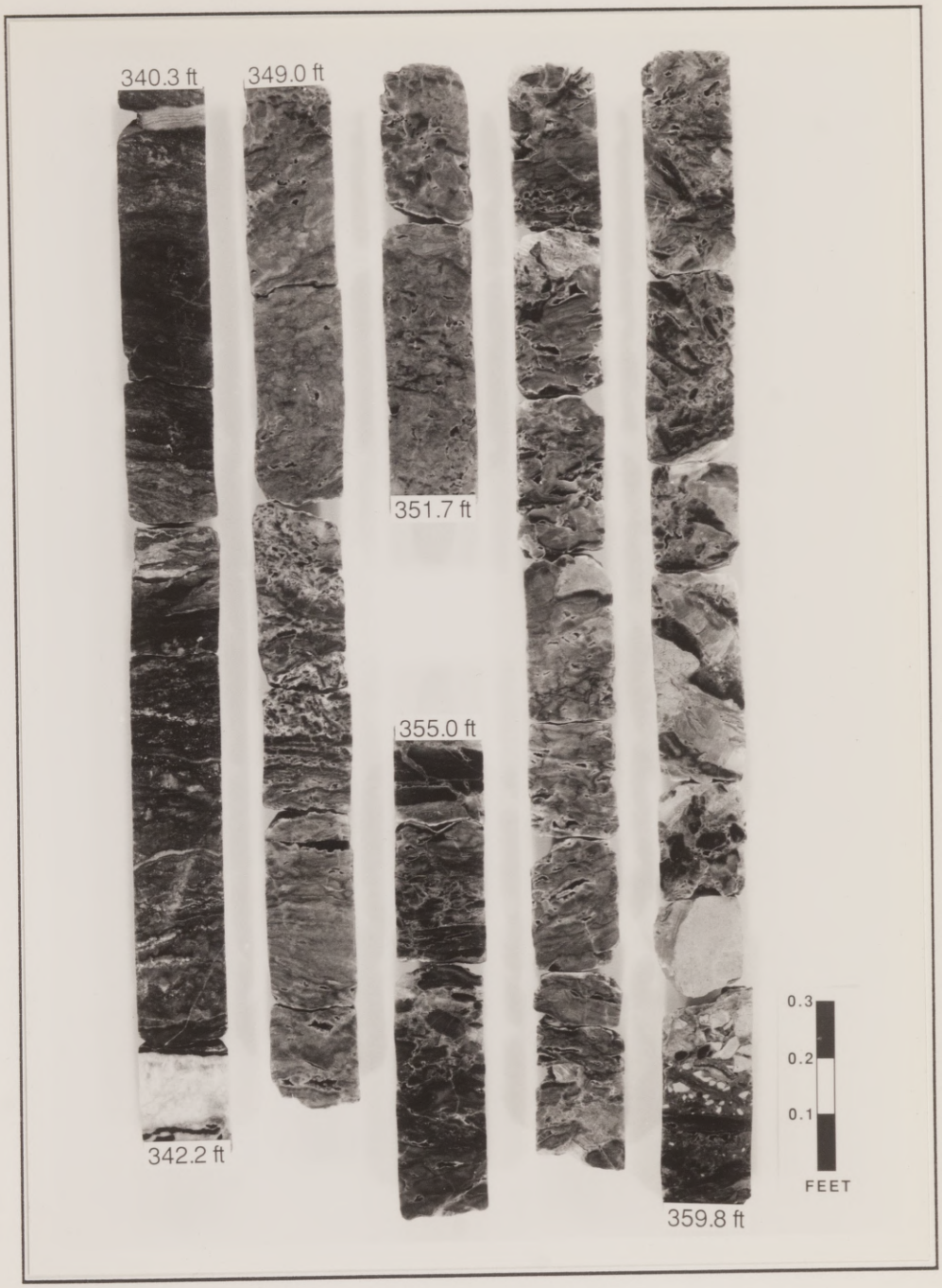

Fig. 3.14a. Core photograph of type hole HB3.

Fig. 3.14b. Core photograph of type hole HB3.

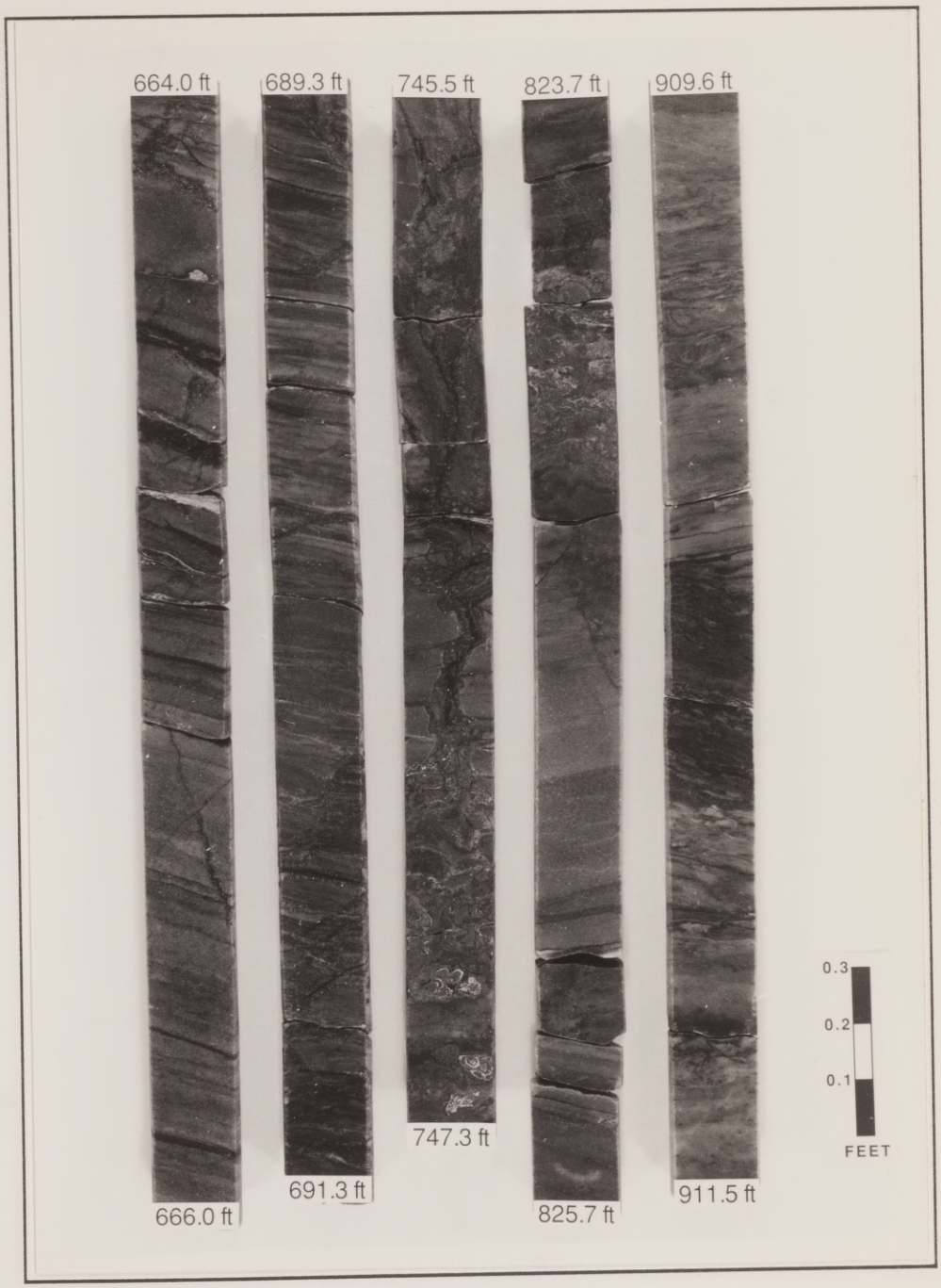

Fig. 3.14c. Core photograph of type hole HB3.

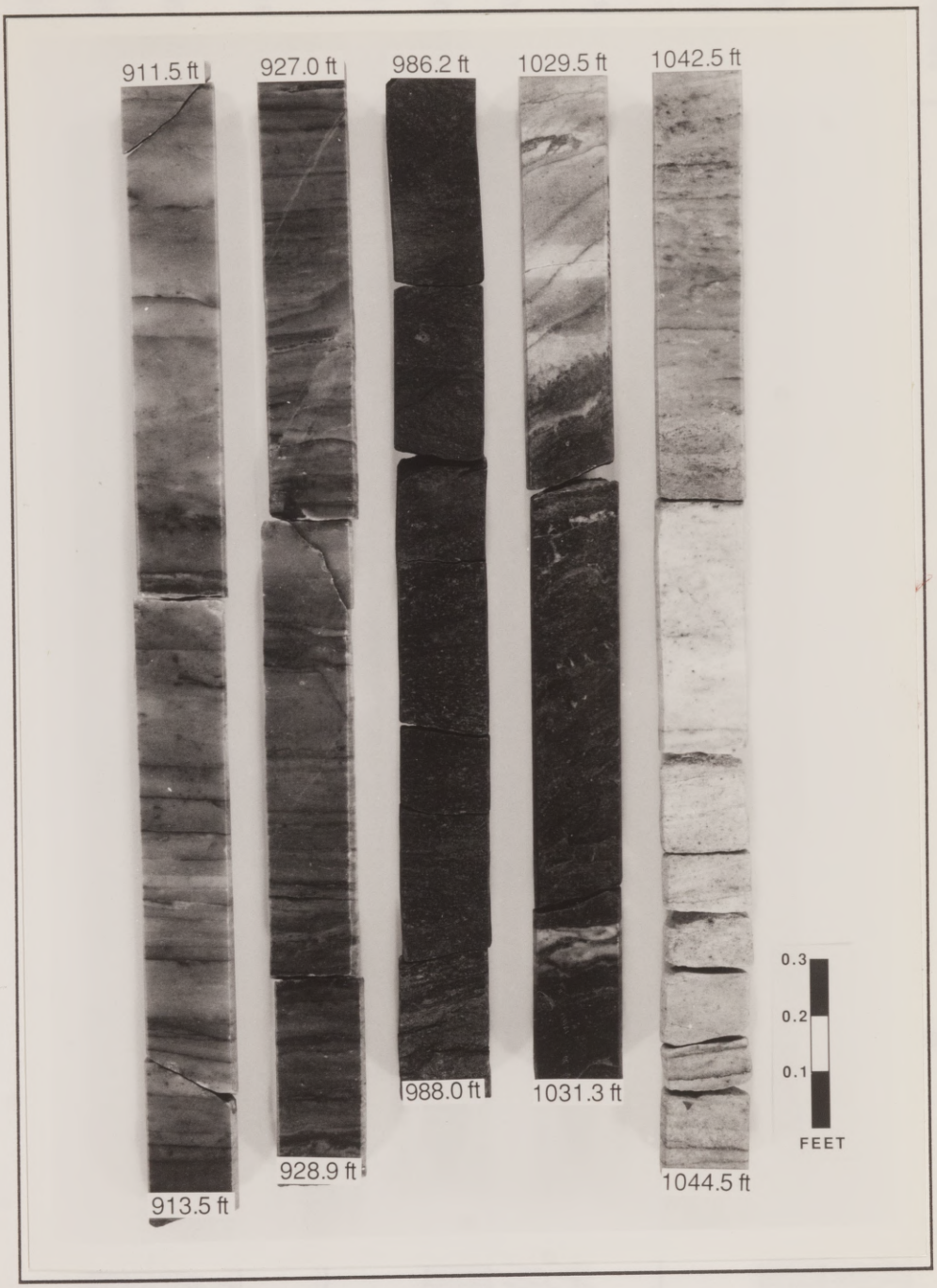

Fig. 3.14d. Core photograph of type hole HB3.

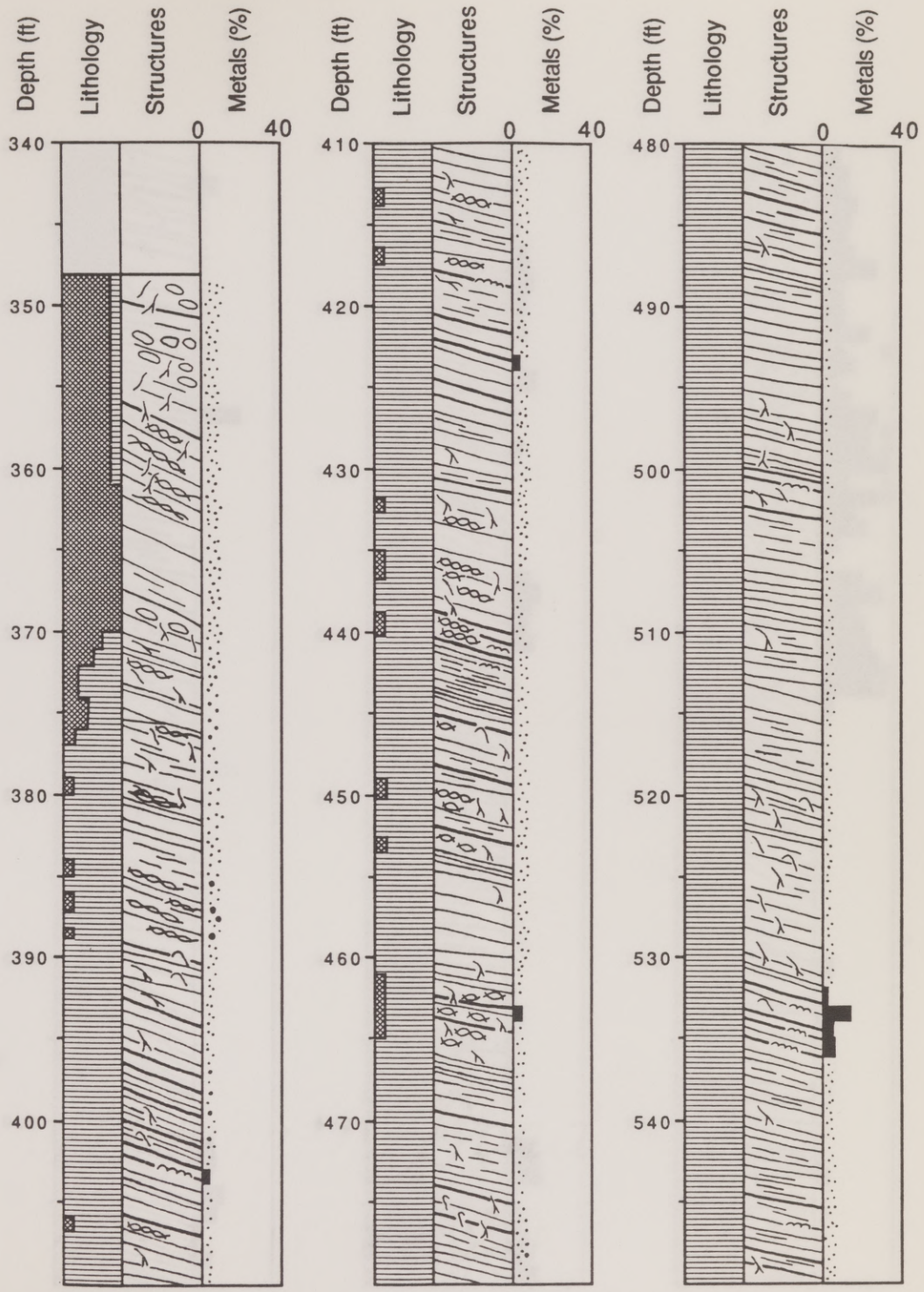

Fig. 3.15. Graphic cap rock description of type hole HH2.
See Figure 3.13 for core explanation.

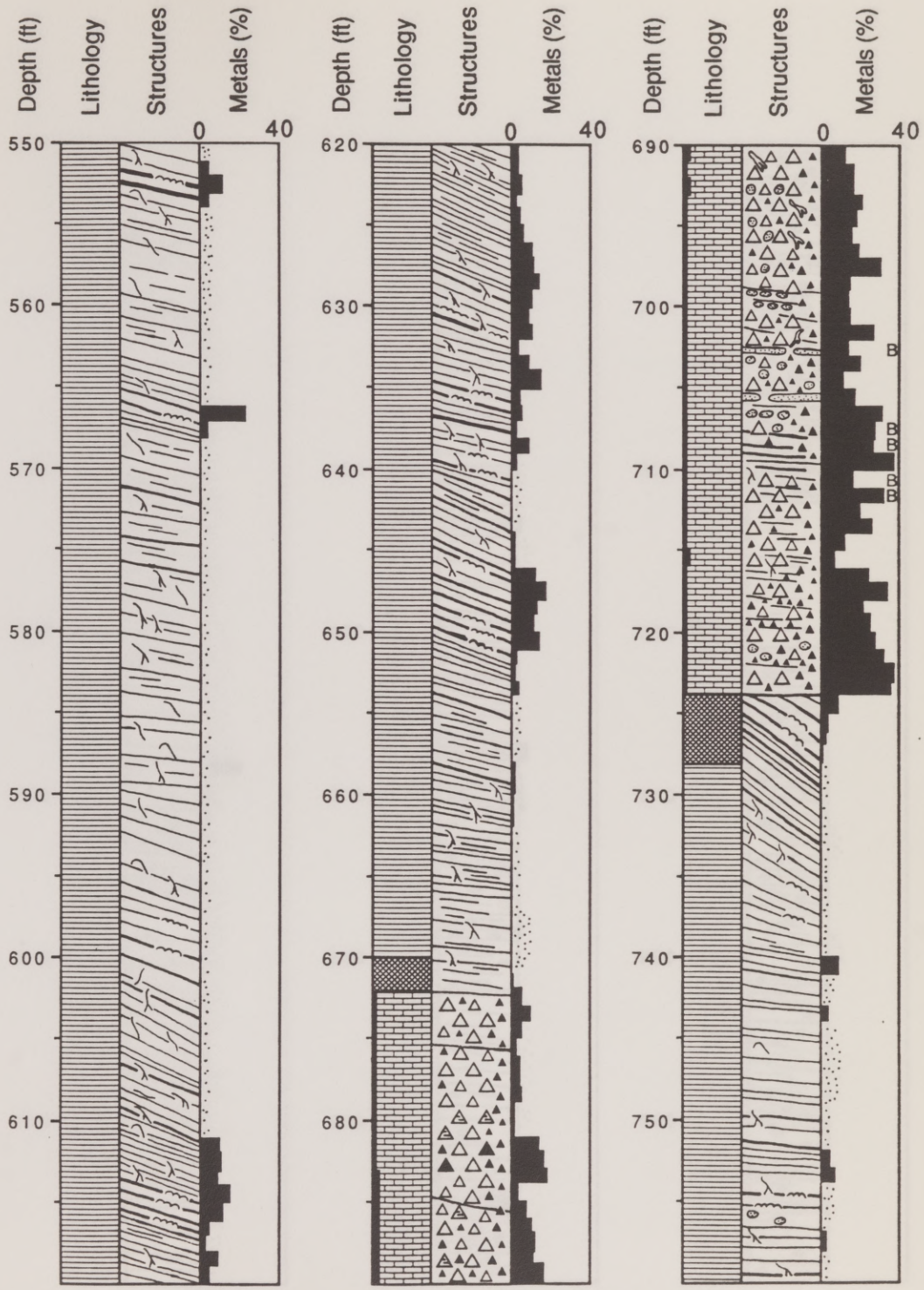

Fig. 3.15. Graphic cap rock description of type hole HH2 (cont.).

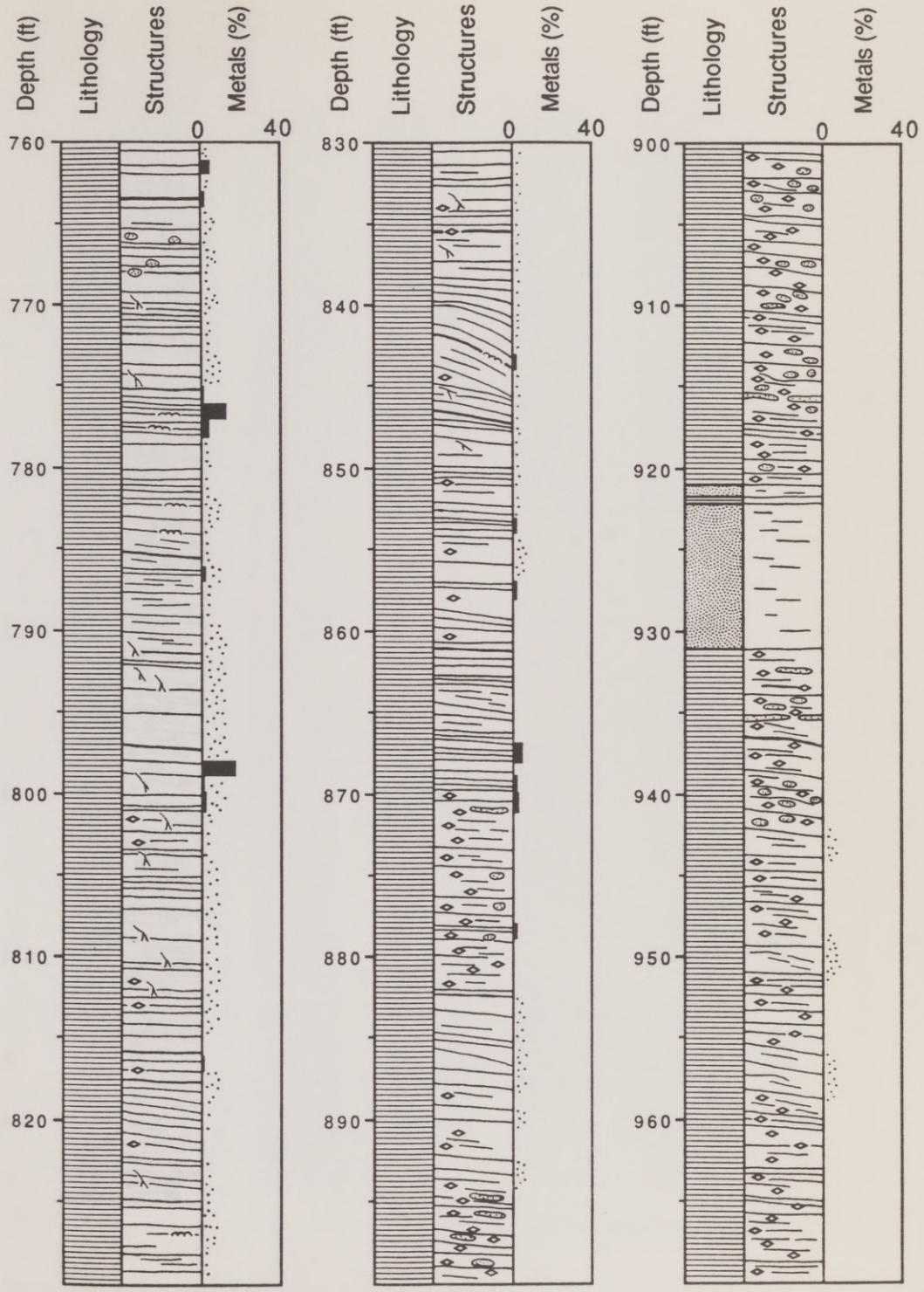

Fig. 3.15. Graphic cap rock description of type hole HH2 (cont.).

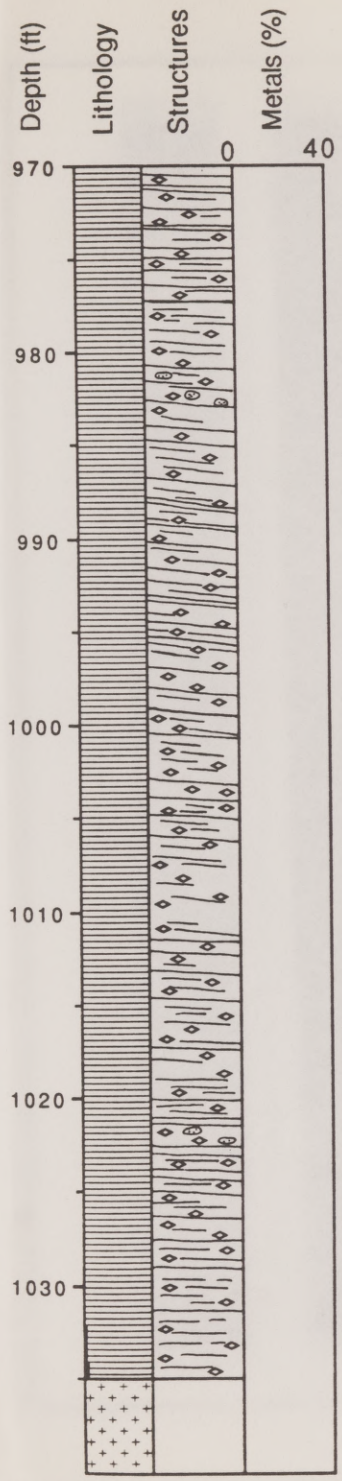

Fig. 3.15. Graphic cap rock description of type hole HH2 (cont.).

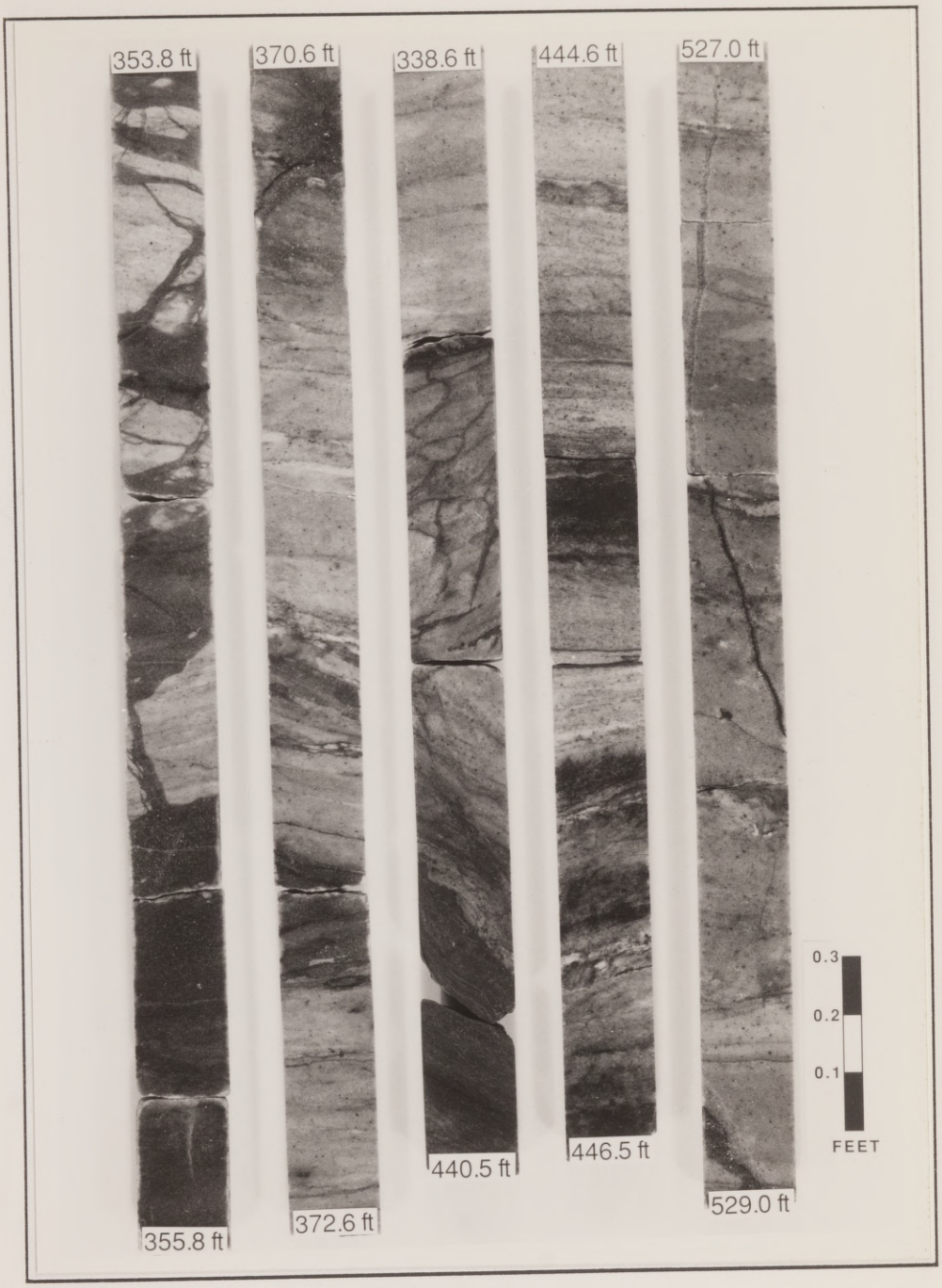

Fig. 3.16a. Core photograph of type hole HH2.

Fig. 3.16b. Core photograph of type hole HH2.

Fig. 3.16c. Core photograph of type hole HH2.

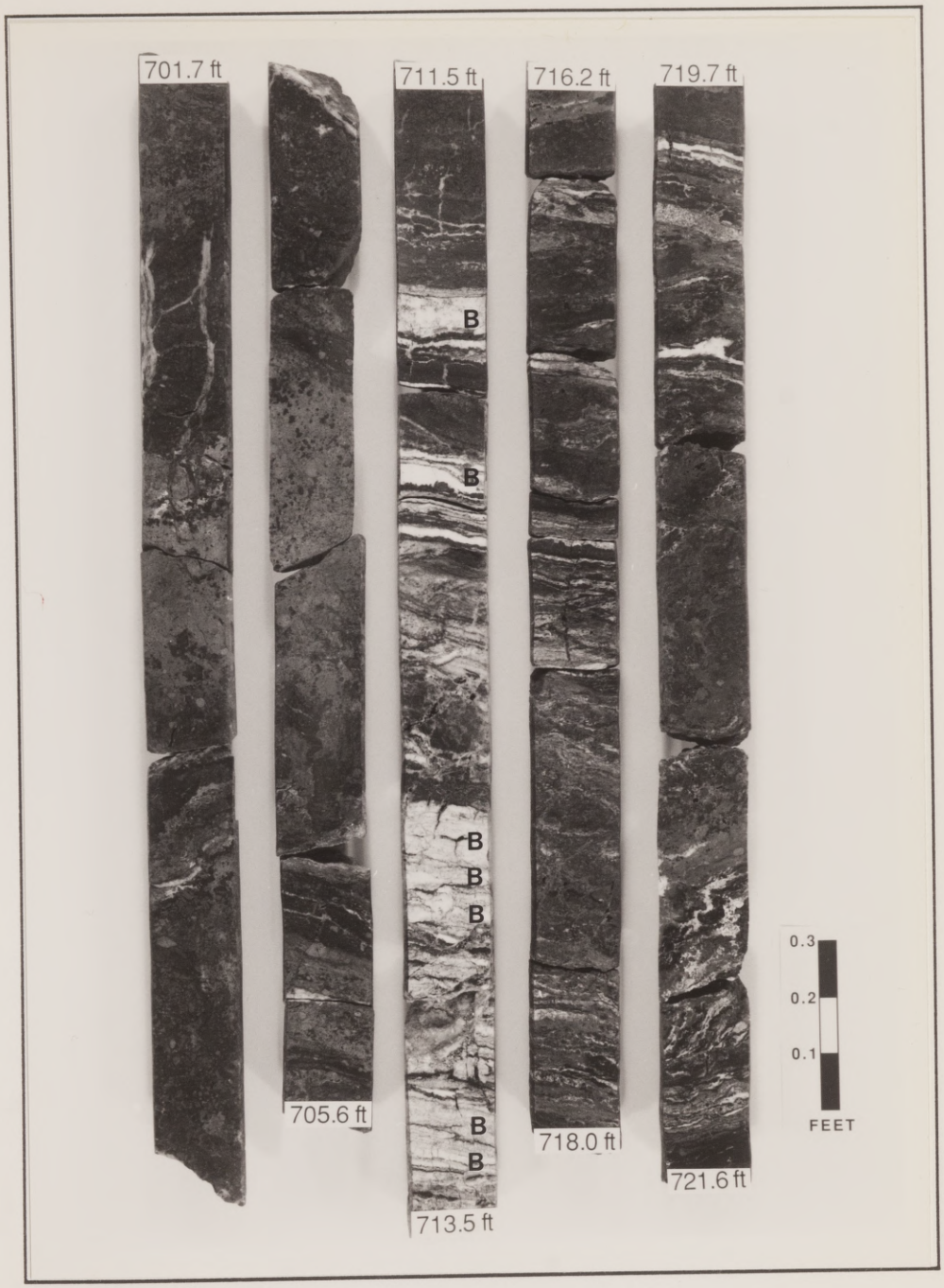

Fig. 3.16d. Core photograph of type hole HH2.

Fig. 3.16e. Core photograph of type hole HH2.

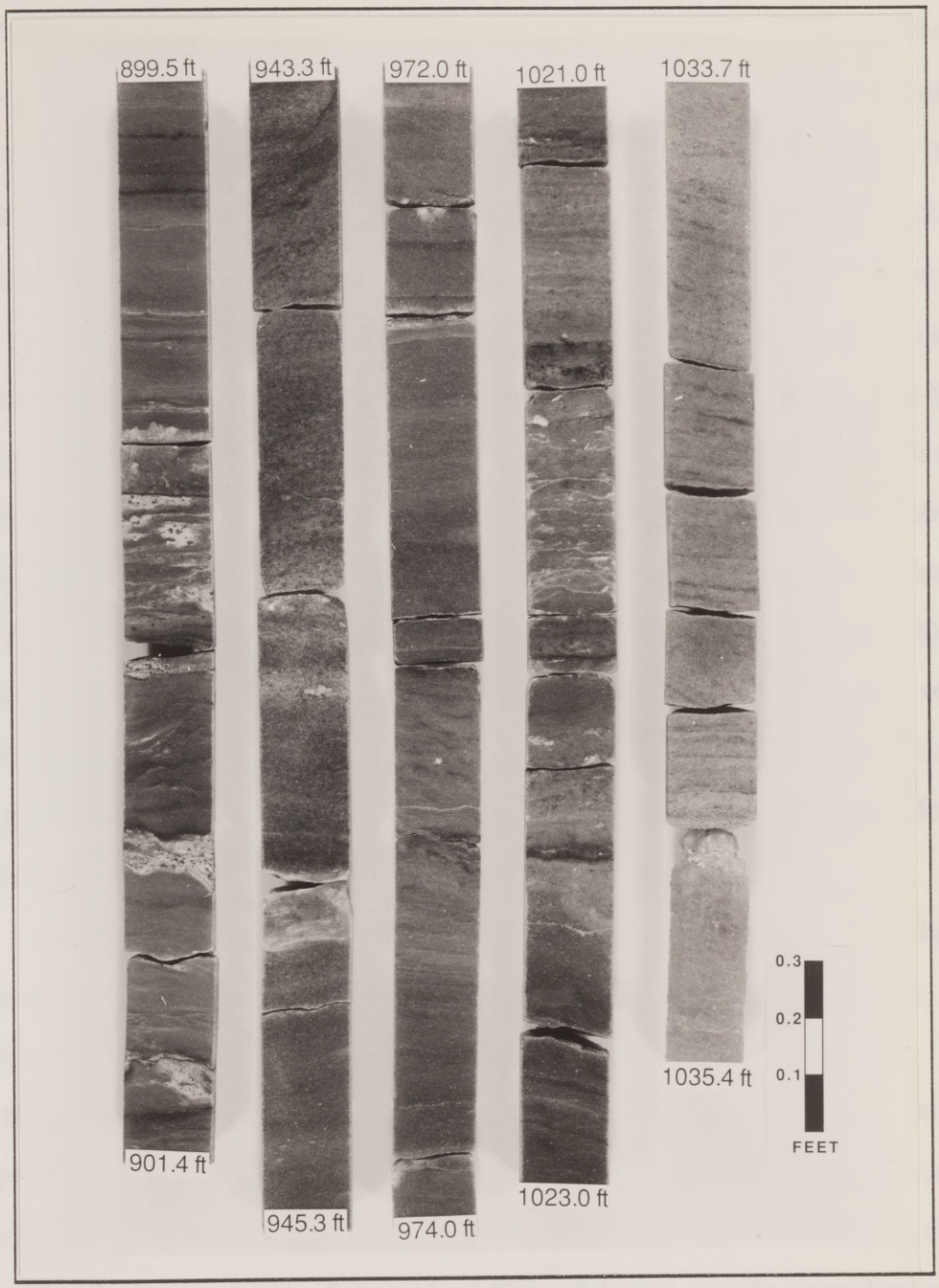

Fig. 3.16f. Core photograph of type hole HH2.

The deepest cap rock strata from HB3 and HH2, recovered at depths of 1048 and 1035 ft, respectively, is a porous (5 to 10 %) anhydrite zone (Fig. 3.17) with obvious but undetermined high permeability. This basal interval, located at the salt/anhydrite contact, is composed of prismatic anhydrite crystals (0.2 to 1.3 mm long) (Fig. 3.17) that are similar in dimension to idioblastic anhydrite disseminated in the salt stock. Approximately one foot above the salt/anhydrite interface pore-filling halite is not present (Hallager, 1984); porosity and permeability (< 0.05 md, measured from several unidentified core holes; Hallager, 1984) are also drastically reduced within a six-ft zone above the base of the cap rock due to grain compaction. This indurated zone consists of recrystallized, predominantly xenoblastic anhydrite prisms that commonly show evidence of pressure dissolution, i.e., sutured grain boundaries (Fig. 3.18). Many of the anhydrite grains exhibit undulose extinction and microfractures (Fig. 3.18) indicating the presence of mechanical strain and grain failure. Deformation is a result of overburden pressure or continued movement of the underlying salt stock (halokinesis). In general, there does not appear to be any visible preferred orientation of anhydrite crystals.

Anhydrite cap rock is light to dark gray and generally well layered. These layers may represent repeated cycles of halite dissolution and anhydrite accretion at the salt/anhydrite interface. Layering in the anhydrite section is readily observed throughout the core but is difficult to distinguish in thin section. Some of the banding appears to be caused by changes in anhydrite grain size. For example, a pale 2 cm thick layer is bordered by gray sections of core (Fig. 3.19a). Petrographically, this pale zone is characterized by finer-grained (0.3 to 0.1 mm), heavily sutured anhydrite crystals (Fig. 3.19b), with coarser-grained (0.5 to 0.2 mm) anhydrite bordering both above and below (Fig. 3.19c).

Fig. 3.17. Photomicrograph of a loosely compacted porous anhydrite (an) zone located at the base of cap rock; sample HH3-1046.
Porosity (p) is 5 to 10 %. Photo width is 2.5 mm; transmitted plane polarized light.

Fig. 3.18. Photomicrograph of recrystallized, xenoblastic anhydrite; sample HH2-799. Many of the anhydrite crystals show evidence of pressure dissolution, i.e., sutured grain boundaries, undulose extinction, and microfracturing. Photo width is 2.5 mm; transmitted light, crossed nicols.

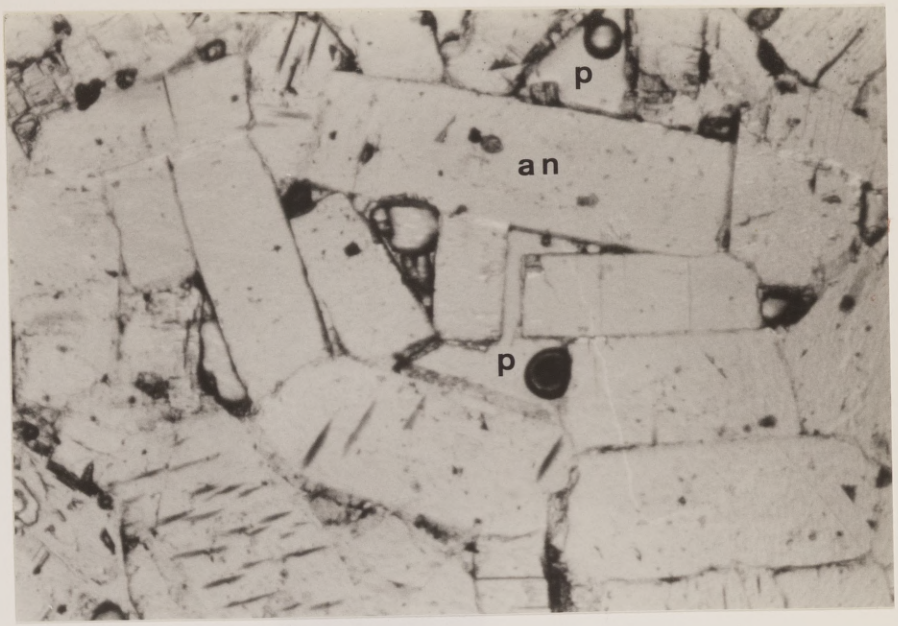
p
an
p

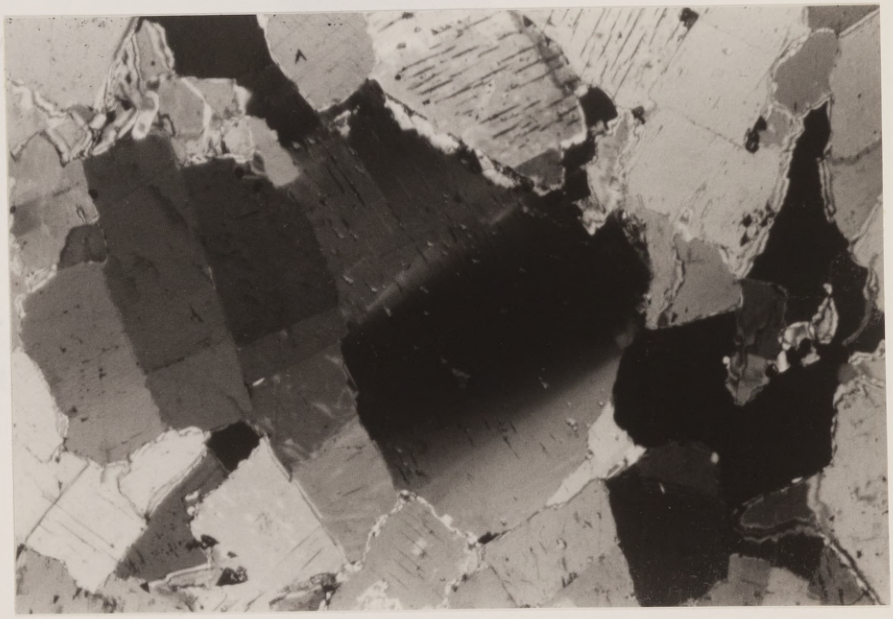

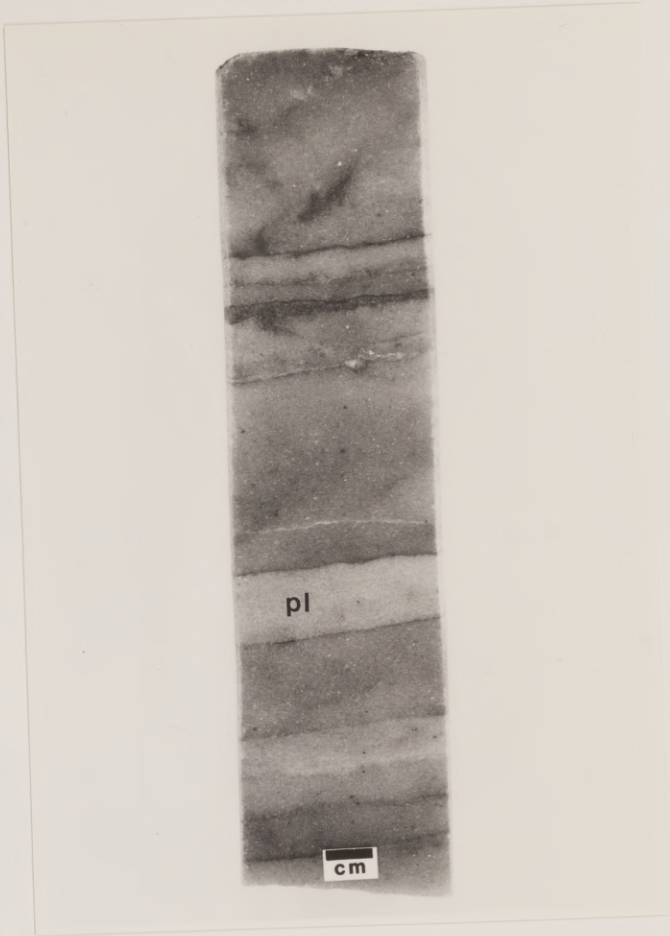

Fig. 3.19a. Core photograph of layered light and dark gray anhydrite cap rock; sample HH3-601.
Note pale (pl) 2 cm layer bordered by gray anhydrite sections of core.

Fig. 3.19b. Photomicrograph of tightly interlocking anhydrite crystals from the pale zone; sample HH3-601.
Crystals are fine-grained and heavily sutured. Photo width is 2.5 mm; transmitted light, crossed nicols.

Fig. 3.19c. Photomicrograph of tightly interlocking anhydrite crystals from the gray zone; sample HH3-601.
Crystals are medium-grained and less embayed than the bordering pale band. Photo width is 2.5 mm; transmitted light, crossed nicols.

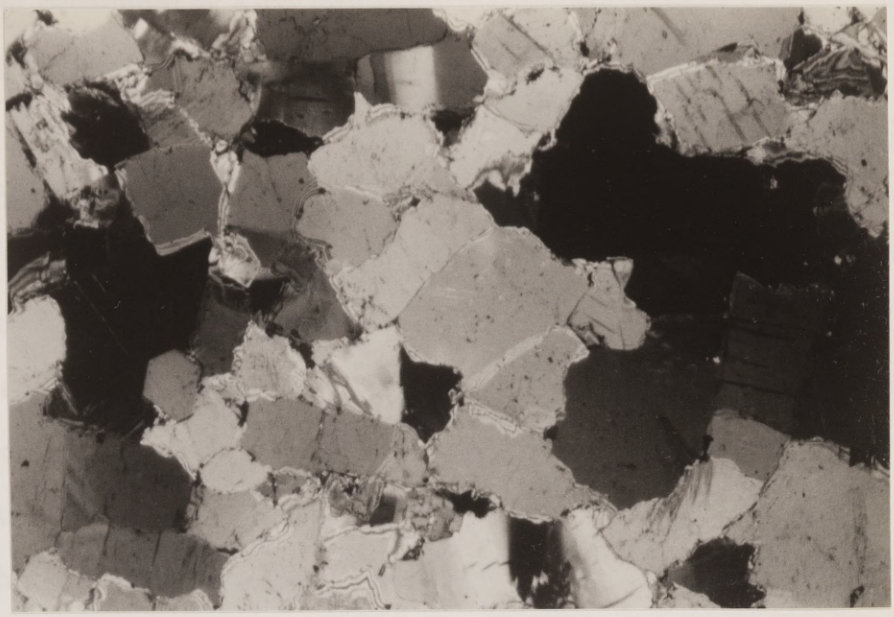

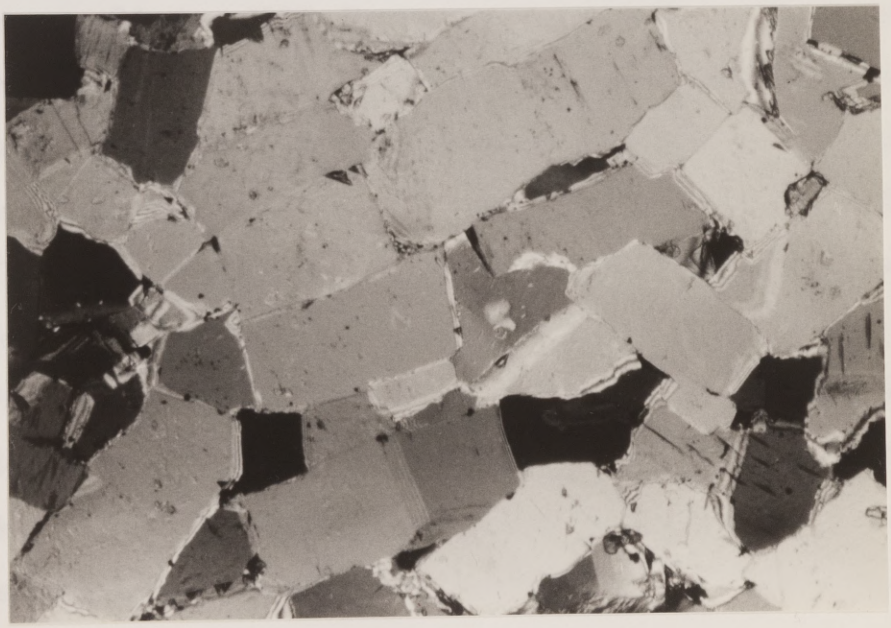

Siderite, determined by X-ray diffraction, is found throughout the lower anhydrite section in both core holes. It occurs as euhedral rhombic grains (0.3 to 1.0 mm) commonly intergrown with the anhydrite matrix (Fig. 3.20). Siderite is commonly observed from depths of 840 ft (HB3) and 800 ft (HH2) to the base of cap rock; its frequency appears to increase with depth. Two intense siderite-rich zones occur within HB3 at interval depths of 975 to 988 ft (Figs. 3.13 and 3.14d, i.e., 986.2 to 988.0 ft) and 1030 to 1032 ft (Figs. 3.13 and 3.14d, i.e., 1030.0 to 1031.3 ft). These zones consist of one to four ft thick intervals of approximately 10 % siderite.

Fractures and slickensides are commonly observed throughout the anhydrite cap rock but their density is greatest in the upper anhydrite zone (Figs. 3.13 and 3.15), and decrease markedly with depth (Fig. 3.13); e.g., in HH2 fractures were absent below a depth of 850 ft (Fig. 3.15). It is proposed that the reduction in fracture density may signify a decrease in the rate of diapiric uplift and indirectly a decrease in cap rock accumulation rates (Martinez, 1980). Fracture zones are typically 1 to 10 mm thick and healed with fine-crystalline Fe-sulfides and gypsum selvages of varying thicknesses (Fig. 3.16b, i.e., 606.0 to 608.0 ft). Locally, anhydrite-hosted fracture-fill sulfides are volumetrically significant. An example of this type of fracturing is observed in HB3 at a depth of 745.5 to 747.0 ft (Fig. 3.14c). Note that horizontal displacement is roughly 10 to 15 mm, whereas there has been very little vertical movement (5 mm) across the fracture. Fracture angles vary greatly ranging from near horizontal to vertical planes. Most small-scale faults in core cause slight vertical displacement (1 to 10 mm) of some anhydrite layers and sulfide laminae (Fig. 3.14d, e.g., 927.5 ft). Slickensides are present along some fault planes and have measured inclinations of 20 to 35 degrees (Fig. 3.16b, e.g., 637.1 ft).

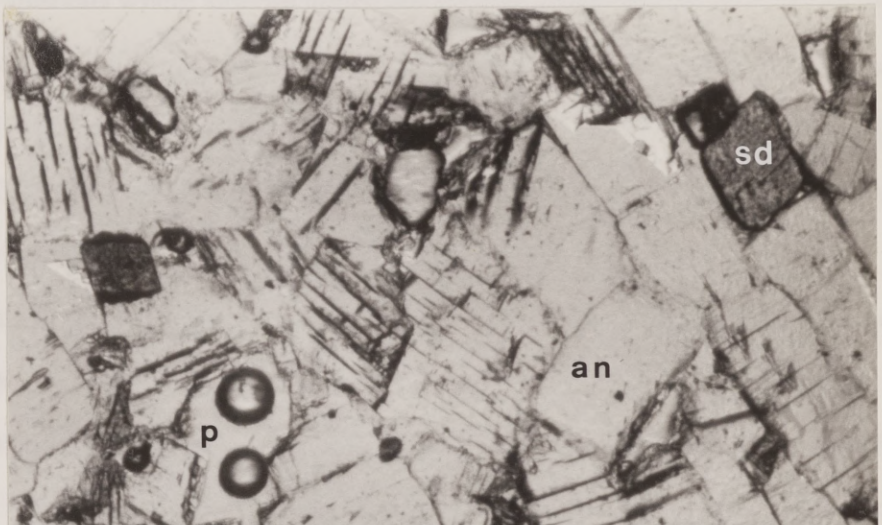

Fig. 3.20. Photomicrograph of porous anhydrite (an) with disseminated and slightly corroded siderite rhombs (sd); sample HH3-1046 occurs at base of cap rock. Porosity (p) ranges from 5 to 10 %. Photo width is 2.5 mm; transmitted plane polarized light.

Disseminated Fe-sulfides (marcasite/pyrite) are relatively uncommon within anhydrite cap rock, but in some intervals they are the most abundant sulfide type. They commonly appear as rhombic grains (i.e., sulfidized pseudomorphs of siderite) within the middle one-third of HB3 and the upper two-thirds of HH2 (Figs. 3.13 and 3.15). Barren intervals of disseminated sulfides occur within the lower 150 and 70 ft of HB3 and HH2, respectively, and correspond to a relative increase in siderite. It appears that in intervals where siderite grains are present, disseminated Fe-sulfides are rarely observed. Because they were difficult to quantify disseminated Fe-sulfides were treated as relative abundances; their distribution varying greatly over short distances (Figs. 3.13 and 3.15). However, a rough estimate of their concentration ranges from barren intervals to zones slightly in excess of 5 %.

Sandstone inclusions within anhydrite occur as spheroids (0.5 to 2.0 cm in diameter) and as thin wispy bands (approximately 0.5 to 2.0 cm thick) (Fig. 3.21). Concentrations of these features are significantly greater in HH2 than in HB3 (Figs. 3.13 and 3.15). However, thick sandstone intervals measuring 12 and 10 ft are observed at depths of 694.8 in HB3 (Fig. 3.13) and 921.0 in HH2 (Fig. 3.15). Some laminae with appreciable amounts of sulfides were observed only in HB3. Porosity of the sandstone inclusions was estimated to be between 5 to 10 % with moderate permeabilities.

Sulfide laminae are observed throughout the anhydrite section (Figs. 3.13 and 3.15). Their thickness ranges from less than one mm to extensive sulfide zones that may exceed several feet. Examples of these thick sulfide zones are generally restricted to the lower half of the anhydrite cap rock. Intervals with 20 % or greater combined metals occur at depths of 745.0 to 748.0 ft (Figs. 3.13 and 3.14c, i.e., 745.5 to

Fig. 3.21. Core photograph of sandy zones (white) in anhydrite cap rock; sample HH2-900.
Clastic material also occurs as isolated dark rimmed clusters.

747.3 ft), 934.0 to 935.0 ft (Fig. 3.13); and 985.0 to 991.0 ft (Figs. 3.13 and 3.14d, i.e., 986.2 to 988.0 ft) from HB3 and 646.0 to 651.0 ft (Fig. 3.15) and 681.0 to 724.0 ft (Figs. 3.15, 3.16c and d) from HH2. However, there is a noticeable decrease in combined metal concentrations within the upper anhydrite zone. This is exemplified by a decrease in sulfide laminae within the upper 320 ft of both core holes (Figs. 3.13 and 3.15). An exception is a 40-ft metal-rich interval in HH2 (Figs. 3.15, i.e., 611.0 to 651.0 ft, and 3.16b, i.e., 633.4 to 637.4 ft) that is slightly above an internal calcite zone.

Sulfide laminae generally appear laterally continuous within the restrictions provided by the scale of the core, although some laminae bifurcate and/or develop a wispy texture. Their inclination varies greatly ranging from horizontal to steeply dipping (45°) (Fig. 3.16b, e.g., 633.4 to 637.4 ft). Dramatic changes in their orientation and thickness are generally abrupt and lack an apparent stratigraphic relationship (Figs. 3.13 and 3.15). The overall inclination of anhydrite layers and sulfide laminae is slightly steeper in the upper two-thirds of both holes. However, in the lower 230 and 290 ft of the anhydrite section of HB3 and HH2, respectively, the inclination of anhydrite layers and sulfide laminae are near horizontal (Figs. 3.13 and 3.15). With the exception of this lower anhydrite zone, there does not appear to be a correlation between stratigraphic position and relative inclination of anhydrite layers and sulfide laminae.

Lower Calcite Zone

Located within the middle of HH2 a lower (internal) calcite zone interrupts a generally continuous anhydrite cap rock section. This zone consists of sulfide and dark gray calcite breccia clasts cemented by coarse-crystalline white calcite (Fig. 3.16c). This disturbed sequence is the most heavily mineralized section of the cap rock and is

thought to represent calcite replacement of previously mineralized anhydrite (Kyle and Agee, 1988). Sulfide concentration is anomalously high within this zone and consists of Fe-sulfides, sphalerite, and galena. Late-stage barite also occurs within the lower half of this calcite zone.

Calcite from HH2 ranges from 672 to 724 ft (52 ft thick) and is surrounded by a thin one to four ft thick selenite zone (Fig. 3.15). The upper 12 ft of the calcite zone consists of brecciated calcite clasts cemented by coarse-crystalline white calcite (Figs. 3.15 and 3.16c, e.g., 684.8 to 685.8 ft). Locally, some of these calcite clasts are weakly banded (Figs. 3.15, e.g., 680.0 to 690.0 ft, and 3.16c). Sulfide concentrations within this zone are relatively minor compared to the remaining 42 ft of calcite core. From a depth of 681.0 to 724.0 ft calcite is characterized by brecciated sulfide and calcite clasts of varying dimensions (1 to 6 cm) cemented by a fine-crystalline sulfide matrix (Figs. 3.16c and d) and coarse-crystalline white calcite (Fig. 3.16c, e.g., 693.8 to 697.6 ft). Some of the sulfide matrix is due to late-stage sulfide precipitation. However, a significant portion may have formed as sulfides were detached from their anhydrite substrate during host-rock dissolution and microbial alteration to calcite.

Sandstone inclusions within the lower calcite appear as spheroids (1 to 5 mm diameter) and ameboid-like sandy bodies (2 to 15 cm) (Fig. 3.16d, i.e., 701.7 to 705.6 ft). They are generally restricted to the middle third of this calcite zone (Fig. 3.15) and are cemented by fine-crystalline sulfides. Within and just below this sandy zone many small seams of barite (1 to 20 cm thick and approximately 20 volume %) locally occur from 700.0 to 714.0 ft (Figs. 3.15 and 3.16d, i.e., 711.5 to 712.3 ft). Some sections of barite are interlaminated with thin sulfide bands (1 to 6 mm thick)

(Fig. 3.16d, i.e., 712.9 to 713.5 ft). Porosity in the lower calcite cap rock is primarily due to fracturing with a lesser extent due to vugs.

Gypsum Zone

From a depth of 386 to 394 ft (HB3) and 370 to 377 ft (HH2) there is a transition zone in which anhydrite has progressively hydrated to gypsum. Within this interval, cap rock composition varies between 15 to 80 % gypsum (Figs. 3.13 and 3.15). Above the transition zone the cap rock is composed almost entirely of gypsum, having only a few percent of remnant anhydrite. For example in HH2, a limited number of anhydrite clasts (2 to 8 cm in length) are preserved within gypsum (Fig. 3.16a, e.g., 354.0 to 354.3 ft). Gypsum cap rock is medium to dark gray and is characterized as a massive featureless zone in which pre-existing textures have apparently been destroyed during hydration (Fig. 3.14b, i.e., 365.6 to 367.5 ft). Only a limited number of sulfide laminae are observed within this zone. However, significant amounts of disseminated Fe-sulfides are present in HH2, whereas few are observed in HB3 (Figs. 3.13 and 3.15).

Upper Calcite Zone

The top of calcite cap rock in HB3 and HH2 (estimated from rotary lithologic cuttings) occurs at depths of 339 and 338 ft and extends downward approximately 25 and 10 ft, respectively (Figs. 3.13 and 3.15). In HB3, upper calcite cap rock consists of broken and disrupted bands (2 to 6 mm thick) of dark gray, fine-crystalline calcite. Porosity in this zone occurs primarily in horizontal vugs (Fig. 3.22). However, vuggy porosity is more abundant in the middle to lower section of calcite cap rock (Figs. 3.13 and 3.14a). A drusy coating of calcite lines all pores. Porosity within the lower 10 ft is markedly decreased by late-stage coarse-crystalline selenite. Within this interval,

Fig. 3.22. Core photograph of broken and disturbed bands in upper calcite cap rock; sample HB3-350.
Porosity is abundant and subhorizontal.

Fig. 3.23. Core photograph of angular sandstone inclusions in upper calcite cap rock; sample HB3-359.

angular sandstone inclusions are common with maximum dimensions ranging to 5 cm (Figs. 3.15 and 3.23).

Anhydrite Cap Rock Diagenesis

The anhydrite portion of Hockley Dome cap rock was formed by salt dissolution and accumulation of anhydrite crystals. Examination of anhydrite dissolved from halite and petrographic evidence from cap rock supports the theory that anhydrite originated in the salt stock. The narrow transition zone between halite and indurated anhydrite appears to require compaction and recrystallization shortly after halite dissolution. The anhydrite zone is considered to have formed by salt dissolution in a moderately high-temperature saline environment. The anhydrite has been deformed and recrystallized into a moderately well developed granoblastic texture. Experimental deformation studies show that anhydrite is brittle and will fracture at low confining pressures (< 1 kbar) and temperatures but will deform by recrystallization at higher temperatures (> 75°C) and pressures (> 1 kbar) (Muller and Siemes, 1974).

The anhydrite zone of cap rock developed in an environment in which anhydrite, and not gypsum, was the stable phase. Computer modeling (using PHREEQE; Parkhurst et al., 1982) of salt dome-related solutions was used to examine anhydrite and gypsum stability under a variety of geochemical conditions (Appendix II). The most notable effect on the saturation state of gypsum and anhydrite is the temperature of reaction. Salinity and pCO_2 of the solution(s) had little effect on stability fields of calcium sulfate phases. Results indicate that at temperatures of roughly 75°C and greater, gypsum is no longer the stable calcium sulfate phase. This conclusion agrees with experimental studies which indicate that the solubility of anhydrite in water

decreases rapidly with increasing temperature (Holland and Mallinin, 1979). However, recent data indicate that anhydrite stability occurs at temperatures of roughly 50°C and greater. Solutions originally modeled by PHREEQE were reexamined using PHREPITZ (a modified PHREEQE program that includes Pitzer equations; Parkhurst et al., 1987; Appendix II). PHREPITZ is particularly useful when calculating solution/mineral equilibria under highly saline conditions ($\geq$ 100,000 ppm TDS). By nature, cap rock forming solutions are extremely saline; therefore, modeling results utilizing PHREPITZ are more representative of actual solution chemistry than PHREEQE.

The general size and morphology of anhydrite crystals in Hockley cap rock are very similar to those present in the Hockley salt mass. Sulfur isotope ratios of anhydrite cap rock and salt-hosted anhydrite are also similar. Anhydrite cap rock from a single drill hole (HH3) yields $\delta^{34}S$ values that range from +16.1 to +16.9 ‰ with a mean of +16.4 ‰ (6 analyses; Table I; Appendix III). These $\delta^{34}S$ values are identical within 1 ‰ of salt-hosted anhydrite measured from several Gulf Coast salt domes (+16 $\pm$ 1 ‰) (Feely and Kulp, 1957; Claypool et al., 1980; Posey et al., 1987). Also, these $\delta^{34}S$ values from HH3 lie within the range of Middle Jurassic seawater as defined by Claypool et al. (1980). However, an earlier study reported $\delta^{34}S$ values (approximately +18 to +20 ‰; 4 analyses) from Hockley anhydrite cap rock that are about 3 to 4 ‰ heavier than salt-hosted anhydrite (Price and Kyle, 1986). Posey et al. (1987) suggested that during cap rock formation part of the anhydrite is dissolved, then reduced, leaving a residual heavy sulfate fluid which eventually forms isotopically heavy anhydrite. This relationship involving partial reduction and mixing of aqueous sulfate is not consistent with the most recent data from HH3 (Table I). $\delta^{34}S$ values

Table I. $\delta^{34}S$ ‰ composition of anhydrite cap rock in core HH3.

Sample no.	Anhydrite	Description:
601	+16.57	massive gray section
601 pl	+16.55	pale 2 cm band
701	+16.90	massive gray section
799	--	massive gray section
902	+16.14	massive gray section
1010	+16.18	massive gray section
1043	+16.38	massive gray section

Sample no. represents subsurface depth in feet; see Figure 6.1 for drill hole location.
Sample HH3-601 was collected 3 cm above HH3-601 pl; see Figure 3.19a for photograph.
Sample HH3-799 was not analyzed.

from HH3 and PHREEQE/PHREPITZ calculations suggest that anhydrite remained stable during salt dissolution and residue accumulation.

Further support of the residual accumulation hypothesis is that anhydrite- and salt-hosted carbonate rhombs possess similar dimensions (0.2 to 1.0 mm in length). Some quartz crystals, like carbonate rhombs, appear to be related to a residual material derived from salt stock. However, the morphology and size of quartz crystals in the cap rock vary considerably with respect to salt. Salt-hosted quartz is generally smaller and occurs as clusters of terminated prisims (Fig. 3.6). Cap rock quartz appears as overgrowths nucleating on detrital quartz and on salt-derived quartz clusters. This suggests that quartz overgrowths may have developed during halite dissolution and anhydrite accumulation. In general, cap rock quartz occurs as euhedral, doubly terminated crystals (Fig. 3.24) with rare twinned intergrowths. They are observed throughout the anhydrite section but appear to be concentrated within and near sulfide laminae.

Inclusions of terrigenous sediments commonly occur within Hockley cap rock. Examples of these zones are 12 and 10 ft thick sand-rich intervals described in HB3 and HH2, respectively. Porosity of these massive sandstones is estimated to range between 5 to 10 %. Permeability measurements from similar zones located within HB1 and HB2 range from 0.2 to 0.7 md (Hallager, 1984). Detrital mineralogy of included zones from HB3 and HH2 consists of fine-grained, rounded quartz and rock fragments with minor amounts of anhydrite and euhedral pyrite. There are at least two mechanisms by which clastic intervals could have been incorporated within anhydrite cap rock: (1) emplacement of originally deposited terrigenous clastics into the salt stock along the highly sheared diapiric boundaries, which eventually plate onto cap rock

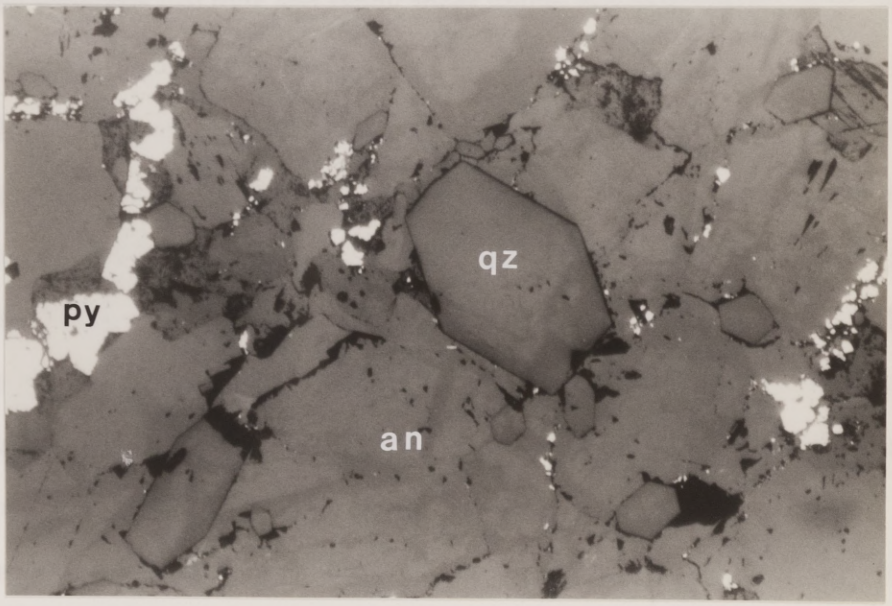

Fig. 3.24. Photomicrograph of euhedral quartz (qz) and interstitial Fe-sulfides (py) intergrown with anhydrite (an) cap rock; sample HH2-878.
Many euhedral quartz crystals have detrital quartz cores. Photo width is 1.2 mm; reflected light.

(Seni, 1987) and (2) salt stock residue that is concentrated in cap rock by intense dissolution of anhydrite and halite (Hallager, 1984).

According to Hallager (1984) the mineral constituents of these "sandy" included zones (at HB1 and HB2) are similar to those of salt residue. Both zones are dominated by anhydrite, quartz, and carbonate. Quartz was reported as euhedral, doubly terminated overgrowths on rounded quartz cores. This observation supports the theory that anhydrite cap rock and sandy zones within cap rock formed under similar conditions. However, clastic ("sandy") zones from HB3 and HH2 are characterized by rounded quartz grains and rock fragments (coated with an iron oxide stain) which is indicative of a detrital origin (E. McBride, pers. commun., 1989). Several intervals from these zones were sampled and examined under both a Zeiss binocular scope and a scanning electron microscope (Appendix IV). Examples of doubly terminated quartz were not observed. Also, "sandy" zones from HB3 and HH2 occur at different depths and are separated by 231 ft in elevation. The irregularity of their depths and localized position within the cap rock suggests that sediment inclusions were randomly incorporated within the salt mass and later plated onto anhydrite. Clearly, laterally extensive zones at uniform depths are required if intense dissolution of salt and anhydrite is to be considered as a possible mechanism responsible for sandy zone development. Therefore, based on the detrital quartz textures and the direct analogy of similar structures observed at Boling dome (Fig. 2.2), it appears from the studied core holes that the clastic zones within anhydrite cap rock are a result of incorporated terrigenous clastics within a rising salt stock, as described by Seni (1987).

Timing of Anhydrite Cap Rock Formation

The presence of cap rock on Hockley salt dome is evidence of dissolution of salt over a lengthy period of time. It is reasonable to assume that cap rock thickness provides an indirect measure of the amount of salt dissolved during diapirism (Martinez, 1980). This cap rock record can be used, with caution, as a basis for determining the growth history of Hockley Dome. The use of cap rock data for a salt dome study is contingent upon a proper understanding of the accumulation and diagenesis of anhydrite. The hypothesis of "residual accumulation" has been adopted as the mode of origin for anhydrite cap rock (Murry, 1966; Posey and Kyle, 1988). Assuming that this is correct, the timing of cap rock formation can be estimated by calculating the volume of salt that must be dissolved to leave the necessary residue of anhydrite. It can then be compared with the geologic history of the salt dome to determine the event(s) in which enough salt was extracted from the rim syncline to account for the dissolved salt. Thickness variations observed in surrounding strata indirectly permit the volumes and rates of salt flow to be measured and thereby determine an incremental cap rock growth history.

In an attempt to determine the age of anhydrite cap rock the following assumptions were made: (1) Based on present cap rock thickness of 910 ft of anhydrite and 25 ft of calcite the average original anhydrite cap rock thickness over the crest of the dome was approximately 940 ft. Chemical conversion of anhydrite to calcite results in an overall volume reduction (Kreitler and Dutton, 1983). Therefore, a section of calcite, 25 ft thick converts to approximately 30 ft of original anhydrite. (2) The average residue content within the salt stock was 5 %. This value, determined by the United Salt Company from mine production, is considered more valid for the salt stock than the

2 % residue measured by Hallager (1984). (3) The source of salt in a diapir is from local mother salt. The volume and rate of salt flow into the diapiric structure can be approximated by the volume of rim syncline sediments that developed within the salt-withdrawal basin. Subsequently, the volume of salt migrating into a diapir can be calculated by measuring the increase in volume of overthickened sediments for that time period. (4) The effect of sediment compaction was not considered. Calculations from the Hockley withdrawal basin regarding volumes and rates of salt flow are based on the present (compacted) volumes of sediments rather than on uncompacted volumes. (5) The salt stock beneath the cap rock is deeply rooted and presumably remains in communication with the underlying mother salt unit. Even though the dimensions of the salt column are certain to vary with depth, salt volume calculations assumed that the diapir radius is approximately 6,750 ft (Halbouty, 1979) and that the salt column is approximately 35,000 ft deep (Ewing, 1986). (6) Cap rocks formed along with diapirism. In the case of Hockley Dome, this assumption strictly dictates that negligible amounts of cap rock were formed during the early pillow stage of halokinesis. Although there is no direct evidence to support this assumption, it appears that because there is little difference between the volume of mobilized pillow salt and the resultant sediment thicknesses, only a minor amount of salt is dissolved during pillow stage development (Seni and Jackson, 1984; S. Seni, pers. commun., 1990). Seismic data from the Katy/Hockley area suggest that pillow stage growth is a late Mesozoic event (Ewing, 1986). (7) Anhydrite was not dissolved and removed from the diapir site; that is, the amount of anhydrite originally present in the salt stock is now entirely preserved in the cap rock. The following discussion is contingent upon the above conditions.

It is inferred that the volume of dissolved salt necessary to form the Hockley cap rock is approximately 16 mi^3 (Table IIa). This calculated volume assumes that accumulation and compaction of anhydrite residue took place in a closed chemical system, i.e., there was no net loss of anhydrite due to residue dissolution. In addition, 34 mi^3 of diapiric salt stock also remains directly under the cap rock (Table IIb). Therefore, an estimated 50 mi^3 of salt appears to have migrated from the Louann Salt to account for the diapiric structure and overlying cap rock (Table IIc). Movement of 50 mi^3 of salt should theoretically result in an equivalent volume of overthickened sediments within the salt-withdrawal basin. Total rim syncline sediments at Hockley Dome are approximately 54 mi^3 (Table III). This estimate is based on a combination of local cross-sections (Figs. 2.5, 2.6, and 2.7) and structure and isopach maps generated on the Wilcox, Claiborne, and Vicksburg/Jackson strata (Ewing, 1986). Principles established by Seni and Jackson (1984) were used to calculate the volume of sediment overthickening in the Hockley salt-withdrawal basin.

There is close agreement between the volume of salt movement into the dome and the resultant development of salt-withdrawal sediments. Given the number of assumptions relied upon to estimate salt and sediment volumes, it is conceptually satisfying that their volumes differ by only 4 mi^3 (approximately 10 %) (Table IIc). This difference is acceptable considering that calculated volumes of diapiric salt, that dissolved to form anhydrite cap rock, are sensitive to the percentage of the salt-hosted residue (e.g., 40 mi^3 of salt is required at 2 % residue; Table IIa). Another sensitive factor is the volume of overthickened sediments within the salt-withdrawal basin; this can be misleading if the basin boundaries are poorly selected. Definition of the salt-withdrawal basin boundaries is subjective and at Hockley is complicated by interference of neighboring salt domes. Local rim anticlines proved to be the best sedimentological

Table IIa. Volume of salt dissolved from Hockley Dome to form its cap rock.

Cap rock thickness (anhydrite and adjusted calcite)	940 ft	
Cap rock radius	6,250 ft	
Cap rock volume	1.15×10^{11} ft^3	
Residue (anhydrite) content of Hockley salt stock	5%	2%
Amount of salt dissolved	16 mi^3	40 mi^3

Table IIb. Volume of diapiric salt beneath Hockley Dome cap rock.

Vertical column of salt[1,2]	35,000 ft
Salt stock radius[3]	6,750 ft
Salt stock volume	34 mi^3

1 depth infered from regional cross-section over San Felipe Dome (Ewing, 1986)
2 1000 vertical feet of salt = roughly 1 mi^3
3 determined from Halbouty (1979)

Table IIc. Mass balance of Hockley diapiric salt and overthickened sediments.

Amount of salt dissolved (at 5% residue)	16 mi^3	
Column of salt beneath cap rock (based on 35,000 ft)	34 mi^3	
Volume of evacuated salt	Total: 50 mi^3	
Volume of overthickened sediments	54 mi^3	

Table III. Timing and volumes of overthickened sediments surrounding Hockley Dome.

Stratigraphic Interval	Overthickened Sediments*	Cap Rock Accretion**	Age (Ma)	Accretion Rate (ft/m.y.)
Lower Wilcox[1]	20 mi^3	350 ft	56 - 52	87.5
Middle and upper Wilcox[1,3]	7 mi^3	110 ft	52 - 48	27.5
Claiborne[2]	8 mi^3	140 ft	48 - 40	17.5
Vicksburg and Jackson[2,3]	4 mi^3	70 ft	40 - 31	7.8
Catahoula (Frio)[2]	12 mi^3	210 ft	31 - 24	30.0
Subtotal:	(51 mi^3)	(880 ft)	(32)	Ave. (27.5)
Lagarto, Oakville, Goliad, and younger[2]	3 mi^3	60 ft	24 - 0	2.5
Total:	54 mi^3	940 ft	56	Ave. 16.8

* Volume of overthickened sediments is considered equivalent to the volume of salt that flowed into the dome. Volume calculations done by grid overlay.

** Cap rock thicknesses are incremental and range from top to bottom.

1 from seismic data (Ewing, 1986)

2 from electric log data (this study)

3 calculated from structure and isopach maps (Ewing, 1986)

guide to define the basin extent. Despite the above problems, results of this study represent an approximation of cap rock growth history based on salt flow and sediment overthickening relationships.

Thickness variations in surrounding strata indirectly permit the incremental timing of cap rock formation to be recognized and estimated. Sediment thickening in the Hockley withdrawal basin consists of approximately 54 mi^3 that has been subdivided according to defined stratigraphic units (Table III). The Wilcox Group represents the lowest stratigraphic unit associated with the initial stages of salt dipirism (approximately 56 Ma). This unit corresponds to early cap rock formation and, based on the underplating concept, represents the upper half (roughly 460 ft) of Hockley Dome cap rock (Table III). This thickness estimate is based on the assumption that cap rock accumulation is in direct response to salt dissolution. An extrapolation of this relationship yields estimates of cap rock growth during Claiborne and Vicksburg/ Jackson time. Approximately 140 and 70 ft of anhydrite cap rock formed during these depositional events, respectively. Interpretation of geologic cross-sections across Hockley Dome shows a massive rim syncline in the Catahoula Group (Frio Formation) (Figs. 2.6 and 2.7). The overthickened volume of this Upper Oligocene unit is approximately 12 mi^3 and is associated with major post-Wilcox salt movement into the diapir (Table III). Consequently, the formation of roughly 210 ft of cap rock at Hockley Dome is considered to have developed during this event (roughly 31 to 24 Ma). Miocene and younger sediments overlie the Catahoula Group and appear to correspond to the lowest 60 ft of cap rock.

Although halokinetic growth may be dated by stratigraphic effects produced in the withdrawal-basin sediments, the exact age and volume of sedimentary units are difficult to define precisely. It is evident that salt dome cap rock preserves a record of geologic

processes. The interpretation of this record does not yield unequivocal solutions, therefore, cap rock and diapir growth rates determined solely on sedimentation events may not be exact. Nevertheless, the average rates of diapir growth (and indirectly anhydrite accumulation) at Hockley Dome (as estimated by sediment response to salt withdrawal) compare favorably with published results of Northern Louisiana (i.e., Winnfield Dome; Kyle et al., 1987) and East Texas salt domes (Seni and Jackson, 1984).

For example, rates of halokinetic growth for Winnfield Dome are well constrained by paleomagnetic reversals identified within the cap rock. The average cap rock accretion rate for Winnfield Dome is roughly 15 ft/m.y. (Kyle et al., 1987). By comparison, the average accretion rate for anhydrite cap rock at Hockley is approximately 27.5 ft/m.y. (if for the moment the lower 60 ft of anhydrite is not considered in the cap rock accretion rate calculations) (Table III). Calculations indicate that Hockley has a greater average cap rock accretion rate than Winnfield, however, it appears that both domes have similar diapir growth rates. That is, the vertical movement of Hockley and Winnfield salt through a cross-sectional area of the diapiric neck is roughly equivalent per unit of time. To equate Hockley and Winnfield Dome diapir rates the difference in the percent of salt-hosted anhydrite must be considered. For example, to account for 27.5 ft (one m.y.) of Hockley anhydrite cap rock, approximately 550 vertical feet of salt stock (at 5 % anhydrite content in salt; Table IIa) must be dissolved. A comparable amount of Winnfield salt (roughly 500 vertical feet) containing an average of 3 % anhydrite is required to accrete 15 ft of anhydrite cap rock over the same period of time (one m.y.) (Kyle et al., 1987).

Also, estimated diapir growth rates for Hockley (550 ft/m.y.) and Winnfield (500 ft/m.y.) Domes yield values within the same order of magnitude of growth-rate curves for many of the East Texas Basin diapirs. Seni and Jackson (1984) have calculated maximum vertical growth rates in the range of 300 to 1000 ft/m.y. Similar growth rates may have been attained during the early stages of Hockley salt diapirism (Wilcox time). These results, based on a model of sediment response to salt withdrawal, suggest that the average rate of diapir growth and anhydrite accretion at Hockley are compatible with other domes in adjacent salt basins. These comparisons provide an indirect means of testing the growth history of Hockley salt dome and, thus, age determinations of anhydrite cap rock accumulation.

Chapter 4

SULFIDE CONCENTRATIONS

Ore Reserves

An extensive assay data set exists for Hockley Dome cap rocks as a result of a minerals exploration program that involved the drilling of sixty-five core tests during 1980-82. All core holes were rotary drilled through supracaprock sediments, including the upper portion of calcite cap rock in some holes. Continuous core was then drilled to the salt stock, and core recovery was generally complete. Assay data for all core holes consists of selected intervals that contain visible sulfide concentrations. Geochemical analyses of mineralized zones were generally assayed in one-foot intervals for Pb and Zn by atomic absorption, with selected intervals analyzed for other elements including Fe, Ag and Cd (Appendix I). Although Fe sulfides are generally concentrated with sphalerite and galena in the same intervals, Fe was rarely assayed because of its lack of commercial interest. Intervals not assayed were assumed to contain only minor metal concentrations and were treated as barren host rock for this study.

The cap rock interior represents a normal salt dissolution environment in which anhydrite accumulated with little sulfide precipitation. However, the highest metal sulfide concentrations identified during the drilling project at Hockley occur in a discontinuous annular zone within the cap rock perimeter. This zone consistently contains relatively minor amounts of combined Pb+Zn (at least totalling 10 ft %) (Fig. 4.1). High grade metal-rich zones occur in the northwestern and southern periphery of the cap rock and have total Pb+Zn concentrations that exceed 300 ft % (Fig. 4.1). The western margin of the dome contains lesser metal concentrations

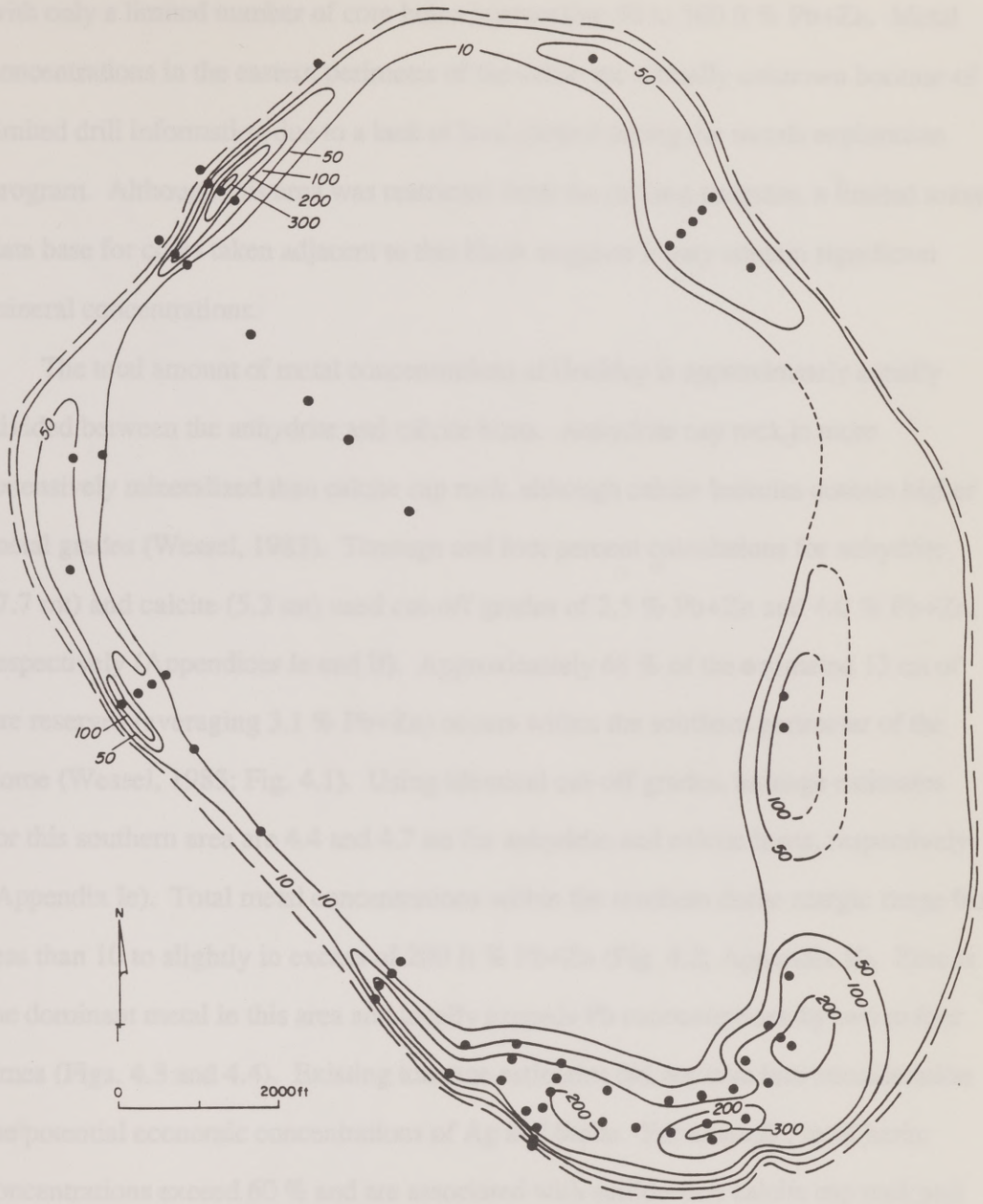

Fig. 4.1. Plan map of Hockley Dome showing isopach thickness of ft % Pb+Zn. Note that greatest metal concentrations are in the southern portion of the dome. Dashed outermost line represents the inferred extent of sulfide mineralization. Data are shown in Appendix If. (See text in Appendix I for additional information on methods of calculation.)

with only a limited number of core holes intersecting 50 to 100 ft % Pb+Zn. Metal concentrations in the eastern perimeter of the dome are virtually unknown because of limited drill information due to a lack of land control during the metals exploration program. Although this area was restricted from the drilling program, a limited assay data base for cores taken adjacent to this block suggests it may contain significant mineral concentrations.

The total amount of metal concentrations at Hockley is approximately equally divided between the anhydrite and calcite hosts. Anhydrite cap rock is more extensively mineralized than calcite cap rock, although calcite breccias contain higher metal grades (Wessel, 1983). Tonnage and foot percent calculations for anhydrite (7.7 mt) and calcite (5.3 mt) used cut-off grades of 2.5 % Pb+Zn and 4.0 % Pb+Zn, respectively (Appendices Ie and If). Approximately 68 % of the estimated 13 mt of ore reserves (averaging 3.1 % Pb+Zn) occurs within the southern perimeter of the dome (Wessel, 1983; Fig. 4.1). Using identical cut-off grades, tonnage estimates for this southern area are 4.4 and 4.7 mt for anhydrite and calcite hosts, respectively (Appendix Ie). Total metal concentrations within the southern dome margin range from less than 10 to slightly in excess of 200 ft % Pb+Zn (Fig. 4.2; Appendix If). Zinc is the dominant metal in this area and locally exceeds Pb concentrations by two to four times (Figs. 4.3 and 4.4). Existing tonnage estimates did not take into consideration the potential economic concentrations of Ag and barite. For example, local barite concentrations exceed 60 % and are associated with sulfide-rich calcite cap rock and supradome sediments (Kyle and Price, 1985). Substantial Ag concentrations are indicated by Ag assay data, with the bulk of the proven reserves located within the southern perimeter of the dome.

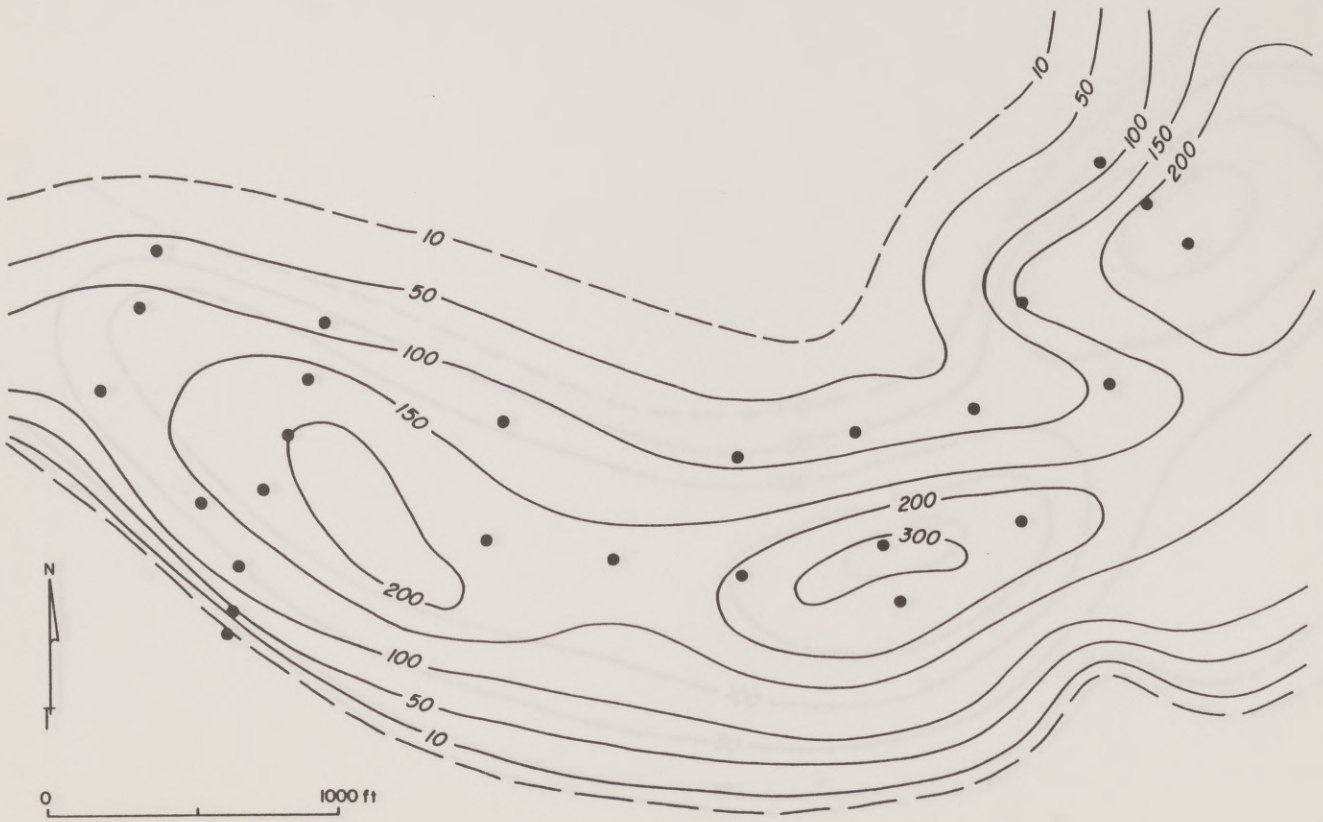

Fig. 4.2. Plan map of southern Hockley Dome showing isopach thickness of ft % Pb+Zn. Dashed outermost line represents the inferred extent of sulfide mineralization.

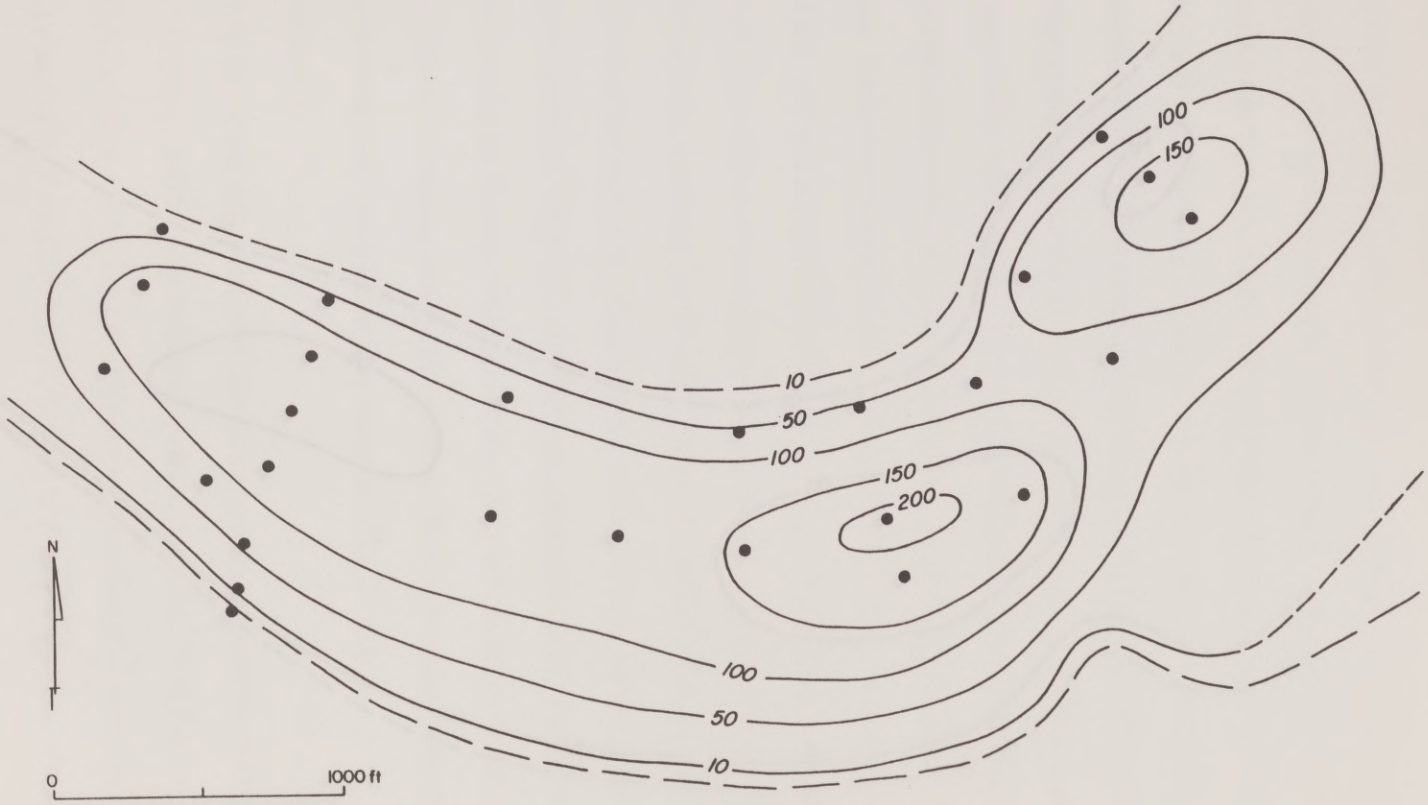

Fig. 4.3. Plan map of southern Hockley Dome showing isopach thickness of ft % Zn. Dashed outermost line represents the inferred extent of sulfide mineralization.

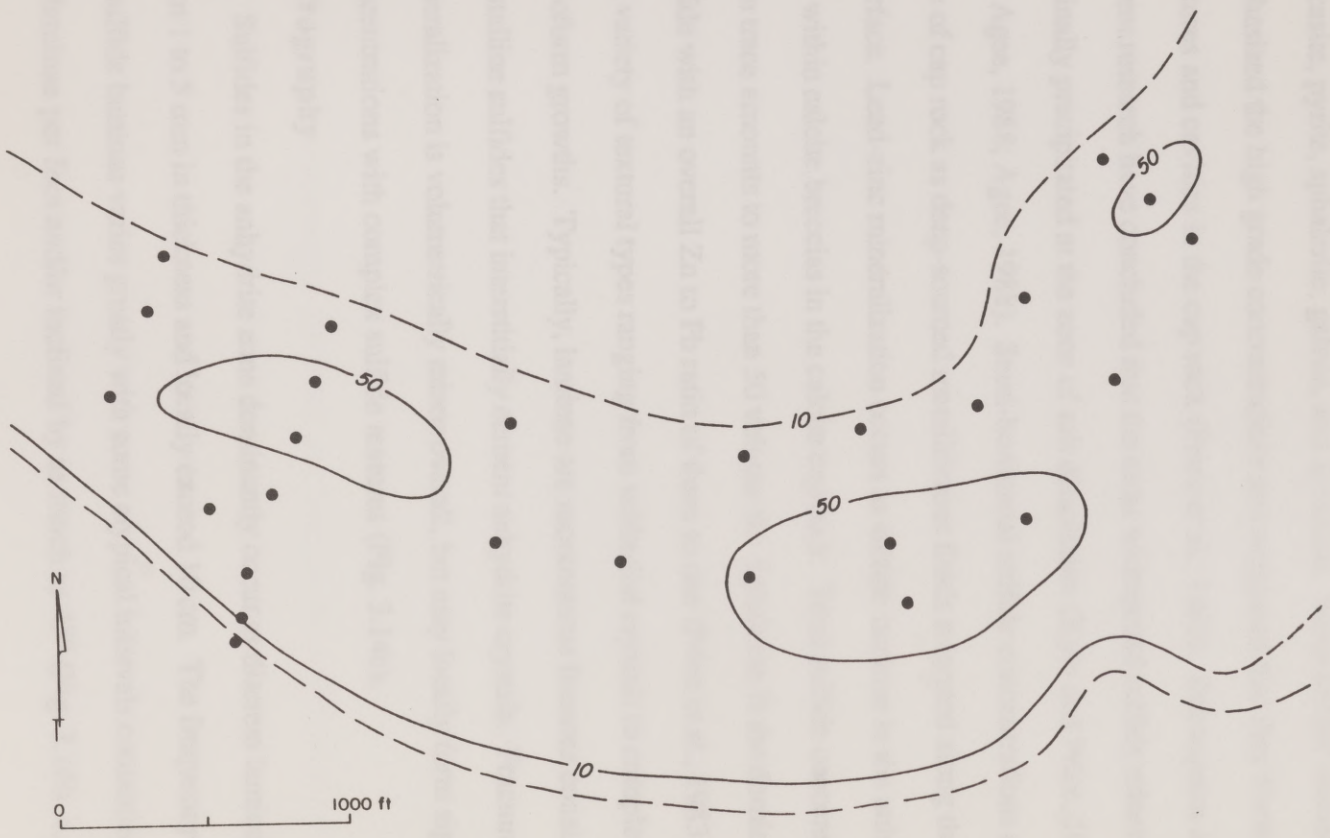

Fig. 4.4. Plan map of southern Hockley Dome showing isopach thickness of ft % Pb. Dashed outermost line represents the inferred extent of sulfide mineralization.

Anhydrite-Hosted Sulfides

General

Sulfide minerals observed at Hockley are, in order of decreasing abundance: marcasite, pyrite, sphalerite, galena, and acanthite. Some earlier studies at Hockley emphasized the high grade concentrations and suggested that they formed along late fractures and cavities in the cap rock (Price et al., 1983). Subsequent studies and current research have concluded that the most widespread sulfide mineralization originally precipitated at the zone of salt dissolution (Kyle and Price, 1985; 1986; Kyle and Agee, 1988; Agee, 1988). Semi-horizontal sulfide concentrations developed at the base of cap rock as deep-sourced metalliferous fluids migrated along the salt/anhydrite interface. Lead-zinc mineralization occurs as sulfide laminae in the anhydrite cap rock and within calcite breccias in the calcite cap rock. Total sulfide concentrations range from trace amounts to more than 50 volume %. Sphalerite is the dominant economic sulfide with an overall Zn to Pb ratio of three to one (Price et al., 1983). Sulfides occur in a variety of textural types ranging from subhedral crystals to complexly banded colloform growths. Typically, laminae are monotonous features consisting of fine-crystalline sulfides that interstitially cement anhydrite crystals. Fracture-related sulfide mineralization is volumetrically minor overall, but may locally form significant concentrations with complex sulfide textures (Fig. 3.14c).

Petrography

Sulfides in the anhydrite zone dominantly occur as discrete laminae that range from 1 to 5 mm in thickness and locally exceed 10 cm. The frequency and orientation of sulfide laminae varies greatly with some atypical intervals containing as many as 10 laminae per foot and/or inclined by as much as 45° (Fig. 3.16b, e.g., 633.4 to

637.4 ft). Some sulfide laminae occur as wispy, irregular zones with poorly defined boundaries. These sulfide laminae/zones are stratiform deposits that appear laterally continuous. By analogy to Winnfield Dome (Ulrich et al., 1984), individual laminae may be traced laterally tens of feet within the anhydrite cap rock. Variable amounts of marcasite, pyrite, sphalerite, and galena form local massive sulfide intervals (Fig. 4.5).

Sulfides commonly occur as interstitial cements of anhydrite grains and colloform aggregates that form on anhydrite substrates. Marcasite and pyrite are the dominant intercrystalline sulfide cements of anhydrite grains (Fig. 4.6a); residues from laboratory dissolution of anhydrite provides the "boxwork" textural type discussed in the subsequent sulfur isotope section (Fig. 4.6b). Marcasite generally occurs as fine-crystalline anhedral aggregates that are commonly intergrown with pyrite. However, in some petrographic sections pyrite is the dominant Fe-sulfide. Sphalerite and lesser amounts of galena also occur as interstitial cements between anhydrite crystals. Sphalerite cement occurs as heavy rinds and as small colloform spheres (roughly 100 microns) on anhydrite crystals. Sphalerite is microcrystalline and appears in hand specimen as dark brown to a tan chalky material (Fig. 4.5). Most "boxwork" sulfides exhibit impressions of relatively flat surfaces that commonly posses geometric, step-like ridges (Fig. 4.6c) resulting from growth on a striated, anhydrite crystal substrate (Fig. 3.4).

Textural relationships and metal and isotopic compositions of sulfide layers in anhydrite cap rock suggest that discrete episodic pulses of deep metalliferous brines entered the cap rock and formed each sulfide laminae. Anhydrite grains that are completely surrounded by sulfides are euhedral and undeformed; grains outside the mineralized zone are deformed and sutured (Ulrich et al., 1984). Clearly, sulfide

Fig. 4.5. Core photograph of steeply inclined sulfide laminae (roughly 45°) consisting of marcasite, pyrite, sphalerite and galena within anhydrite; sample HB3-934.

Fig. 4.6a. Photomicrograph of interstitial Fe-sulfides (py) cementing anhydrite crystals (an); sample HH2-404.
Euhedral anhydrite grains are observed when surrounded by sulfides. Note the sharp nature of the contact between sulfides and sulfates. Photo width is 2.5 mm; reflected and transmitted light.

Fig. 4.6b. SEM photomicrograph of interstitial Fe-sulfides separated from anhydrite cap rock; sample HH2-404.
Note the impressions left by euhedral anhydrite grains within the sulfide residue (i.e., boxwork texture). SEM photo width is 1.5 mm.

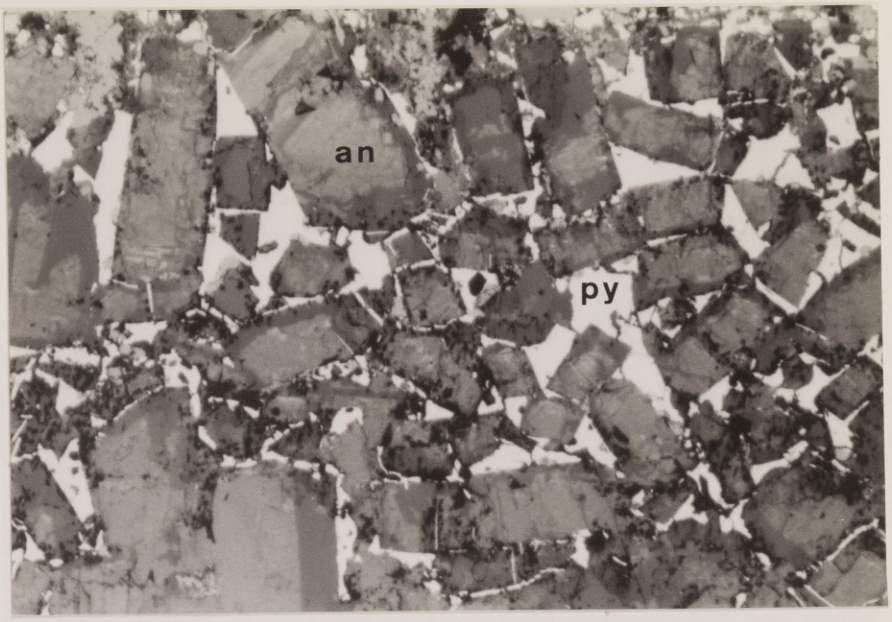
an
py

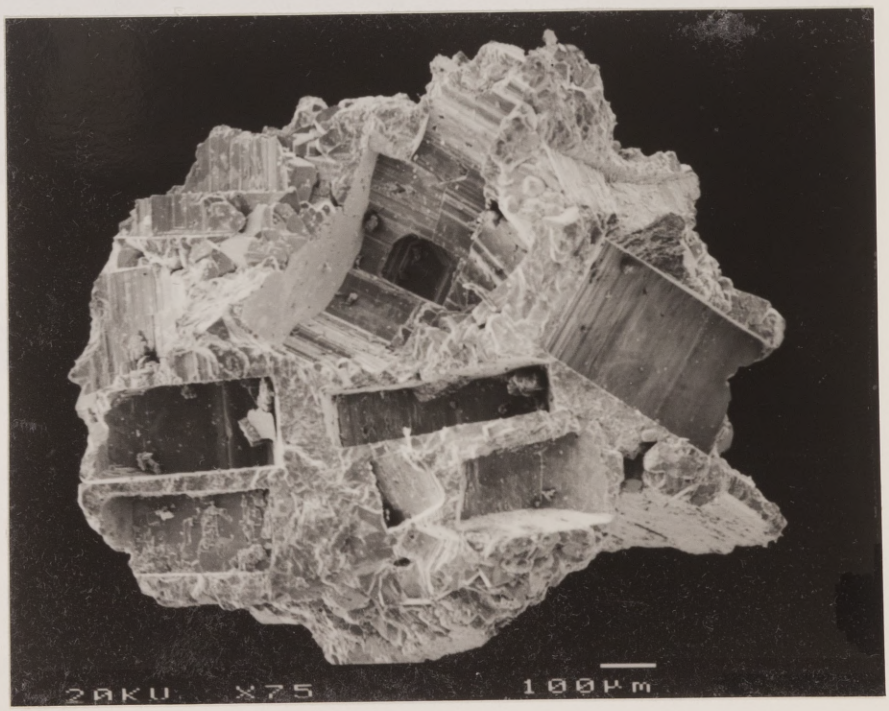
20KU X75
100µm

Fig. 4.6c. SEM photomicrograph of boxwork Fe-sulfide exhibiting geometric impressions left by anhydrite grain; sample HH2-404.
Note sulfide surfaces show little corrosion. SEM photo width is 0.3 mm.

precipitation shields anhydrite grains from halokinetic pressures, thereby preserving their similarity to idioblastic anhydrite grains observed throughout the salt stock. These textures indicate that sulfides precipitated on a grain-supported anhydrite sand at the salt/anhydrite interface. Crystal contacts between anhydrite and sulfide overgrowths rarely show ragged or embayed surfaces (Figs. 4.6a and c). Therefore, it appears that anhydrite remained stable in the highly saline environment of sulfide precipitation. This porous and permeable zone was then compacted and accreted to the overlying anhydrite cap rock.

Marcasite also occurs as radiating colloform or ramose structures that locally form complex intergrowths with lesser aggregates of pyrite and/or sphalerite (Kyle and Price, 1985). Colloform sulfides represent open space precipitation on an anhydrite crystal substrate at the cap rock/salt contact. Euhedral anhydrite crystals provide the local substrate for these Fe-sulfide structures and are commonly preserved at the colloform base (Figs. 4.7a and b). Colloform and ramose aggregates consist of single to multiple generations of Fe-sulfides (Fig. 4.7b) commonly intergrown with sphalerite. These structures may contain internal sphalerite pods (Fig. 4.8) and interlaminated sphalerite bands (Figs. 4.9 and 4.10). Sphalerite bands are microcrystalline and exhibit textural variations within the same Fe-sulfide body. Some bands consist of colloform spheres perched on Fe-sulfides whereas neighboring bands are featureless (Fig. 4.9).

The occurrence of internal sphalerite banding within an Fe-sulfide body suggests that sulfide-precipitating conditions fluctuated. In some instances, it appears that sulfide precipitation was readily reversible such that sphalerite was no longer the stable sulfide during subsequent Fe-sulfide deposition. Contacts between interlaminated Fe-sulfides and sphalerite are variable and may commonly exhibit partial replacement

Fig. 4.7a. Photomicrograph of colloform Fe-sulfide intergrown with minor amounts of banded sphalerite (sl); sample HH1-932.5.
Sulfide aggregate nucleated on euhedral anhydrite grains (an). Note sphalerite is partially replaced by marcasite (mc) at the base of the sulfide structure, and hemispheres of sphalerite appear to float within Fe-sulfide structure.
Photo width is 2.5 mm; reflected light.

Fig. 4.7b. SEM photomicrograph of layered colloform aggregate consisting of multiple generations of Fe-sulfides.
Note irregular cast left by dissolved basal anhydrite grain. SEM photo width is 2.0 mm.

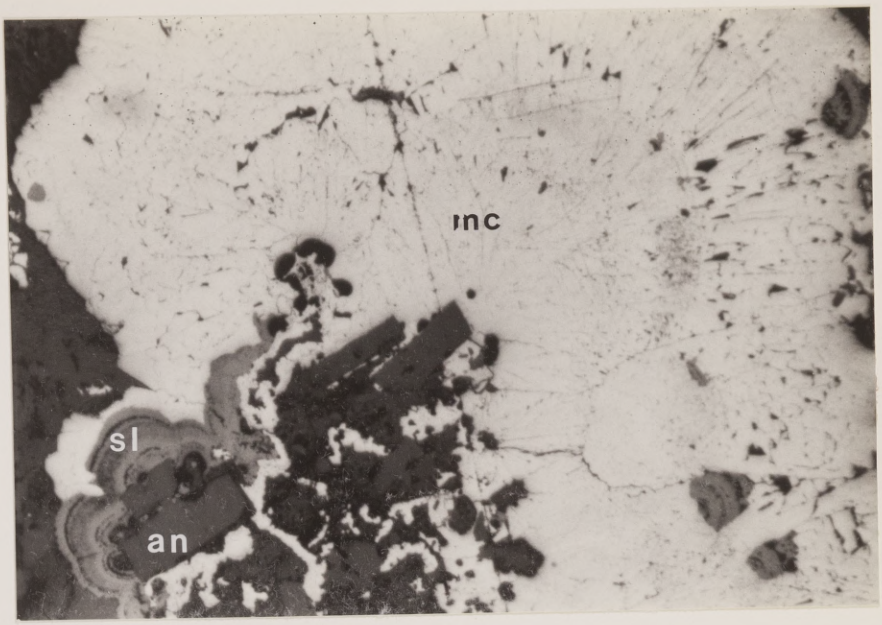
mc
sl
an

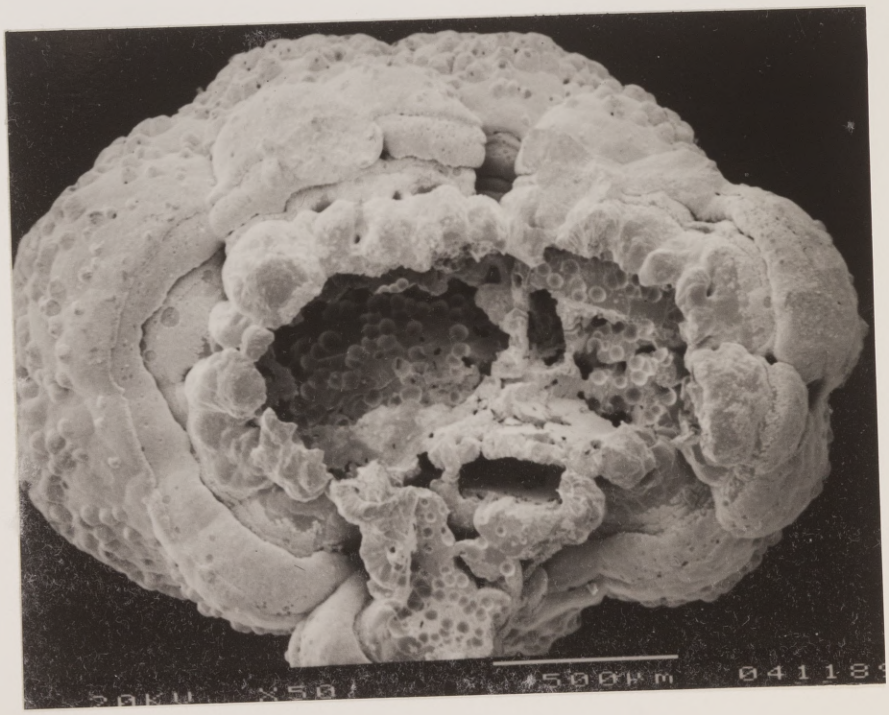
20KV X50
500µm
04118

Fig. 4.8. Photomicrograph of complex sulfide intergrowths consisting of ramose Fe-sulfides (mc) (included with sphalerite pods), microcrystalline sphalerite (sl), and late-stage euhedral galena (ga) with an acanthite inclusion (ac); sample HH1-932.5. Note Fe-sulfides exhibit brittle failure and are cemented by sphalerite matrix. Sphalerite inclusions (*a*, *b*, *c*, and *d*) were analyzed by microprobe, see text for discussion. Photo width is 2.5 mm; reflected light.

Fig. 4.9. Photomicrograph of Fe-sulfide interlaminated with microcrystalline sphalerite bands; sample HB3-990.
Note the corroded crystal boundary between late-stage, pore filling galena (ga) and ramose Fe-sulfide (mc). Sphalerite (sl) bands *A* and *B* (*C* -not shown) and sphere(s) *a* (*b* -not shown) were analyzed by microprobe, see text for discussion. Photo width is 2.5 mm; reflected light.


mc
b
sl
a
ac
d
c
ga
an

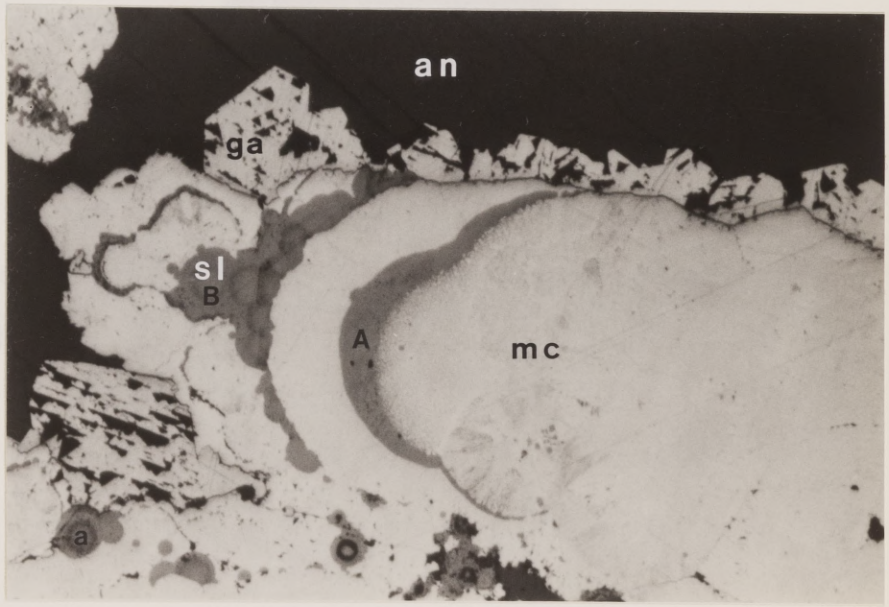
an
ga
sl
B
A
mc
a

Fig. 4.10. Core photograph of massive sulfide section of anhydrite cap rock consisting of ramose Fe-sulfides interlaminated with tan chalky sphalerite; sample HB3-747.

of sphalerite by Fe-sulfides (Fig. 4.7a). In addition, some mineral boundaries appear as a diffuse, embayed zone (50 to 100 microns) characterized by minute interfingering of sphalerite into marcasite/pyrite (Kyle and Price, 1985; Fig. 4.11). These embayed contacts suggest that the underlying sphalerite was partially dissolved when exposed to Fe-sulfide precipitating fluids.

Disseminated rhombic Fe-sulfide grains are relatively minor compared to the overall abundance of sulfide laminae, but they generally occur throughout anhydrite cap rock and in some intervals are very abundant. They typically have a porous, fine-crystalline texture and euhedral habit which suggests they are sulfidized pseudomorphs after disseminated siderite or dolomite grains (Fig. 4.12). Carbonate rhombs with a range of compositions are present in the Hockley salt mass and anhydrite zone.

Galena is a coarse crystalline, late-stage precipitate that generally exhibits euhedral to subhedral cubes (1 to 2 mm) (Figs. 4.8, 4.9, and 4.10). Evidence of sulfide corrosion prior to galena mineralization is common (Fig. 4.9). Galena-precipitating fluids may have etched the underlying sulfide substrate prior to/during sulfide deposition (Fig. 4.9). Galena is commonly intergrown with sphalerite, including rare skeletal crystals (Fig. 4.13), and to a lesser extent with Fe-sulfides. Skeletal textures suggest rapid sulfide deposition resulting in a fine-crystalline precipitate (Ramdohr, 1979; Price et al., 1983). Acanthite is locally associated with galena and has been identified as irregular crystal masses less than one mm in length (Fig. 4.8). Although the Ag content in sphalerite and galena can be high, Ag assay intervals that exceed 50 ppm are attributed to the presence of acanthite.

Fig. 4.11. Photomicrograph of irregular contact between Fe-sulfides (mc) and sphalerite band (sl); sample HB3-990.
The interfingering mineral boundary suggests sphalerite replacement of Fe-sulfides (Kyle and Price, 1985). Photo width is 1.2 mm; reflected light.

Fig. 4.12. Photomicrograph of rhombic Fe-sulfide grain disseminated within anhydrite (an); sample HH3-452.
Note the euhedral habit which suggests that it is a sulfidized pseudomorph of siderite or dolomite. Photo width is 1.2 mm; reflected light.

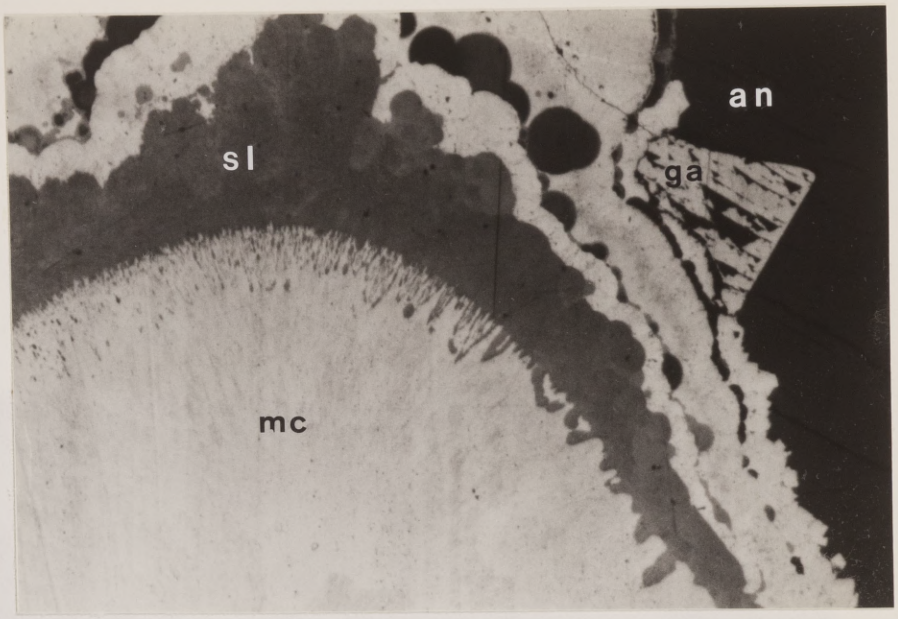
an
sl
ga
mc

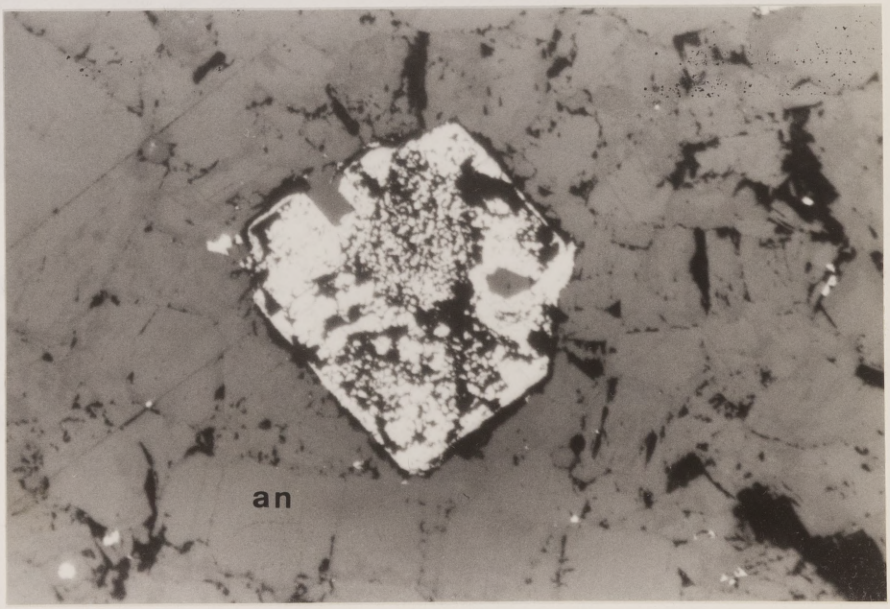
an

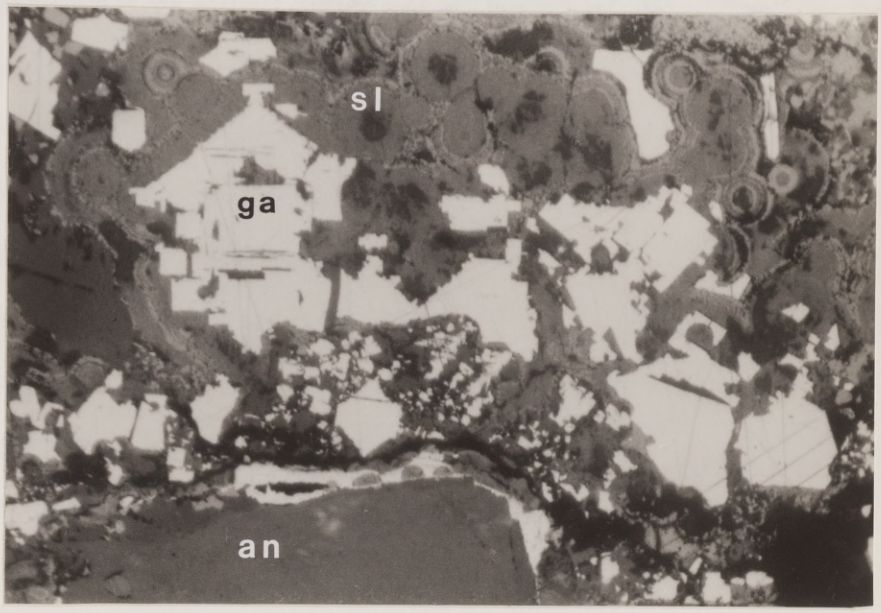

Fig. 4.13. Photomicrograph of complex sulfide intergrowth consisting of colloform sphalerite (sl) and skeletal galena (ga) nucleating on anhydrite grains (an); sample HH2-404.
Skeletal galena suggests that sulfide precipitation was rapid. Photo width is 1.2 mm; reflected light.

Paragenesis

Sulfide laminae are composed of variable amounts of marcasite, pyrite, sphalerite, galena, and acanthite. Most laminae lack one or more base metal sulfides within a given interval. Therefore, a detailed paragenetic sequence that is applicable throughout the cap rock is difficult to establish because of highly variable sulfide textures and composition within individual laminae; a generalized sequence is shown in Figure 4.14. Marcasite is the earliest sulfide mineral in most laminae followed by, and often intergrown with, pyrite. Sphalerite precipitation overlaps the Fe-sulfide stage. Early sphalerite precipitation occurs as fine-crystalline inclusions and bands intergrown with colloform or ramose Fe-sulfides (Figs. 4.8 and 4.9). Late-stage sphalerite is a massive, fine-crystalline cement (Fig. 4.8). Galena may be intergrown with sphalerite (Fig. 4.13), and coarse crystals of cubic and cubo-octahedral galena may also be intergrown with rare acanthite (Fig. 4.8). Galena is generally the last sulfide deposited (Fig. 4.9). Anhydrite/gypsum deposition may follow sulfide precipitation where porosity is still present (Fig. 4.8).

Trace Element Composition of Sulfide Minerals

Major and trace element compositions of some sulfide samples from anhydrite cap rock were determined by microprobe analysis (Appendix V). Results indicate that trace element variations exist, particularly involving Ag and Cd, within sphalerite cements and closely spaced sphalerite bands and inclusions within colloform Fe-sulfides. Local intervals of Hockley sulfides contain significant quantities of Ag and Cd, which can occur as individual mineral phases (e.g., acanthite) and/or in solid solution with sphalerite (Kyle and Price, 1985). In Mississippi Valley-Type deposits, many economically important trace elements occur in solid solution with sphalerite, the more

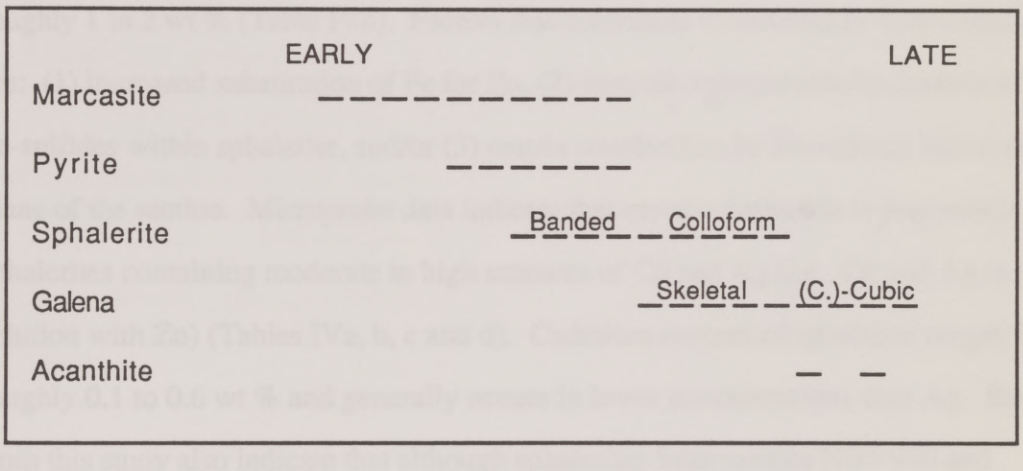

Fig. 4.14. Generalized paragenetic sequence for anhydrite-hosted sulfide laminae.

abundant being cadmium, silver, germanium, and indium (Hagni, 1983). In some sulfide intervals the abundance of these elements could be sufficient to contribute to the economic viability of the Hockley deposit.

Four polished sections consisting of intergrown sulfides were analyzed by electron microprobe. Sphalerites from HB3-990, HH1-932.5, HH2-404, and HH2-878 are relatively pure, generally containing greater than 64 wt % Zn. The Fe content was typically less than 0.6 wt % (Tables IVa, b, c and d). However, some spot analyses of sphalerite inclusions from HH1-932.5 exhibit Fe concentrations that range between roughly 1 to 2 wt % (Table IVb). Factors that contribute to elevated Fe concentrations are: (1) increased substitution of Fe for Zn, (2) intricate intergrowths/inclusions of Fe-sulfides within sphalerite, and/or (3) matrix interference by Fe-sulfides below the plane of the section. Microprobe data indicate that metal substitution is responsible for sphalerites containing moderate to high amounts of Cd and Ag (i.e., Cd and Ag in solid solution with Zn) (Tables IVa, b, c and d). Cadmium content of sphalerite ranges from roughly 0.1 to 0.6 wt % and generally occurs in lower concentrations than Ag. Results from this study also indicate that although sphalerites from sample HB3-990 and HH2-404 appear Ag-poor (Tables IVa and c), other polished sections exhibit elevated Ag values that typically range from 0.1 to 1.3 wt % (Tables IVb and d). One sphalerite analysis from HH1-932.5 is anomalously enriched in Ag, with a maximum Ag content slightly above 3 wt % (Table IVb).

Compositional variations in banded sulfides were tested by microprobe analysis. Results from HB3-990 and HH2-878 indicate that trace element content varies little within individual bands. For example, two well defined sphalerite bands in HB3-990 interlaminated within a ramose Fe-sulfide (Fig. 4.9) are relatively homogeneous

Table IVa. Microprobe analysis of sphalerite from polished section HB3-990.

Analysis no.	Beam Location	Luminescence Color	Zn wt %	Fe wt %	Ag wt %	Cd wt %	S wt %	Total wt %
(0.2mm thick sphalerite band - "A")								
A-1	innermost	pale orange	65.53	0.03	0.00	0.08	32.63	98.27
A-2	inner	pale orange	65.46	0.04	0.00	0.09	32.76	98.35
A-3	middle	pale orange	64.03	0.10	0.00	0.14	29.68	93.95
A-4	outer	pale orange	64.22	0.12	0.00	0.15	31.62	96.11
A-5	outermost	light blue	65.41	0.54	0.00	0.11	33.35	99.41
(0.1mm thick sphalerite band - "B")								
B-1	innermost	pale orange	65.52	0.05	0.00	0.15	32.28	98.00
B-2	middle	pale orange	65.71	0.06	0.00	0.11	32.71	98.59
B-3	middle	pale orange	65.40	0.08	0.00	0.17	32.89	98.54
B-4	outermost	pale orange	60.86	0.05	0.00	0.18	31.11	92.20
(<0.1mm thick sphalerite band - "C")								
C-1	innermost	pale orange	65.70	0.25	0.00	0.17	33.29	99.41
C-2	outermost	pale orange	64.49	0.14	0.00	0.21	31.91	96.75
(0.2mm diameter sphalerite sphere - "a")								
a-1	core	pale orange	62.62	0.05	0.00	0.15	31.48	94.30
a-2	rim	pale orange	65.95	0.11	0.00	0.09	32.79	98.94
(0.2mm diameter sphalerite sphere - "b")								
b-1	core	light blue	66.20	0.47	0.00	0.02	31.23	97.92

Table IVb. Microprobe analysis of sphalerite from polished section HH1-932.5.

Analysis no.	Beam Location	Luminescence Color	Zn wt %	Fe wt %	Ag wt %	Cd wt %	S wt %	Total wt %
(0.1-0.2mm diameter sphalerite inclusions in ramose marcasite)								
a-1	core	deep orange	59.48	1.40	1.00	0.08	30.56	92.52
a-2	core	deep orange	63.03	1.07	1.00	0.18	32.94	98.22
a-3	edge	light blue	64.33	1.24	0.23	0.11	34.03	99.94
b-1	core	deep orange	60.90	1.86	1.23	0.19	32.29	96.47
c-1	core	deep orange	59.31	1.87	1.29	0.16	32.25	94.88
d-1	core	light blue	59.55	2.05	0.08	0.07	30.78	92.53
(late stage sphalerite matrix cement)								
1	random	purple-red	63.04	0.46	0.88	0.55	33.19	98.12
2	random	purple-red	63.75	0.93	0.85	0.41	32.70	98.64
3	random	purple-red	62.08	0.44	1.23	0.37	32.69	96.81
4	random	purple-red	59.98	0.38	1.26	0.50	31.55	93.67
5	random	purple-red	57.79	0.43	3.31	0.41	31.82	93.76

Table IVc. Microprobe analysis of sphalerite from polished section HH2-404.

Analysis no.	Beam Location	Luminescence Color	Zn wt %	Fe wt %	Ag wt %	Cd wt %	S wt %	Total wt %
(fine crystalline sphalerite cement)								
1	random	pale orange	65.72	0.12	0.00	0.26	31.69	97.79
2	random	pale orange	65.24	0.07	0.01	0.25	32.04	97.61
3	random	pale orange	65.92	0.09	0.01	0.29	31.97	98.28
4	random	pale orange	65.63	0.05	0.00	0.14	31.48	97.30
5	random	pale orange	65.74	0.21	0.01	0.22	31.69	97.87

Table IVd. Microprobe analysis of sphalerite from polished section HH2-878.

Analysis no.	Beam Location	Luminescence Color	Zn wt %	Fe wt %	Ag wt %	Cd wt %	S wt %	Total wt %
(1mm thick sphalerite band)								
1	random	mod. orange	59.26	0.63	0.65	0.20	30.89	91.63
2	random	mod. orange	59.74	0.64	0.59	0.20	31.13	92.30
3	random	mod. orange	62.26	0.70	0.78	0.29	31.07	95.10
4	random	mod. orange	62.08	0.64	0.63	0.22	29.90	93.47
5	random	mod. orange	61.16	0.71	0.72	0.24	31.27	94.10
6	random	mod. orange	63.18	0.57	0.70	0.22	30.54	95.21
7	random	mod. orange	62.95	0.79	0.84	0.27	29.32	94.17
8	random	mod. orange	62.09	0.68	0.75	0.24	31.05	94.81
9	random	mod. orange	60.93	0.62	0.60	0.23	31.08	93.46
10	random	mod. orange	62.86	0.66	0.75	0.22	31.33	95.82

features (Table IVa). Small sphalerite spheres (75 to 150 microns in diameter) intergrown with Fe-sulfides from the same sample (Fig. 4.9) have about the same trace element composition as the bands. Random spot analyses of a sphalerite band in HH2-878 also exhibit compositional homogeneity (Table IVd; Fig. 4.15). However, trace element content of Ag and Cd in sphalerite is significantly different between HB3-990 and HH2-878. The most noticeable difference is the presence of roughly 0.7 wt % Ag in HH2-878 compared to undetectable amounts in HB3-990. Sphalerites from HH2-878 also contain Cd concentrations that are slightly greater than HB3-990 (Tables IVa and d).

Section HH1-932.5 consists of large ramose growths of Fe-sulfides (1 to 2 mm length) intergrown with co-precipitated sphalerite pods (50 to 150 microns diameter) (Fig. 4.8). Silver and Cd concentrations measured from inner cores of these isolated pods (i.e., analyses *a* 1, *a* 2, *b* 1, and *c* 1) average 1.0 and 0.2 wt %, respectively (Table IVb). However, Ag and Cd concentrations near the inclusion margin (i.e., analyses *a* 3 and *d* 1) were consistently less than values observed from inner cores (Table IVb). Sphalerite is also present as a microcrystalline cement of fractured sulfides (Fig. 4.8). This paragentically late-stage cement is also enriched in Ag and Cd. Silver and Cd concentrations range from roughly 0.8 to 3.3 wt % and 0.4 to 0.6 wt %, respectively (Table IVb).

Elevated concentrations of Ag and Cd found within sphalerite produce striking luminescent colors when excited under an electron beam. These colors and their intensity are primarily due to variation of Ag, Cd, and Fe concentrations in sphalerites. Silver and Cd are recognized as excellent luminescent activator atoms (Goni and Remond, 1969). In contrast, Fe is a powerful luminescent inhibiter; i.e., small amounts of Fe in sphalerite generally cause the mineral to be nonluminescent

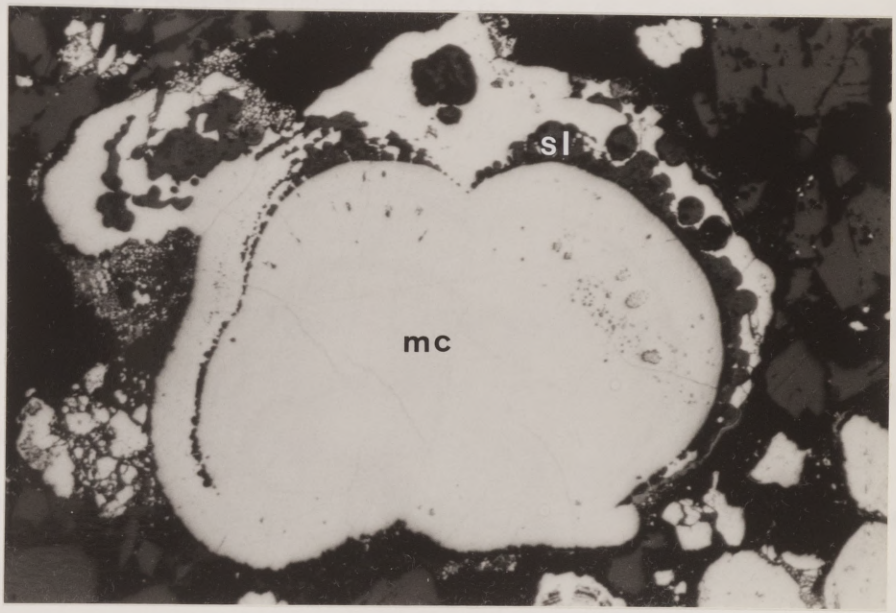

Fig. 4.15. Photomicrograph of colloform Fe-sulfide (mc) interlaminated and included with microcrystalline sphalerite (sl); sample HH2-878.
Sphalerite bands and spheres were analyzed by microprobe, see text for discusson.
Photo width is 2.5 mm; reflected light.

(Robbins, 1983). In a pilot study, Kyle and Price (1985) determined that sphalerites consisting of minor amounts of Fe with high Ag and Cd content produced striking cathodoluminescent colors. Similar luminescent effects were observed in sphalerites from samples HB3-990, HH1-932.5, HH2-404, and HH2-878. However, luminescence was induced by the microprobe electron beam in this study. Microprobe results indicate that moderate to deep orange luminescence occurs in samples containing a considerable Ag content ranging from 0.6 to 1.3 wt % (Tables IVb and d). The moderate orange variety occurs in HH2-878 (Table IVd) as an irregular sphalerite band within a ramose structure (Fig. 4.15). Deep orange sphalerite in HH1-932.5 (Table IVb) was observed within small sphalerite pods that are encapsulated by Fe-sulfides (Fig. 4.8). It appears that deep orange sphalerite is more intense because Ag concentration is slightly higher than the moderate orange variety (Tables IVb, c and d). This relationship is supported by low intensity luminescence of the Ag-poor HB3-990 and HH2-404 sphalerites (Tables IVa and c).

The presence of an intense purple-red luminescence is attributed to sphalerites with enriched Ag and Cd concentrations. Sphalerite of this variety occurs as a late-stage precipitate that clearly post-dates the ramose structures and included pods. Compositional differences of Ag and Cd between pod and cement sphalerite in HH1-935.5 (Table IVb) suggest that fluid composition and/or sulfide precipitating conditions changed. Sphalerite bands within a single ramose structure may also record distinct changes in mineralizing conditions. However, the bulk composition of bands "A" and "B" from HB3-990 appear to be very similar (Table IVa). Other examples of sulfide intergrowths suggest that significant compositional differences between multiple sphalerite bands is anomalous. Luminescent colors and their intensities reflect

variations in trace elements of sphalerite and therefore are sensitive indicators of composition.

Geochemical analyses of these mineralized intervals, HB3-990, HH1-932.5, HH2-404, and HH2-878, were determined in one-foot intervals by atomic absorption (Table V; Appendix I). Trace element analyses of these samples indicate that HH1-932.5 and HH2-878 are anomalously Ag-rich intervals (Tables IVb and d, and V). Acanthite crystals and Ag in sphalerite are responsible for these assay intervals exceeding 170 ppm Ag (Table V). Local Ag-rich zones, e.g. HH1-932.5 and HH2-878, are attributed to mineralizing fluids that were enriched in Ag, and to a lesser extent Cd. HB3-990 and HH2-404 represent mineralized intervals that are Ag-poor (Tables IVa and c, and V). These sulfide intervals presumably precipitated from mineralized fluids that contained only minor amounts of trace element Cd and lesser amounts of Ag. Microprobe analysis of sulfides within assayed intervals is a useful tool to specifically locate Ag and Cd and determine their relationship to sulfide paragenesis and possibly to fluid composition.

Calcite-Hosted Sulfides

Anomalous amounts of sulfides occur in the calcite portion of the cap rock. Both the upper and lower calcite cap rock are extensively fractured and brecciated throughout the section. However, the degree of sulfide mineralization appears to be controlled by the stratigraphic position of calcite within the cap rock. In general, upper calcite zones that develop along flanks of the dome are more heavily mineralized (Fig. 4.16) than calcite that is perched stratigraphically high and away from steeply sloping margins (Fig. 3.14a). Lower (internal) calcite zones also represent a well-developed sulfide-

Table V. Geochemical analyses of HB3-990, HH1-932.5, HH2-404, and HH2-878.

Core Hole	Depth (ft)	Fe (ppm)	Pb (ppm)	Zn (ppm)	Ag (ppm)	Cd (ppm)
HB3	990-991	8,800	87,000	120,000	0.2	- -
HH1	932-933	- -	385	8,100	220.0	69.0
HH2	403-404	24,400	1,710	2,700	- -	- -
HH2	878-879	5,200	2,700	5,200	173.0	- -

Assay data provided by Marathon Mineral Resources.
-- Unanalyzed element

Fig. 4.16. Core photograph of brecciated sulfide clasts (s), composed of Fe-sulfides and minor sphalerite and galena, cemented by fine-grain sulfide matrix and calcite; sample HF2-1095.
Sample is representative of a massive sulfide interval from the deeply flanking portion of the upper calcite zone in Hockley cap rock.

rich interval comparable to sulfide concentrations in deep, flanking calcite sections (Figs. 3.16c and d).

Sulfide accumulations within the heavily mineralized calcite zones consist of broken and disrupted clasts of fine-crystalline sulfides cemented by sulfides and coarse-crystalline calcite (Fig. 3.16c). In some cases, sulfide breccias have been cemented by later-stage sulfides indicating that cap rock mineralization is a multi-stage process. However, it appears that a significant portion of the breccia matrix may have formed as sulfides were disaggregated during anhydrite dissolution. Marcasite and pyrite are the most common accessory minerals in the calcite cap rock where they may locally exceed 60 %. Many of these massive sulfide concentrations also contain minor amounts of sphalerite and galena intergrown with Fe-sulfide clasts (Fig. 4.16).

Pore-filling sulfides in calcite cap rock suggests that a portion of calcite-hosted sulfides may have developed after local sulfide mineralization within the anhydrite cap rock had largely ceased. However, some sulfides within the internal calcite zone of HH1, HH2, and HH2A are attributed to pre-existing sulfides originally in place within anhydrite cap rock. Evidence for pre-existing sulfides is provided by relic sulfide laminae within the lower calcite cap rock (Fig. 4.17). This section of cap rock clearly exhibits calcite replacement of mineralized anhydrite cap rock. Some local occurrences of barite represent late-stage open space filling within calcite cap rock. The origin of the massive barite associated with calcite-hosted sulfides has not been established.

Supracaprock Hosted Sulfides

Pyrite aggregates from supracaprock sediments have been identified from rotary samples collected from HB4 and HH2. There appear to be two distinct pyrite morphologies: (1) very fine-crystalline pyrite aggregates (1 to 2 mm long) from

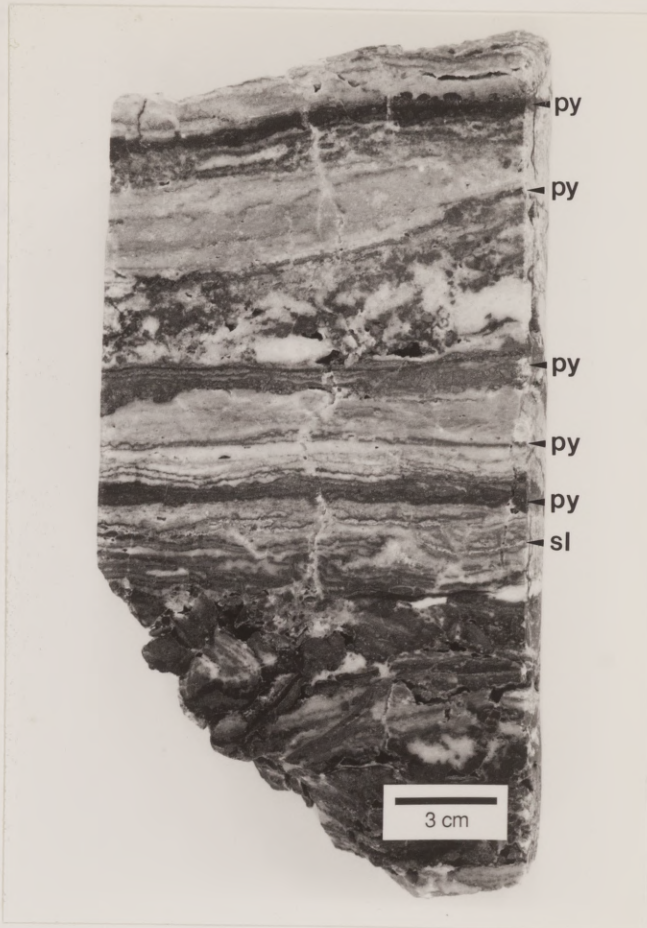

Fig. 4.17. Core photograph of calcite cap rock with slightly disturbed pyrite (py) and sphalerite (sl) laminae.
These laminae are interpreted to represent inherited sulfides from calcite replacement of mineralized anhydrite. Sample from internal calcite zone of hole HH2A. Note sulfide fragments at base of sample.

overlying clay-rich sediments (Fig. 4.18a) and (2) fine-crystalline pyrite (approximately 1 mm long) particularly abundant in fine-grained sandy units (Fig. 4.18b). Sulfides within these sandy-shale sediments are authigenic and volumetrically minor, i.e., less than 1 %. Although both of the sulfide types are authigenic, they are inferred to have different diagenetic histories. Based on textural and isotopic similarities of pyrites between South Texas uranium deposits (Goldhaber et al., 1978; 1979) and Hockley, it appears that very fine-crystalline aggregates are associated with early bacterial reduction of pore-water sulfate whereas fine-crystalline pyrite is related to "ore-stage" mineralization of cap rock.

Fig. 4.18a. SEM photomicrograph of very fine-crystalline pyrite aggregate separated from clay-rich supracaprock sediments, Hockley Dome. SEM photo width is 2.3 mm.

Fig. 4.18b. SEM photomicrograph of fine-crystalline pyrite aggregate separated from sandy supracaprock sediments, Hockley Dome. SEM photo width is 1.2 mm.

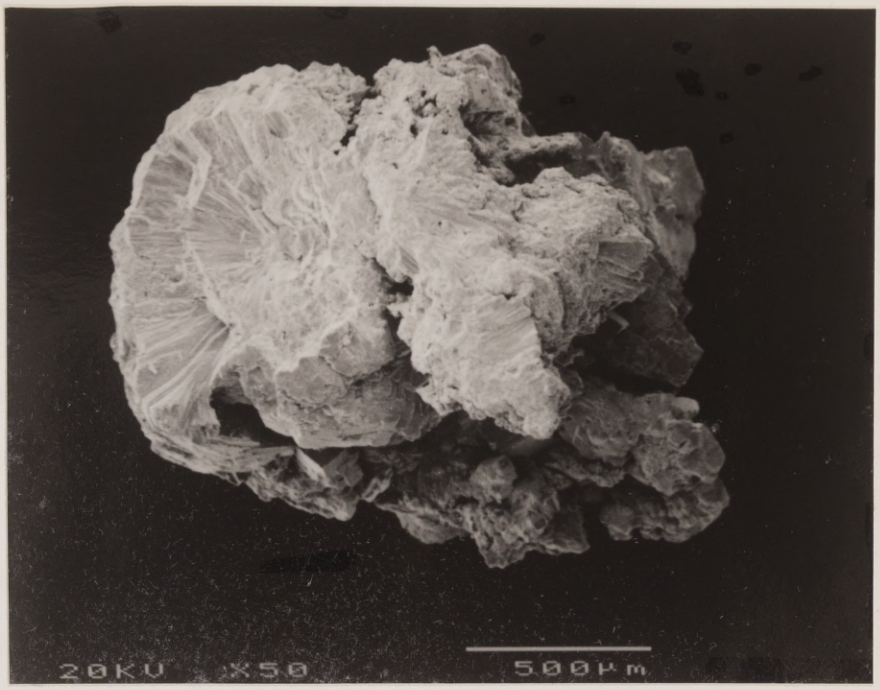

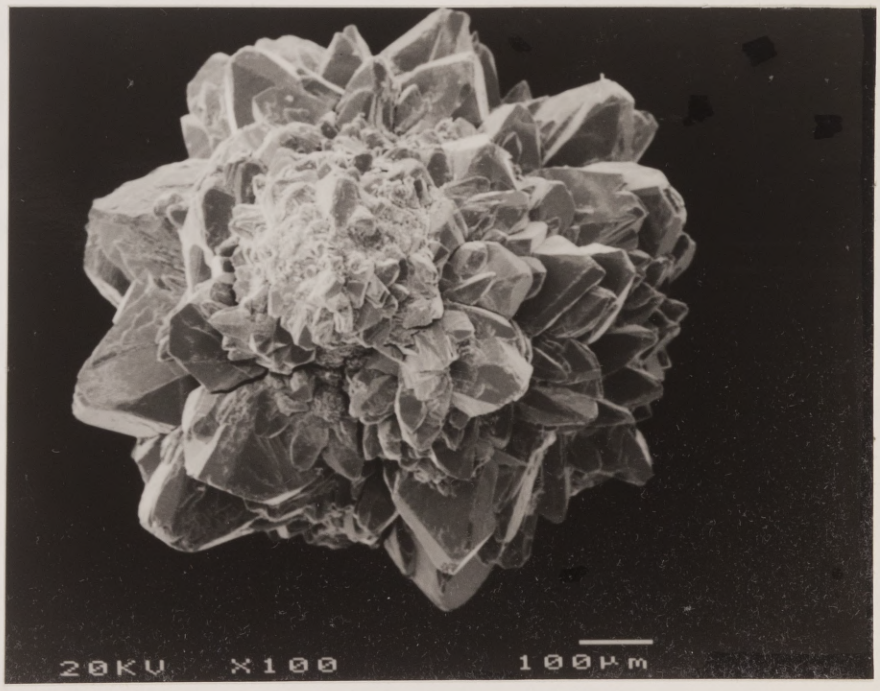

Chapter 5

METAL CONCENTRATIONS

The selected metals, Pb, Zn, Ag, Cd, and Fe, chosen for this study are principally from the "H" and "B" lines of drill holes located on the southern perimeter of the dome (Fig. 5.1). The highly mineralized "H" line (HH1, HH2, and HH3) and to a lesser degree "B" line (HB1, HB3, HB4, and HB5), were selected to study vertical and lateral metals distribution. Additional sites C1, C5, HC1, HD2, HI1, and HW2 were also evaluated for their metal content to examine possible variations around the dome (Fig. 5.2). Assay data are graphically expressed as both metal concentrations and metal ratios. Histogram plots of Pb, Zn, Ag, Cd, and Fe are smoothed by a five-point moving average and illustrate the variation of metals with depth (Appendix I).

Results

Vertical Metal Pattern

One of the principal reasons for studying the metal distribution of the HH section of drill holes was to determine whether mineralized zones within the interior calcite and anhydrite host rock were laterally continuous (Fig. 5.3). Metal distribution of the HB section was also evaluated for lateral continuity but was selected particularly because the anhydrite section is not interrupted by an interior calcite zone (Fig. 5.4). Both the HH and HB drill holes are from dip-oriented sections that intersect gently dipping sulfide laminae within the cap rock. To complement the dip-line studies a strike-oriented profile was constructed through HI1 and HW2, using HB3 and HH2 as endpoints (Fig. 5.2). Also, perimeter (C1, HC1, and HD2) and interior (C5) core holes were examined to determine if the lateral extent and vertical position of sulfide

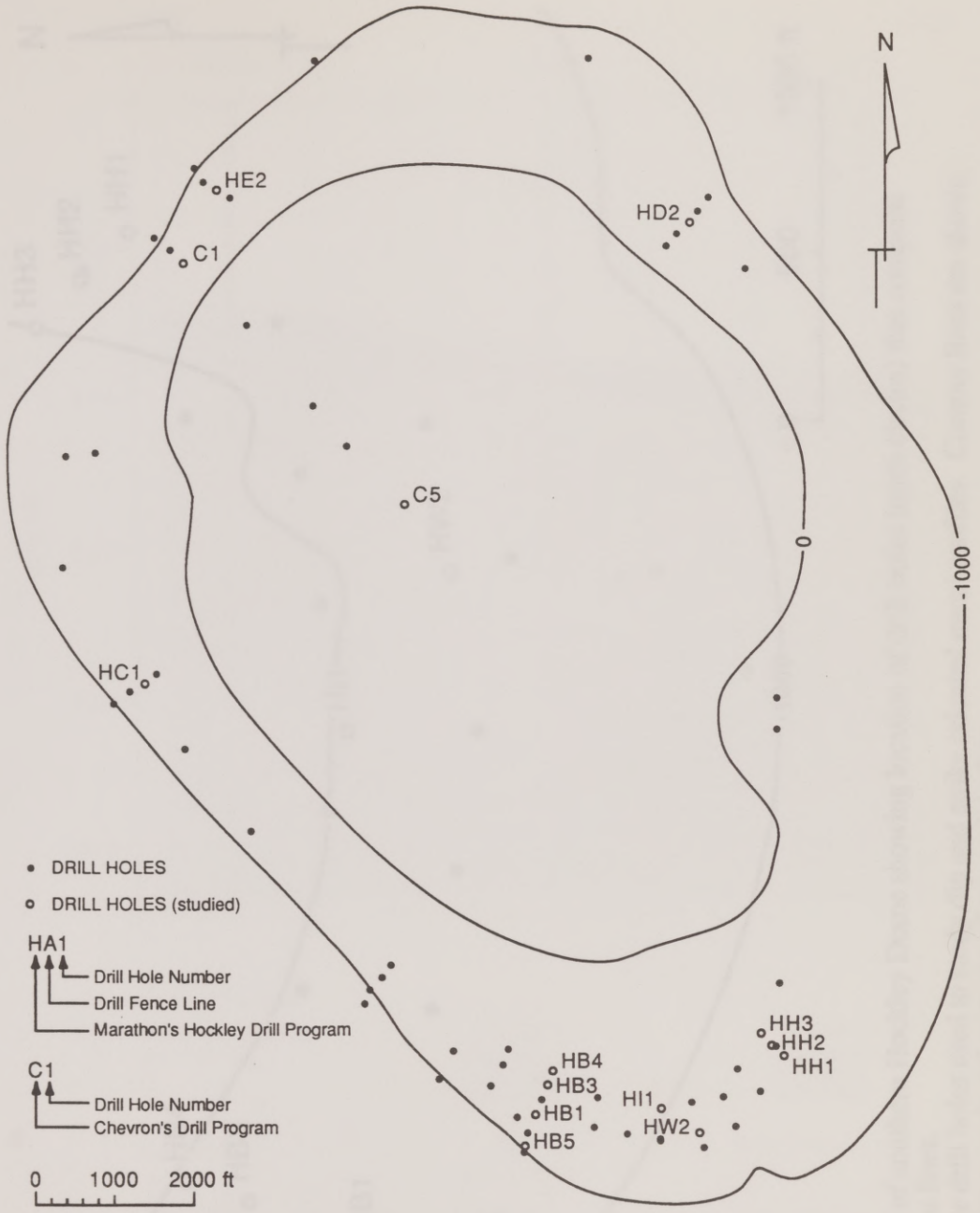

Fig. 5.1. Plan map showing location of drill holes (open circles) utilized in metal abundance and distribution study.
Contour lines are shown for reference and represent elevation of top of cap rock in feet.

Fig. 5.2. Plan map of southern Hockley Dome showing location of drill holes (open circles) that comprise the B- and H-section lines.
Open circles indicate drill holes used to study dip and strike oriented metal profiles. Contour lines are shown for reference and represent elevation to top of cap rock in feet.

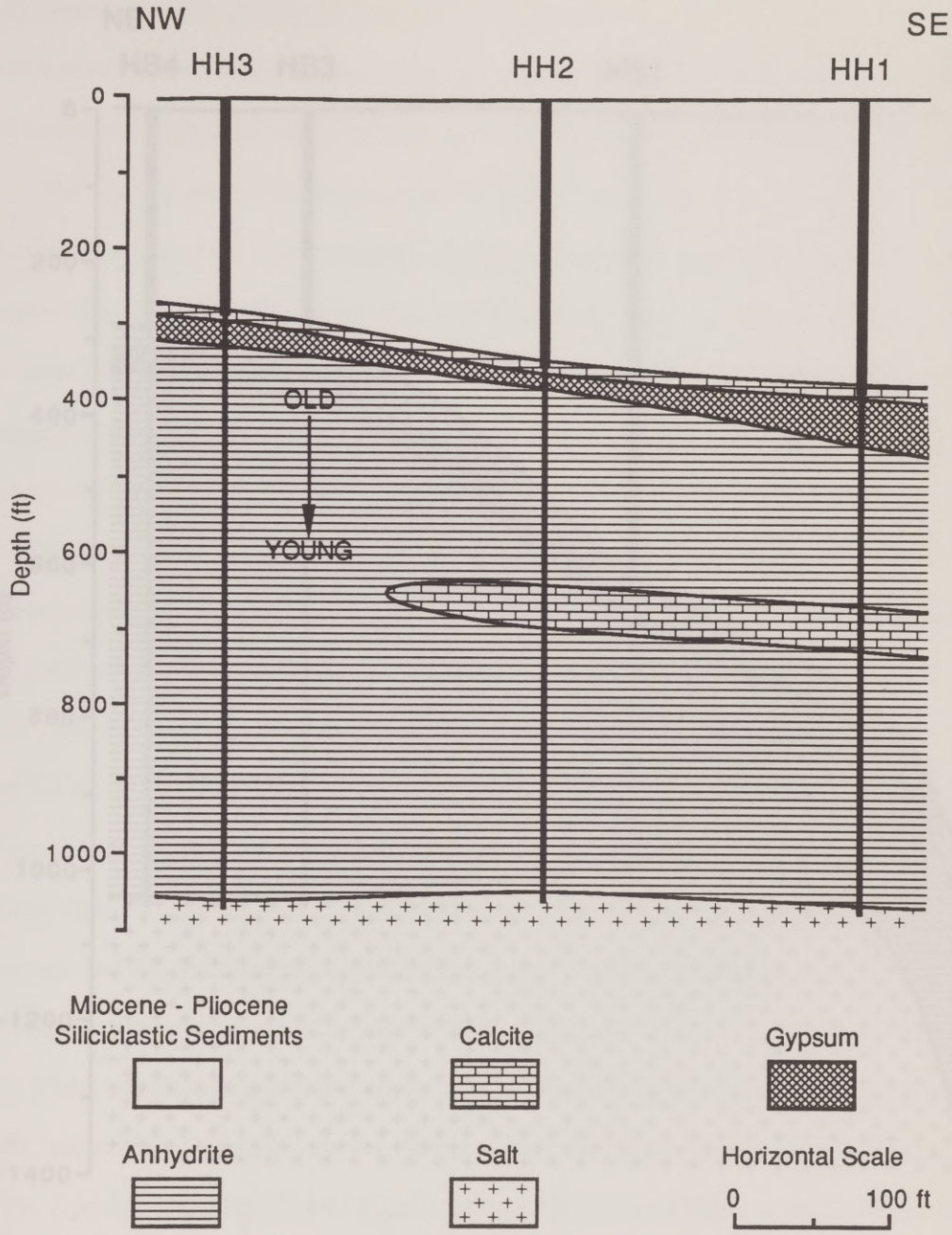

Fig. 5.3. Lithologic cross-section along the H-section line.
Vertical lines represent drill holes. Thick lines are rotary drilled intervals;
thin lines are cored intervals used in this study.

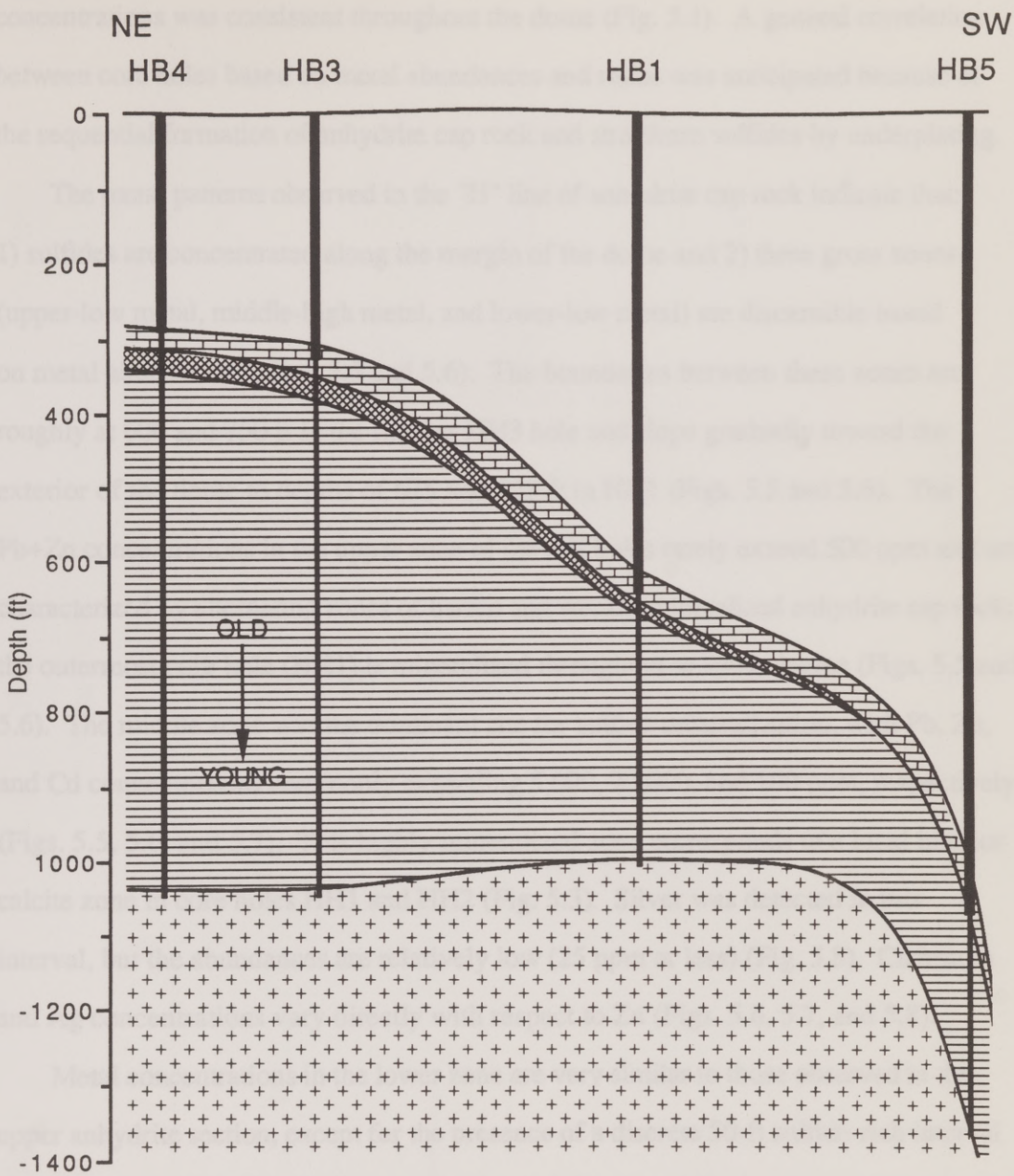

Fig. 5.4. Lithologic cross-section along the B-section line. Vertical lines represent drill holes. Thick lines are rotary drilled intervals; thin lines are cored intervals used in this study. Note the thinning of cap rock toward the dome margin. See Figure 5.3 for lithologic explanation.

concentrations was consistent throughout the dome (Fig. 5.1). A general correlation between core holes based on metal abundances and ratios was anticipated because of the sequential formation of anhydrite cap rock and stratiform sulfides by underplating.

The metal patterns observed in the "H" line of anhydrite cap rock indicate that: 1) sulfides are concentrated along the margin of the dome and 2) three gross zones (upper-low metal, middle-high metal, and lower-low metal) are discernible based on metal abundances (Figs. 5.5 and 5.6). The boundaries between these zones are roughly at 600 and 750 ft in the interior HH3 hole and slope gradually toward the exterior of the dome to depths of 675 and 825 ft in HH1 (Figs. 5.5 and 5.6). The Pb+Zn concentrations in the upper zone of the HH holes rarely exceed 500 ppm and are characterized by alternating zones of barren and weakly mineralized anhydrite cap rock; the outermost core hole (HH1) is mineralized throughout to some degree (Figs. 5.5 and 5.6). The middle zone was the dominant site for sulfide mineralization, with Pb, Zn, and Cd concentrations commonly exceeding 5,000, 20,000, and 100 ppm, respectively (Figs. 5.5, 5.6, and 5.7). This highly mineralized zone corresponds to a local interior calcite zone in core holes HH1 and HH2 (Fig. 5.3). Silver was detected in this interval, but the abundances are relatively low (25 ppm or less) (Fig. 5.8). Cadmium and Ag concentrations vary directly with respect to Zn (Figs. 5.6, 5.7, and 5.8).

Metal concentrations in the lower zone are very similar to those observed in the upper anhydrite section, except for the presence of a discrete 50-ft sulfide-rich interval (Figs. 5.6 and 5.8). This lower zone is best developed in HH1 at a depth of about 925 ft and occurs in HH2 and HH3 at approximately 875 ft. Relatively large amounts of Zn and Ag define this interval along with minor amounts of Pb and Cd. This Ag-rich interval is clearly identified in HH1 and HH2 (Fig. 5.8; Appendix Id). Continuation

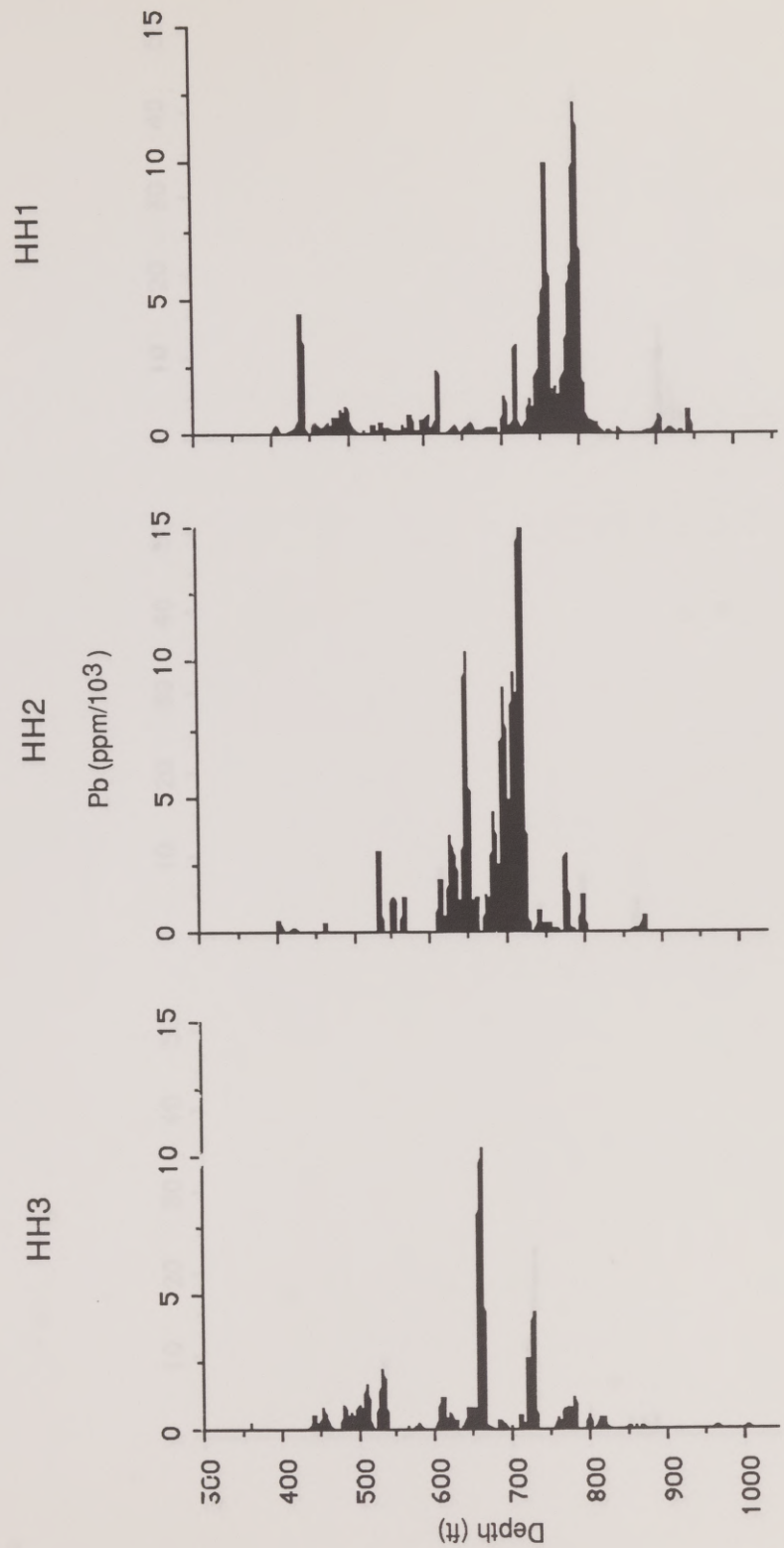

Fig. 5.5. Histogram of Pb content for cored intervals of drill holes on the H-section line.

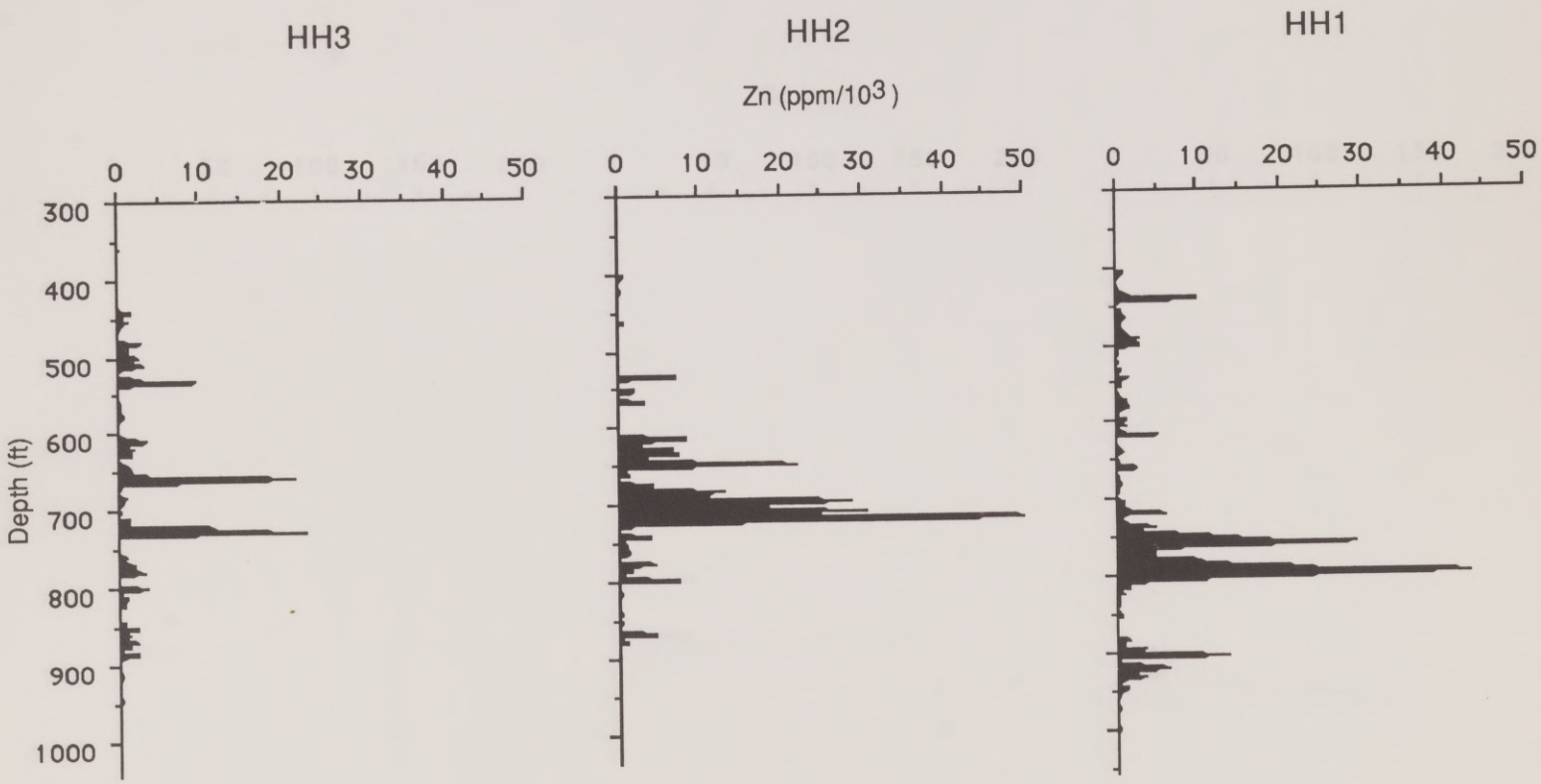

Fig. 5.6. Histogram of Zn content for cored intervals of drill holes on the H-section line.

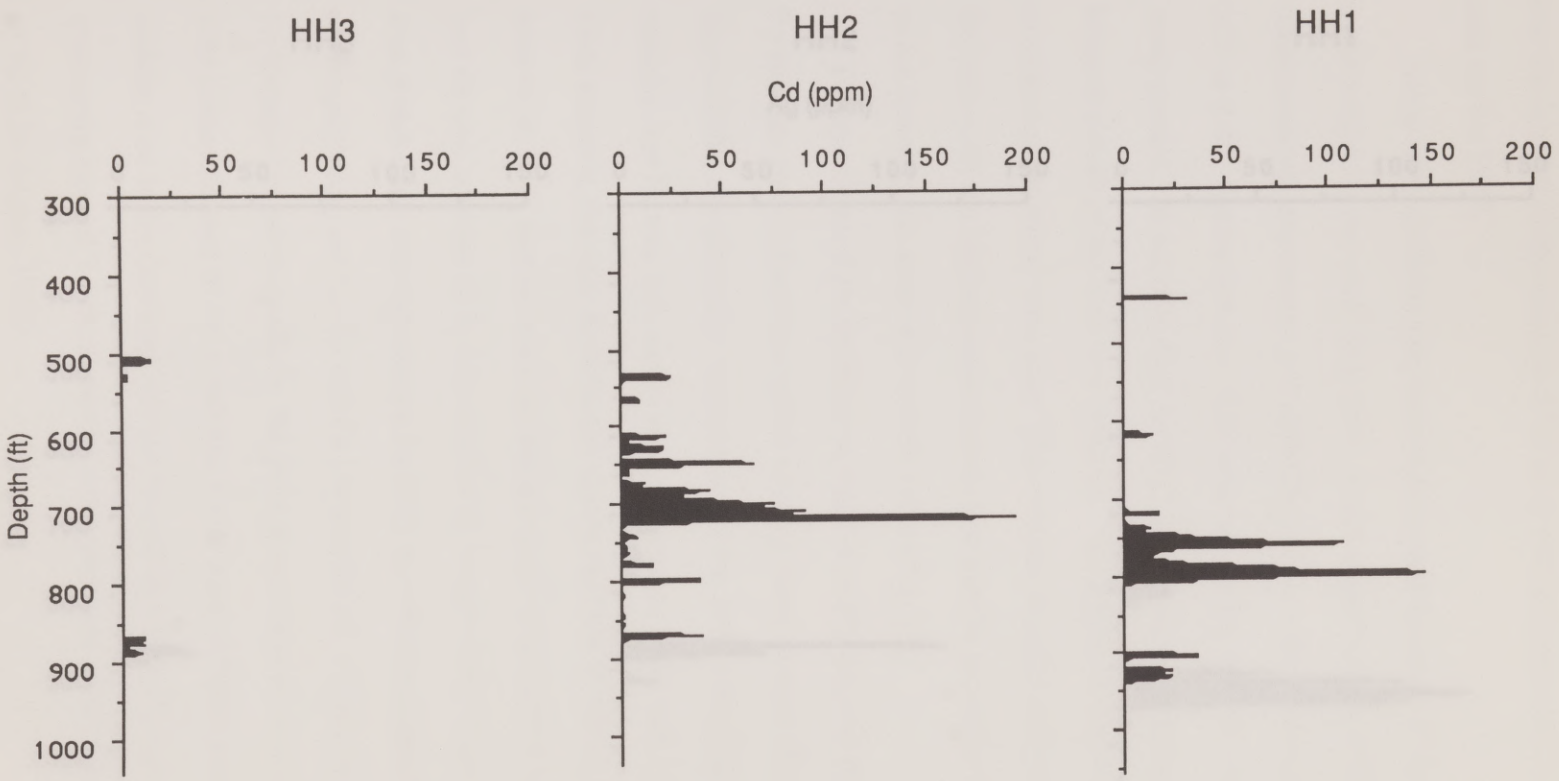

Fig. 5.7. Histogram of Cd content for cored intervals of drill holes on the H-section line.

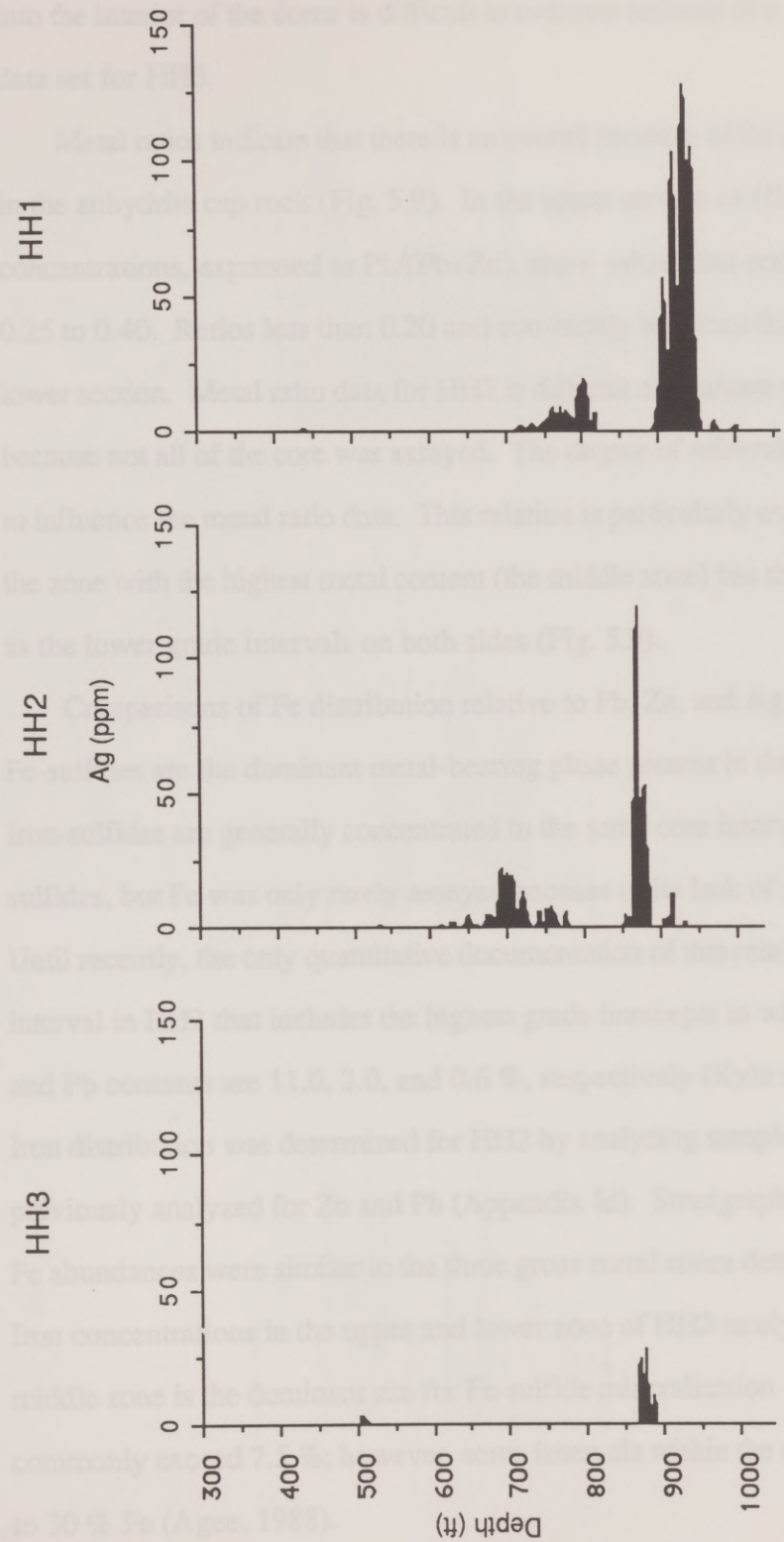

Fig. 5.8. Histogram of Ag content for cored intervals of drill holes on the H-section line.

into the interior of the dome is difficult to evaluate because of a more limited Ag assay data set for HH3.

Metal ratios indicate that there is an overall increase of Zn relative to Pb downward in the anhydrite cap rock (Fig. 5.9). In the upper section of HH1 and HH3, the metal concentrations, expressed as Pb/(Pb+Zn), show values that commonly range from 0.25 to 0.40. Ratios less than 0.20 and commonly less than 0.10 are typical of the lower section. Metal ratio data for HH2 is difficult to evaluate to the same degree because not all of the core was assayed. The degree of mineralization does not seem to influence the metal ratio data. This relation is particularly evident in HH3 where the zone with the highest metal content (the middle zone) has the same metal ratios as the lower grade intervals on both sides (Fig. 5.9).

Comparisons of Fe distribution relative to Pb, Zn, and Ag are desirable because Fe-sulfides are the dominant metal-bearing phase present in the Hockley cap rock. Iron-sulfides are generally concentrated in the same core intervals as Pb and Zn sulfides, but Fe was only rarely assayed because of its lack of commercial interest. Until recently, the only quantitative documentation of this relationship was for a 55-ft interval in HH2 that includes the highest grade intercepts in which the average Fe, Zn, and Pb contents are 11.0, 2.0, and 0.6 %, respectively (Kyle and Price, 1985; 1986). Iron distribution was determined for HH2 by analyzing sample splits from all intervals previously analyzed for Zn and Pb (Appendix Id). Stratigraphic relationships for Fe abundances were similar to the three gross metal zones determined for Pb and Zn. Iron concentrations in the upper and lower zone of HH2 rarely exceed 1.0 %. The middle zone is the dominant site for Fe-sulfide mineralization where Fe concentrations commonly exceed 7.5 %; however, some intervals within the middle zone contain up to 30 % Fe (Agee, 1988).

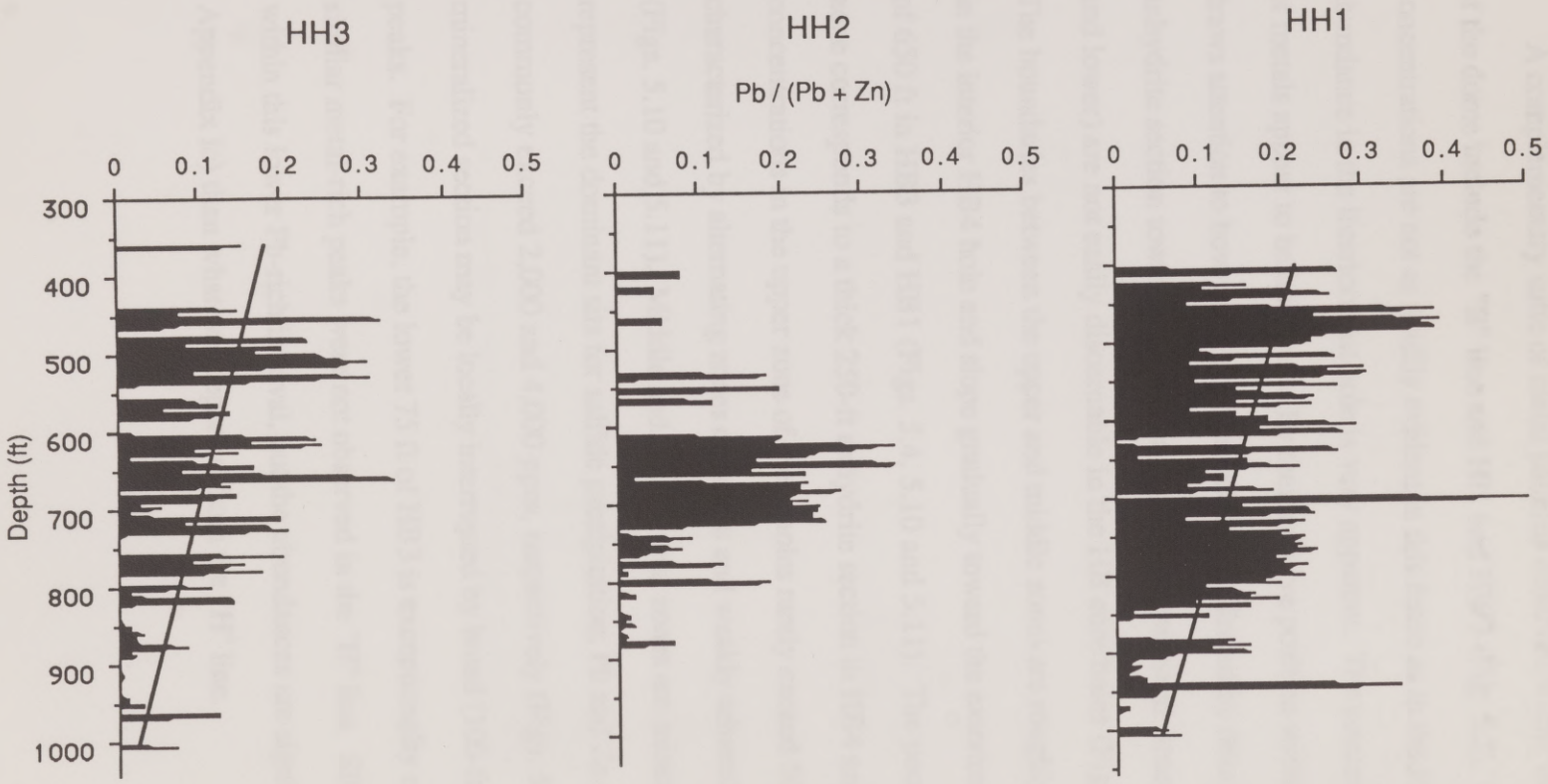

Fig. 5.9. Pb/(Pb+Zn) ratios for cored intervals of drill holes on the H-section line. Sloped regression lines indicate an increase in Zn relative to Pb with depth, corresponding to decreased Pb content in younger mineralizing fluids.

A complementary suite of metal patterns observed within the southern perimeter of the dome include the "B" line and HI1 and HW2 (Fig. 5.2). Although high concentrations are not as readily evident in this fence as in the H-fence, the lower metal abundance in the interiormost hole is very apparent. The concentration and distribution of metals appear to be influenced by their relative position within the cap rock. This draws attention to how metal patterns might be affected by thinning and tilting of the anhydrite section toward the dome margins. Gross metal zones (e.g., upper, middle, and lower) are not easily discernable in the HB core holes (Figs. 5.10 and 5.11). The boundaries between the upper and middle zones are roughly at the 575-ft level in the interior HB4 hole and slope gradually toward the exterior of the dome to depths of 650 ft in HB3 and HB1 (Figs. 5.4, 5.10 and 5.11). The poorly mineralized upper zone corresponds to a thick 250-ft anhydrite section in HB4 and HB3. The Pb+Zn concentrations in the upper zone of these holes rarely exceed 500 ppm and are characterized by alternating zones of barren and weakly mineralized anhydrite cap rock (Figs. 5.10 and 5.11). Middle and lower metal zones are mineralized throughout and represent the dominant sits for sulfide precipitation; Pb and Zn concentrations commonly exceed 2,000 and 4,000 ppm, respectively (Figs. 5.10 and 5.11). This mineralized section may be locally interrupted by broad (100-ft or less) metal enriched peaks. For example, the lower 75 ft of HB3 is exceptionally enriched in Pb, however, similar metal-rich peaks were not observed in the "H" line. Silver was also detected within this lower Pb-rich interval, but the abundances are significantly lower ($\leq$ 9 ppm; Appendix Ic) than what was reported from the "H" line.

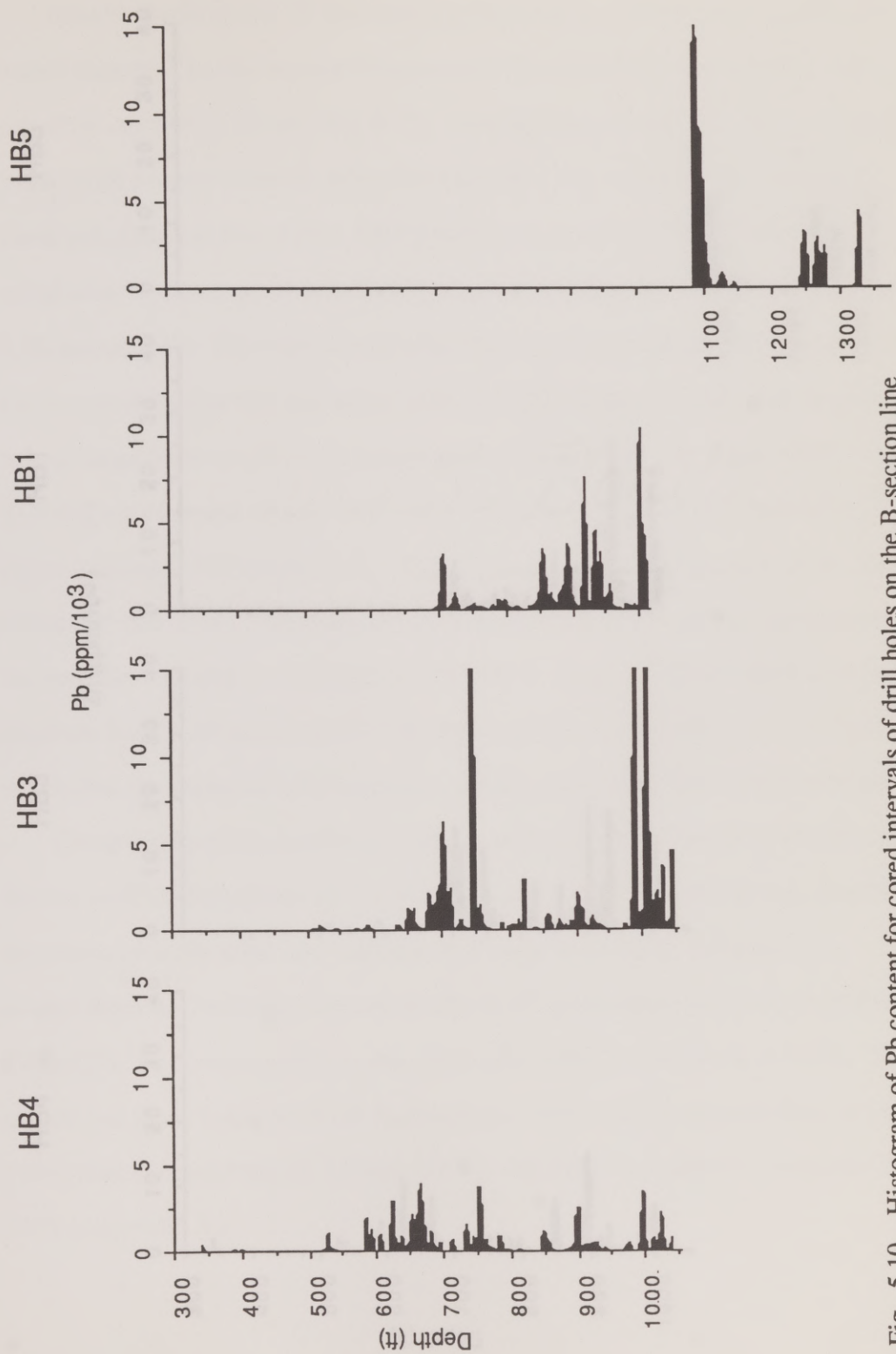

Fig. 5.10. Histogram of Pb content for cored intervals of drill holes on the B-section line

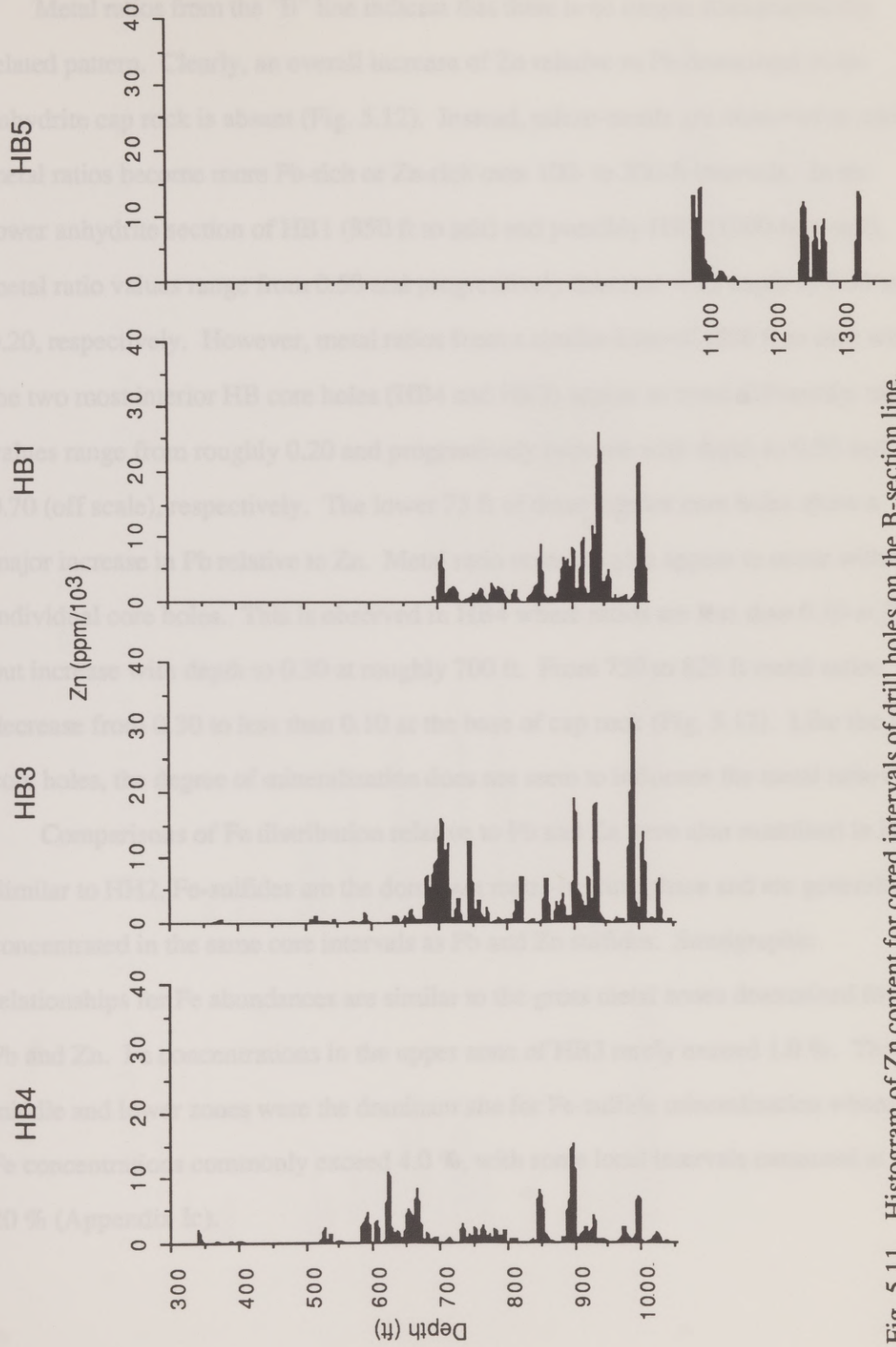

Fig. 5.11. Histogram of Zn content for cored intervals of drill holes on the B-section line.

Metal ratios from the "B" line indicate that there is no simple stratigraphically related pattern. Clearly, an overall increase of Zn relative to Pb downward in the anhydrite cap rock is absent (Fig. 5.12). Instead, micro-trends are observed in which metal ratios become more Pb-rich or Zn-rich over 100- to 200-ft intervals. In the lower anhydrite section of HB1 (850 ft to salt) and possibly HB5 (1090 ft to salt), metal ratio values range from 0.50 and progressively decrease with depth to 0.30 and 0.20, respectively. However, metal ratios from a similar interval (850 ft to salt) within the two most interior HB core holes (HB4 and HB3) appear to trend differently; ratio values range from roughly 0.20 and progressively increase with depth to 0.50 and 0.70 (off scale), respectively. The lower 75 ft of these interior core holes show a major increase in Pb relative to Zn. Metal ratio reversals also appear to occur within individual core holes. This is observed in HB4 where ratios are less than 0.10 at 500 ft but increase with depth to 0.30 at roughly 700 ft. From 750 to 825 ft metal ratios decrease from 0.30 to less than 0.10 at the base of cap rock (Fig. 5.12). Like the HH core holes, the degree of mineralization does not seem to influence the metal ratio data.

Comparisons of Fe distribution relative to Pb and Zn were also examined in HB3. Similar to HH2, Fe-sulfides are the dominant metal-bearing phase and are generally concentrated in the same core intervals as Pb and Zn sulfides. Stratigraphic relationships for Fe abundances are similar to the gross metal zones determined for Pb and Zn. Fe concentrations in the upper zone of HB3 rarely exceed 1.0 %. The middle and lower zones were the dominant site for Fe-sulfide mineralization where Fe concentrations commonly exceed 4.0 %, with some local intervals measured at 20 % (Appendix Ic).

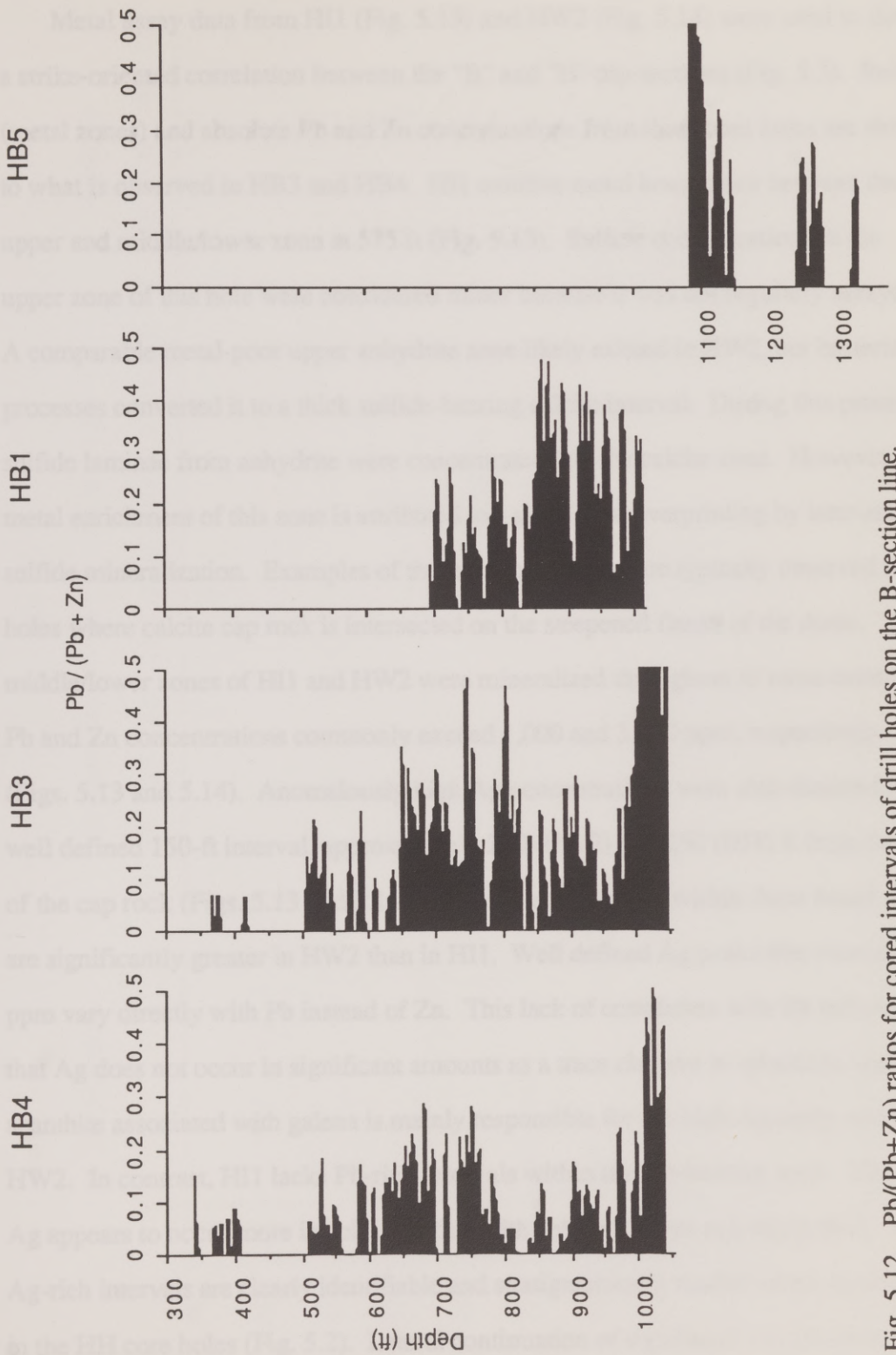

Fig. 5.12. Pb/(Pb+Zn) ratios for cored intervals of drill holes on the B-section line.

Metal assay data from HI1 (Fig. 5.13) and HW2 (Fig. 5.14) were used to develop a strike-oriented correlation between the "B" and "H" dip-sections (Fig. 5.2). Relative (metal zones) and absolute Pb and Zn concentrations from these core holes are similar to what is observed in HB3 and HB4. HI1 exhibits metal boundaries between the upper and middle/lower zone at 575 ft (Fig. 5.13). Sulfide concentrations in the upper zone of this hole were considered minor because it was not regularly assayed. A comparable metal-poor upper anhydrite zone likely existed in HW2, but bacterial processes converted it to a thick sulfide-bearing calcite interval. During this process sulfide laminae from anhydrite were concentrated into the calcite zone. However, metal enrichment of this zone is attributed to a significant overprinting by later-stage sulfide mineralization. Examples of these enriched zones are typically observed in core holes where calcite cap rock is intersected on the steepened flanks of the dome. The middle/lower zones of HI1 and HW2 were mineralized throughout to some extent; Pb and Zn concentrations commonly exceed 1,000 and 3,000 ppm, respectively (Figs. 5.13 and 5.14). Anomalously high Ag concentrations were also detected in a well defined 150-ft interval, approximately 200 (HW2) and 250 (HI1) ft from the base of the cap rock (Figs. 5.13 and 5.14). Silver concentrations within these broad zones are significantly greater in HW2 than in HI1. Well defined Ag peaks that exceed 100 ppm vary directly with Pb instead of Zn. This lack of correlation with Zn indicates that Ag does not occur in significant amounts as a trace element in sphalerite, and that acanthite associated with galena is mainly responsible for the high Ag assay values in HW2. In contrast, HI1 lacks Pb-rich intervals within the Ag-bearing zone. Therefore, Ag appears to occur more in solid solution with sphalerite than as a Ag-sulfide. These Ag-rich intervals are clearly identifiable and stratigraphically similar to the Ag-horizons in the HH core holes (Fig. 5.2). Lateral continuation of significant Ag abundances

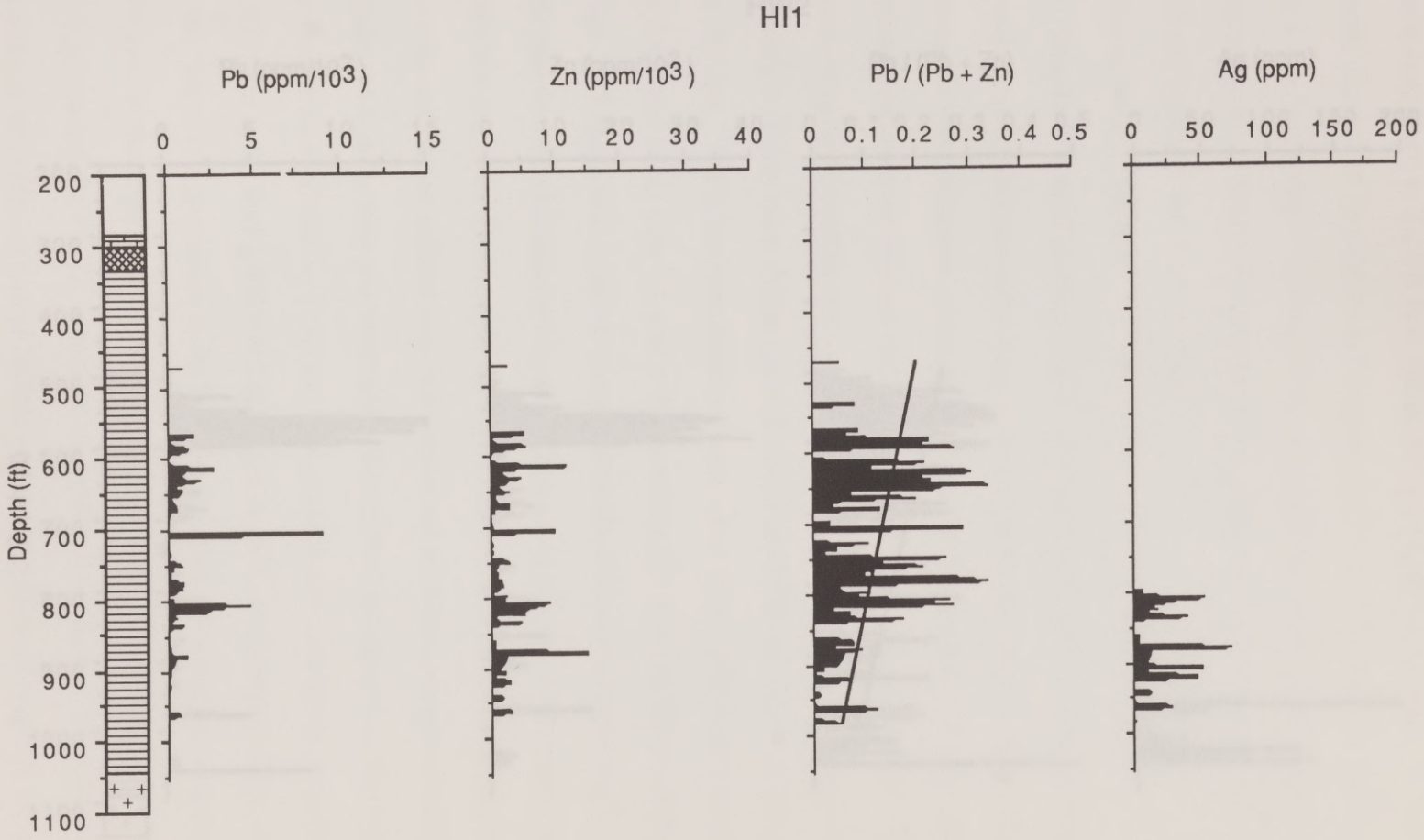

Fig. 5.13. Histogram of Pb, Zn, and Ag content and Pb/(Pb+Zn) ratios of drill hole HI1. Sloped regression line from metal ratios indicate an increase in Zn relative to Pb with depth. See Figure 5.2 for core hole location and Figure 5.3 for lithologic explanation of vertical profile.

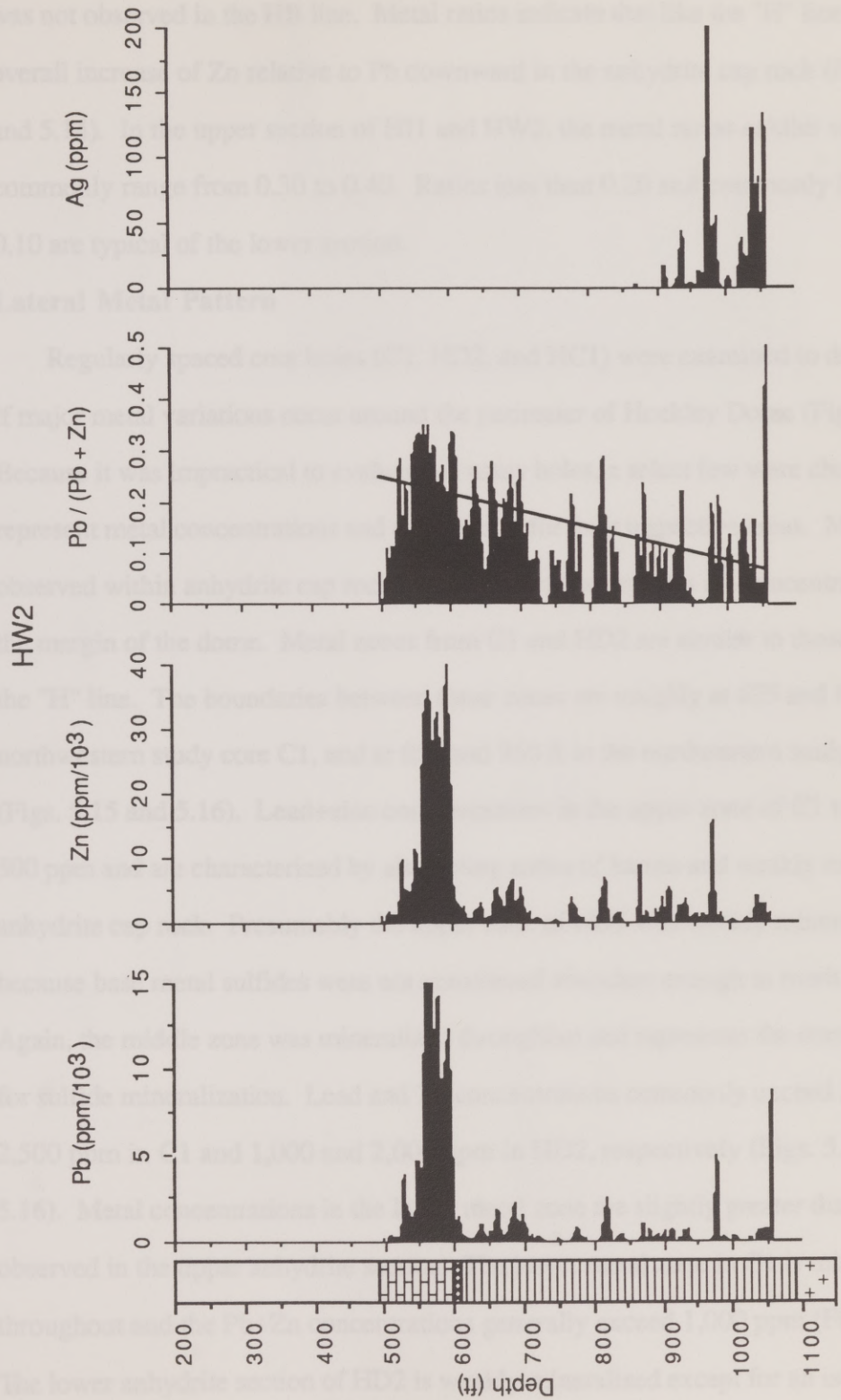

Fig. 5.14. Histogram of Pb, Zn, and Ag content and Pb/(Pb+Zn) ratios of drill hole HW2. Sloped regression line from metal ratios indicate an increase in Zn relative to Pb with depth. See Figure 5.2 for core hole location and Figure 5.3 for lithologic explanation of vertical profile.

was not observed in the HB line. Metal ratios indicate that like the "H" line there is an overall increase of Zn relative to Pb downward in the anhydrite cap rock (Figs. 5.13 and 5.14). In the upper section of HI1 and HW2, the metal ratios exhibit values that commonly range from 0.30 to 0.40. Ratios less than 0.20 and commonly less than 0.10 are typical of the lower section.

Lateral Metal Pattern

Regularly spaced core holes (C1, HD2, and HC1) were examined to determine if major metal variations occur around the perimeter of Hockley Dome (Fig. 5.1). Because it was impractical to evaluate all assay holes, a select few were chosen to represent metal concentrations and distribution for their respective areas. Metal patterns observed within anhydrite cap rock again support that sulfides are concentrated along the margin of the dome. Metal zones from C1 and HD2 are similar to those observed in the "H" line. The boundaries between these zones are roughly at 625 and 825 ft in the northwestern study core C1, and at 650 and 950 ft in the northeastern study core HD2 (Figs. 5.15 and 5.16). Lead+zinc concentrations in the upper zone of C1 rarely exceed 500 ppm and are characterized by alternating zones of barren and weakly mineralized anhydrite cap rock. Presumably the upper zone of HD2 was weakly mineralized because base metal sulfides were not considered abundant enough to merit assaying. Again, the middle zone was mineralized throughout and represents the dominant site for sulfide mineralization. Lead and Zn concentrations commonly exceed 2,000 and 2,500 ppm in C1 and 1,000 and 2,000 ppm in HD2, respectively (Figs. 5.15 and 5.16). Metal concentrations in the lower metal zone are slightly greater than those observed in the upper anhydrite section. The lower metal zone in C1 is mineralized throughout and the Pb+Zn concentrations generally exceed 1,000 ppm (Fig. 5.15). The lower anhydrite section of HD2 is weakly mineralized except for an isolated 20-ft

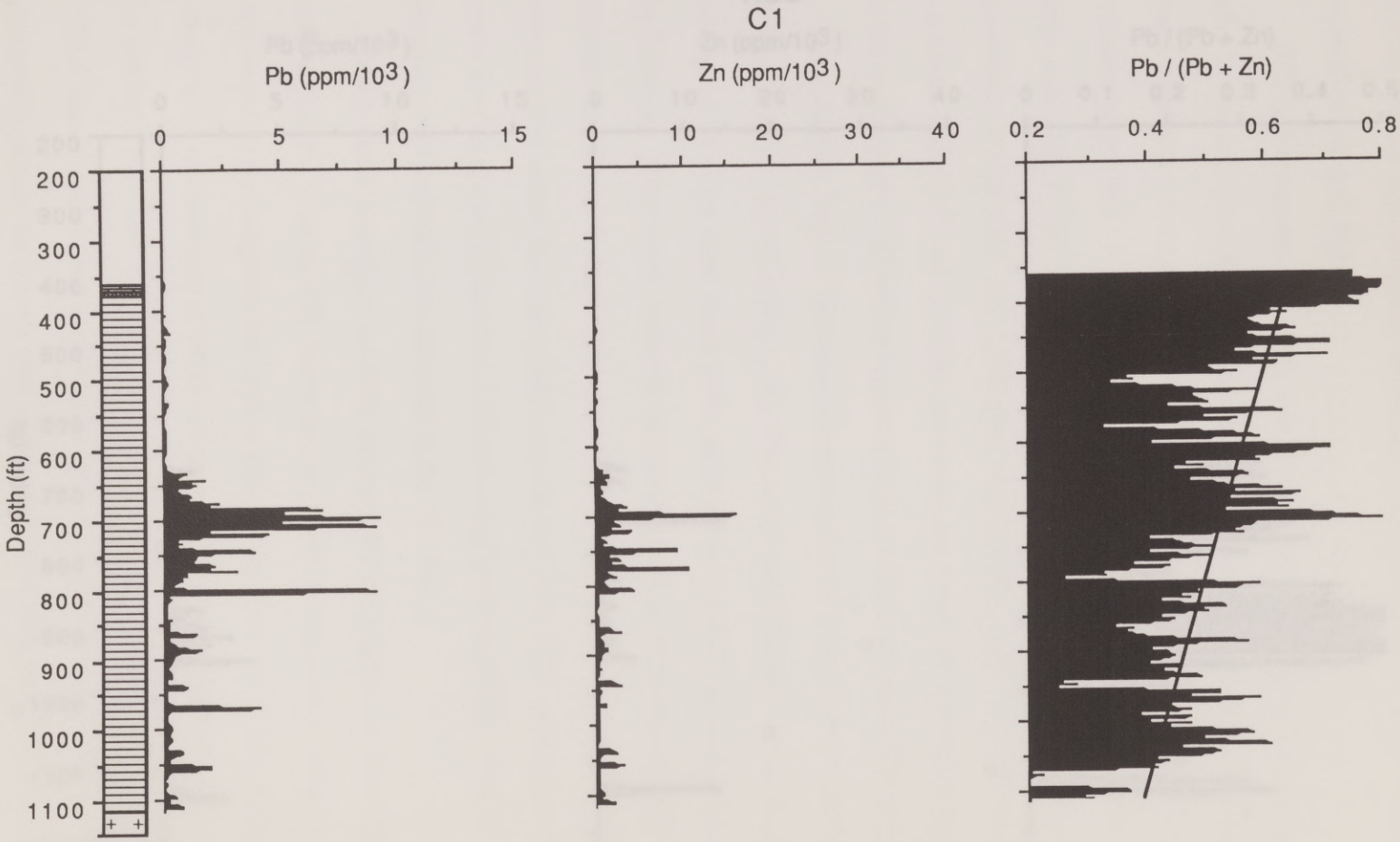

Fig. 5.15. Histogram of Pb and Zn content and Pb/(Pb+Zn) ratios of drill hole C1.
Sloped regression line from metal ratios indicate an increase in Zn relative to Pb with depth.
See Figure 5.1 for core hole location and Figure 5.3 for lithologic explanation of vertical profile.

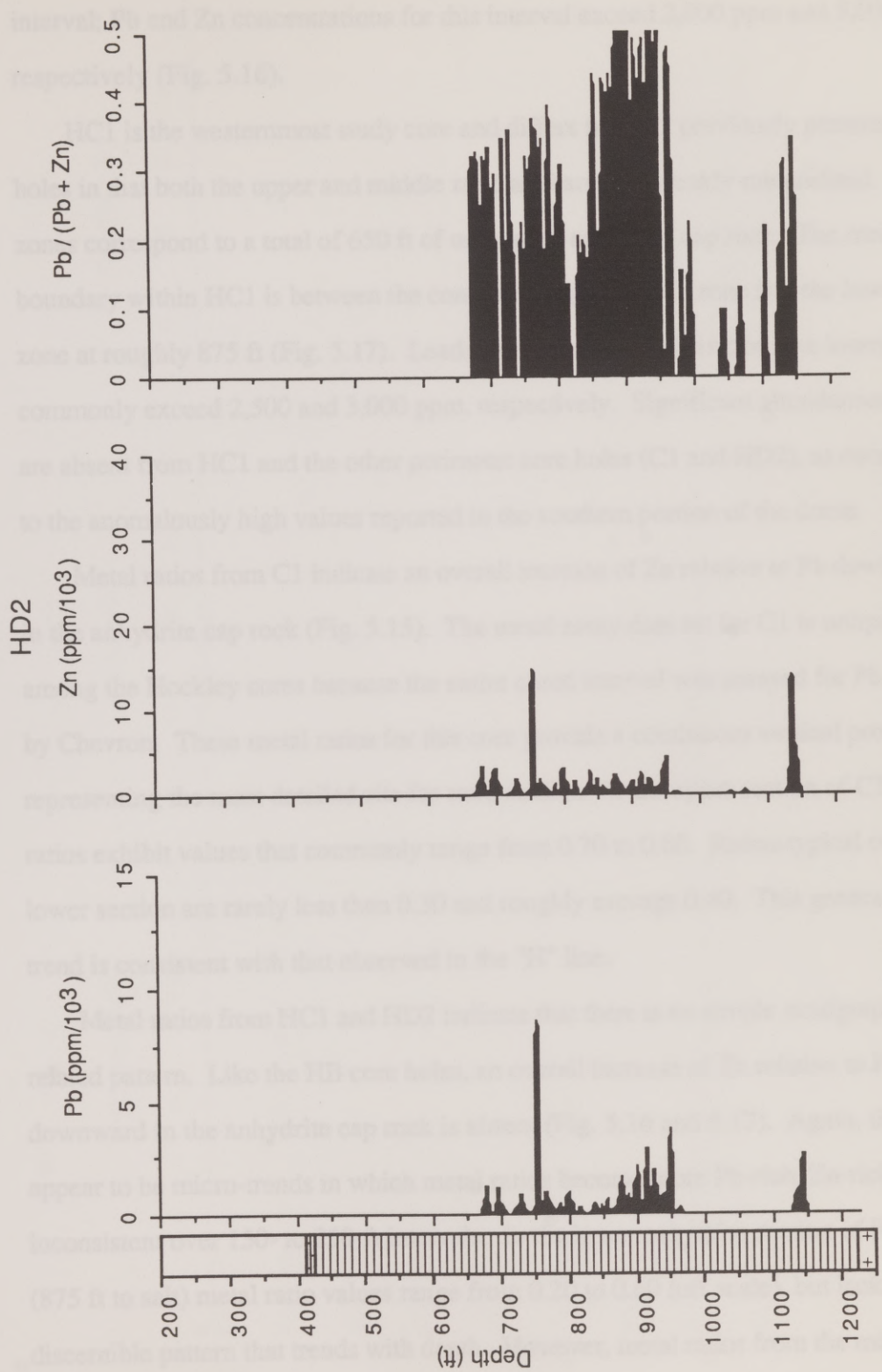

Fig. 5.16. Histogram of Pb and Zn content and Pb/(Pb+Zn) ratios of drill hole HD2. See Figure 5.1 for core hole location and Figure 5.3 for lithologic explanation of vertical profile.

interval; Pb and Zn concentrations for this interval exceed 2,000 ppm and 5,000 ppm, respectively (Fig. 5.16).

HC1 is the westernmost study core and differs from all previously presented core holes in that both the upper and middle zone are barren or weakly mineralized. These zones correspond to a total of 650 ft of unassayed anhydrite cap rock. The metal boundary within HC1 is between the combined upper/middle zone and the lower zone at roughly 875 ft (Fig. 5.17). Lead and Zn concentrations from the lower zone commonly exceed 2,500 and 3,000 ppm, respectively. Significant abundances of Ag are absent from HC1 and the other perimeter core holes (C1 and HD2), as compared to the anomalously high values reported in the southern portion of the dome.

Metal ratios from C1 indicate an overall increase of Zn relative to Pb downward in the anhydrite cap rock (Fig. 5.15). The metal assay data set for C1 is unique among the Hockley cores because the entire cored interval was assayed for Pb and Zn by Chevron. These metal ratios for this core provide a continuous vertical profile representing the most detailed site for ratio studies. In the upper section of C1, metal ratios exhibit values that commonly range from 0.70 to 0.80. Ratios typical of the lower section are rarely less than 0.30 and roughly average 0.40. This general metal trend is consistent with that observed in the "H" line.

Metal ratios from HC1 and HD2 indicate that there is no simple stratigraphically related pattern. Like the HB core holes, an overall increase of Zn relative to Pb downward in the anhydrite cap rock is absent (Fig. 5.16 and 5.17). Again, there appear to be micro-trends in which metal ratios become more Pb-rich, Zn-rich, or inconsistent over 150- to 250-ft intervals. In the lower anhydrite section of HC1 (875 ft to salt) metal ratio values range from 0.20 to 0.60 (off scale), but lack a discernible pattern that trends with depth. However, metal ratios from the middle

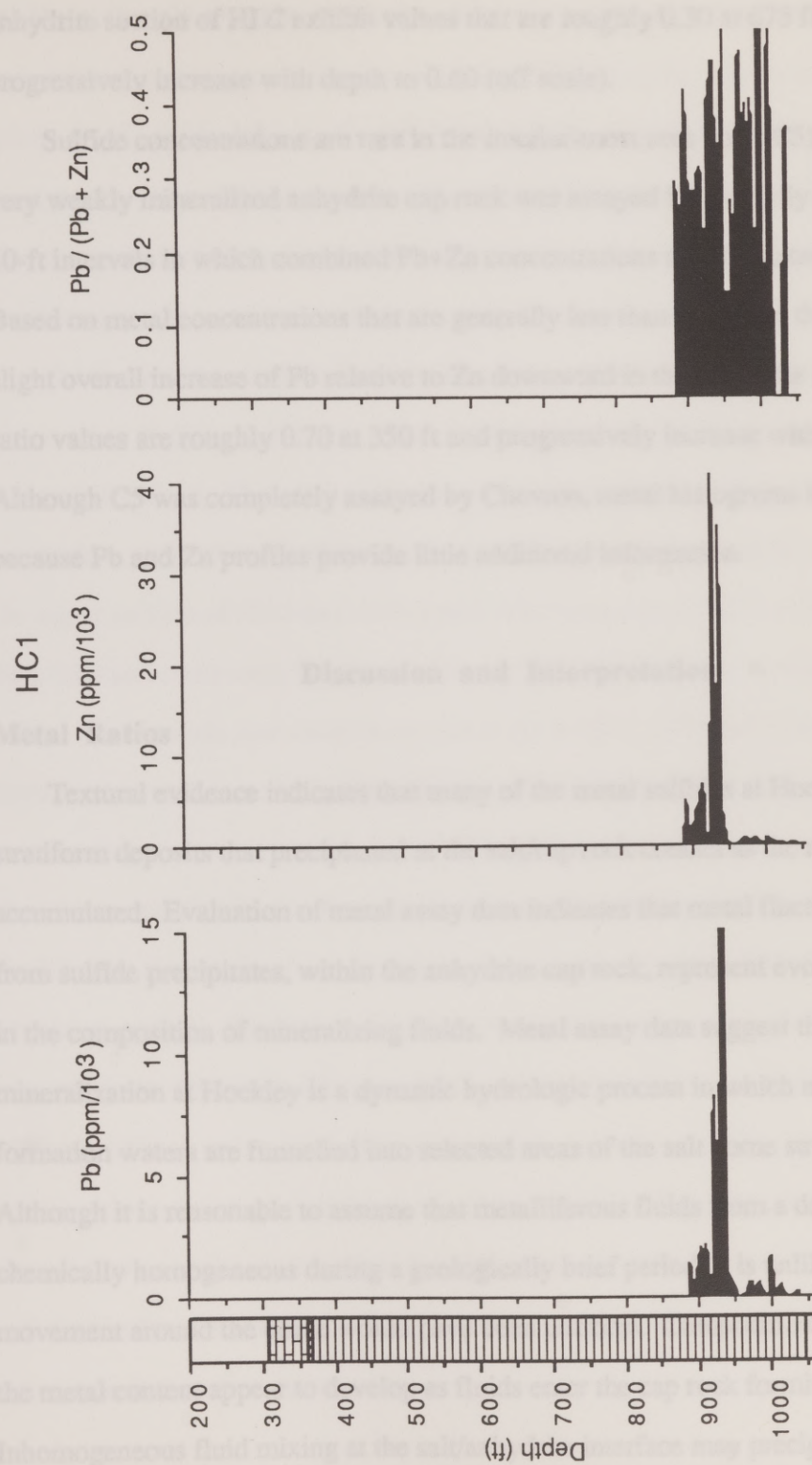

Fig. 5.17. Histogram of Pb and Zn content and Pb/(Pb+Zn) ratios of drill hole HC1. See Figure 5.1 for core hole location and Figure 5.3 for lithologic explanation of vertical profile.

anhydrite section of HD2 exhibit values that are roughly 0.30 at 675 ft and progressively increase with depth to 0.60 (off scale).

Sulfide concentrations are rare in the interior-most core hole (C5). The barren to very weakly mineralized anhydrite cap rock was assayed in randomly spaced 5- to 10-ft intervals in which combined Pb+Zn concentrations slightly exceeded 250 ppm. Based on metal concentrations that are generally less than 100 ppm, there may be a slight overall increase of Pb relative to Zn downward in the anhydrite cap rock. Metal ratio values are roughly 0.70 at 350 ft and progressively increase with depth to 0.85. Although C5 was completely assayed by Chevron, metal histograms are not presented because Pb and Zn profiles provide little additional information.

Discussion and Interpretation

Metal Ratios

Textural evidence indicates that many of the metal sulfides at Hockley Dome are stratiform deposits that precipitated at the salt/cap rock contact as the anhydrite zone accumulated. Evaluation of metal assay data indicates that metal fluctuations measured from sulfide precipitates, within the anhydrite cap rock, represent evolutionary changes in the composition of mineralizing fluids. Metal assay data suggest that sulfide mineralization at Hockley is a dynamic hydrologic process in which metalliferous formation waters are funnelled into selected areas of the salt dome structure. Although it is reasonable to assume that metalliferous fluids from a deep aquifer are chemically homogeneous during a geologically brief period, it is unlikely that fluid movement around the dome would have been uniform. Compositional variations in the metal content appear to develop as fluids enter the cap rock forming environment. Inhomogeneous fluid mixing at the salt/anhydrite interface may precipitate galena and

sphalerite (by pH increase, cooling, or dilution) such that sections of cap rock posses unique metal patterns and abundances. Also, differential movement of salt segments within the diapiric salt mass (Kupfer, 1989) may prevent the development of a metal stratigraphy that would be consistent throughout the entire dome. Despite these local aberrations in vertical and lateral metal concentrations, the majority of the study cores exhibit a general metal trend within the anhydrite cap rock.

Evidence of this trend is large scale metal variations in anhydrite cap rock, best observed as Pb/(Pb+Zn) ratios, which represent overall changes in the character of the mineralizing fluid. The general downward increase of Zn relative to Pb in anhydrite cap rock suggests that late-stage fluids were Zn-rich relative to early-stage fluids. In the upper section of HH1 and HH3 metal ratios range from 0.25 to 0.40; ratios less than 0.20 and commonly less than 0.10 are typical of the lower section of the drill holes. Metal trends and abundances observed in HW2, HI1 and C1 also indicate that there is an overall increase in Zn relative to Pb with depth (Fig. 5.1). This general metal ratio pattern is not observed in HD2, HB4 and HB3, even though their metals abundance and distribution (i.e., metal zones) are relatively similar. This suggests that the HB area is a site in which formation waters with unique/modified metal composition may have entered. This is best exhibited by the local occurrence of a basal Pb-rich interval observed only in HB4 and HB3. Other presented assay data from HB1 and HB5 are difficult to interpret. These core holes intercept relatively thin anhydrite sections along the steeply inclined cap rock perimeter. Therefore, it is not clear how these intercepts relate to thicker and undeformed cap rock sections. Metals abundance and distribution from HB1 and HB5 cannot be confidently compared with holes that cored a thicker section of cap rock.

Correlation of thin mineralized zones between adjacent core holes does not appear to be possible with the existing data base. However, some broader zones (50-feet or greater) are laterally continuous and can be recognized between distant core holes (500 to 1500 ft). For example, the "H" line exhibits a heavily mineralized section of cap rock that extends from the internal calcite zone (HH1 and HH2) and grades into anhydrite (HH3) toward the dome interior (Fig. 5.3). This sulfide-rich zone can be identified in all three core holes and is best defined by relatively high Zn concentrations with lesser amounts of Pb (Figs. 5.5 and 5.6).

The most striking variation in metal concentration and composition is the local occurrence of intense Ag mineralization that is apparently restricted to the southern margin of the dome. Significant concentrations (i.e., 50 ppm or greater) of Ag are observed to be stratigraphically low in the anhydrite cap rock and are generally independent of the major sulfide concentrations. For example, these high Ag concentrations near the base of HH1 (900 to 950 ft) and HH2 (850 to 900 ft) are due to the presence of acanthite and represent the most obvious "statigraphic" marker along the "H" line (Fig. 5.8). The lateral continuity of this mineralized horizon extends from an unknown distance northeast of the "H" line to approximately 1000 ft west of HH2. Silver concentrations of this nature were observed in cores occurring between the "H" line and HI1 (Fig. 5.2). Additional core holes around the dome were selectively analyzed for Ag, but enriched zones were not identified. Clearly, this stratigraphically and spatially localized Ag-rich zone represents selective movement of Ag-enriched, late-stage mineralizing fluids into the southern section of the salt dome.

Timing of Cap Rock Mineralization

The introduction of metal-bearing formation waters along the salt/anhydrite interface was an episodic process perhaps reflecting periodic expulsion from deep overpressured zones. Each infusion of metalliferous fluids was recorded as a thin sulfide laminae that accumulated at the base of the anhydrite cap rock. It may be possible to calibrate these basin dewatering pulses with respect to geologic age by establishing a relationship between sediment overthickening and anhydrite cap rock accumulation. It has been proposed in this study that thickness variations produced within the withdrawl-basin sediments indirectly permit a generalized cap rock stratigraphy to be estimated (Table III). The apparent correlation between cap rock stratigraphy and sediment overthickening is speculative but, at this point, is considered a plausible model to relate cap rock mineralization to age of cap rock formation.

As indicated from metal assay data there appears to be three gross metal zones identified within the cap rock. Generally, the upper metal zone consists of 340 to 450 ft of barren to weakly mineralized cap rock that probably corresponds to Wilcox time (Table III; Fig. 5.18a). During this time, diapirism and cap rock accumulation rates were greatest. This rapidly forming cap rock sequence was exposed to episodic movement of metalliferous formation waters from the deepening Gulf Coast basin. This stage produced alternating zones of barren and weakly mineralized anhydrite cap rock. As cap rock growth rates began to decline (approximately 50 Ma), metal concentrations appear to have increased significantly. Major sulfide-bearing intervals spanning 100 to 150 ft of cap rock are generally representative of the middle metal zone. These sulfide-rich intervals are interpreted to have formed principally during Claiborne time (Fig. 5.18b). Therefore, it is inferred from the stratigraphic position

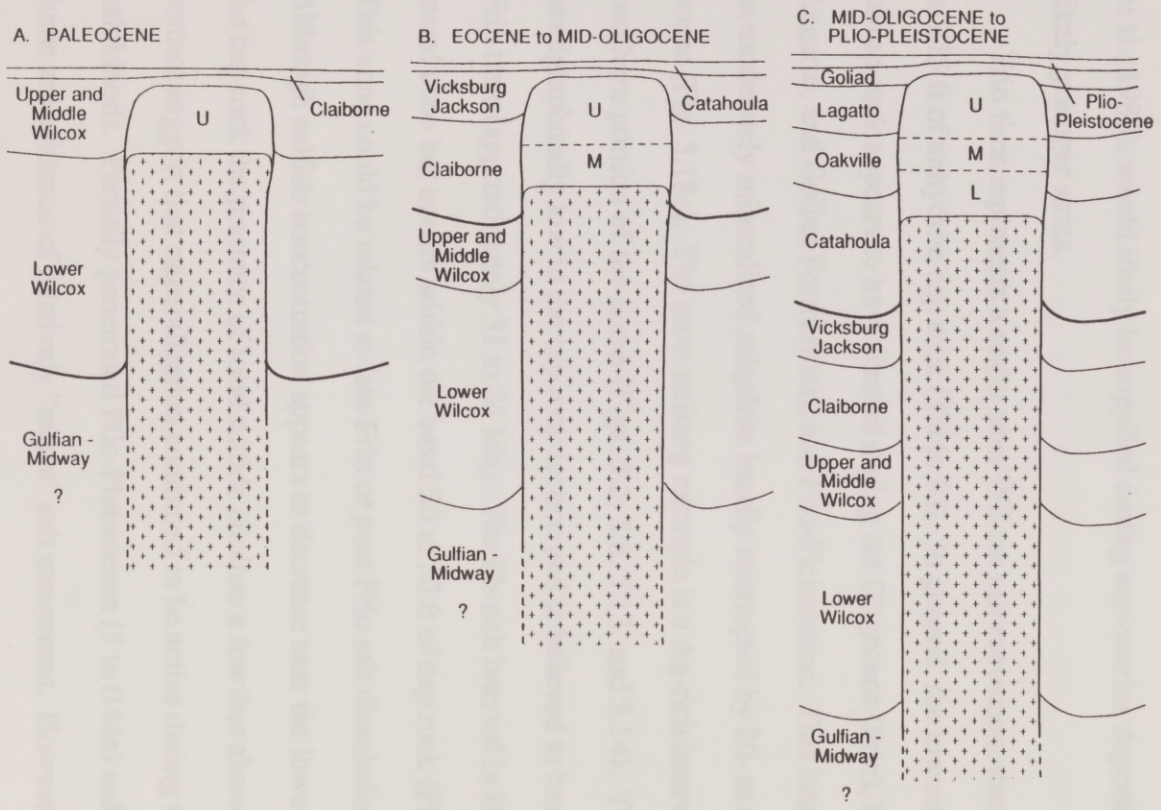

Fig. 5.18. Schematic evolution of Hockley cap rock growth showing general metal abundances and stratigraphic position during (A) Paleocene, (B) Eocene to Mid-Oligocene, and (C) Mid-Oligocene to Plio-Pleistocene.
Brines migrate updip from the overpressured deep Gulf of Mexico basin via formational aquifers and major fault systems. Metalliferous fluids that enter the site of ore deposition are in response to regional sediment deposition and not local sediment loading of Hockley Dome rim synclines. U, M, and L refer to the major cap rock metal zones (Upper, Middle, and Lower) discussed in the text.

of the middle metal zone and the relationship to uppermost Wilcox, Claiborne, and Jackson deposition that the major sulfide interval in C1, HB3, HH1 and HH2 likely developed between 50 to 35 Ma. It appears that bacterial processes then converted the heavily mineralized anhydrite interval in HH1 and HH2 into calcite. Low-temperature meteoric fluids ($\leq 70^{o}C$), required for calcite cap rock formation (Posey, 1986; Prikryl et al., 1988), would likely be supplied during non-marine deposition of Frio or more likely younger strata.

Frio time represents a major post-Wilcox salt movement that rapidly produced 160 to 215 ft of anhydrite cap rock (Table III). In general, the lowermost 200 to 300 ft of cap rock appears to have formed during the Oligocene (Frio), Miocene (Oakville, Lagarto, and Goliad Formations), and Plio-Pleistocene. This interval is characterized as moderately mineralized anhydrite locally interrupted by 20- to 50-ft thick metal-rich zones (Fig. 5.18c). The most striking example is a Ag-rich interval concentrated in the southern portion of the dome (Figs. 5.2, 5.8, 5.13, and 5.14). This metal zone is stratigraphically low in the cap rock section and is believed to have developed during Frio time (approximately 31 to 24 Ma). The Pb-rich interval in HB3 is also a localized metal zone but occurs within the basal 30 to 50 ft of cap rock (Figs. 5.2 and 5.10). This zone could be related to late-Frio or post-Frio salt dissolution (24 to 5 Ma). Although sulfide concentration appears to decrease near the lowermost portion of the cap rock the presence of local sulfide laminae a few feet above the salt/anhydrite contact suggest that mineralization continued to be active during the waning stages of halokinesis. Partially penetrated Plio-Pleistocene (5 to 0 Ma) sediments on top of the dome are evidence of relatively "recent" salt movement. However, the presence of a fused anhydrite/salt contact and the absence of any topographic relief over Hockley Dome indicates that dome growth is inactive. Therefore, it is difficult to determine

when the supply of metalliferous fluids to the cap rock environment was curtailed and the mineralizing system terminated. It is possible that further research will provide a basis for refining cap rock growth/mineralization estimates of this kind in the future.

The question to address at this point is what mechanism(s) controls sulfide concentration in the anhydrite cap rock. Clearly, sulfide concentrations can be strongly influenced by flow rates of metalliferous brines into the cap rock forming environment, i.e., metal concentrations probably will be directly related to mineralizing fluid flow rates. However, it appears that growth rates may indirectly have had a profound effect on the degree of sulfide mineralization. For example, if basin dewatering rates are assumed to be constant over the history of anhydrite cap rock development, then at times of relatively low cap rock growth rates metalliferous fluids may reside longer at the salt/anhydrite interface. Sulfide concentrations will also increase under these slow cap rock growth conditions because a smaller section of anhydrite, representing a longer period of time, may be exposed to a greater number of mineralizing pulses per given unit of cap rock. If cap rock is forming quickly, then an equivalent volume of metalliferous fluids (or number of dewatering events) would be "diluted" over a thicker section of anhydrite cap rock. A balance between these processes may produce the variation in metal abundances observed within cap rock.

Brine Geochemistry

Concentrations of metals in deep formational brines vary widely (e.g., Carpenter et al., 1974). The precise mechanism through which these fluids achieve their elemental metal content is not well understood. The evolution of metalliferous brines is probably tied to progressive diagenesis in deepening sedimentary basins. The formation of approximately 940 ft of original anhydrite cap rock at Hockley represents approximately 50 Ma of episodic sulfide mineralization. Consequently,

changes in fluid character over long periods of time can be recognized by sulfide concentration and occurrence. The shift from relatively Pb- to Zn-rich sulfide laminae with depth in the cap rock is interpreted to represent gradual but significant changes in the mineralizing fluid character over time.

Some geochemical models of metalliferous oil field brines predict that the products of the earliest ore-forming solutions would be sphalerite-rich followed by a second galena-rich stage (Sverjensky, 1984). The relative lengths of time of and between the two stages of deposition should determine the overall Pb/Zn ratio of the deposit. This interpretation does not appear to be influenced by the aquifer type (i.e., siliciclastic or carbonate) with which migrating ore-forming fluids were modeled (Sverjensky, 1984). However, there is a correlation of Zn-rich deposits with carbonate host rocks (e.g., east Tennessee with dolostone aquifers) and Pb-rich deposits with sandstone aquifers (Bjorlykke and Sangster, 1981; Gustafson and Williams, 1981). This sulfide/host rock association suggests that chemical reactions might occur when an oil field brine migrates out of a sedimentary basin and interacts with aquifer units enroute to an ore-forming site. The duration of and type of rock-water interactions encountered by basinal fluids can account for the differences in the composition of modern oil field brines and mineralizing solutions for major sediment-hosted ore deposits (Sverjensky, 1984). According to McLimans et al. (1980) and Sverjensky (1981), oil field brines can become ore-forming solutions and can transport base metals and reduced sulfur to sites of ore formation by large-scale migration through aquifers in sedimentary basins. The movement of significant quantities of both metals and reduced sulfur in formation waters requires moderately low pH's and small, approximately equal quantities of base metals and reduced sulfur (Sverjensky, 1984). However, many authors propose that formation water at pH values generally observed in sedimentary basins (pH of 4 to 7)

can not carry high concentrations of both metals and reduced sulfur (Kharaka et al., 1987). Evidence for Kharaka's et al. (1987) hypothesis is based on chemical composition of formation waters from the central Mississippi Salt Dome basin. These data suggest that high metal concentrations (Fe, Zn, Pb, etc.) are only present in formation waters with extremely low concentrations of H_2S (Kharaka et al., 1987).

For theories which require that metal and reduced sulfur be transported together in the same solution, the problem is not one of just metal transport but of reduced sulfur transport as well. A geochemical consideration is the quantities of Pb and Zn, as chloride complexes, that can be transported at pH values not far from neutrality and at temperatures of 100 to 150°C. Experimental determination of Pb and Zn solubilities under H_2S-saturated conditions has been carried out for a 3.0m NaCl solution at temperatures of 100°C. At 100°C, the neutral point is pH 6.13, so pH values ranging from 6.0 to 4.0 was considered (Anderson, 1973). Under these conditions, Zn, Pb, and H_2S content in solution ranges from 2.0, 0.6, and 0.6 ppm (pH of 6) to 20.0, 6.0, and 6.0 (pH of 4), respectively (Anderson, 1973). Solubility experiments indicate that by varying the above conditions both Pb and Zn become more soluble in solution as salinity and temperature increase; regardless of any of these changes Zn always remains more soluble than Pb (Anderson, 1973; Barrett and Anderson, 1988). There is little doubt that under the above conditions metalliferous brines can transport and deposit galena and sphalerite in ore quantities. However, if the ore-forming solution need only supply the metals with precipitation brought about by addition of H_2S from another solution, transport of higher metal concentrations are possible. Examples of such formation waters are extremely deficient in H_2S and contain Pb and Zn in much higher concentrations than the minimum values required for the formation of Mississippi Valley-Type deposits (Sverjensky, 1984; Kharaka et al., 1987).

The pore waters of deeply buried sediments undergoing diagenesis in the Gulf Coast basin appear to be a likely source of the ore-forming solutions that produced cap rock-hosted sulfide concentrations at Hockley Dome. However, the predicted metal trends determined by modeling a present-day Gulf Coast metal-bearing oil field brine are not in complete agreement. Results from modeled fluids indicate that the relative Zn/Pb ratio should decrease as a function of time and distance to the ore-forming site (Sverjensky, 1984). This trend is not what is observed at the Hockley Dome; instead the Zn/Pb ratio increases slightly with time. However, deposits with high Zn/Pb ratios suggest that the early Zn-rich stage of ore formation is much longer than the Pb-rich stage in the case of the carbonate aquifer. The opposite occurs in the case of a sandstone aquifer. Although Hockley Dome is emplaced into a thick sequence of siliciclastic sediments, the observed Zn to Pb ratio of three to one suggests that there is a fundamental relationship between Hockley sulfides and a carbonate aquifer flow path for metalliferous fluids.

Minor galena and sphalerite associated with deep subsurface carbonate cements within Lower Cretaceous platform carbonates in south Texas are inferred to have precipitated from relatively hot deep-sourced formation waters (Land and Prezbindowski, 1981; Woronick and Land, 1985). Higher Zn-Pb-Ag sulfide concentrations have been reported from deep Jurassic carbonates in southern Arkansas (Kyle et al., 1988). The metal component in these Mesozoic carbonates may have originated from fluids that migrated up faults after rock-water interactions in more deeply buried formations. For example, high Pb and Zn concentrations in some basinward Cretaceous carbonate-hosted formation waters in south Texas have been suggested to be related to metal release during albitization of detrital plagioclase (Land

and Prezbindowski, 1981). However, in sedimentary basins metal concentrations are typically low in formation water because any metals leached from shale and feldspar are precipitated as sulfides (Kharaka et al., 1987). Exceptionally rich sources of metals, such as red beds, are attractive sources for metals because they are generally low in reduced sulfur - a function of their low organic content. Lead, Zn and other metals absorbed into the red beds are mobilized into solution when the red beds are leached by reducing formation waters (Kharaka et al., 1987). Brines with similar metal compositions migrating along formational aquifers, faults, and diapir margins may have produced cap rock metal concentrations at Hockley and other domes (Kyle and Price, 1986; Light et al., 1987).

Formation Waters

Published chemical analyses of metalliferous Gulf Coast formation waters were compiled to evaluate metal-bearing brines that could have been responsible for sulfide mineralization at Hockley Dome. This data base consists of brine analyses reported by Carpenter et al. (1974) and Carpenter and Trout (1978) from Arkansas, Louisiana, and central Mississippi. Land and Prezbindowski (1981), Kharaka et al. (1977; 1980), and Macpherson (1989) reported analyses of brines from the Texas Gulf Coast. Geochemical analysis by Macpherson (1989) focused on south Texas Tertiary reservoir fluids in which 3 and 22 out of a total of 85 water analyses contained detectable amounts of Pb and Zn, respectively. All formation fluids were evaluated for their Pb and Zn content, host rock age, and lithology type (Tables VI and VII).

A summary of the Pb and Zn concentrations by stratigraphic position clearly indicate a systematic relationship between brine chemistry and reservoir age. The existing data base for Tertiary brines suggests that these fluids typically contain only minor amounts of metals (Table VI; Fig. 5.19). However, the Picaroon field, Brazos

Table VI. Summary of Gulf Coast formation water metal analyses by formation age.

Age	Metal	Number of analyses	Minimum (mg/L)	Maximum (mg/L)	Mean (mg/L)
Tertiary	Pb	6	<0.1	1.1	0.3
		3*	1.1*	6.0*	3.4*
	Zn	25	<0.1	1.6	0.7
		3**	25.0**	194.0**	110.0**
Cretaceous	Pb	57	2.0	226.0	39.0
	Zn	57	4.0	753.0	189.0
Jurassic	Pb	45	1.0	24.0	3.0
	Zn	44	0.4	84.0	14.0

References to data: Carpenter and others (1974), Carpenter and Trout (1978), Kharaka et al. (1977); (1980), Land and Prezbindowski (1981), and Macpherson (1989).

* Pb analyses from the Picaroon field, offshore Texas; reported in Macpherson (1989).
** Zn analyses from the Picaroon field, offshore Texas; reported in Macpherson (1989).

Table VII. Summary of Gulf Coast formation water by reservoir lithology.

Variables	Age	Lithology	No. of analyses	Minimum	Maximum	Mean
				Celsius	Celsius	Celsius
Temp. (°C)	Tertiary	Siliciclastics	25	70	150	108
	Cretaceous	Siliciclastics	44	100	136	123
	Jurassic	Siliciclastics	11	121	158	132
	Tertiary	Carbonates	--	--	--	--
	Cretaceous	Carbonates	13	86	176	134
	Jurassic	Carbonates	43	73	154	117
				mg/L	mg/L	mg/L
T.D.S. (mg/L)	Tertiary	Siliciclastics	25	6,000	132,000	45,000
	Cretaceous	Siliciclastics	44	187,900	319,500	249,000
	Jurassic	Siliciclastics	11	160,300	323,500	278,000
	Tertiary	Carbonates	--	--	--	--
	Cretaceous	Carbonates	8	118,000	344,000	218,000
	Jurassic	Carbonates	35	50,500	364,500	292,080
Pb (mg/L)	Tertiary *	Siliciclastics	6	<0.1	1.1	0.3
	Cretaceous	Siliciclastics	44	2.0	111.0	40.3
	Jurassic	Siliciclastics	11	2.0	24.0	4.4
	Tertiary	Carbonates	--	--	--	--
	Cretaceous	Carbonates	13	2.0	226.0	36.0
	Jurassic	Carbonates	34	1.0	19.0	2.5
Zn (mg/L)	Tertiary *	Siliciclastics	25	<0.1	1.6	0.7
	Cretaceous	Siliciclastics	44	12.0	367.0	173.1
	Jurassic	Siliciclastics	11	4.0	84.0	21.2
	Tertiary	Carbonates	--	--	--	--
	Cretaceous	Carbonates	13	4.0	753.0	247.2
	Jurassic	Carbonates	33	0.4	66.0	10.9

References to data: Carpenter and others (1974), Carpenter and Trout (1978), Kharaka et al. (1977); (1980), Land and Prezbindowski (1981), and Macpherson (1989).

-- Data not available

* Picaroon fluids are excluded from this data set because they appear to have a strong Mesozoic signature (see text for discussion).

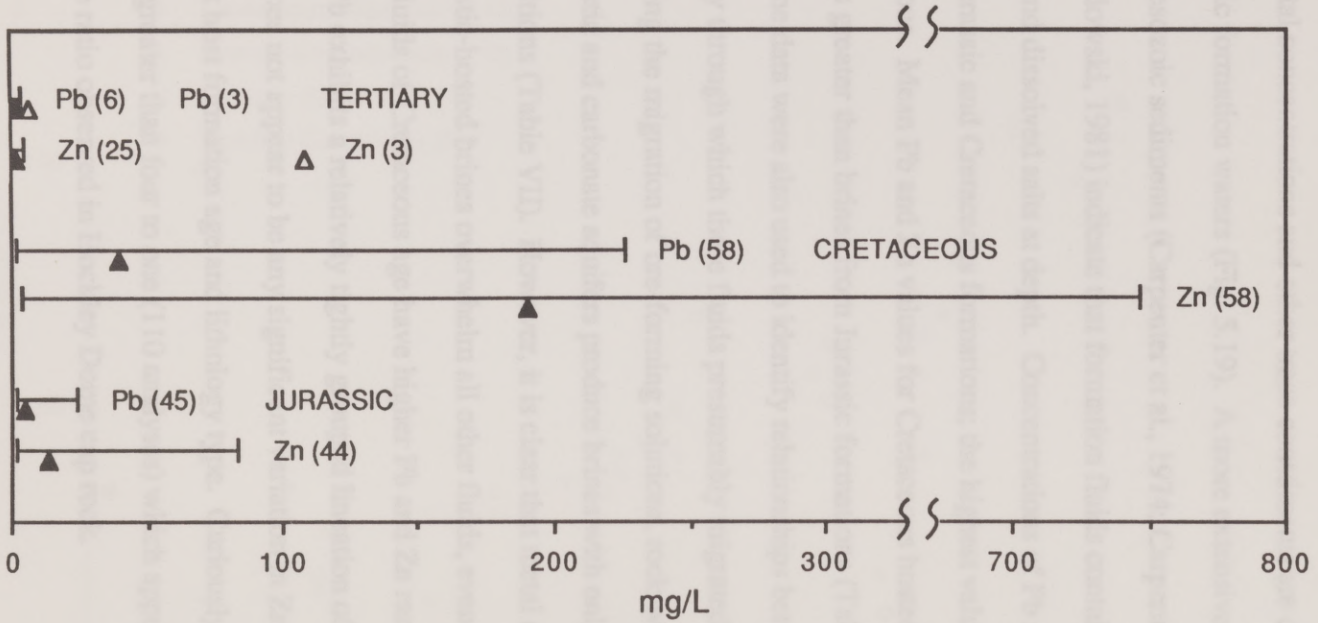

Fig. 5.19. Range and mean (filled triangle) of metal-bearing Gulf Coast formation waters by reservoir age. The numbers in parentheses indicate total number of samples analyzed. The open triangles represent mean values for the Picaroon field, offshore Texas; they are interpreted to have a strong Mesozoic fluid signature. References to data: Carpenter et al. (1974), Carpenter and Trout (1978), Land and Prezbindowski (1981), Macpherson (1989), and Kharaka et al. (1977; 1980).

area, offshore Texas, is an exception to these metal-poor brines. Lead and Zn concentrations are significantly greater than what is typically observed within the Tertiary section. In fact, Picaroon field fluids may have an external source because their metal concentrations and other trace constituents are characteristic of deep Mesozoic formation waters (Fig. 5.19). A more extensive collection of brine analyses from Mesozoic sediments (Carpenter et al., 1974; Carpenter and Trout, 1978; Land and Prezbindowski, 1981) indicate that formation fluids contain higher concentrations of metals and dissolved salts at depth. Concentrations of Pb and Zn are greatly elevated in the Jurassic and Cretaceous formations; the highest values are restricted to the lower Cretaceous. Mean Pb and Zn values for Cretaceous hosted fluids are approximately 13 times greater than brines from Jurassic formations (Table VI; Fig. 5.19).

Brine data were also used to identify relationships between metal content and the lithology through which these fluids presumably migrated. Brine analyses suggest that during the migration of ore-forming solutions, rock-water interactions between siliciclastic and carbonate aquifers produce brines with only moderately different metal compositions (Table VII). However, it is clear that metal concentrations for Cretaceous siliciclastic-hosted brines overwhelm all other fluids, even though some carbonate-hosted fluids of Cretaceous age have higher Pb and Zn ranges. A scatter plot of Zn versus Pb exhibits a relatively tightly grouped lineation of data points (Fig. 5.20). There does not appear to be any significant variation in Zn to Pb ratios for brines of different host formation age and lithology type. Curiously, mean Zn to Pb ratio is slightly greater than four to one (110 analyses) which approximates the three to one Zn to Pb ratio observed in Hockley Dome cap rock.

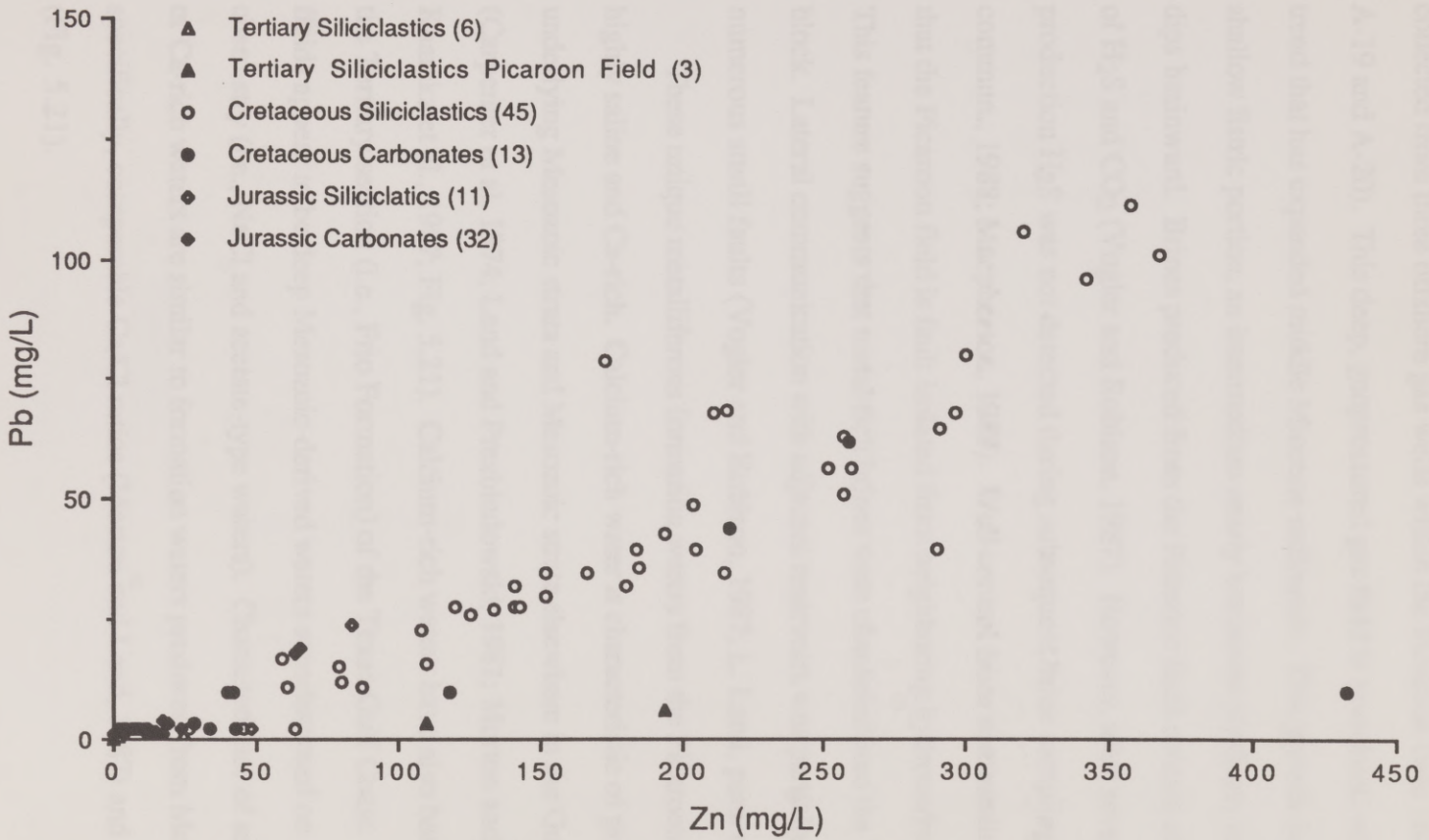

Fig. 5.20. Scatter plot of metal-bearing formation waters from Gulf Coast region.
Fluids from Tertiary siliciclasitics (six values) plot within the black area near the origin, i.e., very low metal values. The three most metal-rich brines produced within Tertiary siliciclasitics are from the Picaroon field. Three high metal brines from Cretaceous carbonates (Land and Prezbindowski, 1981) are off the field of this diagram. References to data: Carpenter et al. (1974), Carpenter and Trout (1978), Land and Prezbindowski (1981), Macpherson (1989), and Kharaka et al. (1977; 1980).

An intriguing situation is provided by the anomalously metal-rich formation waters collected from three offshore gas wells within the Picaroon field (Brazos area, Blocks A-19 and A-20). This deep, geopressured gas field is associated with the Corsair fault trend that has expanded middle Miocene sediments. This growth fault consists of a shallow listric portion, an intermediate nearly horizontal platform, and a deep ramp that dips basinward. Brines produced from the Picaroon field contain corrosive amounts of H_2S and CO_2 (Vogler and Robison, 1987). However, after several months of production H_2S was not detected during subsequent brine sampling (L. Land, pers. commun., 1988; Macpherson, 1989). Well control from surrounding fields indicates that the Picaroon field is fault isolated from neighboring hydrocarbon-producing fields. This feature suggests that metal-rich brines were channeled into the Picaroon fault block. Lateral communication with adjacent reservoirs was partially obstructed by numerous small faults (Vogler and Robison, 1987; L. Land, pers. commun., 1988).

These unique metalliferous formation waters from the Picaroon field are also highly saline and Ca-rich. Calcium-rich water is characteristic of presumably underlying Mesozoic strata and Mesozoic strata elsewhere in the Gulf Coast basin (Carpenter et al, 1974; Land and Prezbindowski, 1981; Morton and Land, 1987; Kharaka et al., 1987; Fig. 5.21). Calcium-rich waters have also been recognized in the Tertiary section (i.e., Frio Formation) of the Texas Gulf Coast. However, these fluids appear to be deep Mesozoic-derived waters superimposed on the regional water chemistry (i.e., NaCl and acetate-type waters). Characteristics of several components of Ca-rich waters are similar to formation waters produced from Mesozoic rocks; specifically, comparable Ca/Cl ratios (Morton and Land, 1987) and Pb and Zn (Fig. 5.21).

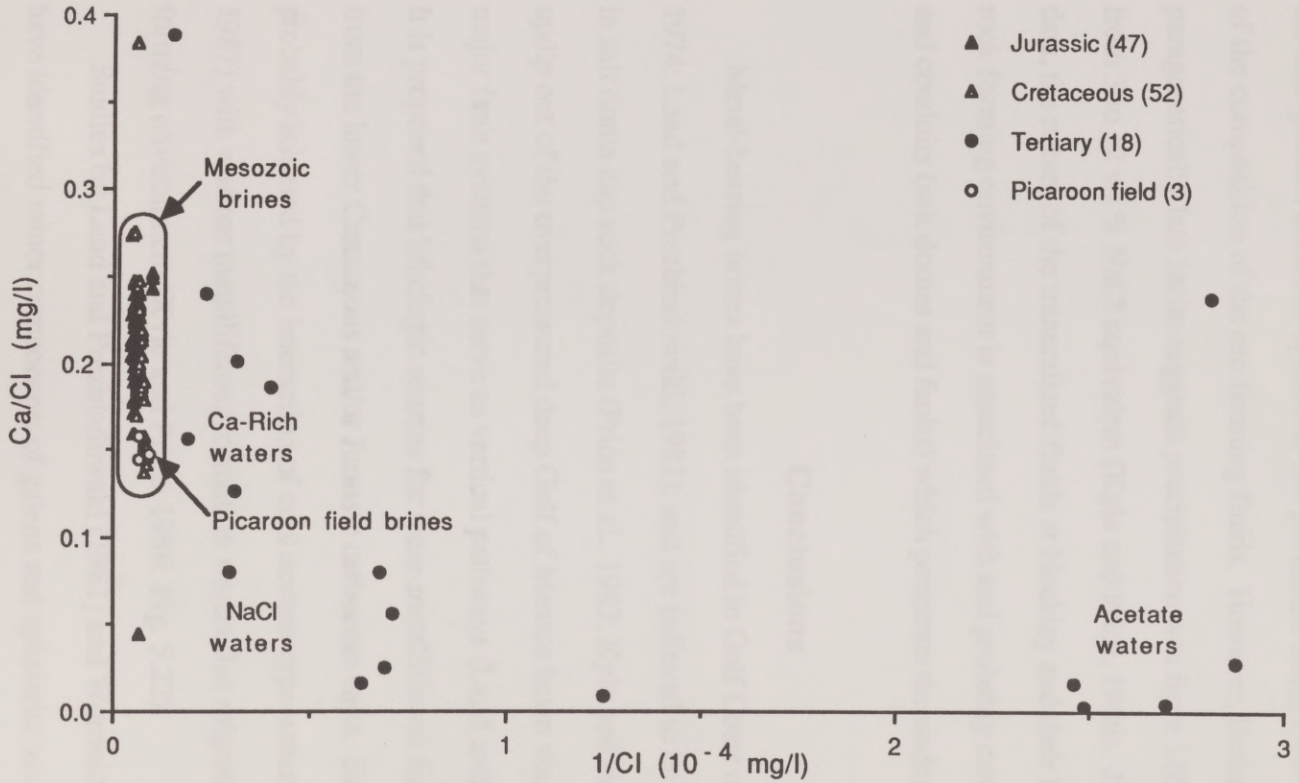

Fig. 5.21. Scatter plot of Ca versus Cl concentrations for metal-bearing formation waters from the Gulf Coast region. Almost all of the formation waters that contain > 1 mg/L Pb+Zn are Na-Ca-Cl brines. Calcium-rich, metal-bearing waters from Frio reservoirs (south Texas) have Ca/Cl ratios similar to brines in Cretaceous rocks (Texas and Mississippi) and in Jurassic rocks (Mississippi). Underlying Mesozoic fluids have probably been circulated into the Tertiary section resulting in elevated Ca and metal concentrations (Morton and Land, 1987). Ca/Cl ratios from Picaroon fluids fall within the Mesozoic brine field suggesting a direct conduit (fault) of metalliferous fluids from the Mesozoic section. NaCl-type water is derived by dissolution of diapiric salt, and Acetate-type water is derived from diagenetic clay mineral reactions that release water (Morton and Land, 1987). References to data: Carpenter et al. (1974), Carpenter and Trout (1978), Land and Prezbindowski (1981), Macpherson (1989), and Kharaka et al. (1977; 1980).

It appears that Ca-rich, saline waters were injected along fault conduits from underlying Mesozoic units resulting in anomalously high metal abundances in the Picaroon field. A similar hydrologic scenario may have existed at Hockley Dome, but the fine-grained nature of sphalerite has prevented direct fluid-inclusion investigations of the composition of the ore-forming fluids. However, limited fluid inclusion data for paragenetically late barite suggests precipitation was from 110 to 140°C fluids ranging from 3 to 12 wt % NaCl equivalent (Kyle and Price, 1986). Judging from the available data, the nature of the mineralized fluids at Hockley and their flow path into the cap rock forming environment is associated with and probably controlled by local structures and conduits (salt domes and faults) which penetrate the underlying Mesozoic strata.

Conclusions

Metal-bearing brines have been identified in Gulf Coast oil wells (Carpenter et al., 1974; Land and Prezbindowski, 1981), and are believed to be the source of the metals in salt dome cap rock deposits (Price et al., 1983; Kyle and Price, 1986). Brines move updip out of the overpressured deep Gulf of Mexico basin via formation aquifers and major fault systems that serve as vertical pathways (Land and Prezbindowski, 1981). It is proposed that lithologic sources for these metalliferous formation waters originate from the lower Cretaceous and/or Jurassic carbonate units. Sulfide precipitation was probably initiated by the interaction of cool acetate-type waters (Morton and Land, 1987) with warmer metalliferous formation waters that migrated into the cap rock forming environment (Kyle and Price, 1986; Fig. 5.22).

Studies by Land and Prezbindowski (1981) and Woronick and Land (1985) have identified minor components of galena and sphalerite associated with late subsurface carbonate cements within Lower Cretaceous platform carbonates and

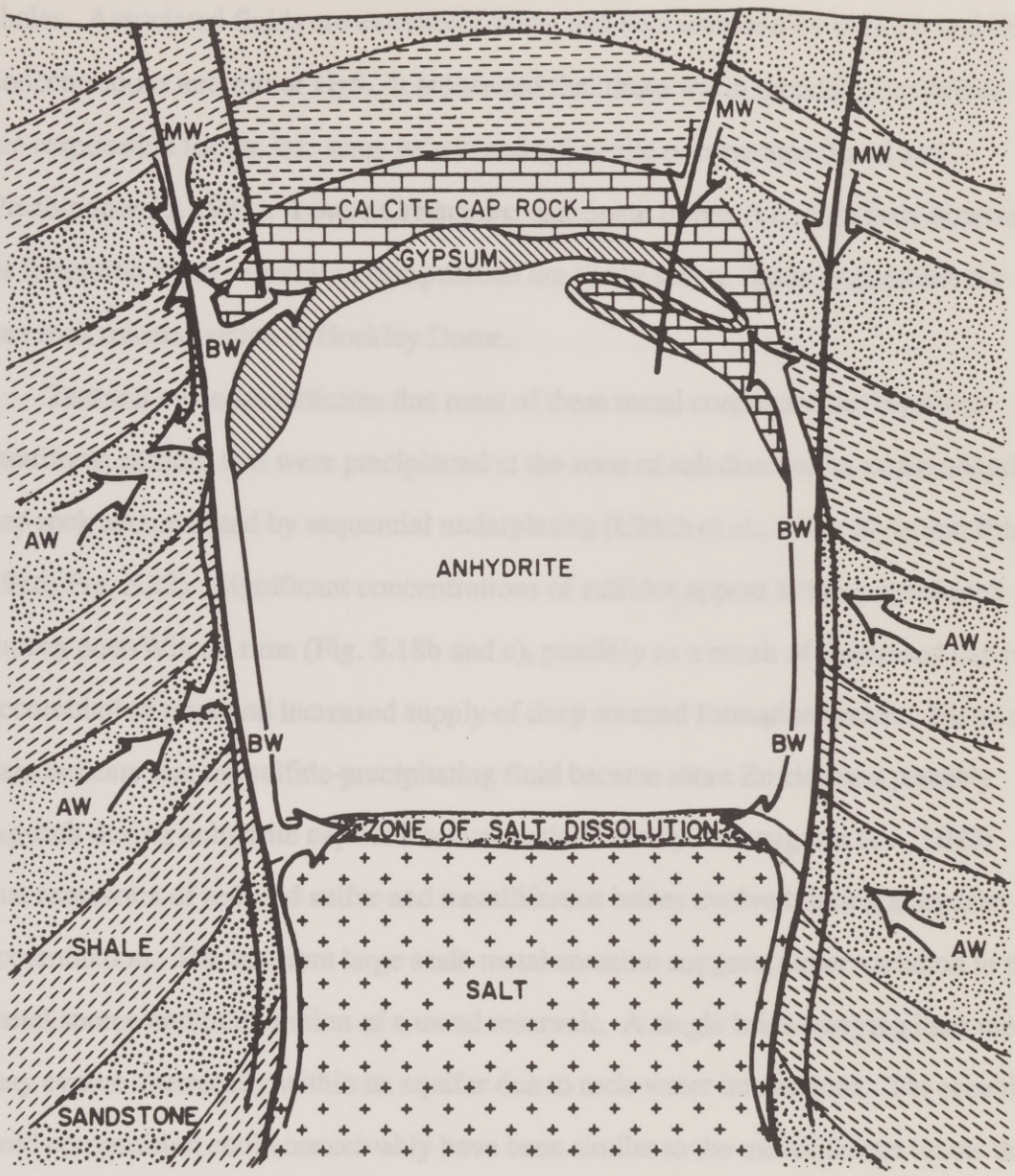

Fig. 5.22. Hypothesized fluid flow pattern of basinal waters (BW), acetate-type waters (AW), and (MW) meteoric waters into the cap rock forming environment. See text for discussion. Note illustration not drawn to scale (modified after Price et al., 1983).

shales. Associated fluids are extremely saline and characterized by high Pb and Zn concentrations and minor H_2S. It is inferred that these warm metalliferous brines are responsible for the late stage galena and sphalerite occurrences (Land and Prezbindowski, 1981). Lower Cretaceous carbonate brines (i.e., Edwards limestone) or formation waters similar in composition are likely source fluids responsible for cap rock mineralization at Hockley Dome.

Textural evidence indicates that most of these metal concentrations represent stratiform sulfides that were precipitated at the zone of salt dissolution as the anhydrite cap rock accumulated by sequential underplating (Ulrich et al., 1984; Kyle and Price, 1986; Fig. 5.22). Significant concentrations of sulfides appear to have developed during post-Wilcox time (Fig. 5.18b and c), possibly as a result of decreased cap rock accumulation rates and increased supply of deep sourced formation waters. Metal ratio data indicate that the sulfide-precipitating fluid became more Zn-rich and possibly Ag-rich during anhydrite cap rock accumulation. Assay data suggest (i.e., HH2) that reservoirs of reduced sulfur and metalliferous brines evolved during anhydrite accumulation. The apparent large scale metal zonation suggests either variation in the metal source and/or evolution of a metal reservoir. A single brine carrying base metals may evolve chemically within its aquifer due to rock-water interactions. The resulting fluid composition could conceivably have been similar to the metalliferous brines that mineralized the Hockley Dome.

Chapter 6

SULFUR ISOTOPES

Textural characteristics of euhedral anhydrite grains surrounded by sulfides indicate that cap rock accumulation and mineralization were cogenetic processes. Mineralizing fluids entered the salt/anhydrite interface and precipitated sulfides as discrete subhorizontal laminae. The anhydrite cap rock and the stratiform sulfide laminae form an inverted stratigraphic sequence (Ulrich et al., 1984). This orderly accumulation of cap rock and sulfides permits examination of the evolution of the sulfide-mineralizing system. Sulfides analyzed for $\delta^{34}S$ were obtained from the calcite, gypsum, and anhydrite zones and sediments at Hockley Dome (Kyle and Agee, 1988). Sulfide samples from core hole HH2 were collected at regular intervals of 33 to 50 ft. Samples from an earlier $\delta^{34}S$ study (Kyle and Price, 1986) concentrated on textural and host rock types and were collected from core holes spaced around the dome (Table VIII; Fig. 6.1).

Marcasite, pyrite, sphalerite, and galena were collected for $\delta^{34}S$ analysis. In hand samples and mineral separates, marcasite and pyrite commonly are fine-crystalline intergrowths and cannot be consistently distinguished; thus, mechanical separation is impractical. Fortunately, there is limited isotopic fractionation between marcasite and pyrite (M. Goldhaber, pers. commun., 1982). $\delta^{34}S$ analyses reported as "pyrite" represent samples of pyrite and/or marcasite (Table IX). Iron-sulfide separates were carefully prepared to reduce the effects of contamination by other mineral phases. $\delta^{34}S$ analyses are reported to be accurate to $\pm$ 0.5 ‰ or better (Appendix VI).

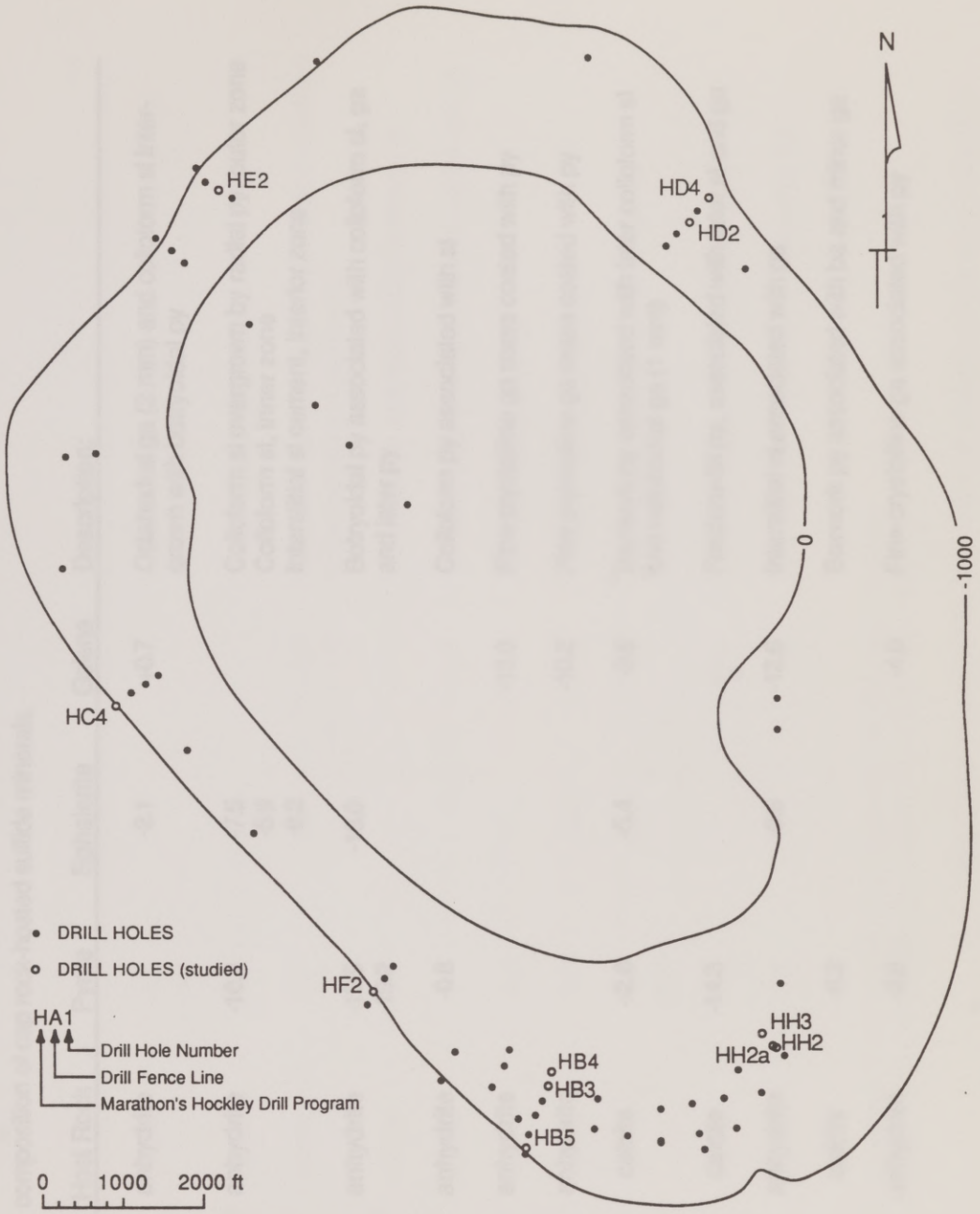

Fig. 6.1. Plan map showing location of drill holes (open circles) utilized in $\delta^{34}S$ study. Contour lines are shown for reference and represent elevation of top of cap rock in feet.

Table VIII. $\delta^{34}S$ ‰ composition of cap rock-hosted sulfide minerals.

Core	Sample no.	Host Rock	Pyrite	Sphalerite	Galena	Description:
HB3	824	anhydrite		-2.1	+0.7	Octahedral ga (2 mm) and colloform sl intergrown with botryoidal py
	935	anhydrite	-10.2	-7.5		Colloform sl overgrown by radial py, outer zone
				-5.9		Colloform sl, inner zone
				-8.2		Interstitial sl cement, interior zone
	990	anhydrite	-15.5	-16.0		Botryoidal py associated with colloform sl, ga
			-19.2			and later py
	996	anhydrite	-0.8			Colloform py associated with sl
HB5	1089	anhydrite			-13.0	Fine-crystalline ga mass coated with py
	1097	anhydrite			-10.2	Fine-crystalline ga mass coated with py
HC4	1013	calcite	+2.6	-5.4	-9.6	Boxwork py associated with later colloform sl and octahedral ga (1 mm)
	1025	calcite	-14.3			Fracture-fill py, associated with later sl and ga
HD2	755	anhydrite		-9.6	-12.6	Interstitial sl associated with ga
HD4	862	calcite	-6.2			Boxwork py associated with ba and minor ga
	1049	anhydrite	-3.8		-4.0	Fine-crystalline ga associated with py

Table VIII. (Cont.)

Core	Sample no.	Host Rock	Pyrite	Sphalerite	Galena	Description:
HE2	739	calcite	-5.0 -4.7			Massive fine-grain py associated with ga and boxwork py
	745	calcite	-5.6	-1.4		Radial py associated with sl
	746	calcite	-6.7	-3.8	-6.9	Boxwork and radial py associated with colloform sl and octahedral ga (1 mm)
	765	calcite	-10.5			Botryoidal py associated with massive ba
	784	calcite			-9.9	Octahedral ga (1 mm) associated with sl and py
HF2	1091	calcite	-8.9			Massive fine grained py
	1096	calcite	-0.7	+3.4		Colloform py overgrown by sl
	1099	calcite	-1.1 +2.0	+4.0	-2.2	Colloform py associated with sl and ga
	1120	calcite			-12.6	Octahedral ga (1 mm) associated with S
HH2A	737	calcite	-1.8			Botryoidal py intergrown with massive ba

Sample no. represents subsurface depth in feet; See Figure 6.1 for drill hole locations.
Mineral abbreviations: py = pyrite; sl = sphalerite; ga = galena; ba = barite; S = sulfur

From Kyle and Agee (1988); data summary originally in Kyle and Price (1986)

Table IX. $\delta^{34}S$ ‰ composition of cap rock-hosted Fe-sulfides in core HH2.

Sample no.	Host Rock	Sulfides	Description (in situ):	(separate):
350	gypsum	-18.1*	Disseminated py	100% rhombic
360 a	gypsum	-13.3	Disseminated py	50% rhombic, 50% boxwork
360 b	gypsum	-18.3*	Disseminated py	90% rhombic, 10% boxwork
404 a	anhydrite	-30.2, -30.6	Broad lamination (1-2 cm) of disseminated and interstitial py with colloform sl and minor ga	75% rhombic, 25% boxwork
404 b	anhydrite	-34.6*	Disseminated py	100% rhombic
404 c	anhydrite	-35.4*	Broad laminae (1 cm) of interstitial py, sl, and ga	100% boxwork
404 d (sl)	anhydrite	-26.1*	Broad laminae (1 cm) of interstitial py, sl, and ga	100% flocculant powder
404 e (ga)	anhydrite	-32.0*	Broad laminae (1 cm) of interstitial py, sl, and ga	100% cubic and dodecahedron
407	anhydrite	-24.2*	Broad laminae (1 cm) of interstitial py	90% rhombic, 10% boxwork
440 a	anhydrite	-20.4, -20.5*	Broad laminae (1.5 cm) of colloform py and minor sl	100% colloform - smooth surface
440 b	anhydrite	-21.7*	Broad laminae (1.5 cm) of colloform py and minor sl	100% colloform - sugary surface
452	anhydrite	-14.4	Broad laminae (5 mm) of disseminated and interstitial py associated with minor sl	90% rhombic, 10% boxwork
499 a	anhydrite	-18.1	Thin laminae (2 mm) of interstitial py and lesser sl; minor colloform and disseminated py	100% rhombic
499 b	anhydrite	-20.2	Thin laminae (2 mm) of interstitial py and lesser sl; minor colloform and disseminated py	65% boxwork, 35% botryoidal

Table IX. (Cont.)

Sample no.	Host Rock	Sulfides	Description (in situ):	(separate):
533	anhydrite	-13.4	Massive sulfide laminae (6 mm) of colloform py intergrown with colloform sl and minor ga	70% rhombic, 30% boxwork
566 a	anhydrite	-6.7	Colloform and disseminated py with minor interstitial sl and py	100% rhombic
566 b	anhydrite	-7.1	Colloform and disseminated py with minor interstitial sl and py	80% colloform, 20% boxwork
612	anhydrite	-7.3, -7.7	Thin laminae of colloform py and interstitial py and sl (3 mm); minor disseminated py	75% rhombic, 25% boxwork
649 a	anhydrite	-1.3	Laminae of colloform py (5 mm) and interstitial sl, minor ga; adjacent to a massive sulfide zone	40% massive, 30% colloform, 20% boxwork, 10% rhombic
649 b	anhydrite	-4.6	Massive sulfide zone (5 cm); isolated (1.5 cm) ramose py structure	100% inner (3 mm) core
649 c	anhydrite	-4.2	Massive sulfide zone (5 cm); isolated (1.5 cm) ramose py structure	100% outer (2 mm) rind
704	calcite	-2.8	Highly disturbed massive sulfide zone, colloform py intergrown with lesser sl and minor ga	60% boxwork, 40% colloform
723	calcite	-3.9	Highly disturbed massive sulfide zone, colloform py intergrown with minor sl and ga	60% boxwork, 40% colloform
757	anhydrite	+3.5, +3.8	Massive sulfide zone; laminae of interstitial and colloform py associated with minor sl	70% boxwork, 30% colloform

Table IX. (Cont.)

Sample no.	Host Rock	Sulfides	Description (in situ):	(separate):
780	anhydrite	-12.0	Broad lamination (1-2 cm) of interstitial py, sl and minor ga	100% boxwork
811	anhydrite	-14.6	Thin laminae (2 mm) of interstitial py and sl	70% colloform, 30% boxwork
830 a (sl)*	anhydrite	-2.9	Thin laminae (5 mm) of interstitial py and sl	100% boxwork
830 b (ga)*	anhydrite	-7.2	Thin laminae (5 mm) of interstitial py and sl	100% boxwork
861	anhydrite	-6.3	Thin laminae (2 mm) of interstitial py and minor sl	70% colloform, 30% boxwork
878	anhydrite	-7.7	Thin laminae (2 mm) of interstitial py and sl	75% colloform, 25% boxwork
910	anhydrite	-18.3, -18.7	Broad lamination (1 cm) of colloform and interstitial py	75% colloform, 25% boxwork
941	anhydrite	-14.8	Thin laminae (2 mm) of colloform and interstitial py and interstitial sl; minor disseminated py	75% colloform, 25% boxwork
975	anhydrite	-15.7	Broad laminae (1 cm) of colloform and interstitial py intergrown with minor sl and ga	75% colloform, 25% boxwork
1026	anhydrite	-20.0	Thin laminae (2 mm) of interstitial and minor colloform py	75% colloform, 25% boxwork

Sample no. represents subsurface depth in feet; See Figure 6.1 for drill hole location.
Mineral abbreviations: py = pyrite; sl = sphalerite; ga = galena
All seperate anayses are for Fe-sulfides except for 404d (sl), 404e (ga), 830a (sl), and 830b (ga)
* Includes samples reported in Kyle and Agee (1988)

Iron-sulfides are the most abundant and easiest sulfide to cleanly separate from anhydrite and other sulfides. Therefore, pyrite was used to characterize the sulfur isotopic composition of sulfides with the assumption that these data would adequately represent the sulfur reservoir. Three distinct pyrite textural types (boxwork, colloform/ ramose, and rhombic) were identified in the vertical profile of the anhydrite cap rock in drill hole HH2 (Kyle and Agee, 1988). To determine if the pyrite type influenced the $\delta^{34}S$ values, some sample intervals were analyzed for more than one textural type.

Results

General $\delta^{34}S$ Study

An earlier $\delta^{34}S$ study of Hockley Dome cap rock minerals concentrated on textural and host rock types and were collected from randomly selected cores and intervals (Kyle and Price, 1986; Table VIII; Fig. 6.1). Pyrite, marcasite and lesser amounts of sphalerite and galena were analyzed and generally represent the highly mineralized zones commonly exceeding 50 % metal sulfides. This initial study indicated that $\delta^{34}S$ values of sulfide minerals within the Hockley Dome cap rock range from +4 to -20 ‰ (CDT) with a mean of -6 ‰ (39 analyses; Table VIII). Data from these scattered holes do not permit detailed evaluation of $\delta^{34}S$ trends with depth in the cap rock which might provide information about evolution of the mineralizing system.

Vertical $\delta^{34}S$ Marcasite/Pyrite Profile

Iron-sulfides from a single drill hole (HH2) were systematically sampled at regular intervals to generate a vertical profile of sulfur isotope composition (Kyle and Agee, 1988; Table IX; Figs. 6.1 and 6.2). The Kyle and Agee (1988) study

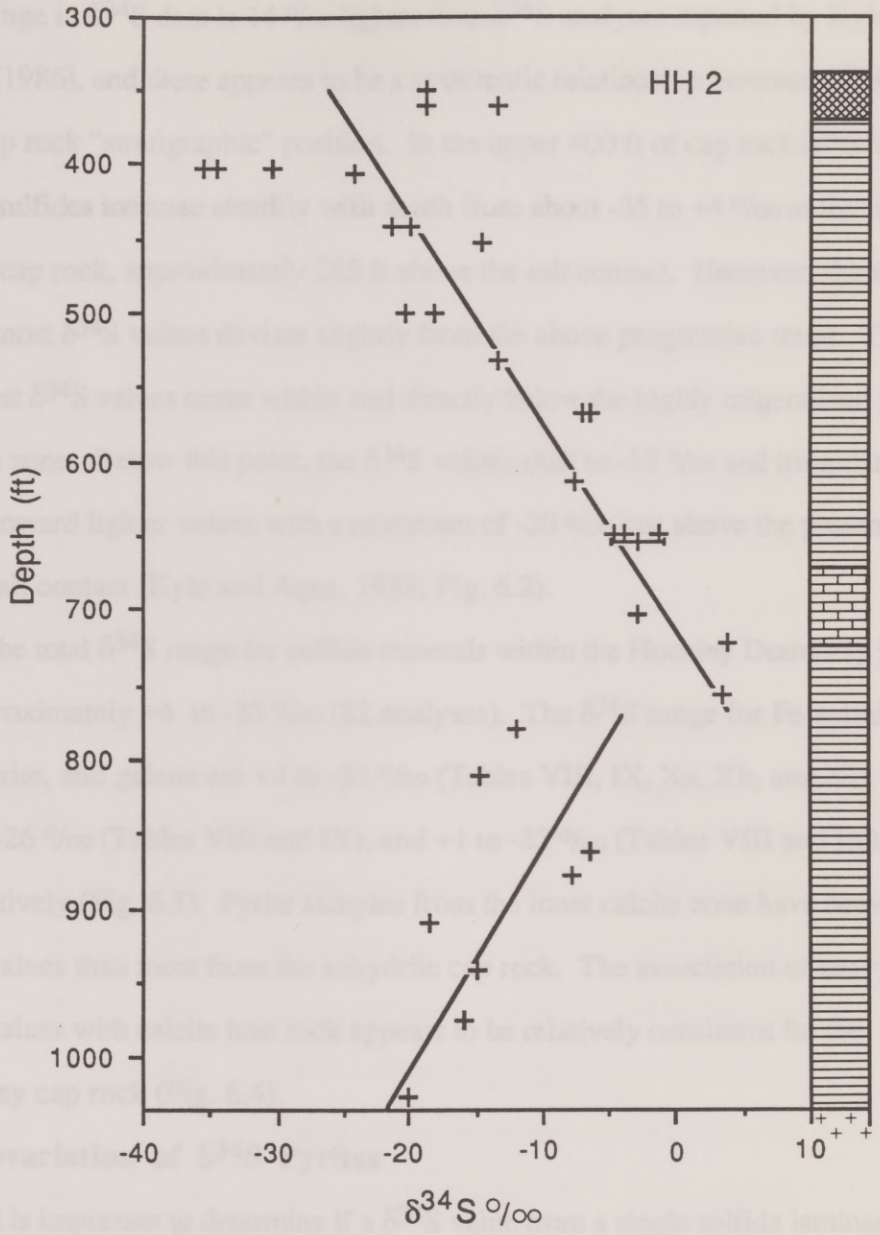

Figure. 6.2. Profile of $\delta^{34}S$ values of pyrite for HH2 plotted as depth below surface. The least-squares best-fit lines for the upper and lower isotope trends have correlation coefficients of 0.86 and 0.79, respectively (modified from Kyle and Agee, 1988).

of HH2 was later infilled to complete the uppermost portion of the $\delta^{34}S$ profile. The range in $\delta^{34}S$ data is 14 ‰ lighter than $\delta^{34}S$ analyses reported by Kyle and Price (1986), and there appears to be a systematic relationship between $\delta^{34}S$ values and cap rock "stratigraphic" position. In the upper 400 ft of cap rock $\delta^{34}S$ values of Fe-sulfides increase steadily with depth from about -35 to +4 ‰ to the middle of the cap rock, approximately 265 ft above the salt contact. However, the three uppermost $\delta^{34}S$ values deviate slightly from the above progressive trend. The heaviest $\delta^{34}S$ values occur within and directly below the highly mineralized internal calcite zone. Below this point, the $\delta^{34}S$ values shift to -12 ‰ and irregularly trend toward lighter values with a minimum of -20 ‰ just above the present cap rock/salt contact (Kyle and Agee, 1988; Fig. 6.2).

The total $\delta^{34}S$ range for sulfide minerals within the Hockley Dome cap rock is approximately +4 to -35 ‰ (82 analyses). The $\delta^{34}S$ range for Fe-sulfides, sphalerite, and galena are +4 to -35 ‰ (Tables VIII, IX, Xa, Xb, and XI), +4 to -26 ‰ (Tables VIII and IX), and +1 to -32 ‰ (Tables VIII and IX), respectively (Fig. 6.3). Pyrite samples from the inner calcite zone have heavier $\delta^{34}S$ values than most from the anhydrite cap rock. The association of heavy $\delta^{34}S$ values with calcite host rock appears to be relatively consistent for the Hockley cap rock (Fig. 6.4).

Microvariation of $\delta^{34}S$ Pyrites

It is important to determine if a $\delta^{34}S$ value from a single sulfide laminae properly represents the general composition of the sulfur reservoir. In other words, are the isotopic trends observed within a $\delta^{34}S$ vertical profile (i.e., HH2) indicative of an evolving sulfur reservoir or the result of local $\delta^{34}S$ variations. Iron-sulfides were sampled from two densely laminated core sections (approximately six inches

Table Xa. $\delta^{34}S$ ‰ composition of anhydrite-hosted Fe-sulfides from HH2-652.

Sulfide: Band	Set		Description (in situ):	(separate):
A	1	-2.3	Sulfide laminae (1.0 mm)	100% boxwork
B	2	-0.4	Sulfide laminae (<0.5 mm)	100% boxwork
C	3	-1.9	Sulfide laminae (<0.5 mm)	100% boxwork
D	3	-2.2	Sulfide laminae (2.0 mm)	80% colloform, 20% boxwork
E	4	-4.4	Sulfide laminae (2.0 mm)	50% colloform, 50% boxwork
F	4	-3.0	Sulfide laminae (0.5 mm)	100% boxwork
G	5	-1.8	Sulfide laminae (4.0 mm)	100% colloform
H	5	-2.2	Sulfide laminae (1.0 mm)	100% boxwork
I	6	-3.7	Fracture-fill (1.0 mm)	100% fine grain

Table Xb. $\delta^{34}S$ ‰ composition of anhydrite-hosted Fe-sulfides from HH3-837.

Sulfide: Band	Set		Description (in situ):	(separate):
A	1	-2.6	Sulfide laminae (0.5 mm)	100% boxwork
B	2	-1.2	Sulfide laminae (1.0 mm)	100% boxwork
C	2	-1.4	Sulfide laminae (1.5 mm)	100% boxwork
D	2	-0.3	Sulfide laminae (0.5 mm)	100% boxwork
E	2	-1.1	Sulfide laminae (0.5 mm)	100% boxwork
F	3	-2.5	Sulfide laminae (<0.5 mm)	100% boxwork
G	3	-2.7	Sulfide laminae (0.5 mm)	100% boxwork
H	4	-5.0	Sulfide laminae (1.0 mm)	100% boxwork
I	4	-4.6	Sulfide laminae (2.0 mm)	100% boxwork

Sample no. represents core hole and subsurface depth in feet.
See Figure 6.1 for drill hole locations.

Table XI. $\delta^{34}S$ ‰ composition of supracaprock-hosted Fe-sulfides in core HB4.

Sample no.	Sediment		Description (separate):
R1 a	clay-rich	-25.0	Very fine-crystalline py aggregates (1-2 mm)
R1 b	sand-rich	+1.5	Fine-crystalline py aggregates (1-2 mm)
R5 a	clay-rich	-24.6, -25.0	Very fine-crystalline py aggregates (1-2 mm)
R5 b	sand-rich	+2.1	Fine-crystalline py aggregates (1-2 mm)
R15 a	clay-rich	-25.4	Very fine-crystalline py aggregates (1-2 mm)

Sample no. represents rotary subsurface depth in feet; See Fig 6.1 for drill hole location.
Mineral abbreviation: py = pyrite

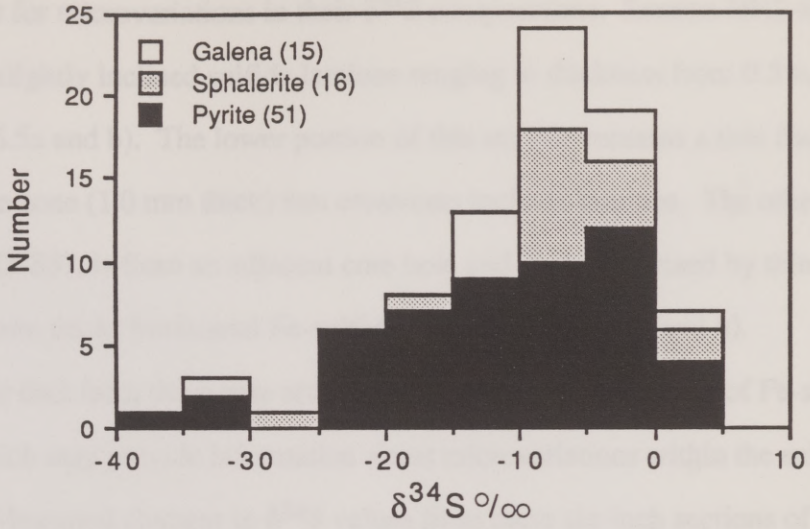

Fig. 6.3. $\delta^{34}S$ composition of all sulfide minerals in the Hockley dome cap rock. Mean $\delta^{34}S$ values for pyrite/marcasite, sphalerite, and galena are roughly -11°/oo, -6°/oo, and -9 °/oo, respectively. Plot includes data reported in Kyle and Price (1986) and Kyle and Agee (1988).

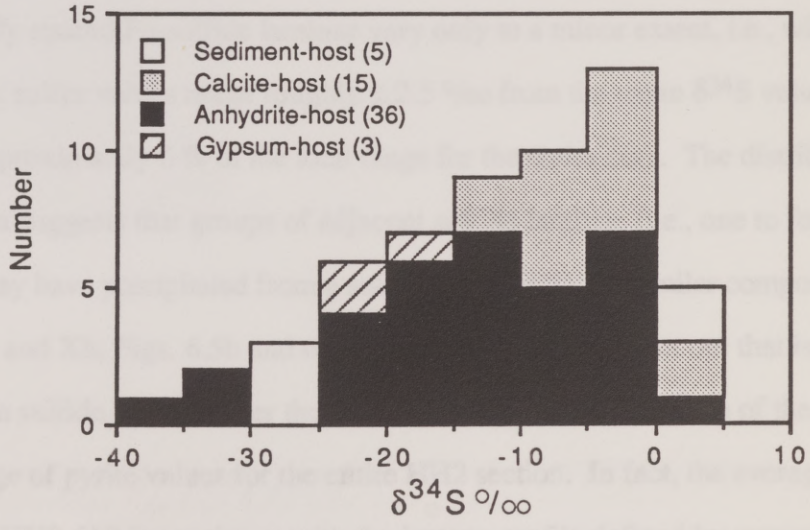

Fig. 6.4. $\delta^{34}S$ values of pyrite relative to host rock.
Note that heavier $\delta^{34}S$ values are associated with calcite-hosted sulfides.
Plot includes data reported in Kyle and Price (1986) and Kyle and Agee (1988).

long) to test for microvariations in their $\delta^{34}S$ compositions. Section HH2-652 consists of slightly inclined sulfide laminae ranging in thickness from 0.5 to 4.0 mm (Figs. 6.5a and b). The lower portion of this sample contains a thin fracture-filled sulfide zone (1.0 mm thick) that cross-cuts inclined laminae. The other test section, HH3-837, is from an adjacent core hole and is characterized by thin (0.5 to 1.5 mm thick) horizontal Fe-sulfide laminae (Figs. 6.6a and b).

Isotopic data from these core sections permit detailed evaluation of Fe-sulfide laminae which may provide information about microvariations within the sulfur reservoir. Measured changes in $\delta^{34}S$ values from these six-inch sections of core corresponds to approximately 25,000 to 30,000 yr of cap rock growth (based on general accumulation rates of 27.5 ft/m.y.; Table III). $\delta^{34}S$ values from these test core range from -0.4 ‰ to -4.4 ‰ (HH2-652; Fig. 6.5b) and -0.3 ‰ to -5.0 ‰ (HH3-837; Fig. 6.6b) with a mean of -2.4 ‰ (9 analyses; Table Xa) and -2.4 ‰ (9 analyses; Table Xb), respectively. These data indicate that $\delta^{34}S$ values from densely spaced Fe-sulfide laminae vary only to a minor extent, i.e., within this data set sulfur values range roughly ± 2.5 ‰ from the mean $\delta^{34}S$ value, which is approximately 6 % of the total range for the entire core. The distribution of $\delta^{34}S$ data suggests that groups of adjacent sulfide laminae (i.e., one to four laminae) may have precipitated from a sulfur reservoir with a similar composition (Tables Xa and Xb; Figs. 6.5b and 6.6b). It is important to point out that isotopic variations in sulfide laminae over these short intervals is only 4.7 ‰ of the total 39 ‰ range of pyrite values for the entire HH2 section. In fact, the average $\delta^{34}S$ value from HH2-652 is consistent with the isotope profile defined by systematic sampling of single Fe-sulfide laminae (Fig. 6.2).

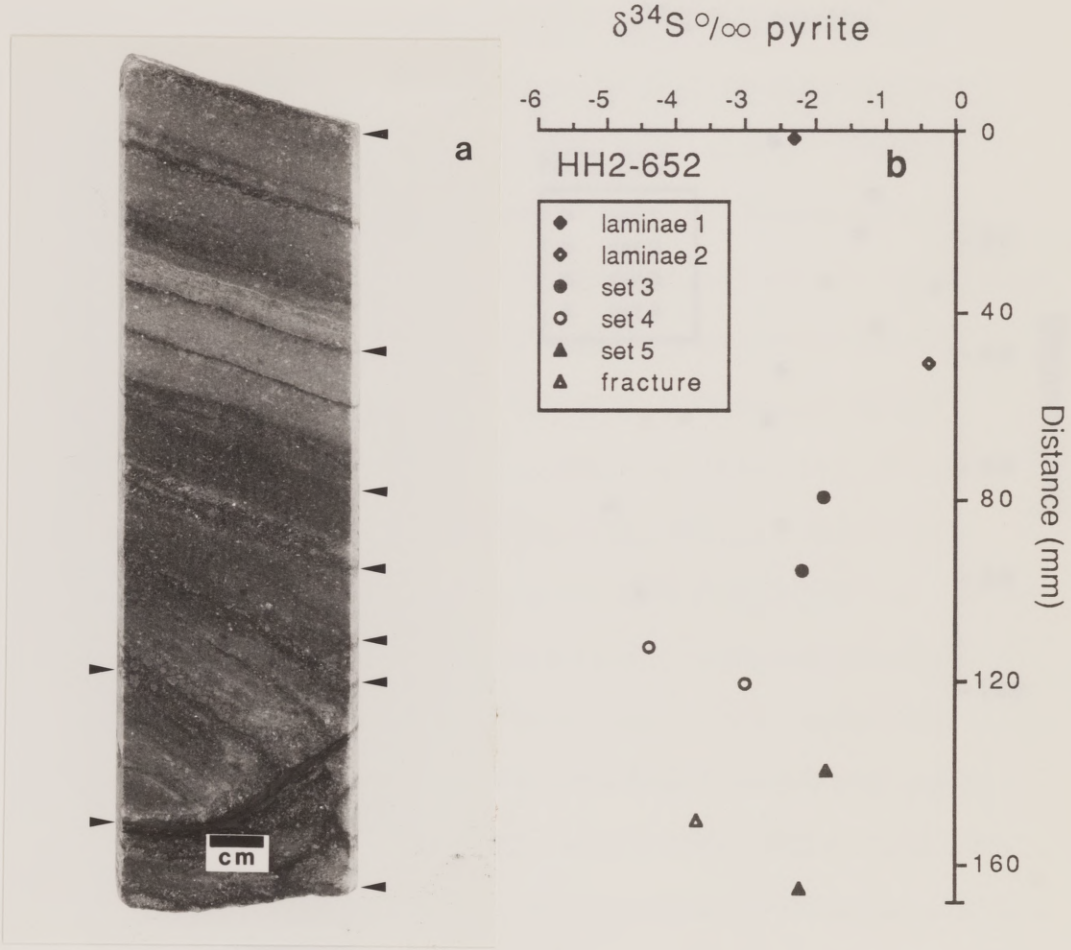

Fig. 6.5a. Photograph of anhydrite cap rock core containing numerous, inclined Fe-sulfide laminae; sample HH2-652.
Note the fracture-fill Fe-sulfide zone in the lower core section..

Fig. 6.5b. Scatter plot of $\delta^{34}S$ pyrite values versus laminae distance from HH2-652.
Note grouping of adjacent laminae that have similar $\delta^{34}S$ values.

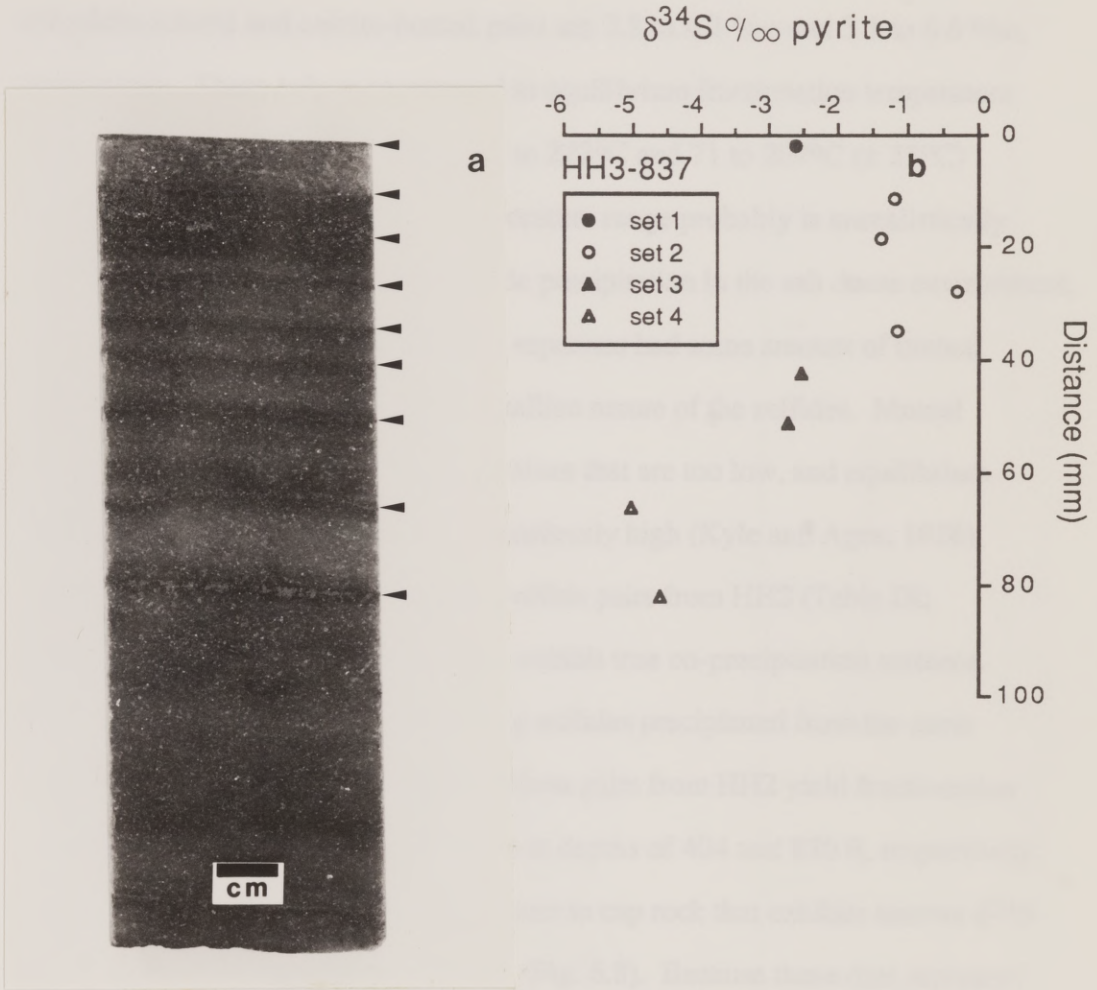

Fig. 6.6a. Photograph of anhydrite cap rock core containing numerous, horizontal Fe-sulfide laminae; sample HH3-837.

Fig. 6.6b. Scatter plot of $\delta^{34}S$ pyrite values versus laminae distance from HH3-837. Note grouping of adjacent laminae that have similar $\delta^{34}S$ values.

Sphalerite-Galena Sulfide Pairs

The $\Delta^{34}S_{sl\text{-}ga}$ values for seven co-existing sulfide pairs range from 2.8 to 6.6 ‰ (Table VIII, Price et al., 1983; Table IX). The $\Delta^{34}S_{sl\text{-}ga}$ ranges for anhydrite-hosted and calcite-hosted pairs are 2.8 to 4.3 ‰ and 3.1 to 6.6 ‰, respectively. These values correspond to equilibrium fractionation temperature ranges (Ohmoto and Rye, 1979) of 73 to 222°C and 71 to 207°C (± 25°C) (Fig. 6.7). The upper part of this temperature range probably is unrealistically high for the general conditions of sulfide precipitation in the salt dome environment. It is probable that the analyzed mineral separates had some amount of mutual contamination because of the fine-crystalline nature of the sulfides. Mutual contamination would yield $\Delta^{34}S_{sl\text{-}ga}$ values that are too low, and equilibrium fractionation temperatures that are anomalously high (Kyle and Agee, 1988). With the exception of two co-existing sulfide pairs from HH2 (Table IX; Figs. 6.7 and 6.8), none of the textures exhibit true co-precipitation textures. Thus, it is not certain that the co-existing sulfides precipitated from the same fluid. The two co-existing sphalerite-galena pairs from HH2 yield fractionation temperatures of 78 and 138°C (± 25°C) at depths of 404 and 830 ft, respectively. This suggest that temperatures were greater in cap rock that exhibits heavier $\delta^{34}S$ values and greater metal concentrations (Fig. 6.8). Because these data represent samples from widely spaced drill holes, it is not possible to evaluate these data in terms of thermal evolution of the cap rock mineralization system.

Supracaprock $\delta^{34}S$ Pyrites

Pyrite aggregates identified in supracaprock sediments provide a limited $\delta^{34}S$ data base. The two types of pyrite morphologies exhibit a bimodal $\delta^{34}S$ distribution with isotopically light values ranging from -24.6 to -25.4 ‰ and

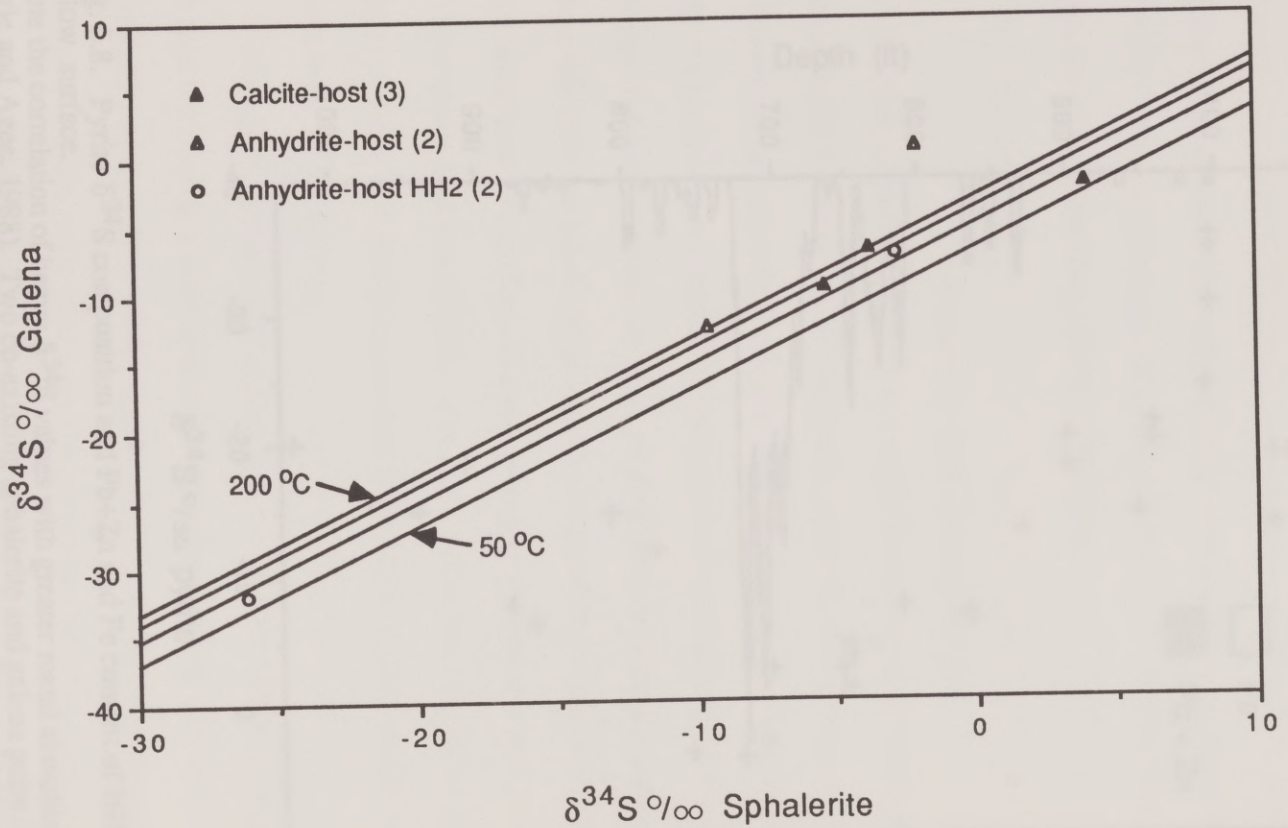

Fig. 6.7. Scatter plot of $\delta^{34}S$ sphalerite versus galena within equilibrium fractionation temperature fields. Equilibrium lines are calculated every 50° C (equation in Ohmoto and Rye, 1979)

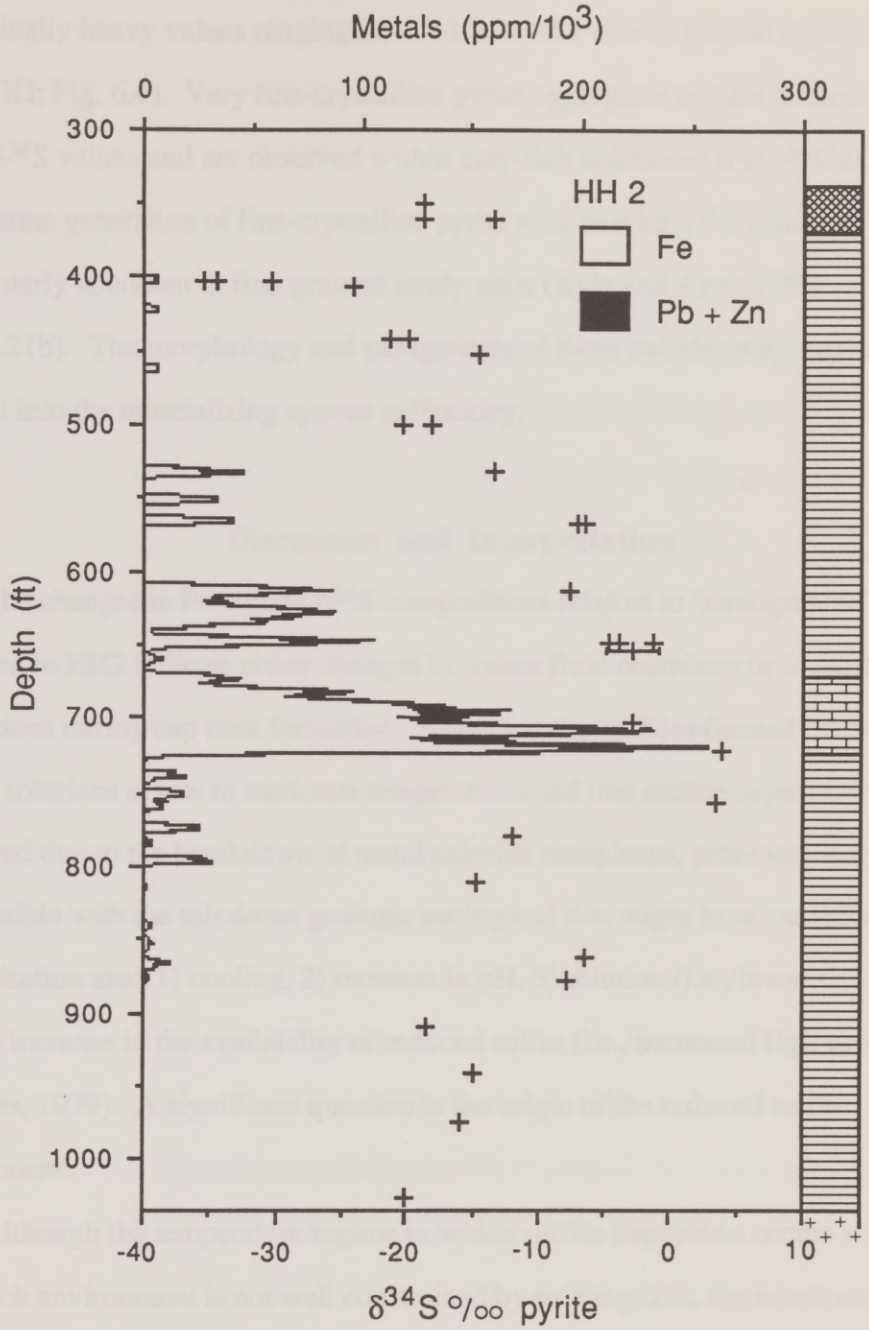

Fig. 6.8. Pyrite δ^{34}S composition and Pb+Zn and Fe content of HH2 plotted as depth below surface.
Note the correlation of heavy δ^{34}S values with greater metal abundances (modified from Kyle and Agee, 1988). Two co-existing sphalerite and galena pairs (not shown) exhibit fractionation temperatures of 78 and 139°C at depths of 404 and 830 ft, respectively.

isotopically heavy values ranging from +1.5 to +2.1 ‰ (Kyle and Agee, 1988; Table XI; Fig. 6.4). Very fine-crystalline pyrite aggregates exhibit isotopically light $\delta^{34}S$ values and are observed within clay-rich sediments (Fig. 4.21a). A separate generation of fine-crystalline pyrite with heavier $\delta^{34}S$ values is particularly abundant in fine-grained sandy units (Kyle and Agee, 1988; Fig. 4.21b). The morphology and paragenesis of these sulfides may provide insight into the mineralizing system at Hockley.

Discussion and Interpretation

The changes in Fe-sulfide $\delta^{34}S$ compositions relative to "stratigraphic" position in HH2 indicate either changes in source fluid chemistry or in depositional conditions during cap rock formation. Assuming the sulfides formed from slightly acidic solutions at low to moderate temperatures and that sulfide deposition occurred due to the breakdown of metal chloride complexes, processes that are compatible with the salt dome geologic setting and that might have caused sulfide precipitation are: 1) cooling, 2) increase in pH, 3) dilution (i.e., lower Cl^- activity), and 4) increase in the availability of reduced sulfur (i.e., increased H_2S activity) (Barnes, 1979). A significant question is the origin of the reduced sulfur component.

Although the temperature regime in which sulfide deposition occurs within the cap rock environment is not well constrained by existing data, the maximum range is probably 25 to 200°C. Under equilibrium conditions the maximum amount of isotopic fractionation (at 25°C) resulting from precipitation of pyrite from an H_2S reservoir is 4.5 ‰. Thus, temperature variations during Fe-sulfide precipitation from H_2S-bearing solutions cannot account for the 39 ‰ range of pyrite $\delta^{34}S$

values for HH2 (Fig. 6.8). Furthermore, the trends in sulfide $\delta^{34}S$ values and the correlation of highly mineralized intervals with relatively heavy $\delta^{34}S$ values appear to require at least a two-component mineralizing system (Kyle and Agee, 1988). It is possible that fluctuations in temperature may be responsible for the slight shift in $\delta^{34}S$ pyrite values that correspond to short intervals of time (i.e., $\delta^{34}S$ microvariations). However, it is doubtful that such extreme temperature variations (approximately 200°C required for equilibrium range of 39 ‰) could have occurred during the limited amount of time represented by close-spaced sulfide laminae, e.g., HH2-652 (Table Xa, Figs. 6.5a and b).

Relevant sulfide-producing genetic models that may be responsible for cap rock sulfide mineralization include 1) closed system thermochemical reduction of cap rock-derived sulfate involving Rayleigh-type fractionation, and 2) a mixing system involving contributions of locally reduced sulfate (i.e., biogenic and/or thermochemical) with metal- and possibly H_2S-bearing basinal fluids (Kyle and Agee, 1988). The inorganic generation of reduced sulfur species may occur in sedimentary terrains by reactions involving hydrocarbons at elevated temperatures either by thermal cleavage of organic sulfur compounds in oil or by thermochemical reduction of reservoir sulfate (Orr, 1977; Machel, 1988). It has been estimated that these reactions require minimum temperatures of about 75°C by Orr (1977) and about 100°C by Machel (1988). The most likely local source of aqueous sulfate is anhydrite cap rock dissolution near the salt/anhydrite interface (Kyle and Agee, 1988). Anhydrite residue from Gulf Coast salt stocks show a narrow $\delta^{34}S$ range of 16 ± 1 ‰ (Feely and Kulp, 1957; Posey et al., 1987), characteristic of the middle Jurassic age of the parent Louann evaporites (Claypool et al., 1980).

Sulfur Isotope Model

Heavy Sulfur Source

The $\delta^{34}S$ trends for the HH2 sulfides appear to require varying contributions of both isotopically light and heavy H_2S components to produce a range of intermediate $\delta^{34}S$ sulfide values. As discussed earlier, the shift from light to heavier $\delta^{34}S$ values could not be due to fractionation related to temperature variations. However, there appears to be an association between the episodes of relatively hot metal-bearing brine introduction into the cap rock environment and the precipitation of isotopically heavy sulfides. Isotopically heavy sulfur for the Hockley mineralizing system can be derived from two possible sources. They include H_2S sourced from deep oil and gas fields or locally generated by thermochemical reduction of anhydrite cap rock sulfate (Kyle and Agee, 1988).

The isotopic signature of H_2S is a function of its concentration within an oil and gas reservoir; i.e., as the H_2S concentration increases, its $\delta^{34}S$ value increases (Fig. 6.9). Limited data indicate that sour gas reservoirs with high concentrations of H_2S have $\delta^{34}S$ values that approach the $\delta^{34}S$ value of reservoir sulfate (Orr, 1977). At depth this phenomenon is a result of thermal decomposition of organic sulfur compounds (desulfurization) and thermochemical sulfate reduction (Fig. 6.10). However, thermal desulfurization is unable to account for the high H_2S content found in sour gas fields. Thermochemical sulfate reduction is considered to be the dominant H_2S-producing mechanism (Orr, 1977). Existing H_2S reacts with sulfate to form elemental sulfur followed by subsequent reduction of sulfur by petroleum to form H_2S gas (Fig. 6.10). There is little isotopic fractionation between the two sulfur species in situations where thermochemical reduction of sulfate to H_2S is complete. Therefore, H_2S in oil and gas reservoirs

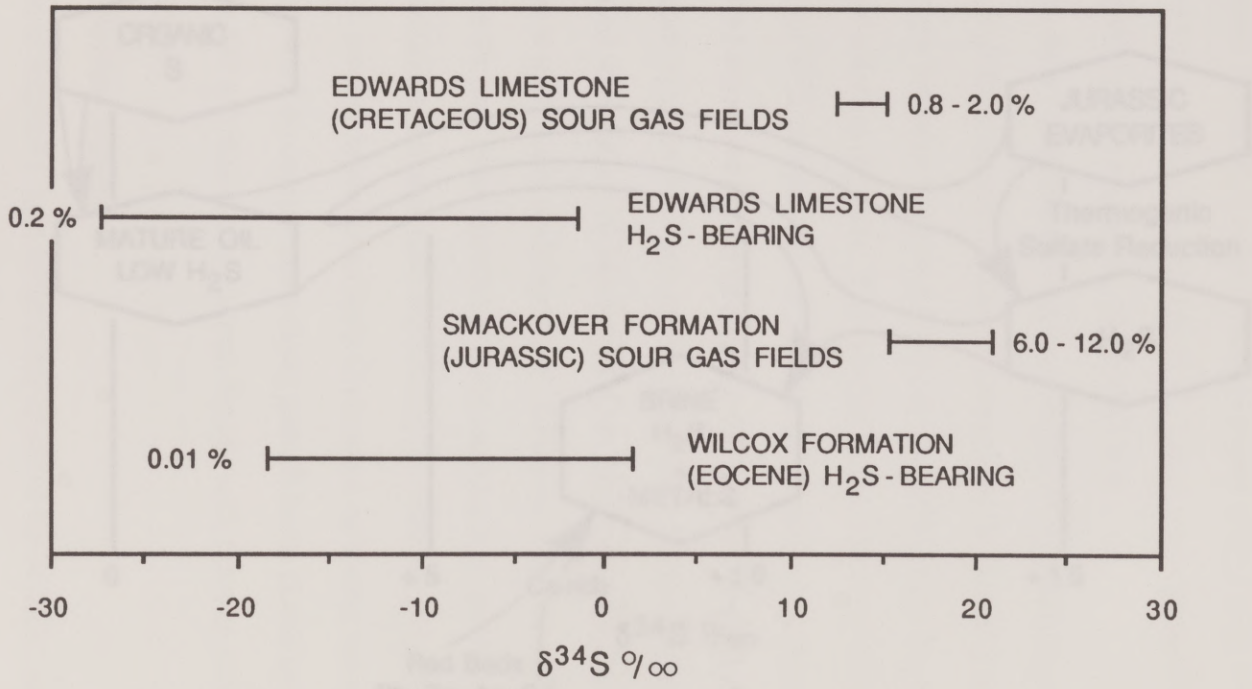

Fig. 6.9. $\delta^{34}S$ range of aqueous and gaseous H2S from Texas.
The isotopic data consist of reported values from sour gas and/or H_2S-bearing gas fields from major producing formations. Sour gas from the Edwards (Lower Cretaceous) and Smackover (Jurassic) formations are interpreted to represent a possible heavy end-member source for the mixed sulfur model. References to data: Goldhaber et al. (1983), Orr (1977), and Pearson and Rightmire (1980).

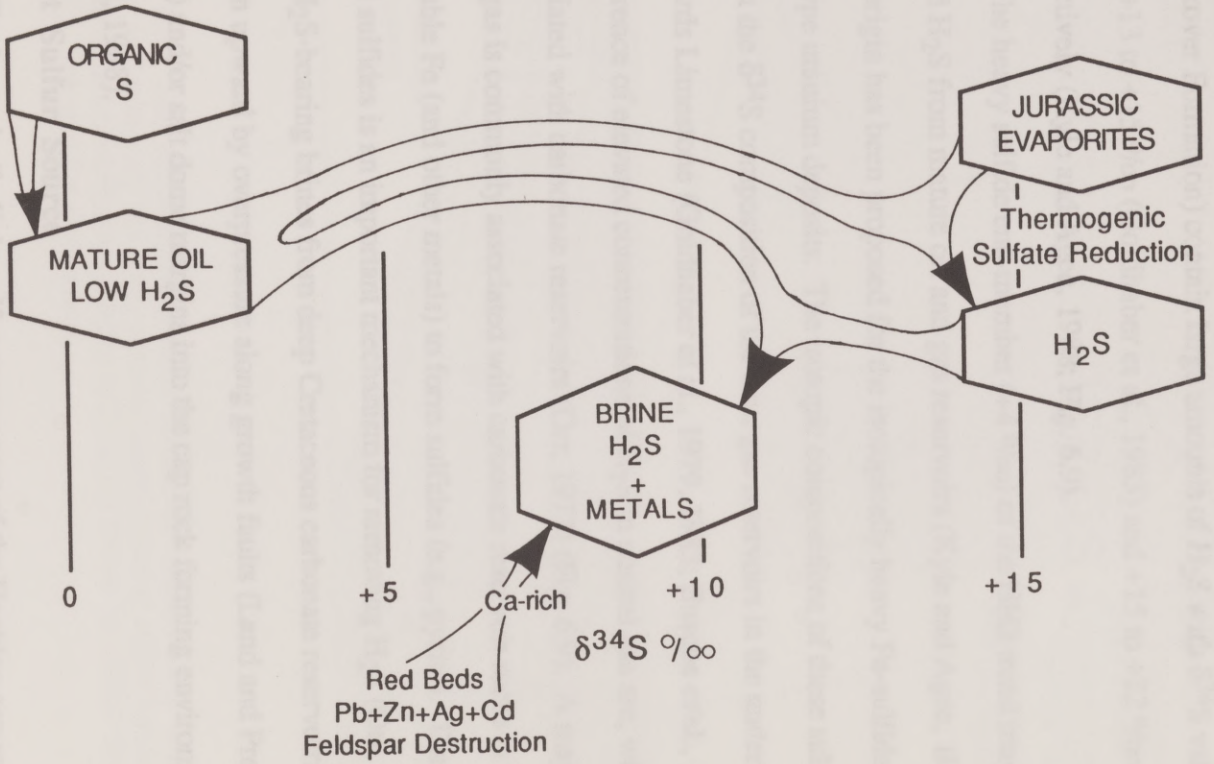

Fig. 6.10. A generalized model for $\delta^{34}S$ changes in Gulf Coast Mesozoic formation waters. Shown is the magnitude of $\delta^{34}S$ changes commonly associated with the various transformations of sulfur (see Orr, 1977). Metals were presumably leached from red beds or feldspar during rock water reactions. The mixing of metalliferous and H_2S fluids may occur at cap rock or within Mesozoic sediments.

that has been exposed to relatively high temperatures exhibits $\delta^{34}S$ values that approach the isotopic ratios of the reservoir sulfate (Orr, 1977; Fig. 6.10). For example, Mesozoic carbonate sour gas reservoirs (i.e., Edwards Limestone and Smackover Formation) contain large amounts of H_2S with $\delta^{34}S$ values that range from +13 to +15 ‰ (Goldhaber et al., 1983) and +15 to +22 ‰ (Orr, 1977), respectively (Kyle and Agee, 1988; Fig. 6.9).

The heavy sulfide end-member (+4 ‰) of the HH2 trend may represent fault-leaked H_2S from mature oil and gas reservoirs (Kyle and Agee, 1988; Fig. 6.11). This origin has been proposed for the isotopically heavy Fe-sulfides in South Texas roll-type uranium deposits. The isotopic compositions of these sulfides directly reflect the $\delta^{34}S$ composition of the sour gas reservoirs in the underlying Cretaceous Edwards Limestone (Goldhaber et al., 1979, 1983; Busche et al., 1982). The occurrence of elevated concentrations of H_2S in natural gas are, without exception, associated with carbonate reservoirs (Orr, 1977) (Fig. 6.9). A major reason that sour gas is commonly associated with carbonate reservoir rocks is that there is little available Fe (and other metals) to form sulfides (e.g., pyrite). The formation of metal sulfides is an important mechanism for removing H_2S (Orr, 1977). Metal- and H_2S-bearing brines from deep Cretaceous carbonate reservoirs may have been driven upward by overpressure along growth faults (Land and Prezbindowski, 1981) and/or salt dome margins into the cap rock forming environment (Kyle and Agee, 1988).

Light Sulfur Source

The isotopically light sulfur component of the Hockley cap rock sulfides is believed to be a result of biogenic reduction of aqueous sulfate derived from local anhydrite dissolution. Sulfate-reducing bacteria (e.g., Desulfovibrio desulfuricans)

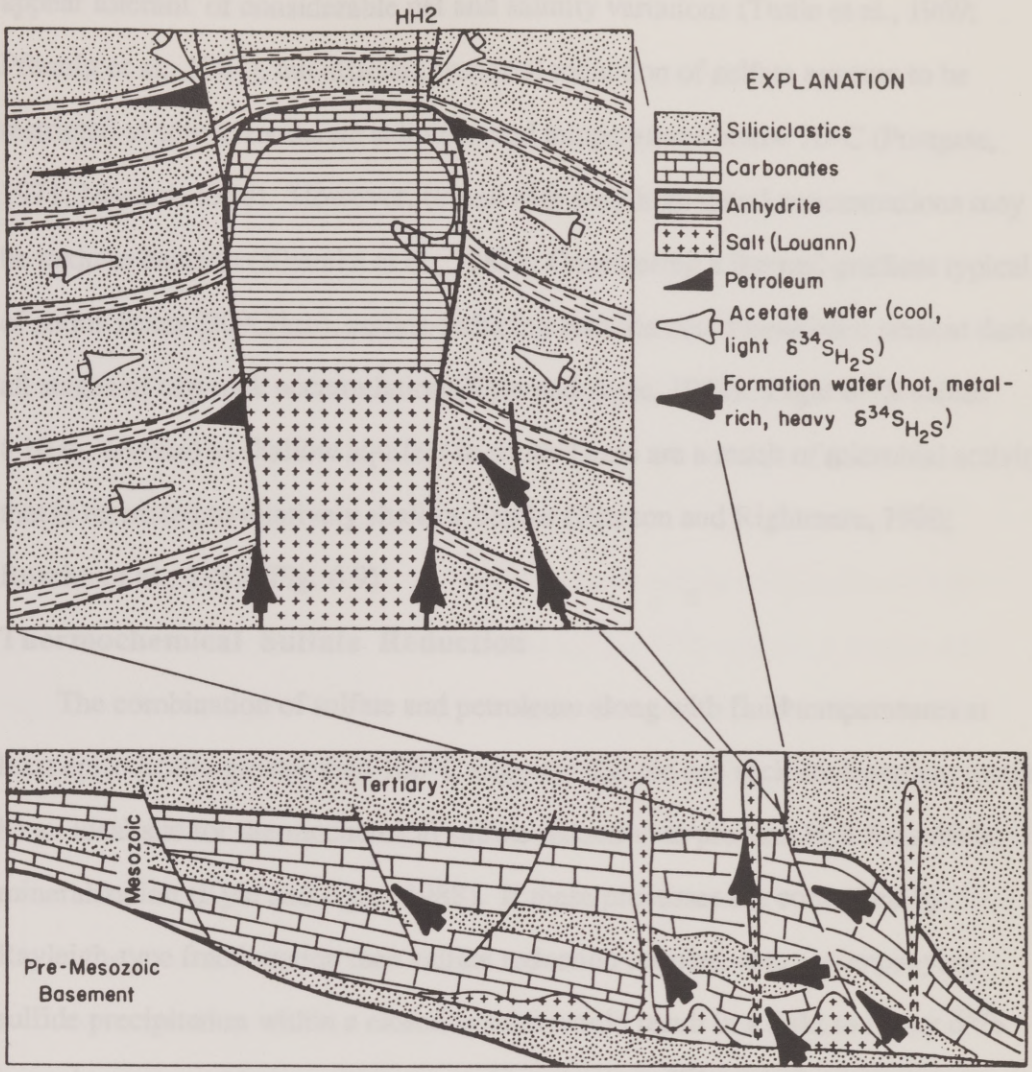

Fig. 6.11. Schematic hydrodynamic model for interaction of cool, shallow acetate water and relatively hot, deep-sourced metal-bearing saline formation water resulting in cap rock sulfide mineralization at Hockley Dome (modified from Kyle and Agee, 1988). See text for discussion.

appear tolerant of considerable pH and salinity variations (Tuttle et al., 1969; Pfennig et al., 1981), but efficient bacterial reduction of sulfate appears to be restricted to low to moderate salinities and temperatures below 70°C (Postgate, 1971; Machel, 1988). However, brines with very high metal concentrations may be toxic to bacteria (Kharaka et al., 1987). Considering a thermal gradient typical of south Texas (30°C/km), sulfate-reducing bacteria could have been present during all stages of cap rock accumulation (Kyle and Agee, 1988). Light $\delta^{34}S$ values (-10 to -60 ‰) in shallow aquifers in south Texas are a result of microbial activity that is restricted to relatively shallow depths (Pearson and Rightmere, 1980; Busche et al., 1982; Fig. 6.9).

Thermochemical Sulfate Reduction

The combination of sulfate and petroleum along with fluid temperatures at least episodically greater than 100°C suggests that the cap rock environment would be an ideal site for thermochemical sulfate reduction to produce H_2S for sulfide mineralization (Kyle and Agee, 1988). If these processes are controlled by Rayleigh-type fractionation then sulfate reduction coupled with accompanying sulfide precipitation within a closed system would result in a light to heavy $\delta^{34}S$ isotopic pattern with time. Using an initial reservoir $\delta^{34}S$ value of +16 ‰ for the Hockley mineralizing system, this model theoretically could explain the light to heavy trend in pyrite $\delta^{34}S$ in the upper part of the anhydrite cap rock (Fig. 6.2). However, Rayleigh-type fractionation appears to be geologically unrealistic for the dynamic salt dome environment and cannot directly explain the heavy to light $\delta^{34}S$ trend in the lower cap rock (See Kyle and Agee, 1988, for further discussion).

Mixed Sulfur Source Model

The mixed sulfur source model requires that the heavy H_2S component ($\geq$ +4 ‰) be thermochemically generated from cap rock sulfate or transported along with metals in the same solution. The co-transportation of metals and H_2S is geochemically feasible in Gulf Coast formation waters but only under restricted conditions of pH, temperature, and salinity (Anderson, 1973; Sverjensky, 1984). Most of the $\delta^{34}S$ values from the upper portion of HH2 fall relatively close to a mixing line defined by the light and heavy sulfide end-members (Kyle and Agee, 1988). The lightest $\delta^{34}S$ value (i.e., -35 ‰) along the upper mixing trend, was presumably generated by biogenically reduced sulfate without discernable contribution of heavy sulfide. The heaviest sulfide $\delta^{34}S$ value (+4 ‰) can be explained by mixing 75 % of anhydrite cap rock or basin-derived H_2S ($\delta^{34}S$ = +16 ‰) with 25 % biogenic H_2S from local reduced sulfate ($\delta^{34}S$ = -35 ‰) (Kyle and Agee, 1988; Fig. 6.2). In the lower anhydrite zone (below the inflection point), biogenic H_2S began to dominate the mixed sulfur reservoir. The increase of relative concentrations of light sulfur with time results in relatively light pyrite $\delta^{34}S$ values with depth (Fig. 6.8). Two $\delta^{34}S$ data points at an interval depth of 165 and 182 ft above salt appear to fall outside the mixing trend. These samples are from a 50-ft zone that contains abundant Fe- and Zn-sulfides and is particularly Ag-rich (Figs. 5.6 and 5.8). This zone is interpreted to represent a late-stage pulse (possibly Frio time) of deep-sourced metal-bearing fluids (Kyle and Agee, 1988).

A test of the mixing model for explaining the $\delta^{34}S$ trends at Hockley is its geologic plausibility. Fluctuations and trends in $\delta^{34}S$ values can be explained by mixing light and heavy components of H_2S fluids. Additional support is provided by limited data for two pyrite types from the Hockley supracaprock sediments.

These sulfides have a bimodal $\delta^{34}S$ distribution (mean values of -25 and +2 ‰) which are interpreted to represent end-member components of the H_2S reservoirs (Kyle and Agee, 1988; Table XI). Very fine-crystalline pyrite aggregates (Fig. 4.21a) have isotopically light $\delta^{34}S$ values and are from supracaprock clay-rich sediments. A later generation of fine-crystalline pyrite (Fig. 4.21b) with heavier $\delta^{34}S$ values is particularly abundant in fine-grained sandy units and may represent the "ore-stage" sulfides with reference to cap rock mineralization (Kyle and Agee, 1988).

A similar $\delta^{34}S$ range of Fe-sulfide minerals (-47 to +27 ‰) has been documented in Tertiary sandstone-hosted roll-front uranium deposits in south Texas. These deposits contain abundant isotopically light ore-stage marcasite (< -20 ‰) and isotopically heavy post-ore pyrite; pre-ore pyrite may be either isotopically heavy or light (Goldhaber et al., 1978, 1979; Reynolds and Goldhaber, 1983). This bimodal distribution of $\delta^{34}S$ values implies that there are two different sulfur sources (Goldhaber et al., 1983). It has been proposed that fault-leaked brines from underlying oil and gas fields (isotopically heavy) and shallow groundwaters representing bacterially metabolized organic matter (isotopically light) are the H_2S sources (Goldhaber et al., 1979; Busche et al., 1982). Although these ore deposit are different in nature, there appears to be a relationship between the Hockley Pb-Zn-Ag deposit and the South Texas uranium deposits with regard to sulfur source (Kyle and Agee, 1988). Conversely, the possibility exists that thermochemically reduced cap rock sulfate (heavy H_2S) leaked into permeable supracaprock sediments resulting in a heavy $\delta^{34}S$ signature of "ore-stage" pyrite.

Conclusions

The Gulf Coast basin is a dynamic hydrologic environment for which mixing of multisource fluids is an attractive and plausible mechanism to explain the metal and sulfur isotope variations at Hockley Dome. It has been proposed that the reservoirs of reduced sulfur and metals evolved during the several million year accumulation history of the anhydrite cap rock (Kyle and Agee, 1988; Table III). The metal assay and $\delta^{34}S$ data for HH2 indicate two isotopically distinct sulfur components. The isotopically heavy H_2S component is believed to be related to deep metalliferous oil field brines that migrated up the flanks of the salt diapir into the cap rock environment (Fig. 6.11). The isotopically light H_2S is attributed to bacterial reduction of local aqueous sulfate. The relative correlation between sulfide mineralization and sulfide $\delta^{34}S$ indicates a genetic relationship between the generation of heavy H_2S and the supply of metals by relatively hot, deep-sourced formation waters (Kyle and Agee, 1988; Fig. 6.8). If petroleum was episodically supplied along with metals, then isotopically heavy H_2S could be produced via thermochemical reduction of cap rock sulfate. Conversely, heavy H_2S could have been supplied along with metals in the formation waters. Potential extrensic sources of the heavy H_2S- and metal-bearing brines are Mesozoic carbonate sour gas reservoirs (Kyle and Agee, 1988; Figs. 6.9 and 6.10).

The highly mineralized intervals with heavy $\delta^{34}S$ values are interpreted to represent a sustained supply and exposure of relatively hot, deep-sourced fluids to the cap rock environment. These events increase the contribution of heavy H_2S to the mixed sulfur reservoir, either through extrensic supply or by local thermochemical production of H_2S. Also, the introduction of large volumes of metalliferous formation waters ($\geq 100^{o}C$), perhaps episodically released during

basin dewatering (Cathles and Smith, 1984), would result in the periodic decimation of the bacterial population in the shallow cap rock environment. These formation waters with very high metal concentrations may have been toxic to bacteria (Kharaka et al., 1987). Until the salt dome environment returned to a more tolerable temperature for bacteria regeneration, heavy H_2S dominated the sulfur reservoir (Kyle and Agee, 1988).

The proposed geological model for cap rock mineralization at Hockley Dome is that hot metal-bearing formation waters mixed with ambient biogenic H_2S. Sulfide precipitation was probably initiated when cool acetate-type water mixed with warmer metalliferous formation waters that migrated up the salt dome flanks (Kyle and Agee, 1988). The upper portion of the anhydrite cap rock is barren to weakly mineralized and corresponds to a trend of relatively light $\delta^{34}S$ values. It appears that biogenic production of H_2S was greatest during events of rapid diapirism and cap rock accumulation (i.e., Lower and Middle Wilcox time). However, as cap rock growth rates began to decline metal concentration and $\delta^{34}S$ values appear to have increased significantly. The episodic introduction of hot metalliferous fluids overwhelmed the light H_2S component through the combined effects of supplying heavy H_2S or by local thermochemical reduction, and suppression of the local bacterial H_2S production (Kyle and Agee, 1988). Heavier $\delta^{34}S$ sulfide values toward the middle of the cap rock along with high metal concentrations suggests that the flux of basin-derived fluids reached a maximum during the middle history of anhydrite cap rock accumulation (i.e., Upper Wilcox, Claiborne, and Jackson time - roughly 50 to 31 Ma ago). Biogenic H_2S then began to dominate the mixed sulfur reservoir resulting in

the trend toward relatively light $\delta^{34}S$ values to the present cap rock/salt contact. Relatively light $\delta^{34}S$ values appear to correspond to a decrease in metal concentrations and a relative increase in anhydrite accumulation rates.

Chapter 7

Pb ISOTOPES

Common Pb refers to Pb in minerals such that no significant radiogenic Pb has been generated in situ since the phase formed. Because Pb has a high atomic mass, it is not susceptible to natural physiochemical or biochemical fractionation processes which are responsible for isotopic variations in sulfur and other light elements (e.g., hydrogen, carbon, and oxygen) (Faure, 1986). The importance of isotopic variations of common Pb is based on the principle that the composition is "frozen" at the time when Pb was isolated from a reservoir that contains U and Th. Therefore, the Pb contained in an ore mineral preserves in its isotope abundances a composite record of its mixing history in previous U-Th-Pb environments. Because different geologic environments have distinct U/Pb and Th/Pb ratios and the isotopic homogenization of Pb is irreversible, the composition of Pb will reflect its sources. This represents a significant analytical tool to help solve problems of ore genesis (Doe and Stacey, 1974; Loveless, 1975; Koppel and Saager, 1976).

Lead isotope abundances in mineral deposits are classified as either "single-stage" or "anomalous". The single-stage model of Pb isotope evolution assumes that the only changes in the value of the parent to daughter ratio in the source environment are those caused by radioactive decay of the parents (U and Th). Moreover, Pb contained in the ore mineral was extracted from a single source. A mathematical model can be derived which utilizes the compositions of primordial Pb and ore Pb to estimate the age of mineralization and the U/Pb ratio in the source environment. These so-called "model Pb" ages approximate the time of formation of the mineral deposit as determined by independent means. Ores which formed as a result of more complex sets of conditions

give rise to more complex Pb chemistry. One possibility of the latter would be variable Pb isotope ratios within the mineralizing fluid due to mixed source terrains. Single-stage model ages calculated from anomalous leads tend to be very much in error, and commonly correspond to future ages because the samples contain more radiogenic Pb than is compatible with the single-stage model. Data from anomalous leads are also useful, not so much in determination of age as in the solution of genetic problems (Doe and Stacey, 1974; Sangster, 1976; Faure, 1986).

The Hockley sulfide deposit has well developed stratiform and stratabound characteristics. Textures of sulfides indicate that anhydrite cap rock accumulation and mineralization were syngenetic processes. Thus there is a potential to study the genetic relationship between ores and their host. Marcasite, pyrite, and galena were obtained from the calcite, gypsum, and anhydrite zones at Hockley Dome and analyzed for common Pb. Lead isotope analyses were determined for galena samples collected from core holes spaced around the dome that include a variety of textural and host rock types (Price et al., 1983; Table XII; Fig. 6.1). Common Pb compositions were determined specifically for a series of samples from core hole HH2 (Table XIII). Plotted data yield a Pb isotope profile that can be compared with metal assay data (Fig. 7.1). Knowledge of the sequence of accumulation of cap rock and sulfides permits examination of the evolution of the sulfide-mineralizing system.

Results

General

Lead isotope data were collected from seven galena separates from randomly selected cores and intervals (Price et al., 1983; Fig. 6.1). Galena occurs as a late-stage (Fig. 4.17), relatively coarse-crystalline (Fig. 4.11) precipitate permitting relatively

Table XII. Isotope analyses of common Pb from cap rock-hosted galena.

Core	Sample no.	Host Rock	206/204	207/204	208/204	Description: in situ
HB3	824	anhydrite	18.747	15.654	38.703	Octahedral ga (2 mm) and colloform sl intergrown with botryoidal py
HB5	1089	anhydrite	18.734	15.641	38.677	Fine-crystalline ga mass coated with py
	1097	anhydrite	18.749	15.647	38.696	Fine-crystalline ga mass coated with py
HD4	1049	anhydrite	18.774	15.652	38.734	Fine-crystalline ga associated with py
HE2	746	calcite	18.793	15.656	38.785	Boxwork and radial py associated with colloform sl and octahedral ga (1 mm)
	784	calcite	18.798	15.652	38.780	Octahedral ga (1 mm) associated with sl and py
HF2	1120	calcite	18.781	15.667	38.760	Octahedral ga (1 mm) associated with S

Sample no. represents subsurface depth in feet; See Figure 6.1 for drill hole locations.
Mineral abbreviations: py = pyrite; sl = sphalerite; ga = galena; S = sulfur

Data summary in Price et al. (1983)

Table XIII. Isotope analyses of common Pb from cap rock-hosted sulfides in core HH2.

Sample no.	Host Rock	206/204	207/204	208/204	Description (abbreviated): in situ
404 ga *	anhydrite	18.774	15.693	38.802	Broad laminae (1 cm) of interstitial py, sl and ga
499 py	anhydrite	18.808	15.723	38.951	Thin laminae (2 mm) of py and lesser sl
533 ga *	anhydrite	18.773	15.698	38.814	Massive sulfide laminae (6 mm) of py, sl and minor ga
566 py	anhydrite	18.749	15.666	38.716	Disseminated py with minor sl
649 ga *	anhydrite	18.769	15.696	38.806	Laminae (5 mm) of py, sl and minor ga
704 py	anhydrite	18.758	15.678	38.754	Disturbed massive sulfide zone of py, sl and minor ga
757 py	anhydrite	18.793	15.709	38.890	Massive sulfide zone of py with minor sl
780 ga *	anhydrite	18.748	15.655	38.690	Broad laminae (1-2 cm) of py, sl and minor ga
830 ga *	anhydrite	18.767	15.676	38.776	Thin laminae (5mm) of sl, ga and minor py
878 py	anhydrite	18.787	15.704	38.874	Thin laminae (2 mm) of py and sl
910 py	anhydrite	18.780	15.690	38.818	Broad laminae (1 cm) of py
975 py a*	anhydrite	18.791	15.701	38.855	Broad laminae (1 cm) of py with minor sl and ga
975 py b	anhydrite	18.748	15.649	38.699	Broad laminae (1 cm) of py with minor sl and ga
975 py c	anhydrite	18.790	15.718	38.974	Broad laminae (1 cm) of py with minor sl and ga

Sample no. represents subsurface depth in feet; See Figure 6.1 for drill hole location.
Mineral abbreviations: py = pyrite; sl = sphalerite; ga = galena
* Sample analyzed at University of California at Santa Barbara; all others analyzed at University of Texas at Austin

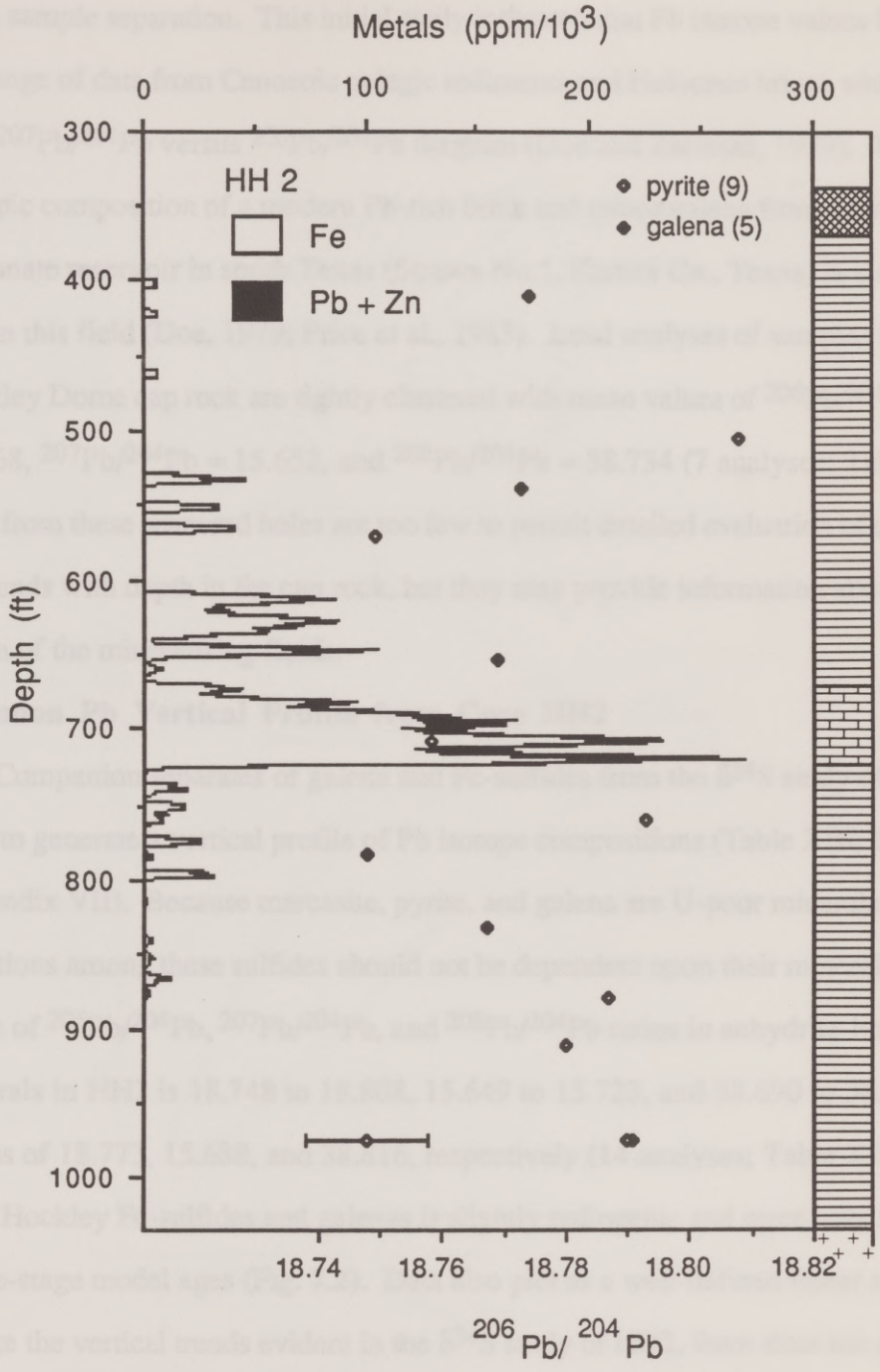

Fig. 7.1. Pyrite and galena $^{206}Pb/^{204}Pb$ compositions and Pb+Zn and Fe content of HH2 plotted as depth below surface.
There is no apparent correlation of $^{206}Pb/^{204}Pb$ ratios with metal abundances or depth.

clean sample separation. This initial study indicated that Pb isotope values lie within the range of data from Cenozoic pelagic sediments and Holocene brines when plotted on a $^{207}Pb/^{204}Pb$ versus $^{206}Pb/^{204}Pb$ diagram (Doe and Zartman, 1979). The Pb isotopic composition of a modern Pb-rich brine and minor galena from a Cretaceous carbonate reservoir in south Texas (Strawn No.1, Karnes Co., Texas) is also reported within this field (Doe, 1979; Price et al., 1983). Lead analyses of samples from Hockley Dome cap rock are tightly clustered with mean values of $^{206}Pb/^{204}Pb$ = 18.768, $^{207}Pb/^{204}Pb$ = 15.652, and $^{208}Pb/^{204}Pb$ = 38.734 (7 analyses; Table XII). Data from these scattered holes are too few to permit detailed evaluation of common Pb trends with depth in the cap rock, but they may provide information about the origin of the mineralizing fluids.

Common Pb Vertical Profile from Core HH2

Companion separates of galena and Fe-sulfides from the $\delta^{34}S$ study of HH2 were used to generate a vertical profile of Pb isotope compositions (Table XIII; Fig. 7.1; Appendix VII). Because marcasite, pyrite, and galena are U-poor minerals, isotope variations among these sulfides should not be dependent upon their mineralogy. The range of $^{206}Pb/^{204}Pb$, $^{207}Pb/^{204}Pb$, and $^{208}Pb/^{204}Pb$ ratios in anhydrite-hosted sulfide minerals in HH2 is 18.748 to 18.808, 15.649 to 15.723, and 38.690 to 38.974 with means of 18.773, 15.688, and 38.816, respectively (14 analyses; Table XIII). Lead from Hockley Fe-sulfides and galenas is slightly radiogenic and represents future single-stage model ages (Fig. 7.2). Data also plot as a well-defined linear array. Unlike the vertical trends evident in the $\delta^{34}S$ study of HH2, there does not appear to be a systematic relationship between Pb isotope values and either cap rock "stratigraphic" position (Fig. 7.1) or to their corresponding $\delta^{34}S$ values (Tables IX and XIII). It has been suggested that a strong correlation of Pb and sulfur isotopic composition is

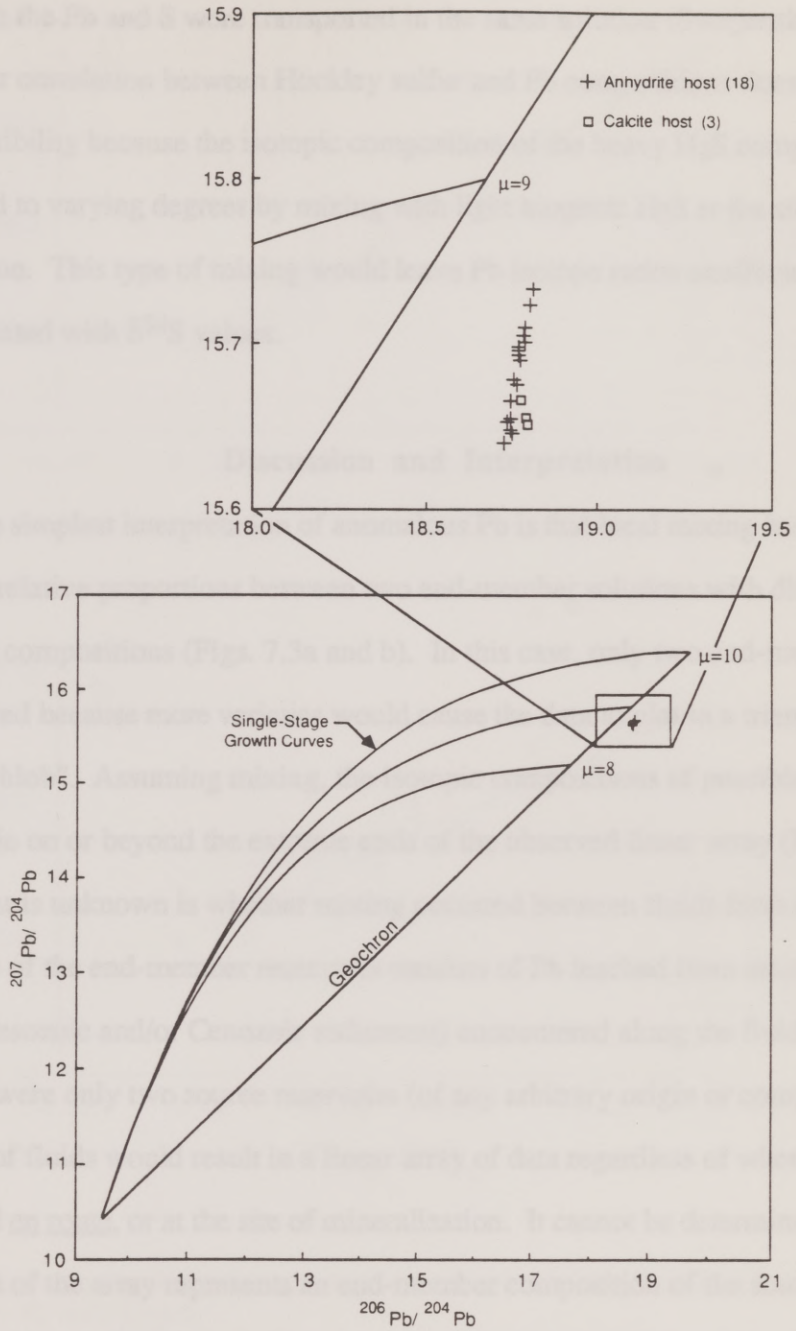

Fig. 7.2. Conventional Pb-Pb diagram showing single-stage growth curves and geochron. The curved lines are Pb growth curves for U-Pb systems having μ values of 8, 9, and 10. Lead isotope compositions from Hockley are slightly radiogenic. These anhydrite- and calcite-hosted leads occur as a linear array of data points that plot to the right of the geochron.

evidence the Pb and S were transported in the same solution (Sverjensky et al., 1979). The poor correlation between Hockley sulfur and Pb compositions does not preclude this possibility because the isotopic composition of the heavy H_2S component was modified to varying degrees by mixing with light biogenic H_2S at the site of ore deposition. This type of mixing would leave Pb isotope ratios unaffected, but uncorrelated with $\delta^{34}S$ values.

Discussion and Interpretation

The simplest interpretation of anomalous Pb is that local mixing has occurred in various relative proportions between two end-member solutions with different Pb isotopic compositions (Figs. 7.3a and b). In this case, only two end-members can be considered because more varieties would cause the data to plot in a triangular field, or as a "blob". Assuming mixing, the isotopic compositions of possible source rocks should lie on or beyond the extreme ends of the observed linear array (Figs. 7.3a and b). What is unknown is whether mixing occurred between fluids from distant sources or if one of the end-member reservoirs consists of Pb leached from intervening wall rock (Mesozoic and/or Cenozoic sediments) encountered along the fluid flow path. If there were only two source reservoirs (of any arbitrary origin or composition), then mixing of fluids would result in a linear array of data regardless of whether the mixing occurred en route, or at the site of mineralization. It cannot be determined if either endpoint of the array represents an end-member composition of the sources. Most likely, neither endpoint does. For example, when a metalliferous brine is episodically released during basin dewatering, the composition of the transported Pb may be modified by contamination from the intervening rocks, depending especially upon the distance of transport from the source rock to the site of ore deposition and the degree

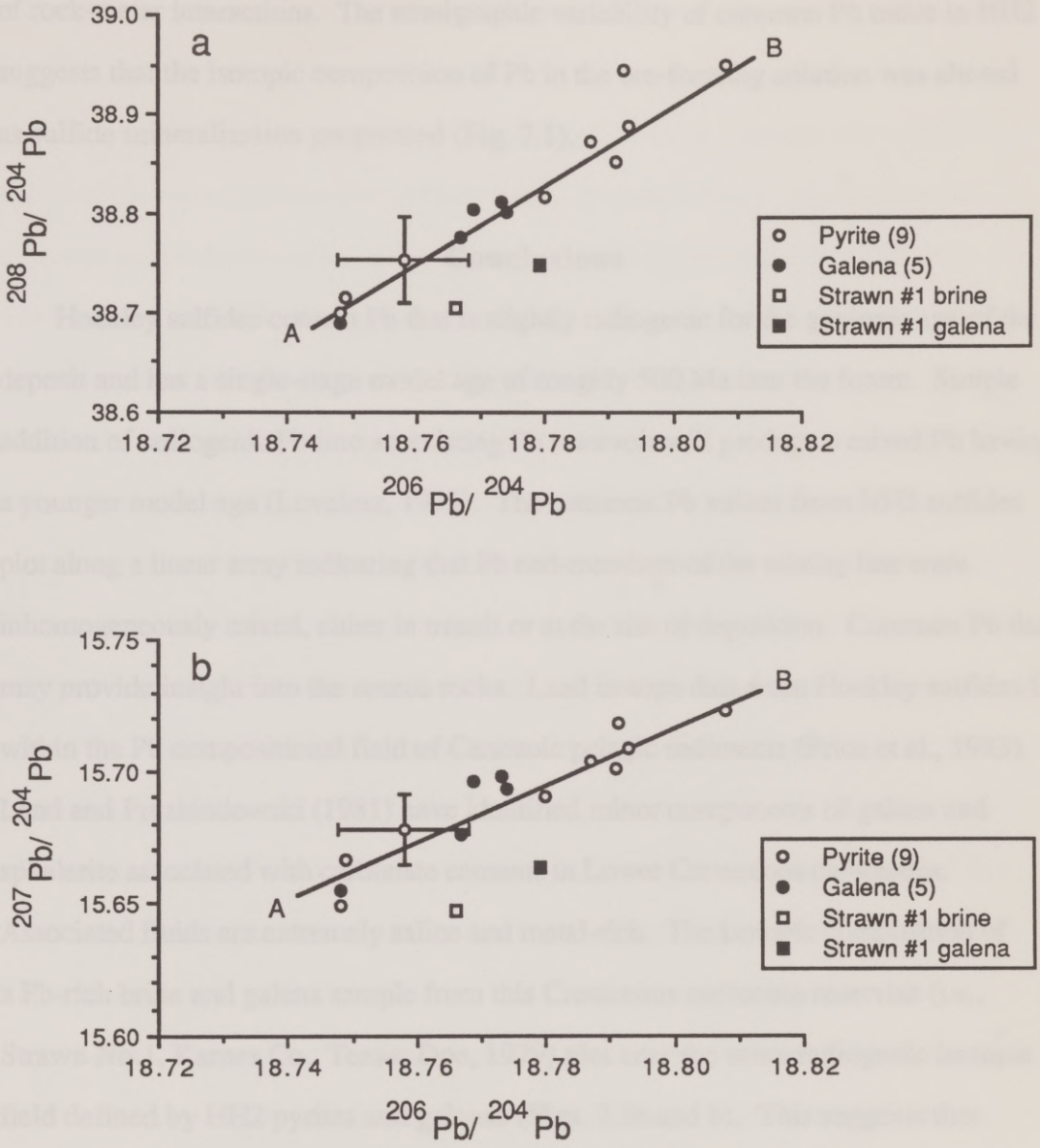

Fig. 7.3a, b. Pyrite and galena isotope values from HH2 produce a liner array of common Pb data points.
Inhomogeneous mixture of component A and B will produce data points that lie on a mixing line. The least-squares best-fit lines through these Pb isotope values (HH2) have correlation coefficients of 0.98 (a) and 0.94 (b). The slope has no age significance because Pb at Hockley have not experienced a single-stage growth history. Note the Pb isotope composition of a Cretaceous-hosted brine and galena from the Srawn #1 plot close to (but slightly below) the same compositional field as Hockley.

of rock-water interactions. The stratigraphic variability of common Pb ratios in HH2 suggests that the isotopic composition of Pb in the ore-forming solution was altered as sulfide mineralization progressed (Fig. 7.1).

Conclusions

Hockley sulfides contain Pb that is slightly radiogenic for the geologic age of the deposit and has a single-stage model age of roughly 500 Ma into the future. Simple addition of radiogenic Pb into an existing Pb reservoir will produce a mixed Pb having a younger model age (Loveless, 1975). The common Pb values from HH2 sulfides plot along a linear array indicating that Pb end-members of the mixing line were inhomogeneously mixed, either in transit or at the site of deposition. Common Pb data may provide insight into the source rocks. Lead isotope data from Hockley sulfides lie within the Pb compositional field of Cenozoic pelagic sediments (Price et al., 1983). Land and Prezbindowski (1981) have identified minor components of galena and sphalerite associated with carbonate cements in Lower Cretaceous carbonates. Associated fluids are extremely saline and metal-rich. The isotopic composition of a Pb-rich brine and galena sample from this Cretaceous carbonate reservoir (i.e., Strawn No.1, Karnes Co., Texas; Doe, 1979) plot near the same radiogenic isotopic field defined by HH2 pyrites and galenas (Figs. 7.3a and b). This suggests that metalliferous fluids at Hockley may have been derived from Mesozoic sediments during burial diagenesis. Rock-water interactions involving red beds and albitization of detrital feldspars are possible sources for metals in the formation fluids (Fig. 6.10).

Chapter 8

SUMMARY

Diagenetic events over an extended period of geologic time resulted in the accumulation and mineralization of cap rock at Hockley Dome. The cap rock is a layered sequence of calcite, gypsum, and anhydrite approximately 900 ft thick. Textural evidence indicates that sulfide mineralization was an integral aspect of anhydrite cap rock formation. The relationship of euhedral anhydrite grains surrounded by sulfides indicates that as mineralizing fluids entered the salt/anhydrite cap rock interface, sulfide precipitation cemented loose anhydrite grains prior to cap rock accretion and compaction. These sulfide-precipitating events are recorded as discrete laminae. Local concentrations of anhydrite-hosted laminae result in sulfide-rich intervals consisting of variable amounts of marcasite, pyrite, sphalerite, galena, and rare acanthite. The highest metal sulfide concentrations occur in an annular zone around the perimeter of the cap rock. Total metal distribution between anhydrite- and calcite-host rock is roughly equally divided. However, anhydrite cap rock is more widely mineralized than calcite cap rock, although the calcite breccias contain higher ore grades.

The following sequence of salt tectonic and diagenetic events is inferred to have formed Hockley Dome and the overlying cap rock. Early stages of halokinesis was initiated by marine carbonate and clastic loading of the thick Louann Salt. Thinning of the Gulfian strata (Ewing, 1986) indicates that pillow stage dome growth occurred during the Upper Cretaceous. Evidence of continued salt movement is preserved in overthickened Wilcox Group sediments (Fig. 2.5). The development of a salt withdrawal basin was in response to this initial stage of diapiric salt movement

(approximately 56 Ma). Wilcox deposition represents an eight m.y. period in which salt diapirism and cap rock accumulation were greatest, resulting in the formation of slightly less than half (roughly 460 ft) of the anhydrite section (Table III). Salt rise and brine expulsion may have been driven by the rapid loading which occurred as Wilcox deltas prograded into the area. The upper anhydrite zone is characterized by alternating zones of barren to weakly mineralized anhydrite cap rock. It is also densely fractured which may be indicative of rapid accumulation rates. During post-Wilcox time, cap rock growth rates were considerably slower and possibly correspond to an overall increase in sulfide concentration and decrease in fracture density. Although the lower portion of the cap rock is mineralized to some degree, the greatest sulfide bearing interval generally occurs within the middle 100 to 150 ft of anhydrite cap rock. It appears that metalliferous fluids responsible for this major sulfide-rich zone entered the cap rock during Claiborne time (approximately 40 and 50 Ma ago) (Fig. 5.18b). A second potentially economic interval occurs stratigraphically low in the cap rock section and appears to have developed during Frio time, again associated with rapid sediment loading of the basin. This Ag-rich zone represents the most obvious geochemical marker within the southern portion of the cap rock. In general, it appears that intervals with significant concentrations of sulfides developed during post-Wilcox time (approximately 50 to 20 Ma ago). This was possibly in response to a decrease in cap rock accumulation rates (slower salt supply) synchronized with an increased availability of or connection to deep sourced metalliferous formation waters.

Most metal concentrations at Hockley represent stratiform sulfides that were precipitated in the zone of salt dissolution as anhydrite cap rock accumulated by sequential underplating. The anhydrite portion of the cap rock provides a chronological record of these fluid events. In general, metal ratio data suggest that sulfide-

precipitating fluid(s) became more Zn-rich (or Pb-poor) and possibly Ag-rich during anhydrite cap rock accumulation. Assay data suggest that reservoirs of metalliferous brines evolved during 940 ft of anhydrite cap rock accumulation. The apparent large scale metal zonation is attributed to variation in the metal source(s) and/or evolution of metal reservoirs. Common Pb data confirm that non-uniform mixing of isotopically different Pb likely occurred. These processes could produce an evolved metal-bearing solution that exhibits variations in its metal ratios and Pb isotopic composition consistent with what is observed at Hockley.

The ore-forming fluids appear to be metalliferous formation waters, perhaps originating from the lower Cretaceous and/or Jurassic carbonate units. A modern example of a potential mineralizing fluid is observed in the Picaroon field, offshore Texas. This fluid, like Mesozoic brines, is extremely saline, Ca-rich and characterized by high Pb and Zn concentrations and extremely low H_2S. Brines of this composition have been rarely identified in the Cenozoic section. Therefore, it is believed that these fluids were injected into Miocene sediments of the Picaroon field along fault conduits from underlying Mesozoic sediments. Considering that local growth faults at Hockley may extend into Lower Cretaceous carbonates, a hydrologic scenario similar to that of the Picaroon field may have channeled fluids into the cap rock forming environment. It is inferred that a warm metalliferous brine, originally derived from the Mesozoic section, is a likely source fluid responsible for cap rock mineralization at Hockley Dome.

Salt movement was such that as metalliferous formation waters were expelled from the sedimentary basin they intercepted the cap rock forming environment. During cap rock generation reduced sulfur must be available for metals to precipitate as sulfides.

It is proposed that mixing of multisource fluids is the mechanism most likely responsible for metal and sulfur isotope variations at Hockley Dome. The reservoirs of reduced sulfur and metals evolved over 50 m.y. of diapiric cap rock accumulation. Complementary metal and $\delta^{34}S$ data for HH2 indicate two isotopically distinct sulfur components. The isotopically heavy H_2S component is believed to be related to deep metalliferous oil field brines that migrated up the flanks of the salt diapir into the cap rock environment (Fig. 6.11). The isotopically light H_2S involved in cap rock sulfide mineralization is attributed to bacterial reduction of aqueous sulfate derived from dissolution of anhydrite cap rock. The correlation between intensity of sulfide mineralization and sulfide $\delta^{34}S$ indicates a genetic relationship between the generation of heavy H_2S and the supply of metals by relatively hot, deep-sourced formation waters. It is possible that heavy H_2S could have been supplied along with metals in the formation waters. Potential sources of the heavy H_2S- and metal-bearing brines are Mesozoic carbonate sour gas reservoirs. However, precipitation of galena and sphalerite from metal-rich brines such as those described in the Picaroon field requires a separate source of H_2S. Isotopically heavy H_2S can be obtained by thermochemical reduction of dissolved sulfate derived from anhydrite cap rock. This reaction is driven thermally at temperatures in excess of 80 to 100°C and in the presence of petroleum (Orr, 1977). This scenario allows high concentrations of metals to enter the cap rock forming environment. Because formation waters high in metals are incompatible with large concentrations of H_2S, mixing of metal-rich brines with local H_2S-rich brines is the simplest mechanism for deposition of ores at Hockley.

A generalized geological model for Pb-Zn-Ag cap rock mineralization at Hockley Dome is as follows: Sulfide deposition appears to have resulted when relatively hot

(≥ 100°C), deep sourced metalliferous fluids were forced out of the Mesozoic section along zones of structural weakness into the cap rock forming environment. These Mesozoic type fluids were episodically released during basin dewatering and focused along a dècollement plane intersecting the Hockley salt stock at depth (Ewing, 1986). Mineralizing fluids then flowed along salt dome flanks into the salt/anhydrite interface, i.e., the principal site of ore deposition. Greater sulfide abundance and presence of significant Ag concentrations in the southern portion of the dome suggest that greater volumes of geopressured mineralizing fluids entered this section of the dome and then laterally dispersed. Also, fluid movement into cap rock may have been influenced by salt overhangs that restricted metalliferous fluids in areas now characterized by elevated metal concentrations. Interaction between these warm, saline formation waters and cool acetate waters probably initiated sulfide precipitation along the cap rock margins. It is proposed that the above fluid mixing and rock-water interactions produced the complex common Pb and $\delta^{34}S$ isotopic and metal patterns within anhydrite cap rock. The stratigraphic relationship of sulfide $\delta^{34}S$ values and metal concentrations suggests that basin-derived fluids were continuously leaked into the cap rock environment, but only prolonged episodes of fluid flow were maintained during the Eocene (Claiborne and Jackson time) and to a lesser extent the Oligocene (Vicksburg and Frio time), at times of rapid sediment loading. This study has identified spatial, temporal, and geochemical factors likely responsible for sulfide mineralization of Hockley Dome. The implications are that the Gulf Coast is a young evolving sedimentary basin in the process of producing metallic sulfide deposits with genetic similarities to some Mississippi-Valley Type Pb-Zn deposits and sedimentary exhalative Pb-Zn-Ag deposits.

APPENDICES

Methods and Materials Studied

Several analytical techniques and methods of observation were used to identify cap rock mineralogy and determine mineral and isotopic composition of hosted sulfides. These techniques include the use of an electron microprobe, a scanning electron microscope, and gas- and solid-sourced mass spectrometers for sulfur and common Pb isotope measurements. Polished sections prepared from cored samples were petrographically studied under transmitted, reflected, and ultraviolet light. In addition, a large assay data base was used to characterize vertical and horizontal metal distribution. All analyses, with the exception of the assay data and sulfur and Pb isotopes, were performed in the Department of Geological Sciences, University of Texas at Austin. Computer facilities at the University of Texas were also used to model the stability of anhydrite and gypsum under various cap rock forming conditions. The geochemical modeling program, PHREEQE and PHREPITZ (a computer program for geochemical calculations), was made available to the Department of Geological Sciences by the United States Geological Survey.

Appendix I

Assay data base

An extensive core library and assay data set exists for the Hockley Dome cap rock as a result of a minerals exploration program that included the drilling of sixty-five core tests (5-ASARCO, 5-Chevron, and 55-Marathon) during 1980-82 (Appendix Ia). These holes were rotary drilled through supracaprock sediments where the upper calcite cap rock was commonly penetrated; then, continuous 1.85-inch diameter core was

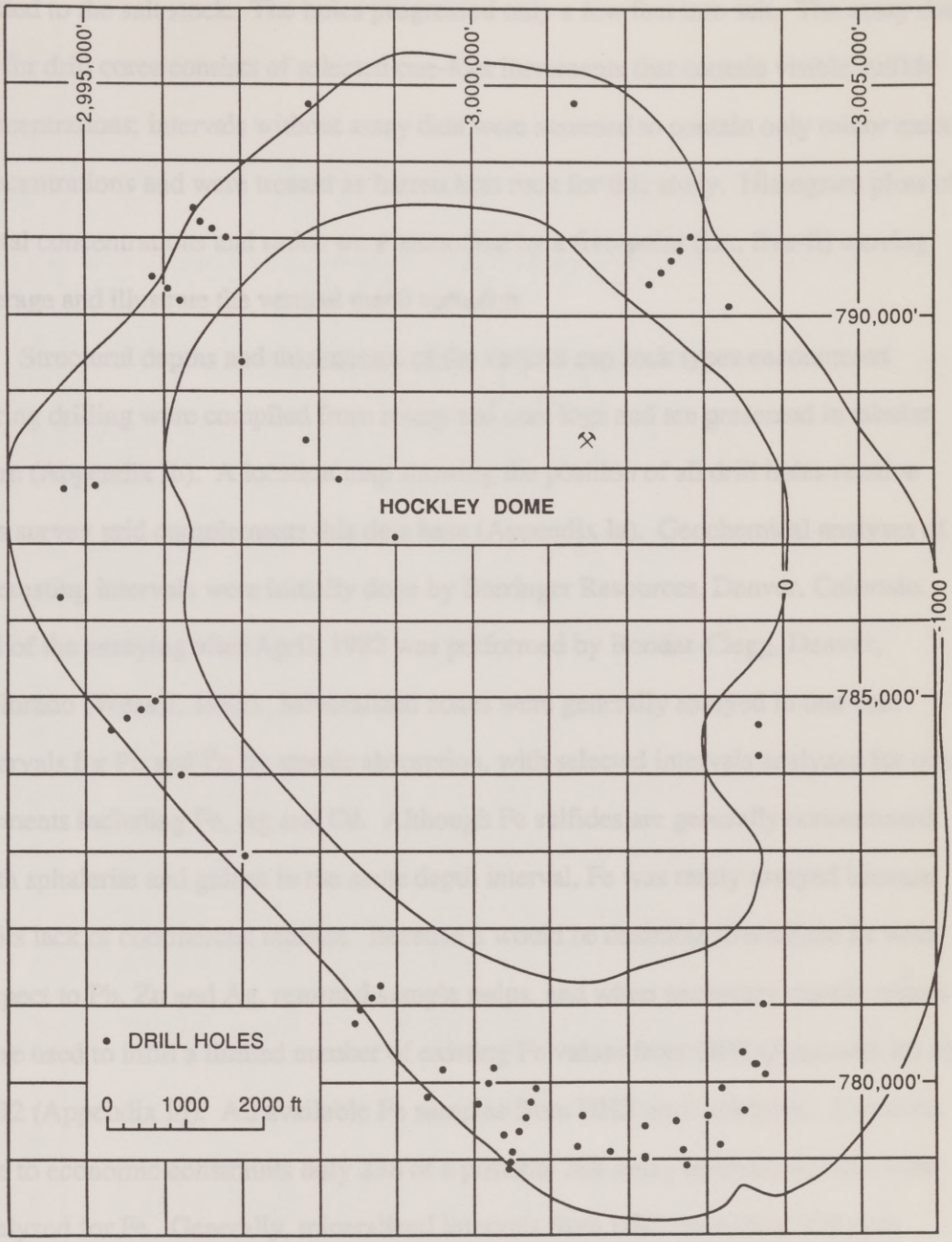

Appendix Ia. Plan map showing the locations of ASARCO, Cheveron, and Marathon drill holes relative to survey grid.
Contour lines are shown for reference and represent elevation to top of cap rock in feet.

drilled to the salt stock. The holes progressed only a few feet into salt. The assay data set for drill cores consists of selected one-foot increments that contain visible sulfide concentrations; intervals without assay data were assumed to contain only minor metal concentrations and were treated as barren host rock for this study. Histogram plots of metal concentrations and ratios were smoothed by a five-point (i.e., five-ft) moving average and illustrate the vertical metal variation.

Structural depths and thicknesses of the various cap rock types encountered during drilling were compiled from rotary and core logs and are presented in tabular form (Appendix Ib). A location map showing the position of all drill holes relative to a survey grid complements this data base (Appendix Ia). Geochemical analyses of interesting intervals were initially done by Barringer Resources, Denver, Colorado. All of the assaying after April, 1982 was performed by Bondar-Clegg, Denver, Colorado (Wessel, 1983). Mineralized zones were generally assayed in one-foot intervals for Pb and Zn by atomic absorption, with selected intervals analyzed for other elements including Fe, Ag and Cd. Although Fe sulfides are generally concentrated with sphalerite and galena in the same depth interval, Fe was rarely assayed because of its lack of commercial interest. Because it would be desirable to evaluate Fe with respect to Pb, Zn and Ag, returned sample pulps, and when necessary, coarse rejects were used to infill a limited number of existing Fe values from HB3 (Appendix Ic) and HH2 (Appendix Id). All available Fe samples from HH2 were analyzed. However, due to economic constraints only 238 of a possible 368 assay intervals in HB3 were analyzed for Fe. Generally, mineralized intervals from HB3 exceeding 500 ppm Pb+Zn were selected for Fe analysis. These samples were analyzed by Cone Geochemical, Inc., Lakewood, Colorado.

Appendix I b. Compilation of Hockley Dome cap rock core.

Well	Coordinates: North	East	Collar Elevation (ft)	Rotary Samples (Depth, ft)	Core Samples (Depth, ft)	Total Depth (ft)	Top of cap rock (ft)	Top of gyp zone (ft)	Top of an zone (ft)	Top of salt (ft)	Thickness upper ca (ft)	Thickness lower ca (ft)	Thickness gypsum (ft)	Thickness anhydrite (ft)	Thickness cap rock (ft)
HA-1a	790,332	2,996,061	188 b	5-855	855-1184	1184	800	855	889	1184	55	2	28	295	384
HB-1	779,362	3,000,598	175 b	5-650	650-1011	1011	635	np	665	1011	30	np	np	346	376
HB-2	779,548	3,000,683	175 b	5-523	523-1070	1070	495	np	523	1064	28	np	np	541	569
HB-3	779,735	3,000,759	175 b	5-333	333-1054	1054	320	np	364	1048	44	np	np	684	728
HB-4	779,921	3,000,819	175 b	5-300	300-1082	1054	296	np	321	1046	25	np	np	725	750
HB-5	778,952	3,000,478	172 b	5-1082	1082-1374	1374	1035	np	1082	1364	47	np	np	170	329
HC-1	784,824	2,995,712	175 b	5-330	330-1054	1054	305	358	365	1045	58	np	2	680	740
HC-2	784,932	2,995,876	176 b	5-84	84-1042	1042	204	np	285	1038	12	np	np	753	834
HC-3	784,709	2,995,535	175 b	0-425	433-1064	1064	433	635	488	1060	55	46	93	378	627
HC-4	784,570	2,995,328	174 b	5-1005	1005-1072	1072	1012	np	np	1062	37	np	np	np	50
HD-1	790,565	3,002,455	188 b	5-383	383-1140	1140	380	np	388	1120	5	np	np	732	740
HD-2	790,707	3,002,598	189 b	5-665	666-1234	1234	410	np	425	1228	15	np	np	803	818
HD-3	790,850	3,002,711	191 b	5-460	465-1244	1244	473	517	518	1239	36	np	15	689	766
HD-4	791,020	3,002,840	194 b	0-700	704-1274	1274	704	np	1033	1263	323	np	np	230	559
HD-5	790,403	3,002,304	186 b	0-300	304-1184	1184	304	414	417	1181	80	np	1	764	877
HE-1	791,212	2,996,486	197 b	0-970	974-1124	1124	974	np	974	1112	np	np	np	138	138
HE-2	791,113	2,996,647	197 b	0-582	582-1070	1070	582	844	860	1063	252	np	16	203	481
HE-3	791,011	2,996,822	195 b	0-378	378-1044	1044	378	534	415	1042	37	np	85	542	664
HF-1	781,089	2,998,693	172 b	0-615	615-1124	1124	615	785	741	1124	107	np	2	381	509
HF-2	780,941	2,998,527	171 b	5-945	952-1174	1174	1030	np	1157	1167	121	np	np	10	137
HF-3	780,757	2,998,468	171 b	nr	nr	nr	nr	nr	nr	nr	nr	nr	nr	nr	nr
HF-4	781,248	2,998,799	172 b	0-405	409-1090	1090	409	520	615	1083	102	2	118	402	674
HG-1	784,225 a	3,003,682 a	162 b	0-216	216-1013	1013	185	292	210	1012	20	np	137	649	827
HH-1	780,095	3,003,754	171 b	0-380	384-1056	1056	365	384	444	1056	19	65	61	547	691
HH-2	780,235	3,003,611	170 b	0-345	348-1043	1043	338 c	348	368	1035	10 c	52	25	610	697
HH-2a	780,220	3,003,630	170	0-640	640-752	752	nr	nr	nr	nr	nr	58	nr	nr	nr
HH-3	780,376	3,003,465	168 b	0-280	280-1047	1047	270	280	312	1044	10	np	32	732	774
HI-1	779,429	3,002,211	176 b	0-290	290-1053	1053	285 c	295	333	1043	10 c	np	52	640	758
HI-2	779,030	3,002,214	177 b	0-475	475-1088	1088	460	580	600	1083	101	np	20	483	623
HI-2a	778,997	3,002,212	177	0-465	465-558	558	nr	nr	nr	nr	nr	nr	nr	nr	nr
HJ-1	779,568	3,001,414	177 b	0-289	289-1067	1067	280 c	289	368	1050	9 c	3	59	699	770
HJ-2	779,172	3,001,353	177 b	5-490	494-1070	1070	502	629	650	1062	127	np	21	412	560
HK-1	779,989	3,000,197	172	0-357	357-1072	1072	357	380	392	1070	23	np	12	677	713
HK-2	780,178	3,000,262	172	5-325	331-1037	1037	320	345	351	1033	19	45	41	598	713
HK-3	779,716	3,000,055	171	0-646	646-1084	1084	646	824	845	1077	175	np	21	235	431
HL-1	780,157	2,999,590	172 b	0-495	497-1104	1104	497	667	677	1100	169	np	29	405	603
HL-2	779,801	2,999,405	171 b	0-1067	1067-1234	1234	1065	np	1211	1224	149	np	np	10	159

Appendix I b. (Cont.)

Well	Coordinates: North	East	Collar Elevation (ft)	Rotary Samples (Depth, ft)	Core Samples (Depth, ft)	Total Depth (ft)	Top of cap rock (ft)	Top of gyp zone (ft)	Top of an zone (ft)	Top of salt (ft)	Thickness upper ca (ft)	Thickness lower ca (ft)	Thickness gypsum (ft)	Thickness anhydrite (ft)	Thickness cap rock (ft)
HN-1	779,568	3,003,011	175 b	5-525	527-1079	1079	520 c	706	527	1075	7 c	22	5	521	555
HN-2	779,184	3,003,167	172	0-704	704-1095	1095	700	775	784	1082	50	np	9	313	382
HO-1	782,928 a	2,997,043 a	173	5-577	577-1084	1084	577	np	936	1075	297	np	np	139	498
HP-1	783,991	2,996,215	175 b	5-413	413-1075	1075	413	np	516	1071	3	np	np	555	658
HQ-1	787,709	2,994,730	179	5-419	419-1050	1050	380 c	419	426	1040	39 c	19	56	430	660
HQ-2	787,750	2,995,125	179	5-287	287-1027	1027	287	601	320	1027	33	np	53	707	740
HR-1	786,292	2,994,681	178	5-500	514-1044	1044	514	734	741	1037	209	np	21	288	523
HS-1	790,126	3,003,323	188 b	5-405	405-1242	1242	405	np	441	1240	36	np	np	799	835
HT-1	792,771	3,001,340	188 b	5-740	740-1194	1194	740	797	745	1183	5	np	16	382	443
HU-1	779,635	3,003,475	175	5-377	377-1089	1089	352 c	np	377	1082	25 c	np	np	705	730
HU-2	779,915	3,003,185	174	0-216	216-1070	1070	215 c	220	267	1065	5 c	34	46	764	850
HV-1	792,742	2,997,889	204	0-1220	np	1220	np	np	np	np	np	np	np	np	np
HW-1	779,502	3,002,609	177	5-270	288-1090	1090	260	288	319	1078	10	np	31	759	818
HW-2	779,117	3,002,698	176	5-494	494-1096	1096	494	598	606	1090	104	np	18	484	596
HW-3	778,921	3,002,748	175	0-495	514-1098	1098	514	609	631	1088	95	np	28	457	574
HX-1	784,625	3,003,683	165	5-229	229-703	703	214 c	np	229	nr	15 c	np	np	np	np
HY-1	781,005	3,003,723	165	5-270	270-1034	1034	265 c	630	270	1020	5 c	np	10	740	755
HZ-1	779,094	3,001,779	177	0-423	423-1048	1048	423	623	642	1036	151	np	68	394	613
C-1	790,180 a	2,996,215 a	186 b	0-360	360-1120	1120	360	370	373	1115	10	np	3	742	755
C-2	789,333 a	2,996,990 a	182 b	0-88	88-1021	1021	108	140	206	1021	32	np	66	815	913
C-3	788,458 a	2,997,708 a	179 b	0-82	82-1021	1021	82	110	215	1019	28	np	105	804	937
C-4	787,960 a	2,998,183 a	174 b	0-104	104-1021	1021	104	121	152	1019	17	np	31	867	915
C-5	787,185 a	2,998,850 a	165 b	0-130	130-1018	1018	130	140	204	1013	10	np	64	809	883
H-1	778,880 a	3,000,460 a	172 b	0-965	965-1092	1092	930	np	np	1092	47	np	np	np	162
H-2	791,385 a	2,996,385 a	197 b	0-1368	1368-1466	1466	1373	np	1397	1466	6	np	np	69	93
H-3	779,105 a	3,000,505 a	174 b	0-737	737-1054	1054	737	np	782	1054	45	np	np	272	317
H-4	779,325 a	3,000,385 a	174 b	0-720	720-1108	1108	720	766	798	1091	46	np	67	258	371
H-5	790,500 a	2,995,870 a	187 b	0-1205	1205-1418	1418	1309	np	1341	1344	15	np	np	3	35

a - hole location coordinates estimated from 1:24,000 (1in = 2,000 ft) base map.
b - collar elevation estimated from 1:24,000 (1in = 2,000 ft) topographic map.
c - contact and thickness estimates include rotary samples.
(thickness of units may represent totals from multiple discontinuous intervals)

np - not present
nr - not recorded

Appendix I c. Metal assay data, HB3.

Depth (ft)	Fe (ppm)	Pb (ppm)	Zn (ppm)	Ag (ppm)	Pb/(Pb+Zn)
365	-	25	150	-	0.14
366	-	100	855	-	0.10
367	-	15	150	-	0.09
374	1470	15	1400	-	0.01
375	1680	35	725	-	0.05
376	1260	55	140	-	0.28
415	-	5	35	-	0.13
416	-	20	265	-	0.07
417	-	35	255	-	0.12
507	-	5	20	-	0.20
508	-	5	40	-	0.11
509	-	270	1270	-	0.18
510	-	25	155	-	0.14
511	-	5	65	-	0.07
512	-	30	550	-	0.05
513	-	20	165	-	0.11
514	-	15	380	-	0.04
515	-	35	275	-	0.11
516	6930	110	920	-	0.11
517	9520	255	1595	-	0.14
518	8890	165	1335	-	0.11
519	2100	190	435	-	0.30
520	700	10	135	-	0.07
521	980	805	1015	-	0.44
522	-	5	40	-	0.11
523	-	15	285	-	0.05
524	-	5	100	-	0.05
527	-	5	150	-	0.03
529	-	65	685	-	0.09
530	-	5	80	-	0.06
531	-	5	75	-	0.06
532	-	5	105	-	0.05
533	-	5	5	-	0.50
534	-	50	245	-	0.17
535	-	5	100	-	0.05
536	-	5	85	-	0.06
537	1190	30	415	-	0.07
544	3360	385	1615	-	0.19
545	1050	70	335	-	0.17
546	1540	50	450	-	0.10
547	-	5	50	-	0.09
570	-	55	165	-	0.25
571	-	20	175	-	0.10
572	1400	65	510	-	0.11
573	7280	155	560	-	0.22
574	490	50	280	-	0.15

Depth (ft)	Fe (ppm)	Pb (ppm)	Zn (ppm)	Ag (ppm)	Pb/(Pb+Zn)
587	-	90	150	-	0.38
588	2380	105	520	-	0.17
589	4340	135	485	-	0.22
590	6930	165	715	-	0.19
591	15330	345	1565	-	0.18
592	5530	890	4150	-	0.18
608	-	30	140	-	0.18
609	-	15	145	-	0.09
610	-	40	135	-	0.23
629	-	10	60	-	0.14
630	-	35	285	-	0.11
631	-	10	125	-	0.07
635	7070	630	2700	-	0.19
636	3640	590	1850	-	0.24
637	-	60	365	-	0.14
647	-	25	190	-	0.12
648	-	65	310	-	0.17
649	-	255	1645	-	0.13
650	-	4800	1750	-	0.73
651	-	945	900	-	0.51
652	-	80	290	-	0.22
653	-	70	1055	-	0.06
657	7210	55	1095	-	0.05
658	3710	4950	7150	0.2	0.41
659	5880	160	490	-	0.25
660	3780	645	1080	-	0.37
661	2240	85	1080	-	0.07
662	2030	275	335	-	0.45
663	18130	505	1700	-	0.23
664	-	190	565	-	0.25
665	-	65	180	-	0.27
666	-	60	490	-	0.11
667	-	20	85	-	0.19
668	-	35	155	-	0.18
669	-	55	150	-	0.27
670	-	55	215	-	0.20
671	-	220	1850	-	0.11
672	-	120	375	-	0.24
673	-	195	490	-	0.28
676	2520	70	355	-	0.16
677	5670	845	2700	-	0.24
678	6510	175	1280	-	0.12
679	4060	1295	1000	-	0.56
680	7770	2750	7400	-	0.27
681	4970	225	1215	-	0.16
682	3990	150	545	-	0.22

Appendix Ic. (Cont.)

Depth (ft)	Fe (ppm)	Pb (ppm)	Zn (ppm)	Ag (ppm)	Pb/(Pb+Zn)
683	19740	6150	25000	-	0.20
684	10500	885	1645	0.2	0.35
688	19880	3150	6250	-	0.34
689	8820	510	2750	-	0.16
690	23170	990	8100	-	0.11
691	19670	1705	5650	-	0.23
692	33880	720	5500	-	0.12
693	22400	2600	13000	0.2	0.17
694	55300	3350	8550	0.4	0.28
695	77000	2800	9750	0.6	0.22
696	60480	1310	7150	0.4	0.15
697	69650	1515	8950	1.0	0.14
698	62090	1365	4550	0.5	0.23
699	51590	1730	4600	0.6	0.27
700	59500	4650	10000	0.5	0.32
701	61040	5900	15000	1.2	0.28
702	49910	7250	11000	0.4	0.40
703	51030	5250	14000	0.3	0.27
704	43680	7650	27000	0.3	0.22
705	61390	5000	13000	0.2	0.28
707	21910	2600	13000	-	0.17
708	26950	3200	10000	-	0.24
709	33880	1175	6150	-	0.16
710	22540	1460	5700	-	0.20
711	29820	770	9550	-	0.07
712	61740	3950	21000	0.2	0.16
713	40390	1695	9100	-	0.16
714	70000	4300	15000	0.2	0.22
715	28280	1490	6120	-	0.20
716	-	105	390	-	0.21
717	-	220	300	-	0.42
718	-	40	255	-	0.14
719	-	55	240	-	0.19
720	-	55	875	-	0.06
721	-	65	575	-	0.10
722	-	120	695	-	0.15
723	6160	110	1055	-	0.09
724	2170	75	525	-	0.13
725	2030	30	220	-	0.12
727	7210	1005	5650	-	0.15
728	16450	795	5600	-	0.12
730	-	70	465	-	0.13
731	-	190	585	-	0.25
732	-	65	460	-	0.12
733	-	140	2750	-	0.05
737	-	55	150	-	0.27
738	-	80	380	-	0.17
739	-	135	540	-	0.20
742	-	125	355	-	0.26
743	-	45	195	-	0.19
744	7350	715	2400	-	0.23
745	78000	14000	11000	0.2	0.56
746	154000	47000	34000	0.5	0.58
747	58000	26000	14000	0.4	0.65
748	2870	390	595	-	0.40
752	5880	190	1260	-	0.13
753	11620	440	765	-	0.37
754	41440	3850	5650	-	0.41
755	29610	525	545	-	0.49
756	3290	135	345	-	0.28
757	10000	175	765	0.4	0.19
758	78000	2350	5800	0.5	0.29
759	6000	115	1750	0.2	0.06
760	5040	1580	7750	-	0.17
762	-	220	720	0.2	0.23
763	-	565	960	-	0.37
764	-	90	725	-	0.11
767	-	120	255	-	0.32
768	2450	35	2400	-	0.01
769	3570	85	190	-	0.31
770	4200	45	1215	-	0.04
771	4760	105	485	-	0.18
772	3080	60	7000	-	0.01
773	-	60	680	-	0.08
782	-	75	575	-	0.12
783	-	50	180	-	0.22
784	-	5	35	-	0.13
787	-	40	165	-	0.20
788	-	440	535	-	0.45
789	-	1380	2150	-	0.39
790	-	275	405	-	0.40
794	-	20	45	-	0.31
795	-	65	105	-	0.38
796	10500	80	540	-	0.13
797	11060	45	120	-	0.27
798	2170	40	510	-	0.07
799	7700	710	725	-	0.49
800	3500	165	475	-	0.26
801	1330	105	850	-	0.11
802	2100	175	270	-	0.39
803	770	30	60	-	0.33
804	2100	45	30	-	0.60

Appendix I c. (Cont.)

Depth (ft)	Fe (ppm)	Pb (ppm)	Zn (ppm)	Ag (ppm)	Pb/(Pb+Zn)
805	12110	1090	810	-	0.57
806	10780	215	1165	-	0.16
807	-	130	60	-	0.68
811	-	45	425	-	0.10
812	8610	100	1745	-	0.05
813	2730	1385	555	-	0.71
814	2870	85	4700	-	0.02
815	1400	115	210	-	0.35
816	3080	1065	9750	0.2	0.10
817	-	60	520	-	0.10
822	-	75	85	-	0.47
823	15400	14000	34000	0.2	0.29
824	-	245	875	-	0.22
825	-	95	165	-	0.37
838	-	205	205	-	0.50
839	-	65	1850	-	0.03
840	-	280	490	-	0.36
854	4060	185	1060	-	0.15
855	3500	215	1070	-	0.17
856	1820	180	660	-	0.21
857	7350	1430	1595	0.2	0.47
858	14700	1520	10000	0.2	0.13
859	32900	575	9850	-	0.06
860	35280	785	8950	-	0.08
861	10080	170	2900	-	0.06
862	7420	180	1535	-	0.10
863	15820	610	3150	-	0.16
864	28910	42	2350	-	0.02
865	-	60	445	-	0.12
873	3010	620	1005	-	0.38
874	55790	625	6500	-	0.09
875	5180	65	210	-	0.24
876	49070	460	4050	-	0.10
877	59150	875	2650	-	0.25
878	54040	510	1415	-	0.26
879	22470	180	1850	-	0.09
880	2730	35	325	-	0.10
881	1820	10	210	-	0.05
882	5250	75	1670	-	0.04
883	43260	470	7300	-	0.06
884	11690	100	2100	-	0.05
885	10780	475	2150	-	0.18
886	29540	265	8800	-	0.03
887	4970	275	1275	-	0.18
892	3500	1035	825	-	0.56
893	6440	520	1900	-	0.21
894	6650	180	395	-	0.31
895	2800	565	1625	-	0.26
899	11130	1105	835	-	0.57
900	15000	695	8800	0.2	0.07
901	13000	1255	15000	0.2	0.08
902	33000	6500	13000	0.2	0.33
903	15000	1130	55000	0.2	0.02
904	20650	800	2750	-	0.23
905	25900	325	3900	-	0.08
906	5950	225	4350	-	0.05
907	3570	170	965	-	0.15
908	3640	1490	6050	-	0.20
909	4830	765	360	-	0.68
910	11060	3550	13000	0.2	0.21
911	3220	170	710	-	0.19
912	4900	305	1275	-	0.19
913	5040	320	5650	-	0.05
914	5950	100	1355	-	0.07
915	6580	220	2650	-	0.08
916	1960	445	5800	-	0.07
917	4060	70	500	-	0.12
918	3640	135	255	-	0.35
919	5110	10	960	-	0.01
920	3570	30	865	-	0.03
921	1190	115	2000	-	0.05
922	1680	55	1165	-	0.05
923	1960	915	16000	0.2	0.05
924	9240	1535	13000	0.2	0.11
925	3430	340	2000	-	0.15
926	3150	720	915	-	0.44
927	2170	520	1210	-	0.30
928	4970	85	5050	-	0.02
929	5530	70	4950	-	0.01
930	-	115	335	-	0.26
931	-	115	165	-	0.41
932	-	15	160	-	0.09
933	3920	25	1100	-	0.02
934	123200	755	88000	8.9	0.01
935	2170	325	685	0.2	0.32
936	-	50	500	0.2	0.09
937	-	50	140	0.2	0.26
938	-	75	1590	0.2	0.05
939	-	5	95	0.2	0.05
940	9590	45	1700	-	0.03
941	5460	105	1750	-	0.06
942	3080	20	675	-	0.03

Appendix I c. (Cont.)

Depth (ft)	Fe (ppm)	Pb (ppm)	Zn (ppm)	Ag (ppm)	Pb/(Pb+Zn)
943	3080	15	145	-	0.09
944	3780	65	1685	-	0.04
945	-	20	310	-	0.06
946	-	15	465	-	0.03
948	-	25	190	-	0.12
949	-	5	170	-	0.03
950	-	5	105	-	0.05
951	-	35	100	-	0.26
952	-	40	315	-	0.11
953	-	5	105	-	0.05
955	-	20	280	-	0.07
956	-	5	70	-	0.07
957	-	5	55	-	0.08
958	-	20	235	-	0.08
959	-	5	120	-	0.04
960	-	5	155	-	0.03
963	-	5	345	-	0.01
964	14560	90	975	-	0.08
965	2170	55	455	-	0.11
966	1960	10	80	-	0.11
967	1820	5	1415	-	0.00
968	-	10	95	-	0.10
969	-	105	455	-	0.19
970	-	105	240	-	0.30
973	-	130	200	-	0.39
974	-	925	2050	-	0.31
975	-	275	320	-	0.46
982	-	15	135	-	0.10
983	5250	1020	320	-	0.76
984	149000	3350	25000	0.2	0.12
985	229000	2450	28000	0.2	0.08
986	207000	2650	8000	0.2	0.25
987	12000	1110	6050	0.2	0.16
988	137000	780	9950	0.2	0.07
989	16000	520	2050	0.2	0.20
990	229000	87000	120000	0.2	0.42
991	68000	4000	12000	0.2	0.25
992	27000	1420	13000	0.2	0.10
993	3640	615	1130	-	0.35
994	2870	560	1035	-	0.35
995	5180	365	3700	-	0.09
996	7070	435	1800	-	0.19
997	13790	840	3100	-	0.21
998	9170	2300	3750	0.2	0.38
999	3010	530	585	-	0.48
1000	5740	1125	1100	-	0.51
1001	3500	430	1695	-	0.20
1002	1470	75	155	-	0.33
1003	980	210	125	-	0.63
1004	6020	3150	3800	-	0.45
1005	24000	15000	38000	-	0.28
1006	53000	2150	11000	-	0.16
1007	117000	41000	16000	-	0.72
1008	15000	11000	855	-	0.93
1009	11000	11000	140	-	0.99
1010	11830	5950	395	-	0.94
1011	35070	3550	245	-	0.94
1012	88900	1160	410	-	0.74
1013	5530	1470	230	-	0.86
1014	3640	50	25	-	0.67
1015	3500	325	290	-	0.53
1016	8820	1090	995	-	0.52
1017	10010	310	205	-	0.60
1018	18270	1185	1485	-	0.44
1019	18690	4650	550	-	0.89
1020	3920	1950	890	-	0.69
1021	4340	1150	610	-	0.65
1022	3150	175	80	-	0.69
1023	4200	3300	295	-	0.92
1024	4200	110	80	-	0.58
1025	5040	125	45	-	0.74
1026	9520	745	1005	-	0.43
1027	5320	365	535	-	0.41
1028	27300	1530	23000	0.2	0.06
1029	20020	460	1715	-	0.21
1030	11000	11000	6400	-	0.63
1031	44000	4050	1850	-	0.69
1032	-	1230	165	-	0.88
1033	-	1090	1080	-	0.50
1034	-	235	195	-	0.55
1035	-	170	400	-	0.30
1036	-	70	65	-	0.52
1037	-	45	5	-	0.90
1038	-	165	175	-	0.49
1043	3640	645	195	-	0.77
1044	1750	3950	1285	0.2	0.75
1045	4270	16000	265	0.2	0.98
1046	1680	2100	1285	-	0.62

- represents intervals where core was not assayed for that element

Appendix I d. Metal assay data, HH2.

Depth (ft)	Fe (ppm)	Pb (ppm)	Zn (ppm)	Ag (ppm)	Cd (ppm)	Pb/(Pb+Zn)
403	24400	1710	2700	-	-	0.39
423	26700	655	2200	-	-	0.23
463	27600	1335	3650	-	-	0.27
532	20000	200	2250	0.9	-	0.08
533	70000	12000	25000	3.1	-	0.32
534	39400	1020	2800	0.7	-	0.27
535	43300	1675	5650	1.7	-	0.23
551	32700	1040	3600	-	-	0.22
552	79800	4900	5400	-	-	0.48
553	35300	205	505	-	-	0.29
566	161000	4800	14000	1.1	-	0.26
567	20400	1200	2600	1.1	-	0.32
611	70000	610	2900	0.9	-	0.17
612	65900	2550	11000	1.3	-	0.19
613	60300	1610	5250	0.7	-	0.24
614	105700	3800	7450	0.7	-	0.34
615	74200	835	15000	0.5	-	0.05
616	31400	740	3150	-	-	0.19
617	16300	165	855	-	-	0.16
618	61300	715	4350	-	-	0.14
619	25600	1125	3550	-	-	0.24
620	22700	175	1800	-	-	0.09
621	23100	320	1165	-	-	0.22
622	40200	725	2800	-	-	0.21
623	21100	235	720	-	-	0.25
624	31900	355	1670	-	-	0.18
625	39300	5300	4900	1.6	-	0.52
626	72800	2450	9100	1.3	-	0.21
627	77000	3200	9700	2.1	-	0.25
628	102900	1260	4800	2.3	-	0.21
629	71400	5650	5150	1.4	-	0.52
630	63600	1190	3100	2.1	-	0.28
631	72800	1310	5700	2.2	-	0.19
632	5600	5600	14000	1.8	-	0.29
633	64100	730	4850	-	-	0.13
634	108500	1290	6000	-	-	0.18
635	25200	705	6150	-	-	0.10
636	30800	2950	6400	-	-	0.32
637	18000	525	1215	-	-	0.30
638	60400	985	5550	-	-	0.15
639	16200	825	1545	-	-	0.35
644	15000	185	525	-	-	0.26
645	9200	325	1265	-	-	0.20
646	54300	8850	32000	2.8	-	0.22
647	97300	12000	26000	6.1	-	0.32
648	63600	14000	24000	5.2	-	0.37
649	68900	7950	13000	4.6	-	0.38
650	83300	8750	15000	4.7	-	0.37
651	16000	765	2350	2.1	-	0.25
652	13700	590	1190	1.8	-	0.33
653	18500	2800	5300	3.0	-	0.35
659	4100	5850	1520	1.5	-	0.79
660	9600	130	3350	1.2	-	0.04
661	6800	105	820	1.4	-	0.11
662	7300	335	1335	1.7	-	0.20
671	6800	200	1455	1.6	6.0	0.12
672	36000	1465	3900	6.7	13.0	0.27
673	68000	2600	6850	6.0	21.0	0.28
674	37000	1340	3800	4.2	13.0	0.26
675	18000	520	2250	3.5	11.0	0.19
676	32000	765	3800	2.9	14.0	0.17
677	32000	765	3800	2.9	14.0	0.17
678	35000	905	4250	11.0	16.0	0.18
679	10000	115	495	2.6	4.0	0.19
680	10000	115	495	2.6	4.0	0.19
681	93000	6300	12000	3.8	37.0	0.34
682	110000	4700	18000	2.4	58.0	0.21
683	110000	6050	26000	2.1	80.0	0.19
684	23000	555	1525	1.1	9.0	0.27
685	51000	4600	8300	2.6	31.0	0.36
686	69000	3200	8750	10.0	36.0	0.27
687	86000	2600	8900	5.7	33.0	0.23
688	78000	1425	9250	12.0	28.0	0.13
689	120000	2050	8700	12.0	24.0	0.19
690	83000	2350	10000	15.0	31.0	0.19
691	120000	2400	12000	36.0	39.0	0.17
692	120000	1655	10000	29.0	25.0	0.14
693	140000	5000	21000	19.0	59.0	0.19
694	110000	6250	32000	1.1	112.0	0.16
695	100000	6350	17000	13.0	76.0	0.27

Appendix I d. (Cont.)

Depth (ft)	Fe (ppm)	Pb (ppm)	Zn (ppm)	Ag (ppm)	Cd (ppm)	Pb/(Pb+Zn)
696	120000	8050	27000	21.0	96.0	0.23
697	180000	18000	47000	20.0	208.0	0.28
698	92000	6200	21000	25.0	84.0	0.23
699	96000	1640	12000	10.0	38.0	0.12
700	110000	1780	10000	23.0	27.0	0.15
701	170000	7550	38000	19.0	100.0	0.17
702	89000	5650	16000	19.0	51.0	0.26
703	140000	5750	18000	13.0	54.0	0.24
704	78000	3150	8850	5.8	23.0	0.26
705	130000	2350	7250	31.0	23.0	0.25
706	230000	4300	14000	27.0	40.0	0.24
707	180000	10000	34000	16.0	144.0	0.23
708	180000	6550	26000	14.0	78.0	0.20
709	280000	16000	38000	9.4	128.0	0.30
710	100000	8100	24000	17.0	92.0	0.25
711	220000	7000	31000	7.6	94.0	0.18
712	140000	3650	15000	1.9	45.0	0.20
713	170000	9600	31000	3.6	98.0	0.24
714	83000	2600	11000	4.1	43.0	0.19
715	51000	780	2550	1.6	10.0	0.23
716	130000	22000	43000	9.8	176.0	0.34
717	200000	14000	57000	10.0	220.0	0.20
718	120000	9250	46000	17.0	164.0	0.17
719	120000	19000	66000	14.0	264.0	0.22
720	140000	15000	66000	8.0	240.0	0.19
721	180000	33000	47000	18.0	192.0	0.41
722	310000	16000	47000	7.5	172.0	0.25
723	260000	5600	21000	11.0	69.0	0.21
724	54000	1575	18000	7.4	30.0	0.08
725	11000	2900	13000	2.2	5.0	0.18
726	19000	270	1345	4.0	5.0	0.17
727	8100	175	995	5.9	4.0	0.15
740	50000	2400	16000	16.0	-	0.13
743	22700	1205	2600	11.0	-	0.32
752	30600	155	1355	12.0	-	0.10
753	49700	1130	4200	21.0	-	0.21
757	22400	90	450	17.0	-	0.17
761	28400	225	2000	12.0	-	0.10
763	6000	445	4850	10.0	-	0.08
775	6400	75	710	6.6	-	0.10
776	63000	14000	15000	16.0	-	0.48
777	18100	360	6400	4.3	-	0.05
786	7000	430	8400	-	-	0.05
798	84700	5500	36000	0.5	-	0.13
799	9100	55	690	0.2	-	0.07
800	13700	1330	500	0.2	-	0.73
816	4800	205	1950	0.5	-	0.10
843	13200	125	2100	0.2	-	0.06
853	10500	90	1100	2.8	-	0.08
857	12000	5	295	20.0	-	0.02
867	15000	315	15000	177.0	-	0.02
868		0	0	114.0	-	0.00
869	12000	25	1950	58.0	-	0.01
870	12000	120	5100	169.0	-	0.02
871	-	-	-	79.0	-	-
872	-	-	-	13.0	-	-
873	-	-	-	31.0	-	-
874	-	-	-	31.0	-	-
875	-	-	-	0.0	-	-
876	-	-	-	32.0	-	-
877	-	-	-	14.0	-	-
878	5400	2700	5200	173.0	-	0.34
879	-	-	-	30.0	-	-
880	-	-	-	8.0	-	-
881	-	-	-	24.0	-	-
882	-	-	-	27.0	-	-
883	-	-	-	28.0	-	-
884	-	-	-	65.0	-	-
906	-	-	-	12.0	-	-
907	-	-	-	3.6	-	-
915	-	-	-	41.0	-	-
916	-	-	-	19.0	-	-
934	-	-	-	8.3	-	-

- represents intervals where that element was not assayed

Lead and Zn mineralization is controlled by gently dipping semi-continuous sulfide laminae in anhydrite cap rock, and by vuggy calcite breccias in the calcite cap rock. Anhydrite cap rock is slightly more mineralized than calcite cap rock, with the calcite breccias containing higher (but less extensive) mineralization than the anhydrite (Wessel, 1983). Tonnage and foot percent estimates have been calculated for anhydrite (7.7 mt) and calcite (5.3 mt) using cut-off concentrations of 2.5 % Pb+Zn and 4.0 % Pb+Zn, respectively (Appendices Ie and If). Foot percent estimates represent the sum of all assayed intervals that are above the cut-off percent (e.g., 5 ft of 5 % Pb+Zn = 25 ft % Pb+Zn) (Appendices If). Approximately 68 % of the estimated 13 mt of ore reserves (averaging 3.1 % Pb+Zn) reside within the southern perimeter of the dome (Wessel, 1983). This area of relatively intense mineralization was defined in the later stages of Marathon's drilling program. Additional ore reserves are likely to exist because areas of influence used in tonnage calculations do not represent all of the dome perimeter. The eastern portion of the dome lies outside of Marathon's holdings and may prove to be extensively mineralized. Also, Ag and barite assay data were obtained late in the study, and were not considered during ore reserve calculations (Wessel, 1983). Tonnage estimates and average ore grades were calculated using standard ore reserve techniques. Polygons that define the areas of influence were constructed using perpendicular bisectors of lines that connect adjacent core holes. The size and geometry of the Hockley Dome mineral deposit were evaluated in this manner.

Appendix I e. Tonnage estimates from anhydrite and calcite cap rock.

Drill Holes	Anhydrite (2.5% Pb+Zn)	Calcite (4.0% Pb+Zn)
H-3	495,938	
H-4	556,289	
H-5		358,594
HA-1a	533,203	
HB-1	154,688	
HB-2	332,719	
HB-3	328,125	
HB-5	76,172	
HC-4		337,500
HD-4	112,500	
HD-5	146,250	
HE-2		1,333,125
HF-2		348,750
HH-1	48,516	113,203
HH-2	28,800	126,720
HH-2a		50,344
HH-3	173,672	
HI-2	480,938	
HJ-1	698,625	
HJ-2	129,375	215,625
HK-1	139,219	
HK-3	806,250	
HL-2		1,110,000
HN-2	127,969	566,719
HQ-1	420,000	
HR-1	480,000	
HT-1	300,000	
HU-1	124,688	
HU-2	159,375	
HW-2		564,047
HW-3	588,656	191,953
HX-1	225,000	
HZ-1	93,359	

Total Ore Reserves: Anhydrite 7,760,326 tons

: Calcite 5,316,580 tons

Data originally in Wessel, 1983

Appendix I f. Drill hole concentrations: foot percent Pb and Zn.

Drill Hole	Pb (ft%)	Zn (ft%)	Pb+Zn (ft%)
HA-1a	50.05	58.45	108.50
HB-1	43.29	129.81	173.10
HB-2	49.76	146.44	196.20
HB-3	54.90	132.31	187.21
HB-4	18.62	72.46	91.08
HB-5	31.62	63.10	94.72
HC-1	17.49	28.81	46.30
HC-2	1.45	3.70	5.15
HC-3	5.99	10.21	16.20
HC-4	31.71	106.09	137.80
HD-1	18.50	31.22	49.72
HD-2a	22.92	43.69	66.61
HD-3	11.64	20.42	32.06
HD-4	21.80	45.23	67.03
HD-5	26.25	48.47	74.72
HE-1	6.99	5.99	12.98
HE-2	119.50	245.43	364.93
HE-3	22.64	46.36	69.00
HF-1	2.49	3.77	6.26
HF-2	30.70	137.98	168.68
HF-4	1.13	1.86	2.99
HG-1	49.09	88.83	137.92
HH-1	40.90	157.85	198.75
HH-2	50.32	158.90	209.22
HH-3	19.97	62.56	82.53
HI-1	18.64	63.57	82.21
HI-2	54.10	152.25	206.35
HJ-1	38.50	97.74	136.24
HJ-2	44.50	120.44	164.94
HK-1	27.74	104.96	132.70
HK-2	14.51	44.63	59.14
HK-3	47.37	95.27	142.64
HL-1	8.48	27.39	35.87
HL-2	35.48	137.22	172.70
HN-1	13.55	51.66	65.21
HN-2	60.01	171.99	232.00
HO-1	1.30	5.32	6.62
HP-1	1.10	3.52	4.62
HQ-1	15.70	36.71	52.41
HQ-2	5.36	9.15	14.51
HR-1	40.55	48.93	89.48
HS-1	13.16	18.21	31.37
HT-1	16.59	68.93	85.52
HU-1	31.12	82.19	113.31
HU-2	43.19	114.27	157.46
HW-1	11.83	63.73	75.56
HW-2	78.11	222.92	301.03
HW-3	74.32	188.13	262.45
HX-1	34.69	74.25	108.94
HY-1	22.60	108.74	131.34
HZ-1	31.39	119.15	150.54

Data originally in Wessel, 1983

Appendix II

PHREEQE and PHREPITZ

PHREEQE is a Fortran IV computer program designed to model geochemical reactions. Based on an ion pairing aqueous model, PHREEQE can calculate pH, mass transfer as a function of reaction progress, and composition of solutions in equilibrium with multiple phases. The aqueous model, including the elements, aqueous species, and mineral phases, is exterior to the computer code and is completely user definable (Parkhurst et al., 1982). PHREEQE was used to calculate the stability of anhydrite and gypsum under a variety of cap rock conditions. These conditions (i.e., temperature, fluid salinity, and pCO_2 saturation) were altered slightly with each calculation to measure their effects on saturation states of calcium sulfate phases. PHREPITZ is a modified PHREEQE program that includes pitzer equations (Parkhurst et al., 1987). These equations are useful when calculating solution/mineral equilibria under highly saline conditions ($\geq$ 100,000 ppm TDS). Because cap rock solutions are extremely saline (ionic strength ≥ 0.1) results from mixed solution equilibria modeled with PHREEQE are questionable. Therefore, these solutions were modeled again using PHREPITZ. PHREPITZ was operated by Rachel Eustice in my absence.

Appendix III

Sulfate Preparation for $\delta^{34}S$ Analysis

Anhydrite analyzed for $\delta^{34}S$ was sampled from core hole HH3 at intervals of approximately 100 ft. Separates were carefully prepared to minimize contamination by gypsum. Therefore, samples were examined petrographically under transmitted light to selectively avoid zones that contained gypsum. Invariably, trace amounts of gypsum (< 2 %) were included. Sample material was then lightly disaggregated in a motar and

pestle and sieved (medium to coarse size fraction retained for digestion). Aqueous sulfate was produced by digesting anhydrite (100 to 200 mg) in a solution (200 ml of distilled water) consisting of 13 wt % NaCl brine and 5 % HCl acid. The filtered (i.e., millipore) water sample is acidified with 5 ml of 0.5 N HCl and boiled for 10 minutes. The solution is removed from heat and 20 ml of 0.5 M $BaCl_2$ added. Precipitation of $BaSO_4$ occurred immediately and began to settle out of solution. The solution is then filtered through a millipore filter system and the $BaSO_4$ slurry flushed with distilled water several times. The filter paper with slurry is placed in a drying oven (40 to 50°C) for roughly two hours. When dry, $BaSO_4$ is removed from the filter paper, weighed (yields 150 to 300 mg), and placed in vials.

Data are presented as the per mil deviation ($\delta^{34}S$) of the isotopic ratio $^{34}S/^{32}S$ from the ratio of the Cañon Diablo Triolite standard. All $BaSO_4$ samples were analyzed at the United States Geological Survey, National Headquarters, Reston, Virginia, utilizing the sulfur isotope facilities of W.C. Shanks III. These samples were analyzed on a Finigan MAT 251 gas mass spectrometer equipped with multicup collectors. Reported $\delta^{34}S$ values from this instrument are accurate to $\pm$ 0.1 ‰. Replicate analyses of standards indicate that precision is less than this value with the maximum being 0.1 ‰

Appendix IV

Scanning Electron Microscope

Digested residues from supracaprock sediments, anhydrite cap rock and salt stock were examined by a JEOL JSM-T330A scanning electron microscope equipped with x-ray analyzing capabilities. Loose grains of sulfides (i.e., sphalerite, pyrite, and galena), quartz, and siderite were concentrated by digesting anhydrite cap rock

samples in a 13 wt % NaCl brine. Pyrite grains from supracaprock sediments were concentrated by wet sieving rotary sample material to remove the clay size fraction. The coarse residue consisted of pyrite and sand grains. Salt stock impurities of quartz, anhydrite, and siderite were easily separated by sample dissolution in tap water. All separates were examined under an incident light binocular microscope and hand picked from the prepared residues.

Appendix V

Microprobe Analysis

The trace element chemistry of base metal sulfides can be determined from microprobe analysis of sphalerite, pyrite, and galena. Polished sections prepared from core samples were examined optically in transmitted, reflected, and ultraviolet light (Leitz Ploemopak fluorescence illuminator) to identify the mineralogy and textures (i.e., the spatial and temporal relationships of the metallic sulfides) necessary in guiding microprobe analyses. Analyses were performed on a computer controlled fully automated JEOL Superprobe JAX-733. "TASK" a FLEXTRAN program developed by Tracor Northern was designed to provide computer automation of data acquisition and data reduction. Operating conditions for the electron microprobe were determined by tedious experimentation with spot size, sample current, accelerating voltage, and detector count times on peak. Typically, beam size was adjusted to the smallest possible diameter (approximately 1 micron) to minimize matrix effects from surrounding sulfides. Although matrix effects may extend approximately 10 microns even under the finest focused electron beam diameter. To enhance the peak to background ratios (a crucial requirement when analyzing for trace amounts of Ag and

Cd) elevated accelerating voltage (25 kv) and sample current (30 nanoamps) were used. Without considering the above adjustments or increasing the detector count time (120 seconds) routine wavelength analysis will not yield a sensitivity greater than approximately 500 ppm for most elements (Cabri et al., 1984). However, microprobe detectability limits under these conditions approach 200 ppm at the 99 % confidence level (equation in LeMaitee, 1982). In most cases, trace element metals (i.e., Ag and Cd) were in such abnormally large concentrations that problems with detectability limits were rarely encountered. Typical examples of wavelength scans for Ag (0.75 wt %, Appendix Va) and Cd (0.23 wt %, Appendix Vb) indicate that peaks are well defined and that peak/background ratios are satisfactory to yield meaningful data.

The JEOL electron microprobe used in this study was equipped with four wavelength dispersive spectrometers (WDS) and an energy dispersive spectrometer (EDS) system. The microprobe spectrometers were calibrated against sphalerite grains of near stochiometric composition and homogeneity (Appendix Vc), Mn-glass, and four metal standards. Sphalerite was used for calibrating Zn and S, Mn-glass for Mn, and Ag, Cd, Fe, and Pb were calibrated against their pure elements (see Table below).

Element Table

Element	Analytical Crystal	Peak Position	Peak Type	Correction Factor	Standard
Ag	PET	132.8	L_{alpha}	1.000	Ag metal
Cd	PET	126.5	L_{alpha}	1.000	Cd metal
Fe	LIF	134.7	K_{alpha}	1.000	Fe metal
Pb	PET	169.6	M_{alpha}	1.000	Pb metal
S	TAP	116.7	K_{alpha}	0.205	Sphalerite
Zn	LIF	99.7	K_{alpha}	0.636	Sphalerite
Mn	PET	66.9	K_{alpha}	0.687	Mn-glass

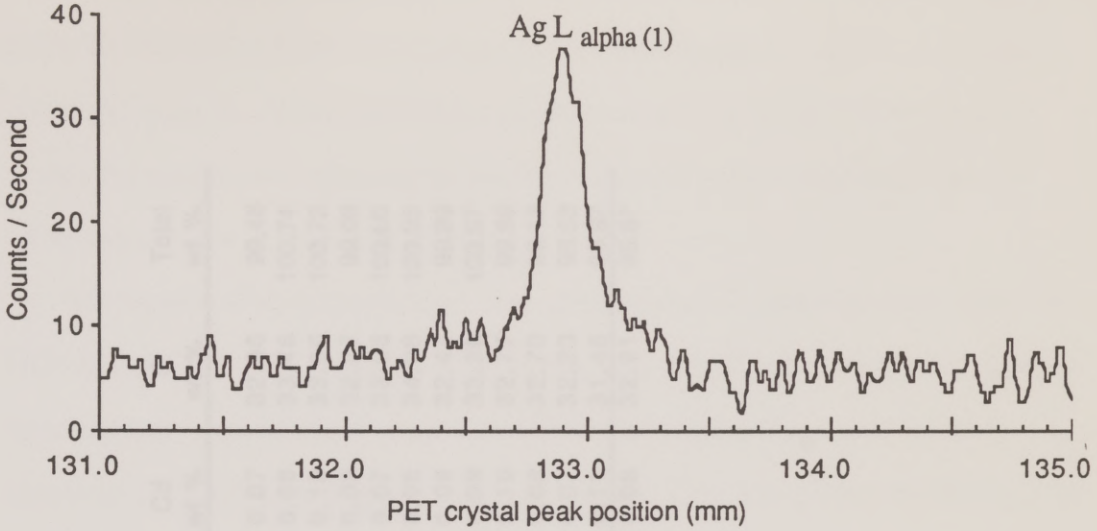

Appendix Va. Wevelength dispersive scan of Ag in sphalerite.

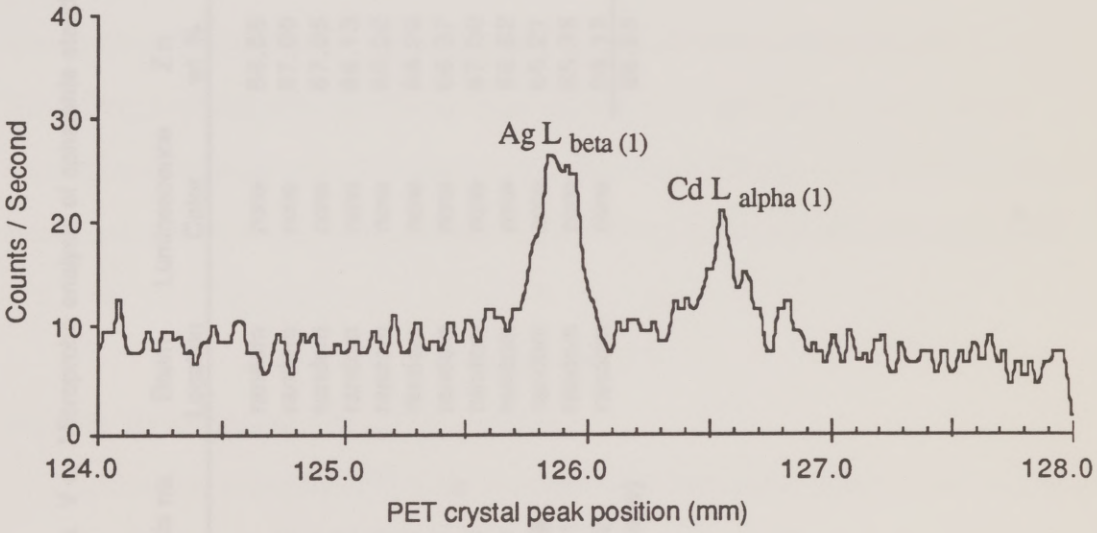

Appendix Vb. Wevelength dispersive scan of Ag and Cd in sphalerite.

Appendix V c. Microprobe analysis of sphalerite standard.

Analysis no.	Beam Location	Luminescence Color	Zn wt %	Fe wt %	Ag wt %	Cd wt %	S wt %	Total wt %
1	random	none	66.88	0.20	0.01	0.07	32.30	99.46
2	random	none	67.00	0.20	0.00	0.08	33.46	100.74
3	random	none	67.05	0.21	0.01	0.10	33.35	100.72
4	random	none	66.13	0.00	0.00	0.08	32.87	99.08
5	random	none	66.22	0.35	0.00	0.07	33.96	100.60
6	random	none	66.20	0.18	0.01	0.08	34.08	100.55
7	random	none	66.37	0.50	0.00	0.08	32.44	99.39
8	random	none	67.00	0.19	0.00	0.08	33.30	100.57
9	random	none	66.62	0.20	0.00	0.10	32.77	99.69
10	random	none	66.21	0.19	0.00	0.08	32.70	99.18
11	random	none	65.98	0.24	0.01	0.07	32.23	98.53
12	random	none	68.13	0.18	0.00	0.11	31.45	99.87
(average)			66.65	0.22	0.00	0.08	32.91	99.87

Primary (sphalerite) and secondary standards (pyrite) were routinely analyzed after every 20 analyses to detect any changes in peak measurements. Sulfide data were processed using the theoretical correction program ZAF, a FLEXTRAN program written for quantitative correction of matrix effects that reduces data to atomic and wt % values (Tracor Northern, 1986).

Microprobe analysis focused on four sphalerite-bearing intervals from HB3-990, HH1-932.5, HH2-404, and HH2-878 (Tables IVa, b, c, and d). Samples examined by microprobe consist of colloform Fe-sulfides that commonly contain internal sphalerite pods and interlaminated sphalerite bands. Microcrystalline sphalerite is also observed as a matrix cement within complexly intergrown sulfides. In general, element totals by microprobe analyses ranged between 95 and 100 wt %. In instances where total wt % fell below 90 the analyses were either repeated or discarded from the data set. Low wt % totals are attributed to sulfur volatilization under a concentrated beam and/or poorly polished sulfide surfaces. However, the purpose of this study was to identify and measure trace Ag and Cd concentrations within sphalerite. Therefore, analyses with low elemental totals were still considered useful. The cathodoluminescence color of sphalerite samples was observed while the samples were under electron excitation and later used to characterize Ag and Cd composition.

Appendix VI

Sulfide Preparation for $\delta^{34}S$ Analysis

Sulfides analyzed for $\delta^{34}S$ were obtained from the calcite, gypsum, and anhydrite zones at Hockley Dome. Sulfide samples from core hole HH2 were collected at intervals of 33 to 50 ft. Samples from an earlier $\delta^{34}S$ study (Kyle and Price, 1986) concentrated on textural and host rock types and were collected from core holes spaced

around the dome (Table VIII; Fig. 6.1). Sulfides were concentrated by digesting the calcium sulfate-rich samples in a 13 wt % NaCl brine and the calcite-rich samples in 10 % acetic acid.

Marcasite, pyrite, sphalerite, and galena were collected for $\delta^{34}S$ analysis. In hand samples and mineral separates, marcasite and pyrite commonly occur as fine-crystalline intergrowths and cannot be consistently distinguished; thus, mechanical separation is impractical. Fortunately, there is limited isotopic fractionation between marcasite and pyrite (M. Goldhaber, pers. commun., 1982). $\delta^{34}S$ analyses reported as "pyrite" represent samples of pyrite and/or marcasite (Table IX). Iron-sulfide separates were carefully prepared to reduce the effects of contamination by other mineral phases. This procedure involved hand picking of Fe sulfide grains (0.2 to 1.0 mm) from the prepared residue under an incident light binocular microscope. Separates were "scrubbed" with dilute (2N) HCl at 50°C in an ultrasonic bath to remove sphalerite, galena and calcium-sulfate minerals.

Iron-sulfides are the most abundant and easiest to cleanly separate from anhydrite and other sulfides. Therefore, pyrite was used to characterize the sulfur isotopic composition of sulfides with the assumption that these data could adequately represent the sulfur reservoir. Three distinct pyrite textural types (boxwork, colloform/ramose, and rhombic) were identified in the vertical profile study of HH2. To determine if the pyrite type influenced the $\delta^{34}S$ values, some sample intervals were analyzed for more than one textural type (Table IX).

Galena and sphalerite separates were considerably more difficult to prepare because they are commonly fine-crystalline and tightly intergrown. Minimizing

the effects of cross-contamination between galena and sphalerite is essential when evaluating $\Delta^{34}S_{sl\text{-}ga}$ values for equilibrium fractionation temperatures. Ultraclean samples are prepared by hand picking relatively clean separates (grain size ranges from 0.1 to 1.0 mm) of galena and sphalerite and chemically "scrubbing" them with concentrated (6N) HCl in an ultrasonic bath. This selectively dissolves sphalerite and galena impurities from their respective concentrate. Repeated chemical attack augmented by continued mechanical separation and hand picking resulted in the ultraclean samples (97 to 100 % pure) necessary for geothermometry studies. Some sphalerite samples required additional mechanical agitation in an ultrasonic bath. Separation was achieved by suspending microcrystalline sphalerite and collecting the supernatant; this appears to result in a sphalerite-rich powder. Purity was estimated by backlighting the supernatant and sphalerite powder under binocular magnification. Fine-grain opaque material is indicative of pyrite and galena.

Data are presented as the per mil deviation ($\delta^{34}S$) of the isotopic ratio $^{34}S/^{32}S$ from the ratio of the Cañon Diablo Triolite standard. Data reported in Kyle and Price (1986) were determined at McMaster University, Hamilton, Ontario, and are reported to be accurate to $\pm$ 0.25 ‰. $\delta^{34}S$ analyses for HH2 were run by Coastal Science Laboratories, Austin, Texas, and are reported by the laboratory to be accurate to $\pm$ 0.5 ‰. Replicate analyses on blind duplicates (H. Posey, unpubl. data) indicate that precision and intrasample variation are less than this value with the maximum being $\pm$ 0.2 ‰.

All subsequent sulfide samples were analyzed at the United States Geological Survey, National Headquarters, Reston, Virginia, utilizing the sulfur isotope facilities of W.C. Shanks III. Initial samples submitted for $\delta^{34}S$ measurement were analyzed on a Nuclide gas mass spectrometer. These samples consisted of two sphalerite-galena

pairs (HH2-404 and HH2-830) and a small number of pyrites (six) used to confirm isotopic trends observed in the upper anhydrite cap rock of HH2 (Table IX). The following suites of samples from HH2-652 (8 pyrites; Table Xa), HH3-837 (9 pyrites; Table Xb), and HB4 (5 pyrites; Table XI) were analyzed on a Finigan MAT 251 gas mass spectrometer equipped with multicup collectors. Reported $\delta^{34}S$ values from this instrument are accurate to ± 0.1 ‰. Replicate analyses of standards indicate that precision is less than this value with the maximum being 0.1 ‰.

Appendix VII

Sulfide Preparation for Common Pb Analysis

Common Pb separates were prepared by hand picking Fe-sulfide and galena grains (0.4 to 1.0 mm) from the prepared residue under an incident light binocular microscope. These separates were also "scrubbed" with dilute (2N) HCl at 50°C in an ultrasonic bath to remove any loose contaminant. Common Pb data presented in Kyle and Price (1986) were determined at the Department of Physics, University of Alberta, Edmonton, Alberta, and are reported to be accurate to the third decimal place (Table XII). Sample material (3 to 5 mg of galena) was dissolved in a $HCl\text{-}HNO_3$ solution and passed through an ion exchange column to separate Pb. Lead (0.5 µg) concentrate was loaded on a Re filament using the standard silica gel-phosphoric acid technique and analyzed on a Micromass MM30 mass spectrometer.

Galenas (7 samples) were analyzed for their Pb isotope composition. The uncertainty (at the one-sigma level) of the measured ratios were better than 0.3 % for $^{206}Pb/^{204}Pb$, $^{207}Pb/^{204}Pb$, and $^{208}Pb/^{204}Pb$, as determined by replicate analyses of NBS SRM981. The correction factor was close to 1.5 ‰ per mass unit difference. Data generated prior to 1981 were reexamined and found to contain a small analytical

bias due to imperfect calibration of the standard reference (NBS SRM981). However, measured precision for Hockley Dome galenas (1982) are consistent with more recent analyses.

In a more recent study common Pb analyses were determined specifically from core hole HH2 (Table XIII). This was done to generate a Pb isotope profile that could be directly compared with an existing sulfur isotope profile. Therefore, sulfide separates that were originally prepared for $\delta^{34}S$ analyses were later submitted for Pb isotope analyses. Samples were submitted in two batches to laboratories at The University of California at Santa Barbara and The University of Texas at Austin in 1987 and 1988, respectively. Both laboratories use similar Finigan MAT 261 solid source mass spectrometors equipped with multicup collectors and both report Pb isotope ratios to be accurate to the third decimal place. All ratios have been corrected for mass fractionation based on replicate analyses of NBS SRM981. Uncertainty (at the two-sigma level) of the measured ratio is 0.06 % for $^{206}Pb/^{204}Pb$, 0.09 % for $^{207}Pb/^{204}Pb$, and 0.12 % for $^{208}Pb/^{204}Pb$. Although the observed range in Pb isotope ratios is small it is not due to analytical error.

Samples analyzed at The University of California at Santa Barbara consisted of five galenas and one pyrite. Seven additional pyrite samples were later analyzed at The University of Texas to complete a Pb isotope profile of HH2. One sample (HH2-975a and b) was duplicated for comparison between both laboratories. A discrepancy between both analyses is apparent and can not be explained by analytical error. Isotopic variations can occur even within growth zones of single galena crystals (Loveless, 1975). This local variability may account for the compositional differences between replicate Pb analyses from HH2-975 (Table XIII). However, both samples (including a third analysis, HH2-975c, analyzed at The University of Texas) seem to

be well-behaved as members of the total group (i.e., 14 analyses from HH2). For example, the correlation coefficient (0.94) from least-squares fitting calculations suggests that the data are of good quality. However, because these data points plot as a linear array, it is possible that all of the dispersion is due to error in measurement of the small Pb^{204} signal. If this were the case, then a projection of the trend should pass through the origin (0, 0). The y-intercept value of the best-fit line is -6.2 ± 2.3. A Pb^{204} error is rejected because the y-intercept can not be zero even considering analytical error (L. Long, pers. commun., 1989).

REFERENCES CITED

Agee, Jr., W.N., 1988, Gulf Coast formation waters as potential source fluids for cap rock-hosted sulfide mineralization, Hockley Dome, Texas, *in* A. Weidie, B. Kohl, and R. Fillon, eds., Trans: Gulf Coast Assoc. Geol. Soc., v. 38, p. 561-568.

Anderson, G.M., 1973, The hydrothermal transport and deposition of galena and sphalerite near 100°C: Econ. Geol., v. 68, p. 480-492.

Barnes, V.F., 1968, Geologic Atlas of Texas, Houston Sheet (1:250,000): Texas Bur. Econ. Geol., Austin.

Barrett, T.J, and Anderson, G.M., 1988, The solubility of sphalerite and galena in 1 to 5 m NaCl solutions to 300°C: Geochem. et Cosmochimica Acta, v. 52, p. 813-820.

Bebout, D.G., Weis, B.R., Gregory, A.R., and Edwards, M.B., 1982, Wilcox sandstone reservoirs in the deep subsurface along the Texas Gulf Coast, their potential for production of geopressured geothermal energy: Texas Bur. Econ. Geol., Austin., Report of Investigations, no. 117, 125 p.

Bjorlykke, A. and Sangster, D.F., 1981, An overview of sandstone lead deposits and their relationship to red-bed copper and carbonate-hosted lead-zinc deposits, *in* B.J. Skinner, ed., Econ. Geol. 75th Anniversary Volume: The Econ. Geol. Pub. Co., El Paso, Texas, p. 179-213.

Buffler, R.T. and Sawyer, D.S., 1985, Distribution of oceanic versus transitional crust in deep Gulf of Mexico Basin; implications for early history: Abstract with program, AAPG annual convention, Bull. Am. Assoc. Petrol. Geol., v. 69, p. 241.

Busche, F.D., Reynolds, R.L., and Goldhaber, M.B., 1982, Fault leaked H_2S and the origin of south Texas uranium deposits: implications of sulfur isotopic studies: Soc. of Mining Engineers of AIME annual meeting, Dallas, Texas, Preprint, 13 p.

Cabri, L. J., Harris, D. C., and Nobiling, R., 1984, Trace silver analysis by proton microprobe in ore evaluation, *in* V. Kudryk, D.A. Corrigan, and W.W. Liang, eds., Precious Metals: Mining, Extraction, and Processing, Conferences and Proceedings: Metallurgical Society of AIME, p. 93-100.

Carpenter, A.B., Trout, M.L., and Pickett E.E., 1974, Preliminary report on the origin and chemical evolution of lead- and zinc-rich oil field brines in central Mississippi: Econ. Geol., v. 69, p. 1191-1206.

Carpenter, A.B. and Trout, M.L., 1978, Geochemistry of bromide-rich brines of the Dead Sea and southern Arkansas: Oklahoma Geological Survey Circular, no. 79, p. 78-88.

Cathles, L.M. and Smith, A.T., 1983, Thermal constraints on the formation of Mississippi valley-type lead-zinc deposits and their implications for episodic basin dewatering and deposit genesis: Econ. Geol., v. 78, p. 983-1002.

Claypool, G.E., Holser, W.T., Kaplan, I.C., Sakai, H., and Zak, I., 1980, The curves of sulfur and oxygen isotopes in marine sulfate and their mutual interpretation: Chem. Geol., v. 28, p. 199-260.

Deussen, A. and Lane, L.L., 1926, Hockley salt dome, Harris County, Texas, *in* R.C. Moore, ed., Geology of Salt Dome Oil Fields: Am. Assoc. Petrol. Geol., p. 570-599.

Dix, O.R. and Jackson, M.P.A., 1982, Lithology, microstructures, fluid inclusions, and geochemistry of rock salt and of the cap rock contact in Oakwood Dome, East Texas: Significance for nuclear waste storage: Texas Bur. Econ. Geol., Austin., Report of Investigations, no. 120, 59 p.

Doe, B.R., 1970, Lead Isotopes: Springer-Verlag, Berlin, West Germany, 137 p.

Doe, B.R. and Stacey, J.S., 1974, The application of lead isotopes to the problems of ore genesis and ore prospect evaluation: A review: Econ. Geol., v. 69, p. 757-776.

Doe, B.R. and Zartman, R.E., 1979, Plumbotectonics, the Phanerozoic, *in* H.L. Barnes, ed., Geochemistry of Hydrothermal Ore Deposits (2nd Edition): John Wiley and Sons, New York, p. 22-70.

Ewing, T.E., 1986, Structural style of the Wilcox and Frio growth-fault trends in Texas: Constraints on Geopressured Reservoirs: Texas Bur. Econ. Geol., Austin., Report of Investigations, no. 154, 86 p.

Faure, G., 1986, Priciples of Isotope Geology (2nd Edition): John Wiley and Sons, New York, 464 p.

Feely, H.W., and Kulp, J.L., 1957, Origin of Gulf Coast salt dome caprock minerals: Bull. Am. Assoc. Petrol. Geol., v. 18, p. 212-225.

Fisher, W.L. and McGowen, J.H., 1967, Depositional systems in the Wilcox Group of Texas and their relationship to occurrence of oil and gas: Texas Bur. Econ. Geol., Austin., Geological Circular, no 67-4, 20 p.

Goldhaber, M.B., Reynolds, R.L., and Rye, R.O., 1978, Origin of a South Texas roll-type deposit: II. Sulfide petrography and sulfur isotope studies: Econ. Geol., v. 73, p. 1690-1705.

Goldhaber, M.B., Reynolds, R.L., and Rye, R.O., 1979, Formation and resulfidization of a south Texas roll-type uranium deposit: U.S. Geological Survey Open-File Report, no. 79-1651, 41 p.

Goldhaber, M.B., Reynolds, R.L., and Rye, R.O., 1983, Role of fluid mixing and fault-related sulfide in the origin of the Ray Point uranium district, South Texas: Econ. Geol., v. 78, p. 1043-1082.

Goldman, M.I., 1952, Deformation, metamorphism, and mineralization in gypsum-anhydrite cap rock, sulphur salt dome: Louisiana. Mem. Geol. Soc. Am., v. 50, 169 p.

Goni, J. and Remond, G., 1969, Localization and distribution of impurities in blend by cathodoluminescence: Mineralogical Magazine, v. 37, p. 153-155.

Gustafson, L.B. and Williams, N., 1981, Sediment-hosted stratiform deposits of copper, lead and zinc, *in* B.J. Skinner, ed., Econ. Geol. 75th Anniversary Volume: The Econ. Geol. Pub. Co., El Paso, Texas, p. 139-178.

Hagni, R. G., 1983, Minor elements in Mississippi Valley-type ore deposits, *in* W.C. Shanks, III, ed, Unconventional Mineral Deposits: The Metallurgical Society of AIME, p. 71-87.

Halbouty, M.F., 1979, Salt domes, Gulf region, United States and Mexico (2nd edition): Gulf Publishing Co., Houston, Texas, 561 p.

Halland, H.D., and Mallinin, S.D., 1979, Solubilities of ore minerals, *in* H.L. Barnes, ed., Geochemistry of Hydrothermal Ore Deposits (2nd Edition): John Wiley and Sons, New York, p. 404-460.

Hallager, W.S., 1984, Geologic summary of Hockley Dome, Texas: Unpublished project report, Chevron Oil, 35 p.

Hamlin, H.S., 1986, Texas Coastal salt domes: stratigraphic and structural interrelationships, *in* S. Seni and R. Kyle, eds., Comparison of cap rocks, mineral resources, and surface features of salt domes in the Houston diapir province: Geol. Soc. of Amer. National Meeting, San Antonio, Texas, p. 27 -42.

Hanna, M.A, and Wolf, A.G., 1934, Texas and Louisiana salt-dome cap rock minerals: Bull. Am. Assoc. Petrol. Geol., v. 18, p. 212-225.

Hanor, J.S., and Workman, A.L., 1988, Distribution of dissolved volatile fatty acids in some Louisiana oil field brines: Appl. Geochem., v. 1, p. 37-46.

Jackson, M.P.A. and Galloway, W., 1984, Structural and depositional styles of Gulf Coast Tertiary continental margins; applications to hydrocarbon exploration: Am. Assoc. Petrol. Geol. continuing education course note series, no. 25, 226 p.

Jackson, M.P.A. and Seni, S.J., 1983, Geometry and evolution of salt structures in a marginal rift basin of the Gulf of Mexico, East Texas: Geology, v. 11, p. 131-135.

Kharaka, Y.K. Callender, E., and Carothers, W.W., 1977, Geochemistry of geopressured geothermal waters from the Texas Gulf Coast, *in* J. Meriwether, ed., Proceedings, third United States Gulf Coastal geopressured-geothermal energy conference: University of Southwestern Louisiana, Lafayette, p. 121-165.

Kharaka, Y.K., Michael, S.L., and Wright, V.A., 1980, Geochemistry of formation waters from Pleasant Bayou no. 2 well and adjacent areas in coastal Texas, *in* M.H. Dorfman and W.L. Fisher, eds., Proceedings, fourth United States Gulf Coastal geopressured-geothermal energy conference: University of Texas, Austin, p. 168-198.

Kharaka, Y.K., Maest, A.S., Carothers, W.W., Law, L.M., Lamothe, P.J., and Fries, T.L., 1987, Geochemistry of metal-rich brines from central Mississippi Salt Dome basin, U.S.A.: Applied Geochemistry, v. 2, p. 543-561.

Koppel, V. and Saager, R., 1976, Uranium, Thorium- and Lead-isotope studies of strata-bound ores, *in* K.H. Wolf, ed., Sulphur and Lead Isotopes in Strata-bound Deposits, Geochemical Studies, v. 2: Elsevier, New York, p. 267-316.

Kreitler, C.W. and Dutton, S.P., 1983, Origin and diagenesis of cap rock, Gyp Hill and Oakwood Salt Domes, Texas: Texas Bur. Econ. Geol., Austin., Report of Investigations, no. 131, 58 p.

Kupfer, D.H., 1989, Internal kinematics of salt diapirs: Discussion: Bull. Am. Assoc. Petrol. Geol., v. 73, p. 939-942.

Kyle, J.R. and Price, P.E., 1985, Mineralogical investigation of sulfide concentrations in the Hockley salt-dome cap-rock, Texas, *in* C.P. Park, et al., eds., Applied Mineralogy, Proceedings of The Second International Congress on Applied Mineralogy in the Minerals Industry: The Metallurgical Society of AIME, p. 1065-1082.

Kyle, J.R. and Price, P.E., 1986, Metallic sulfide mineralization in salt-dome cap rocks, Gulf Coast, U.S.A: Trans. Instn. Min. Metall., v. 95, p. 6-16.

Kyle, J.R., Ulrich, M.R., and Gose, W.A., 1987, Textural and paleomagnetic evidence for the mechanism and timing of anhydrite cap rock formation, Winnfield salt dome, Louisiana, *in* J. Lerche and J.J. O'Brien, eds., Dynamical Geology of Salt and Related Structures: Academic Press, Inc., New York, p. 497-542.

Kyle, J.R. and Agee, Jr., W.N., 1988, Evolution of metal ratios and $\delta^{34}S$ composition of sulfide mineralization during anhydrite cap rock formation, Hockley Dome, Texas, *in* H.H. Posey and J.R. Kyle, guest eds., Fluid-Rock Interactions in the Salt Dome Environment: Chemical Geology, v. 74, p. 37-55.

Land, L.S. and Prezbindowski, D.R., 1981, The origin and evolution of saline formation water, lower Cretaceous carbonates, southcentral Texas, USA: Jour. Hydrology,v. 54, p. 439-74.

Land, L.S., Kupecz, J.A., and Mack, L.E., 1988, Louann salt geochemistry (Gulf of Mexico sedimentary basin, U.S.A.): A preliminary synthesis, *in* H.H. Posey and J.R. Kyle, guest eds., Fluid-Rock Interactions in the Salt Dome Environment: Chemical Geology, v. 74, p. 25-35.

Le Maitre, R.W., 1982, Numerical Petrology: Statistical Interpretation of Geochemical Data: Elseiver, New York, p. 188-191.

Light, M.P.R., Posey, H.H., Kyle, J.R., and Price, P.E., 1987, Integrated hydrothermal model for the Texas Gulf Coast Basin; origins of geopressured brines and lead-zinc, uranium, hydrocarbon, and cap rock deposits, *in* J. Lerche and J.J. O'Brien, eds., Dynamical Geology of Salt and Related Structures: Academic Press, Inc., New York, p. 787-830.

Loveless, A.J., 1975, Lead isotopes - A guide to major mineral deposits: Geoexploration, v. 13, p. 13-27.

Lydon, J.W, 1983, Chemical parameters controlling the origin and deposition of sediment-hosted stratiform lead-zinc deposits, *in* D.F. Sangster, ed., Short Course in Sediment-hosted Stratiform Lead-Zinc Deposits: Mineral Assoc. of Canada, p. 175-250.

Machel, H.G., 1988, Some aspects of diagenetic sulphate-hydrocarbon redox reactions, *in* Marshal, ed., Diagenesis of Sedimentary Sequences: Geol. Soc. London, Special Publication (in press).

Macpherson, G.L., 1989, Lithium, Boron, and Barium in formation waters and sediments, Northwest Gulf Coast of Mexico sedimentary basin: Unpublished Dissertation, University of Texas at Austin, p. 314.

Martinez, J.D., 1980, Salt dome cap rock - A record of geologic processes, *in* A.H. Coogan and L. Hauber, eds., Fifth Symposium on Salt, Volume I: The Northern Ohio Geological Society, Inc., Dept. of Geology, Case Western Reserve University, Cleveland, Ohio, p. 143-151.

McLimans, R.K., Barnes, H.L., and Ohmoto, H., 1980, Sphalerite stratigraphy of the upper Mississippi valley zinc-lead district, southwest Wisconsin: Econ. Geol., v. 75, p. 351-361.

Meltzer, L.H. and Boyd, D.R., 1972, Tectonic map of the Gulf Coast region: Am. Assoc. Petrol. Geol., Tulsa, Oklahoma.

Morton, R.A. and Land, L.L., 1987, Regional variations in formation water chemistry, Frio Formation (Oligocene), Texas Gulf Coast: Bull. Am. Assoc. Petrol. Geol., v. 71, p. 191-206.

Morton, R.A., Ewing, T.E., and Tyler, N., 1983, Continuity and internal properties of Gulf Coast sandstones and their implications for geopressured fluid production: Texas Bur. Econ. Geol., Austin., Report of Investigations, no. 132, 70 p.

Muller, P. and Seimes, H., 1974, Festigkeit, Verformbarkeit und Gefugeregelung von anhydrit-experimentele Stauchverformung unter Manteldrucken bis 5 Kbar bei Temperaturen bis 300°C (Strength, ductility, and preferred orientation of anhydrite-experimental deformation by axial compression under mantle pressure up to 5 kbar and at temperatures up to 300°C): Tectonophysics, v. 23, p. 105-127.

Murray, G.E., 1966, Salt structures of Gulf of Mexico Basin-a review, Bull. Am. Assoc. Petrol. Geol., v. 50, p. 439-478.

Ohmoto, H. and Rye, R.O., 1979, Isotopes of sulfur and carbon, *in* H.L. Barnes, ed., Geochemistry of Hydrothermal Ore Deposits (2nd Edition): John Wiley and Sons, New York, p. 509-567.

Orr, W.L., 1977, Geologic and geochemical controls on the distribution of hydrogen sulfide in natural gas, *in* J. Campos and J. Goni, eds., Advances in Organic Geochemistry: Empresa Nacional Adaro de Investigation Mineras, S.A. Madrid, Spain, p. 572-597.

Parkhurst, D.L., Thorstenson, D.C., and Plummer, L.N., 1982, PHREEQE - A Computer Program For Geochemical Calculations: U.S.G.S. National Headquarters, Reston, Virgina, 216 p.

Parkhurst, D.L., Thorstenson, D.C., and Plummer, L.N., 1987, PHREPITZ - A Computer Program For Geochemical Calculations: U.S.G.S. National Headquarters, Reston, Virgina, 216 p.

Pearson, F.J. Jr. and Rightmere, C.T., 1980, Sulfur and oxygen isotopes in aqueous sulfur compounds, *in* P. Fritz and J.C. Fontes, eds., Handbook of Envirionmental Isotope Geochemistry: Elseiver, New York, p. 227-258.

Pfenning, N., Widdel, F., and Truper, H.G., 1981, The dissimilatory sulfate-reducing bacteria, *in* M.P. Starr, ed., The Prokaryotes, Springer-Verlag: Berlin, West Germany, p. 926-940.

Posey, H.H., 1986, Regional characteristics of strontium, carbon and oxygen isotopes in salt dome cap rocks of the Western Gulf Coast: Unpublished Dissertation, University of North Carolina at Chapel Hill, p. 248.

Posey, H.H., Kyle, J.R., Jackson, T.J., Hurst, S.D., and Price, P.E., 1987, Multiple fluid components of salt diapirs and salt dome cap rocks, Gulf Coast, U.S.A: Applied Geochemistry, v. 2, p. 523-534.

Posey, H.H. and Kyle, J.R., 1988, Fluid-rock interactions in the salt dome environment: An introduction and review, *in* H.H. Posey and J.R. Kyle, guest eds., Fluid-Rock Interactions in the Salt Dome Environment: Chemical Geology, v. 74, p. 1-23.

Postgate, J., 1971, Sulfate reduction-microbial, *in* R.W. Fairbridge, ed., The Encyclopedia of Geochemistry and Environmental Sciences: Van Nostrand Reinhold Co., New York, v. 14, p. 1127-1129.

Price, P.E., Kyle, J.R., and Wessel, G.R., 1983, Metallic sulfide deposits in Gulf Coast salt dome cap rocks, *in* G. Kisvarsanyi, et al., eds., International conference on Mississippi Valley-type lead-zinc deposits, proceedings volume: Rolla, Missouri: Univ. of Missouri, (1983), p. 558-568.

Price, P.E. and Kyle, J.R., 1986, Genesis of salt dome hosted metallic sulfide deposits: The role of hydrocarbons and related fluids, *in* W.E. Dean, ed., Proceedings of the Symposium on Organics and Ore Deposits: Denver Region Exploration Geologists Society, p. 171-184.

Prikryl, J.D., Posey, H.H., and Kyle, J.R., 1988, A petrographic and geochemical model for the origin of calcite cap rock at Damond Mound salt dome, Texas, U.S.A., *in* H.H. Posey and J.R. Kyle, guest eds., Fluid-Rock Interactions in the Salt Dome Environment: Chemical Geology, v. 74, p. 67-97.

Robbins, M., 1983, The Collector's Book of Fluorescent Minerals: Van Nostrand Reinhold Co., New York, 290 p.

Ramdohr, P., 1979, The Ore Minerals and their Intergrowths (2nd Edition): Pergamon Press Inc., New York, 1207 p.

Reynolds, R.L. and Goldhaber, M.B., 1983, Iron disulfide minerals and the genesis of roll-type uranium deposits: Econ. Geol., v. 78, p. 105-120.

Sakai, H., 1968, Isotopic properties of sulfur compounds in hydrothermal processes: Geochem. Jour., v. 2, p. 29-49.

Sangster, D.F., 1976, Sulphur and lead isotopes in strata-bound deposits, *in* K.H. Wolf, ed., Handbook of Strata-bound and Stratiform Ore Deposits, Geochemical Studies, v. 2: Elsevier, New York, p. 219-266.

Sassen, R., 1980, Biodegradation of crude oil and mineral deposition in a shallow Gulf Coast salt dome: Organic Geochem., v. 2, p. 153-166.

Sassen, R., Chinn, E.W., and McCabe, C., 1988, Recent hydrocarbon alteration, sulfate reduction and formation of elemental sulfur and metal sulfides in salt dome cap rock, *in* H.H. Posey and J.R. Kyle, guest eds., Fluid-Rock Interactions in the Salt Dome Environment: Chemical Geology, v. 74, p. 57-66.

Seni, S.J. and Jackson, M.P.A., 1984, Sedimentary record of Cretaceous and Tertiary salt movement, East Texas basin: Times, rates, and volumes of salt flow and their implications for nuclear waste isolation and petroleum exploration: Texas Bur. Econ. Geol., Austin., Report of Investigations, no. 139, 89 p.

Seni, S.J., 1987, Evolution of Boling Dome cap rock with emphasis on included terrigenous clastics, Fort Bend and Wharton Counties, Texas, *in* J. Lerche and J.J. O'Brien, eds., Dynamical Geology of Salt and Related Structures: Academic Press, Inc., New York, p. 543-591.

Sharp, Jr., J.M., Galloway, W.E., Land, L.S., McBride, E.F., Blanchard, P.E., Bodner, D.P., Dutton, S.P., Farr, M.R., Gold, P.B., Jackson, T.J., Lundegard, P.D., Macpherson, G.L., and Millikan, K.L., 1988, Diagenetic processes in northwest Gulf of Mexico sediments: *in* G.V. Chilingarian and K.H. Wolf, eds., Developments in Sedimentology, Diagenesis II, v. 43, Elsevier, New York, p. 43-113.

Smith, Jr., A.E., 1970, Minerals from Gulf Coast salt dome (part I): Rocks and minerals, v. 45, p. 299-303.

Sverjensky, D.A., Rye, D.M., and Doe, B.R., 1979, The lead and sulfur isotopic compositions of galena from a Mississippi Valley-type deposit in the New Lead Belt, southeast Missouri: Econ. Geol., v. 74, p. 149-152.

Sverjensky, D.A., 1981, The origin of a Mississippi valley-type deposit in the Viburnum trend southeast Missouri: Econ. Geol., v. 76, p. 1848-1872.

Sverjensky, D.A., 1984, Oil field brines as ore-forming solutions: Econ. Geol., v. 79, p. 23-37.

Tracor Northern, 1986, FLEXTRAN - A computer program for data acquisition and reduction: Tracor Northern, Middleton, Wisconsin, 43 p.

Tuttle, J.H., Dugan, P.R., Macmillan, C.B., and Randles, C.I., 1969, Microbial dissimilatory sulfur cycle in acid mine waters: Jour. of Bacteriology, v. 97, p. 594-602.

Ulrich, M.R., Kyle, J.R., and Price, P.E., 1984, Metallic sulfide deposits in the Winnfield salt dome, Louisiana: evidence for episodic introduction of metalliferous brines during cap rock formation, *in* B.R. White, ed., Trans: Gulf Coast Assoc. Geol. Soc., v. 34, p. 435-442.

Vogler, H.A. and Robison, B.A., 1987, Exploration for deep geopressured gas: Corsair trend, offshore Texas, Bull. Am. Assoc. Petrol. Geol., v. 71, no. 7, p. 777-787.

Wessel, G.R., 1983, Geologic summary of Hockley Dome, Texas: Unpublished project report, Marathon Mineral Resources, 43 p.

Woronick, R.E. and Land, L.S., 1985, Late burial diagenesis, lower Cretaceous Pearsall and lower Glen Rose formations, south Texas, *in* N. Schneidermann and P.M. Harris, eds., Carbonate Cements, Special Publication: The Soc. of Econ. Paleontologists and Min., v. 36, p. 265-275.

The vita has been removed from the digitized version of this document.